

**ADSORPTION OF HYDROGEN SULFIDE  
FROM SIMULATED WASTE WATER USING  
LOCALLY-SOURCED ADSORBENTS**



**OMAR ABED HABEEB**

**UMP**

Doctor of Philosophy

**UNIVERSITI MALAYSIA PAHANG**

## UNIVERSITI MALAYSIA PAHANG

### DECLARATION OF THESIS AND COPYRIGHT

Author's Full Name : OMAR ABED HABEEB

Date of Birth : 01 JULY 1980

Title : ADSORPTION OF HYDROGEN SULFIDE FROM  
SIMULATED WASTE WATER USING LOCALLY –  
SOURCED ADSORBENTS

Academic Session : \_\_\_\_\_

I declare that this thesis is classified as:

- CONFIDENTIAL (Contains confidential information under the Official Secret Act 1997)\*
- RESTRICTED (Contains restricted information as specified by the organization where research was done)\*
- OPEN ACCESS I agree that my thesis to be published as online open access (Full Text)

I acknowledge that Universiti Malaysia Pahang reserves the following rights:

1. The Thesis is the Property of Universiti Malaysia Pahang
2. The Library of Universiti Malaysia Pahang has the right to make copies of the thesis for the purpose of research only.
3. The Library has the right to make copies of the thesis for academic exchange.

Certified by:

\_\_\_\_\_  
(Student's Signature)

PKC15016/ A8437802

\_\_\_\_\_  
New IC/Passport Number  
Date: 20/ 12 / 2017

\_\_\_\_\_  
(Supervisor's Signature)

RAMESH KANTHASAMY

\_\_\_\_\_  
Name of Supervisor  
Date: 20 /12 / 2017

NOTE : \* If the thesis is CONFIDENTIAL or RESTRICTED, please attach a thesis declaration letter.

## THESIS DECLARATION LETTER (OPTIONAL)

Librarian,  
*Perpustakaan Universiti Malaysia Pahang,*  
Universiti Malaysia Pahang,  
Lebuhraya Tun Razak,  
26300, Gambang, Kuantan.

Dear Sir,

### CLASSIFICATION OF THESIS AS RESTRICTED

Please be informed that the following thesis is classified as RESTRICTED for a period of three (3) years from the date of this letter. The reasons for this classification are as listed below.

Author's Name  
Thesis Title

Reasons           (i)  
  
                         (ii)  
  
                         (iii)

Thank you.

Yours faithfully,

---

(Supervisor's Signature)

Date:

Stamp:

Note: This letter should be written by the supervisor, addressed to the Librarian, *Perpustakaan Universiti Malaysia Pahang* with its copy attached to the thesis.

## SUPERVISOR'S DECLARATION

I/We\* hereby declare that I/We\* have checked this thesis/project\* and in my/our\* opinion, this thesis/project\* is adequate in terms of scope and quality for the award of the degree of \*Doctor of Philosophy of Engineering in Chemical and Natural Resources Engineering.

---

(Supervisor's Signature)

Full Name :

Position :

Date :

---

(Co-supervisor's Signature)

Full Name :

Position :

Date :

### STUDENT'S DECLARATION

I hereby declare that the work in this thesis is based on my original work except for quotations and citations which have been duly acknowledged. I also declare that it has not been previously or concurrently submitted for any other degree at Universiti Malaysia Pahang or any other institutions.

---

(Student's Signature)

Full Name : OMAR ABED HABEEB

ID Number : PKC15016/A8437802

Date : , 2018



UMP

ADSORPTION OF HYDROGEN SULFIDE FROM SIMULATED WASTE  
WATER USING LOCALLY-SOURCED ADSORBENTS



OMAR ABED HABEEB

Thesis submitted in fulfillment of the requirements  
for the award of the degree of  
Doctor of Philosophy in Chemical Engineering and Natural Resources

UMP

Faculty of Chemical and Natural Resources Engineering

UNIVERSITI MALAYSIA PAHANG

2018

## ACKNOWLEDGEMENTS

First of all, I would like to thank ALLAH (s.w.t) for giving me the guidance, patience, and perseverance to complete my Doctor of Philosophy thesis.

Secondly, I would like to extend my heartiest thanks to my supervisors, Dr. Ramesh K., Prof. Dato Dr. Rosli bin Mohd Yunus, for the tremendous supervision and guidance; they have given me all the required and support to complete my study. Their constant encouragement,

I am deeply and forever indebted to my parents for their continuous praying to be successful, and encouragement throughout my previous study. I am also very thankful to my brothers and sisters.

Last but not the least; I would like especially thank my wife and my kids for continue praying and support me.



UMP

## ABSTRAK

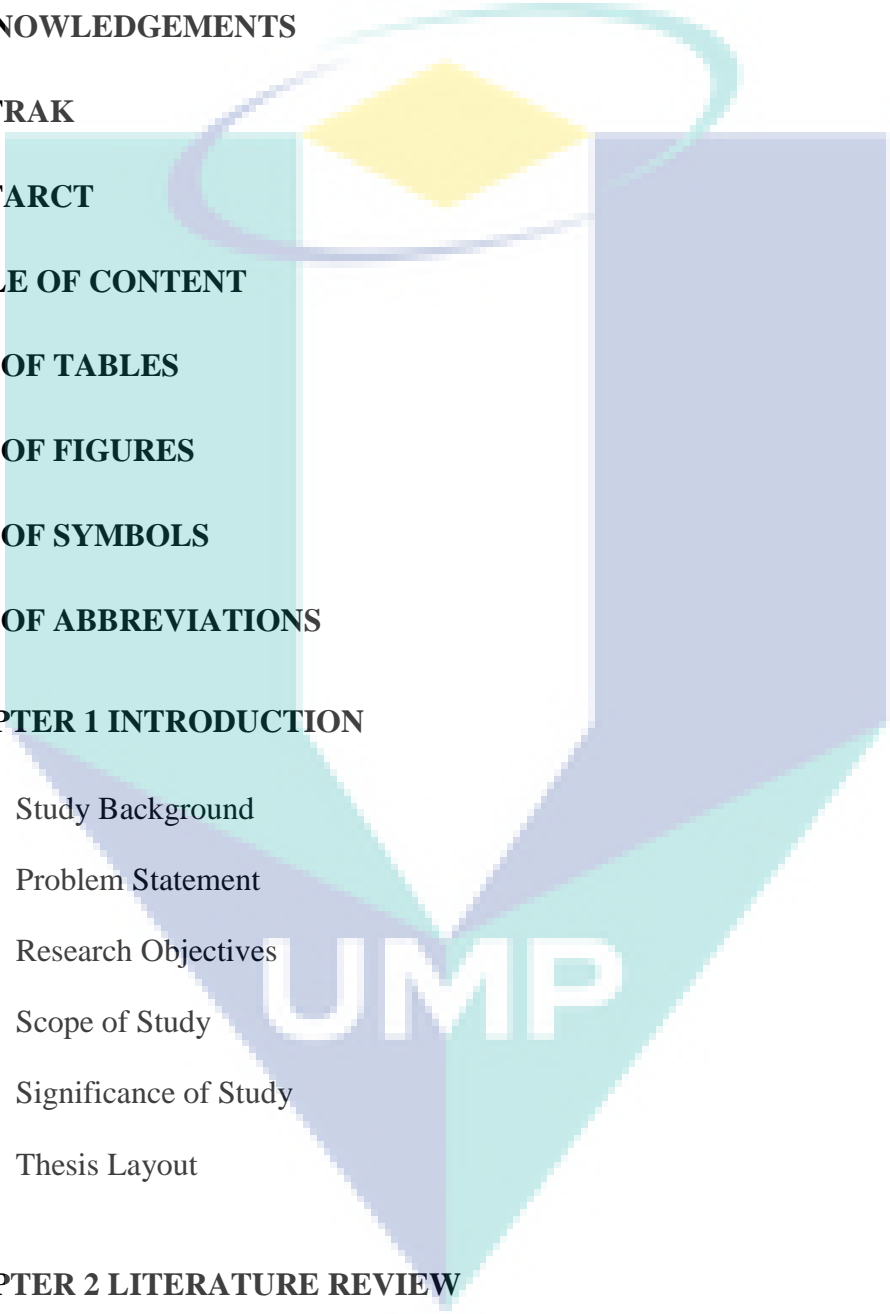
Hidrogen sulfida ( $H_2S$ ) (ak) adalah salah satu bahan pencemar yang paling toksik dalam air sisa dari kilang penapisan petroleum. Ia sangat berbahaya kepada kesihatan manusia dan menyebabkan masalah terhadap alam sekitar dan ekonomi. Penyingkiran  $H_2S$  (ak) dari simulasi air sisa penapisan petroleum menggunakan karbon teraktif yang dihasilkan daripada produk sampingan pertanian seperti tempurung kelapa (CNS), cengkerang biji sawit (PKS), dan habuk kayu papan (WSD) telah dikaji. Karbon teraktif yang diperolehi daripada CNS, PKS, dan WSD diaktifkan secara kimia menggunakan KOH. Karbon teraktif (ACs) diubah suai dengan penghamilan kalsium (Ca) yang diekstrak daripada kulit telur untuk menghasilkan karbon teraktif (IACs) iaitu Ca-ACCNS, Ca-ACPKS dan Ca-ACWSD. Ciri-ciri AC dan IAC yang disediakan akan dianalisis menggunakan SEM / EDX, FTIR, BET, TGA, XRD dan XPS. Kajian perbandingan antara enam penjerap untuk penyingkiran  $H_2S$  (ak) daripada simulasi air sisa telah dijalankan. Kajian penjerapan menunjukkan bahawa karbon teraktif PKS berasaskan Ca (AC-ACPKS) menunjukkan prestasi terbaik untuk penyingkiran  $H_2S$  (ak). Kajian pengoptimuman untuk keadaan penyediaan penjerap terpilih (Ca-ACPKS) telah disiasat menggunakan Kaedah Permukaan Tindak Balas (RSM). Keadaan penyediaan seperti suhu kalsinasi, kepekatan larutan kalsium, dan masa penyentuhan kalsin dioptimumkan. Keadaan penyediaan optimum Ca-ACPKS diperolehi pada suhu kalsinasi  $880\text{ }^\circ\text{C}$ , kepekatan larutan kalsium 49.31 V%, dan masa hubungan penyentuhan kalsinasi selama 57.5 min. Selain itu, faktor-faktor keadaan seperti kepekatan awal  $H_2S$  (ak), masa penyentuhan jerapan, dos, larutan pH, dan kelajuan pengocakan pada mulanya ditapis menggunakan dua pendekatan tahap faktorial. Keputusan menunjukkan bahawa kesan kepekatan awal  $H_2S$  (ak), masa penyentuhan jerapan dan dos adalah penting untuk penyingkiran  $H_2S$  (ak). Tambahan pula, ketiga-tiga parameter keadaan ini disiasat menggunakan teknik reka bentuk composite pusat (CCD) melalui RSM dan keadaan optimum yang diperolehi bagi kepekatan awal  $H_2S$  (ak) ialah 440 mg / L, masa penyentuhan jerapan sebanyak 585 min, dan 1.05 g Ca -ACPKS. Keadaan operasi yang optimum menghasilkan kecekapan penyingkiran sebanyak 99.5% dengan kepekatan pada keseimbangan (0.5-2.2 mg/L) yang berdekatan dengan piawaian Jabatan Alam Sekitar (JAS) B (0.5 mg/L) menggunakan air sisa sebenar. Kajian kinetik mengenai keadaan penjerapan Ca-ACPKS telah menunjukkan bahawa isotherm penjerapan Freundlich lebih sesuai dan proses penjerapan mengikuti model kinetik urutan Pseudo-kedua. Kapasiti penjerapan maksimum Ca-ACPKS adalah 543.4 mg/g. Disimpulkan bahawa CaACPKS adalah penjerap yang berkesan untuk penyingkiran  $H_2S$  (ak) dari air sisa simulasi.



## ABSTARCT

Hydrogen sulfide ( $\text{H}_2\text{S}$ ) (aq) is one of the most toxic pollutants in petroleum refinery waste water. It is very harmful to human health and causes environmental and economic problems. The removal of  $\text{H}_2\text{S}$  (aq) from a simulated petroleum refinery waste water using activated carbons produced from agricultural by-product such as, coconut shell (CNS), palm kernel shell (PKS), and wood sawdust (WSD) were investigated. The activated carbons obtained from the CNS, PKS, and WSD were chemically activated using KOH. The activated carbons (ACs) were modified by impregnating with calcium (Ca) extracted from egg shells to produce impregnated activated carbons (IACs) namely Ca-ACCNS, Ca-ACPKS and Ca-ACWSD. The prepared ACs and IACs were characterized using SEM/EDX, FTIR, BET, TGA, XRD and XPS. Comparative studies between all the six adsorbents for the removal of  $\text{H}_2\text{S}$  (aq) from the simulated waste water were carried out. The adsorption studies revealed that Ca-modified PKS-based activated carbon (Ca-ACPKS) has shown best performance for the removal of  $\text{H}_2\text{S}$  (aq). An optimization studies for the preparation conditions of the selected adsorbent (Ca-ACPKS) was investigated using Response Surface Methodology (RSM) and the optimum preparation conditions were found to be calcination temperature of 880 °C, calcium solution concentration of 49.31 %v, and calcination time of 57.5 min with removal efficiency of 99.2% and yield of 33.8%. Moreover, operating factors such as initial concentration of  $\text{H}_2\text{S}$  (aq), adsorption contact time, dosage, pH of solution, and agitation speed were initially screened using 2 level factorial approach and the resulted significant factors were initial concentration of  $\text{H}_2\text{S}$  (aq), adsorption contact time, and dosage were significant on the removal of  $\text{H}_2\text{S}$  (aq). Furthermore, the effect of these three operating parameters were investigated using the central composite design (CCD) techniques of RSM and the optimum conditions obtained were initial concentration of  $\text{H}_2\text{S}$  of 440 mg/L, adsorption contact time of 585 min, and dosage of 1.05 g Ca-ACPKS. The optimum operating conditions resulted in a removal efficiency of 99.5% with equilibrium concentration (0.5-2.2 mg/L) which was close to Department of Environment (DOE) standard B (0.5 mg/L) using real waste water. The kinetic studies of the adsorption behaviour of Ca-ACPKS have shown that Freundlich adsorption isotherm was fitted well and the adsorption process followed Pseudo- second order kinetic model. The maximum adsorption capacity of Ca-ACPKS was 543.4 mg/g. It can be concluded that Ca-ACPKS has an effective adsorbent for the removal of  $\text{H}_2\text{S}$  (aq) from simulated waste water.

# TABLE OF CONTENT



<b>DECLARATION</b>	
<b>TITLEPAGE</b>	
<b>ACKNOWLEDGEMENTS</b>	<b>ii</b>
<b>ABSTRAK</b>	<b>iii</b>
<b>ABSTARCT</b>	<b>iv</b>
<b>TABLE OF CONTENT</b>	<b>v</b>
<b>LIST OF TABLES</b>	<b>xi</b>
<b>LIST OF FIGURES</b>	<b>xiii</b>
<b>LIST OF SYMBOLS</b>	<b>xvi</b>
<b>LIST OF ABBREVIATIONS</b>	<b>xvii</b>
<b>CHAPTER 1 INTRODUCTION</b>	<b>1</b>
1.1 Study Background	1
1.2 Problem Statement	4
1.3 Research Objectives	5
1.4 Scope of Study	6
1.5 Significance of Study	7
1.6 Thesis Layout	8
<b>CHAPTER 2 LITERATURE REVIEW</b>	<b>9</b>
2.1 Introduction	9
2.2 Sources and Discharge of H <sub>2</sub> S	9
2.2.1 Petroleum Refinery Waste Water	10

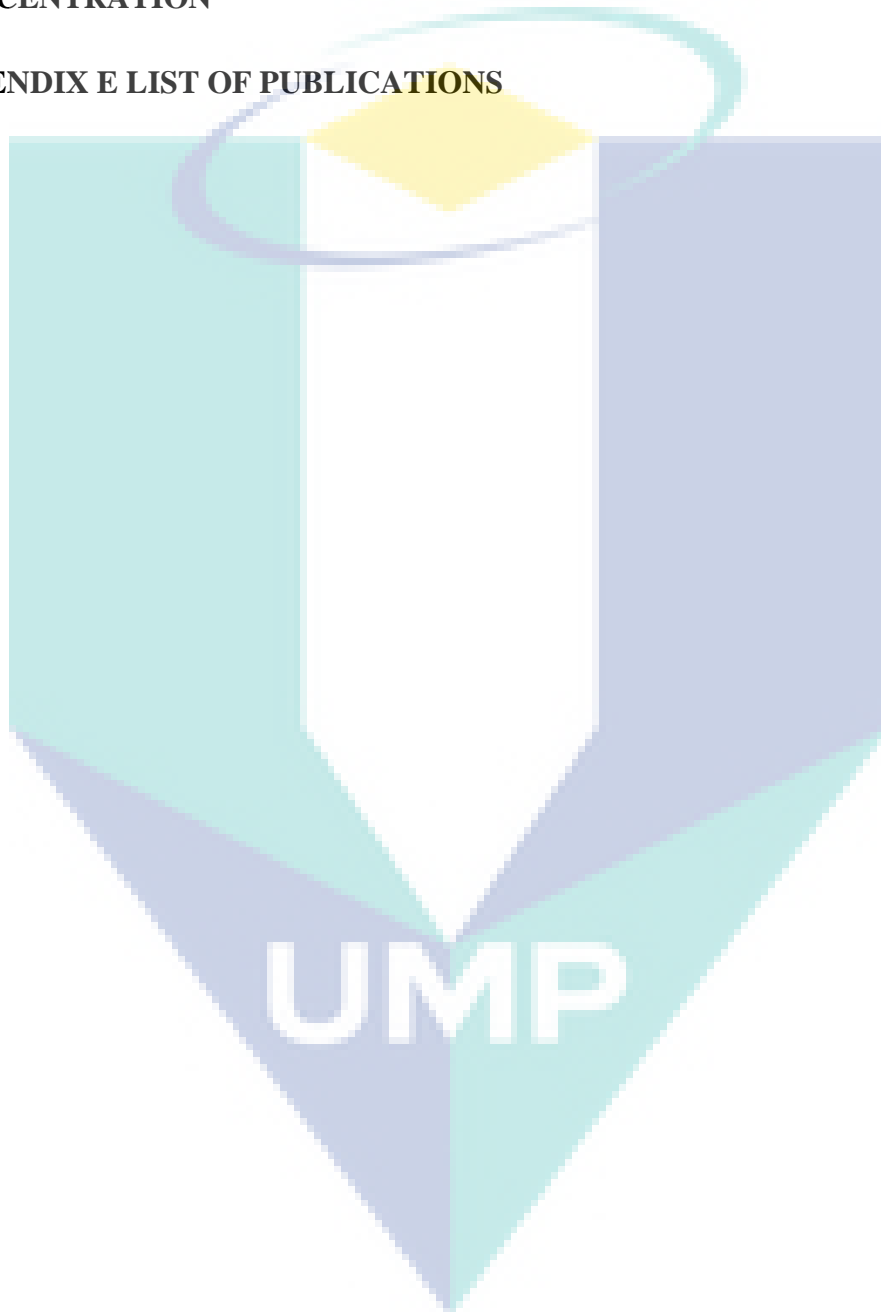
2.2.2	Hydrogen Sulfide in Waste Water	11
2.3	Current Removal Technologies for H <sub>2</sub> S	17
2.3.1	Biological Treatment Method	18
2.3.2	Electrochemical Methods	19
2.3.3	Chemical Method	20
2.3.4	Physiochemical Sorption (Adsorption)	21
2.4	Adsorption of H <sub>2</sub> S	22
2.4.1	Adsorption of H <sub>2</sub> S Using Waste Materials	22
2.4.2	Adsorption of H <sub>2</sub> S on Metal Oxide and Zeolite Materials	23
2.4.3	Adsorption of H <sub>2</sub> S (g) on Composite Materials	24
2.4.4	Adsorption of H <sub>2</sub> S on Activated Carbons	26
2.5	Impregnation of Activated Carbons (IACs)	35
2.5.1	Dispersion of Calcium on Activated Carbon	35
2.5.2	Sources of Calcium	36
2.6	Adsorption of Dissolved H <sub>2</sub> S	37
2.6.1	Factors Affecting the Adsorbent/Adsorbate Interactions	38
2.7	Optimization Studies of Removal Efficiency of H <sub>2</sub> S (aq)	38
2.7.1	Design of Expert (DoE)	39
2.7.2	Statistical and Graphical Analysis.	40
2.8	Adsorption Isotherm Models	40
2.8.1	Langmuir Isotherm	42
2.8.2	Freundlich Isotherm	43
2.8.3	Temkin Isotherm Model	43
2.8.4	Dubinin–Radushkevich Isotherm	44
2.9	Batch Kinetic Models Studies	45
2.9.1	Pseudo–First–Order Kinetic Model	45

2.9.2	Pseudo–Second–Order Kinetic Model	45
2.9.3	Intra-particle Diffusion Model	46
2.10	Thermodynamics of Adsorption Equilibrium	46
2.11	Knowledge Gap	47
<b>CHAPTER 3 RESEARCH METHODOLOGY</b>		<b>49</b>
3.1	Introduction	49
3.2	Synthesis of ACs from Agricultural Wastes	52
3.2.1	Carbonization Process of ACs	52
3.2.2	Activation Process of ACs	53
3.3	Modification and Impregnation Process of ACs	54
3.3.1	Extraction of Calcium from Egg Shells	54
3.3.2	Synthesis Process of IACs	55
3.4	Characterization of the ACs and IACs	56
3.4.1	Scanning Electron Microscope (SEM)	56
3.4.2	Energy Dispersive X-Ray Test (EDX)	57
3.4.3	pH Measurement of Adsorbent Surface and Solution	57
3.4.4	Sorption of Nitrogen	57
3.4.5	Fourier Transform Infrared Spectroscopy (FTIR)	58
3.4.6	Thermal Gravimetric Analysis (TGA)	58
3.4.7	X-Ray Diffraction (XRD)	58
3.4.8	X-ray Photoelectron Spectroscopy (XPS)	58
3.5	Preparation of Simulated and Some of Real Waste Water	59
3.5.1	Preparation of Simulated Waste Water	59
3.5.2	Real Waste Water	59
3.6	Batch Equilibrium Studies of H <sub>2</sub> S (aq) Adsorption by ACs	60

3.6.1	Analysis of H <sub>2</sub> S (aq) Concentration	60
3.6.2	Preliminary Study of the Parameters	61
3.6.3	Comparison Study between the Adsorbents	62
3.7	Optimization of Adsorption Process	62
3.7.1	Optimization of Preparation Conditions of Selected Adsorbent	64
3.7.2	Optimization of Operating Conditions for Adsorption Process	65
3.8	Batch Kinetic and Thermodynamic Study	66
3.8.1	Adsorption Isotherm Models	66
3.8.2	Batch Kinetic Studies	67
3.8.3	Adsorption Thermodynamics	68
<b>CHAPTER 4 RESULTS AND DISCUSSION</b>		<b>69</b>
4.1	Introduction	69
4.2	Characterizations of Adsorbents	69
4.2.1	Morphological Characterization Test	70
4.2.2	pH Measurement	78
4.2.3	Analysis of Nitrogen Sorption	79
4.2.4	FTIR Test	82
4.2.5	Thermal Gravimetric Analysis	86
4.2.6	X-Ray Diffraction (XRD)	91
4.2.7	X-ray Photoelectron Spectroscopy	94
4.3	Batch Adsorption Studies	97
4.3.1	Effect of Initial H <sub>2</sub> S (aq) Concentration	97
4.3.2	Effect of Adsorption Contact Time	98
4.3.3	Effect of Adsorbent Dosage	99
4.3.4	Effect of Initial Solution pH	100

4.3.5	Effect of Agitation Speed	101
4.4	Adsorption of H <sub>2</sub> S (aq) on IACs adsorbents	102
4.4.1	Effect of Preparation Factors on Removal Efficiency	102
4.4.2	Selection of Effective Adsorbent	104
4.5	Optimization of Preparation Conditions of Ca-ACPKS	105
4.5.1	Analysis of Variance Test	105
4.5.2	Combined Effect of 3D Plot on Removal Efficiency	110
4.5.3	Combined Effect of 3D Plot on Ca-ACPKS Yield	112
4.5.4	Validation of preparation conditions of Ca-ACPKS	114
4.6	Optimization of Adsorption Process of Ca-ACPKS	115
4.6.1	Analysis of Variance Test	117
4.6.2	Combined Effect of 3D Plot on Removal Efficiency	118
4.6.3	Validation of Operating Conditions	121
4.7	Equilibrium, Isotherm, and Kinetic Study of Ca-ACPKS	122
4.7.1	Effect of Contact Time and Initial Concentration	122
4.7.2	Adsorption Isotherms Model	124
4.7.3	Kinetics of Adsorption	128
4.7.4	Thermodynamic Study	130
4.7.5	Reaction Mechanisms of Adsorption	131
<b>CHAPTER 5 CONCLUSION AND FUTURE WORK</b>		<b>134</b>
5.1	Overall Conclusion	134
5.2	Future Recommendations	136
<b>REFERENCES</b>		<b>138</b>
<b>APPENDIX A THE IMAGES OF MATERIALS, SIMULATED, AND REAL WASTE WATER BEFORE AND AFTER ADSORPTION PROCESS</b>		<b>163</b>

<b>APPENDIX B CALCULATIONS AND RESULTS</b>	<b>165</b>
<b>APPENDIX C OPTIMIZATION OF THE PREPARATION AND OPERATION CONDITIONS OF CA-ACP KS</b>	<b>167</b>
<b>APPENDIX D THE RESULT OF MEASURING CALCIUM CONCENTRATION</b>	<b>169</b>
<b>APPENDIX E LIST OF PUBLICATIONS</b>	<b>172</b>



## LIST OF TABLES

Table 2.1	Different sources of H <sub>2</sub> S (g)	9
Table 2.2	Typical composition in selected petroleum refinery effluents	11
Table 2.3	Concentration of H <sub>2</sub> S and S <sup>2-</sup> on different kind of waste water	12
Table 2.4	Selected parameter limits of effluent of Standards A and B (Department of Environment, DOE, Malaysia 2009)	15
Table 2.5	Guidelines for Occupational Exposure to H <sub>2</sub> S (g)	16
Table 2.6	Categories of Methods used for H <sub>2</sub> S (aq) removal	17
Table 2.7	Differences between physical and chemical adsorption	22
Table 2.8	Adsorbents derived from wastes materials	23
Table 2.9	The literatures of adsorption process based on composite materials	25
Table 2.10	The literatures of some types of adsorbent and their adsorption capacity	31
Table 2.11	IUPAC classification of pore sizes	34
Table 2.12	Literature summary on adsorption of aqueous H <sub>2</sub> S (aq) using different adsorbents	48
Table 3.1	Equipment employed for characterization study	56
Table 3.2	Preparation of different concentration of dissolved H <sub>2</sub> S (aq) and the weight of Na <sub>2</sub> S.9H <sub>2</sub> O	59
Table 3.3	Characteristics of petrochemical waste water	60
Table 3.4	The experimental rig employed in this study	61
Table 3.5	Preliminary study of operating condition parameters	62
Table 3.6	Independent parameters, ranges and dependent responses for ptimization of preparation conditions of selected adsorbent	64
Table 3.7	Screening removal factors of H <sub>2</sub> S (aq) on selected adsorbent (2 level factorials design)	65
Table 3.8	Optimization of significant factors of adsorption of H <sub>2</sub> S (aq) on the selected adsorbents using (RSM)	66
Table 3.9	List of adsorption isotherms models	67
Table 3.10	List of adsorption kinetic models and thermodynamic equations	68
Table 4.1	The components of ACs for fresh and spent adsorbent	70
Table 4.2	The components of IACs for fresh and spent adsorbent	75
Table 4.3	The values of pH of the solutions and surfaces of adsorbents	78
Table 4.4	Specific surface area and other related parameters of ACs and IACs	80
Table 4.5	The functional group list of ACCNS (fresh and spent)	83



Table 4.6	The functional group list of ACPKS (fresh and spent)	85
Table 4.7	The functional group list of ACWSD (fresh and spent)	86
Table 4.8	Thermal analysis of the materials used to prepare ACs and IACs	87
Table 4.9	Analysis of variance and lack-of-fit test for RE using Ca-ACPKS	106
Table 4.10	Analysis of variance and lack-of-fit test for Ca-ACPKS yield	106
Table 4.11	Regression statistics for RE and yield at equilibrium using Ca-ACPKS	107
Table 4.12	Model validation of preparation conditions of Ca-ACPKS	115
Table 4.13	Analysis of variance (ANOVA) and lack-of-fit test for RE using Ca-ACPKS	117
Table 4.14	Regression statistics for operating conditions of RE using Ca-ACPKS	118
Table 4.15	Validation of operating conditions of RE of H <sub>2</sub> S (aq) using Ca-ACPKS	121
Table 4.16	Isotherm models parameters and correlation coefficients for adsorption of H <sub>2</sub> S on Ca-ACPKS	124
Table 4.17	Kinetic models parameters for adsorption of H <sub>2</sub> S (aq) on Ca-ACPKS	128
Table 4.18	Thermodynamic parameters of H <sub>2</sub> S (aq) adsorption on Ca-ACPKS	130



UMP

## LIST OF FIGURES

Figure 2.1	A schematic example of the typical water balance in a refinery	11
Figure 2.2	Distribution of three sulfide species in water	13
Figure 2.3	Cleaning technologies methods of H <sub>2</sub> S from down stream	17
Figure 2.4	Chemical and biological process for H <sub>2</sub> S emission control in sewer system	19
Figure 2.5	H <sub>2</sub> S (g) adsorption capacities of some composite materials	26
Figure 2.6	Linear dependence of H <sub>2</sub> S adsorption capacity of some carbon based materials on the adsorbent surface area (solid line is the linear fitting)	31
Figure 2.7	(a) Surface functional groups of the activated carbon, (b) Acidic groups, (c) Basic groups	33
Figure 2.8	Schematic representation of external and internal adsorbent surface	34
Figure 2.9	Classification of adsorption isotherm	42
Figure 3.1	Overall methodology flowchart	51
Figure 3.2	Raw materials for preparation of activated carbons from (a) coconut shell, (b) palm kernel shell, (c) wood saw dust	52
Figure 3.3	Carbonization and activation process of ACs	53
Figure 3.4	Preparation and modification of surface chemistry of IACs with calcium extracted from egg shells	55
Figure 3.5	Different techniques of analysis for adsorbents characterization	56
Figure 3.6	Batch equilibrium studies using (DOE)	64
Figure 3.7	Batch equilibrium thermodynamic, isotherm and kinetic modeling studies	67
Figure 4.1	SEM images (a, b) before and after adsorption process for ACCNS.EDX test (c, d) before and after adsorption process for ACCNS, respectively	71
Figure 4.2	SEM images (a, b) before and after adsorption process for ACPKS. EDX test (c, d) before and after adsorption process for ACPKS, respectively	72
Figure 4.3	SEM images (a, b) before and after adsorption process for ACWSD.EDX test (c, d) before and after adsorption process for ACWSD, respectively	73
Figure 4.4	SEM images (a, b) before and after adsorption process for Ca-ACCNS. EDX test (c, d) before and after adsorption process for Ca-ACCNS, respectively	75

Figure 4.5	SEM images (a, b) before and after adsorption process for Ca-ACPKS. EDX test (c, d) before and after adsorption process for Ca-ACPKS, respectively	76
Figure 4.6	SEM images (a, b) before and after adsorption process for Ca-ACWSD. EDX test (c, d) before and after adsorption process for Ca-ACWSD, respectively	77
Figure 4.7	N <sub>2</sub> adsorption–desorption isotherm of ACs	81
Figure 4.8	N <sub>2</sub> adsorption–desorption isotherm of IACs	82
Figure 4.9	FTIR spectrum test for ACCNS fresh and spent	83
Figure 4.10	FTIR spectrum test for ACPKS fresh and spent	84
Figure 4.11	FTIR spectrum test for ACWSD fresh and spent	85
Figure 4.12	TGA curves of ACCNS	87
Figure 4.13	TGA curves of Ca-ACCNS	88
Figure 4.14	TGA curves of ACPKS	89
Figure 4.15	TGA curves of Ca-ACPKS	90
Figure 4.16	TGA curves of ACWSD	90
Figure 4.17	TGA curves of Ca-ACWSD	91
Figure 4.18	The XRD pattern of the ACCNS (fresh) and Ca-ACCNS (fresh and spent)	92
Figure 4.19	The XRD pattern of the ACPKS (fresh) and Ca-ACPKS (fresh and spent)	93
Figure 4.20	The XRD pattern of the ACWSD (fresh) and Ca-ACWSD (fresh and spent)	94
Figure 4.21	X-ray photoelectron spectroscopy (XPS) test for the ACCNS (fresh) and Ca-ACCNS (fresh)	95
Figure 4.22	X-ray photoelectron spectroscopy (XPS) test for the ACPKS (fresh) and Ca-ACPKS (fresh and spent)	96
Figure 4.23	X-ray photoelectron spectroscopy (XPS) test for ACWSD (fresh) and Ca-ACWSD (fresh)	97
Figure 4.24	Effect of initial concentration of H <sub>2</sub> S (aq) on % RE	98
Figure 4.25	Effect of adsorption contact time on % RE	99
Figure 4.26	Effect of amount of adsorbent on % RE	100
Figure 4.27	Effect of initial solution pH on % RE	101
Figure 4.28	Effect of agitation speed on % RE	102
Figure 4.29	Effect of the calcination contact time and types of IACs on RE	103
Figure 4.30	Effect of the calcination temperature and types of IACs on RE	103
Figure 4.31	Effect of the concentration of calcium and types of IACs on RE	104
Figure 4.32	Comparison between adsorbents	105

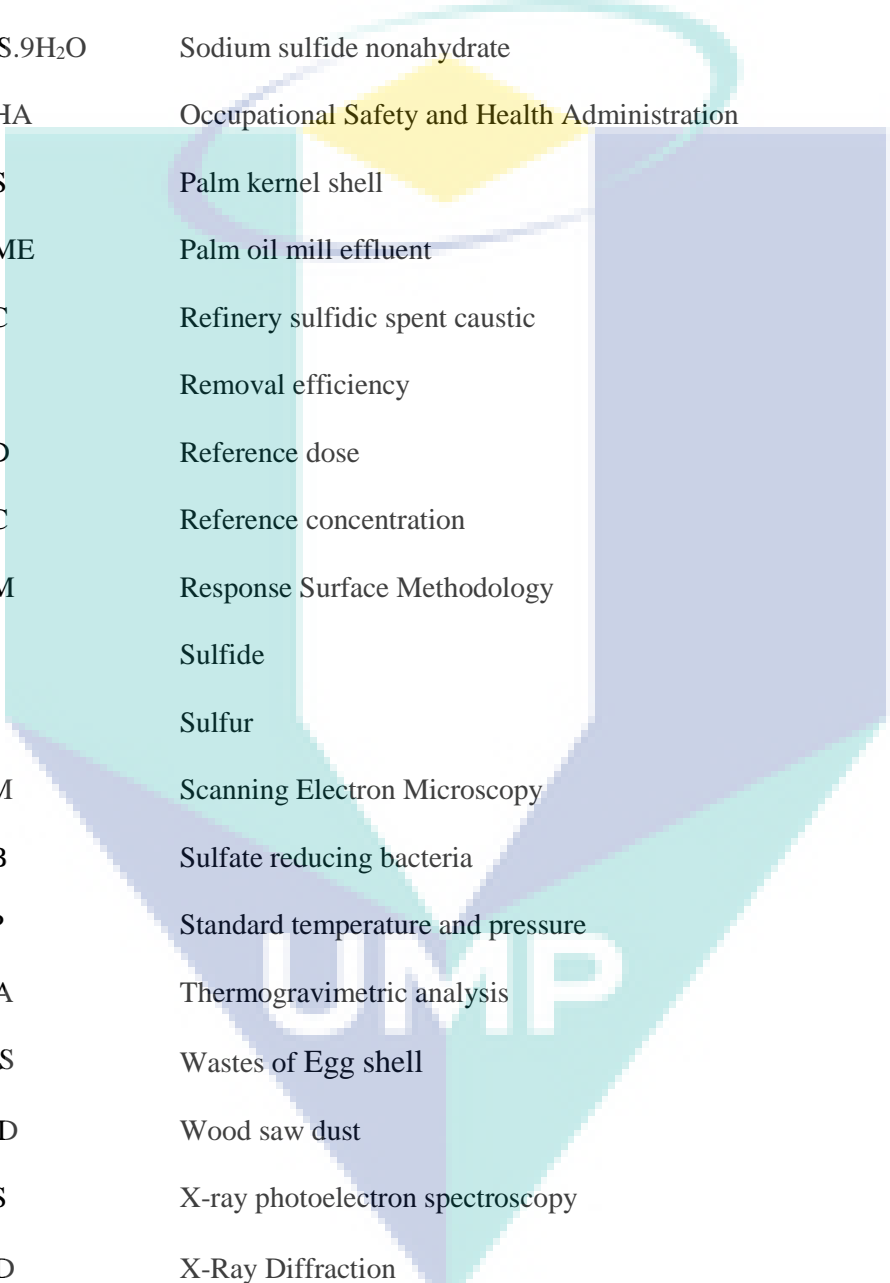
Figure 4.33	(a) The predicted and actual values, (b) Normal plot residual for RE using Ca-ACPKS	108
Figure 4.34	(a) The predicted and actual values, (b) Normal plot residual for the yield of Ca-ACPKS	109
Figure 4.35	The combined effect of calcination temperature and calcium solution concentration on RE	111
Figure 4.36	The influence of combined the calcination temperature and calcination contact time on RE	111
Figure 4.37	The influence of combined of calcium concentration and calcination contact time on RE	112
Figure 4.38	The influence of combined the calcination temperature and calcium concentration on the yield of Ca-ACPKS	113
Figure 4.39	The influence of combined the calcination temperature and calcination time on the yield of Ca-ACPKS	113
Figure 4.40	The influence of combined the concentration of calcium and calcination time on the yield of Ca-ACPKS	114
Figure 4.41	The optimum of the preparation conditions and desirability of Ca-ACPKS	114
Figure 4.42	(a) The predicted vs actual values, (b) Normal plot of residuals for optimization of operating conditions of RE using Ca-ACPKS	116
Figure 4.43	Combined effect of initial concentration of H <sub>2</sub> S(aq) and contact time on RE using Ca-ACPKS	119
Figure 4.44	Combined effect of initial concentration of H <sub>2</sub> S (aq) and dosage on RE using Ca-ACPKS	120
Figure 4.45	Combined effect of dosage and contact time on RE using Ca-ACPKS	121
Figure 4.46	Validation between actual and predicted results of operating conditions of RE using Ca-ACPKS	122
Figure 4.47	The effect of adsorption time with various initial H <sub>2</sub> S(aq) concentrations on RE using Ca-ACPKS	123
Figure 4.48	Langmuir (a), Freundlich (b), Temkin (c) and Dubinin–Radushkevich (d) adsorption isotherms of H <sub>2</sub> S (aq) on Ca-ACPKS at 30 °C	127
Figure 4.49	Pseudo–first–order (a), pseudo–second–order (b) and intra-particle diffusion (c) kinetic models for the adsorption of H <sub>2</sub> S on Ca-ACPKS	129
Figure 4.50	Thermodynamic study of the adsorption of H <sub>2</sub> S on Ca-ACPKS	130

## LIST OF SYMBOLS

B	Heat of adsorption (J/mol)
B <sub>DR</sub>	The constant related to the adsorption energy (mol <sup>2</sup> KJ <sup>-2</sup> )
b <sub>T</sub>	Temkin isotherm constant
C <sub>0</sub>	Initial concentration of H <sub>2</sub> S solution (ppm)
C <sub>e</sub>	Equilibrium concentration (ppm)
E	Mean free energy (KJ/mol)
G	Gibbs free energy (KJ/mol)
K <sub>1</sub>	Pseudo First order equilibrium rate constant (1/min)
K <sub>2</sub>	Pseudo second order rate constant (g/mg.min)
K <sub>f</sub>	Freundlich isotherm constant (mg/g)
K <sub>L</sub>	Langmuir isotherm constant (L/mg)
K <sub>T</sub>	Equilibrium binding constant of Temkin isotherm model (L/g)
M	Mass of adsorbent (g)
n	Adsorption intensity
q <sub>e</sub>	Adsorption capacity (mg/g)
q <sub>s</sub>	D-R monolayer adsorption capacity (mg/g)
q <sub>t</sub>	Uptake of H <sub>2</sub> S at time t (mg/g)
Q <sub>max</sub>	Maximum monolayer coverage uptake (mg/g)
R	Universal Gas constant (8.314 J/mole.K)
R <sup>2</sup>	Correlation coefficient
R <sub>L</sub>	Equilibrium parameter (unitless)
T	Temperature (K)
V	Volume of H <sub>2</sub> S solution (L)
ΔH	Enthalpy (KJ/mol)
ΔS	Entropy (J/mol.K)

## LIST OF ABBREVIATIONS

ACCNS	Activated carbon derived from coconut shell
ACPKS	Activated carbon derived from palm kernel shell
ACs	Activated carbons
ACWSD	Activated carbon derived from wood saw dust
ATSDR	Agency for toxic substances and disease registry
ANOVA	Analysis of variance
BET	Brunauer, Emmet and Teller
Ca-ACCNS	Calcium impregnated activated carbon of coconut shell
Ca-ACPKS	Calcium impregnated activated carbon of palm kernel shell
Ca-ACWSD	Calcium impregnated activated carbon of wood saw dust
CCD	Central Composite Design
CNS	Coconut shell
COD	Chemical oxygen demand
DOE	Design of expert
EPA	Environmental Protection Agency
ES	Egg shell
EDX	Energy-dispersive X-ray spectroscopy
FTIR	Fourier transform infrared spectroscopy
FDA	Food and Drug Administration
FCC	Fluidized Catalytic Crackers
H <sub>2</sub> S	Hydrogen sulfide
HS <sup>-</sup>	Hydrosulfide ion
HDS	Hydro desulfurization unit
IACs	Impregnated activated carbons
KOH	Potassium hydroxide
LPG	Liquefied petroleum gases



NG	Natural gas
NH <sub>3</sub>	Ammonia
NISDWR	US National Interim Secondary Drinking Water Regulations
NIOSH	National Institute of Occupational Safety and Health
Na <sub>2</sub> S.9H <sub>2</sub> O	Sodium sulfide nonahydrate
OSHA	Occupational Safety and Health Administration
PKS	Palm kernel shell
POME	Palm oil mill effluent
RSC	Refinery sulfidic spent caustic
RE	Removal efficiency
RFD	Reference dose
RFC	Reference concentration
RSM	Response Surface Methodology
S <sup>2-</sup>	Sulfide
S	Sulfur
SEM	Scanning Electron Microscopy
SRB	Sulfate reducing bacteria
STP	Standard temperature and pressure
TGA	Thermogravimetric analysis
WES	Wastes of Egg shell
WSD	Wood saw dust
XPS	X-ray photoelectron spectroscopy
XRD	X-Ray Diffraction

## CHAPTER 1

### INTRODUCTION

#### 1.1 Study Background

The activities of downstream petroleum processing such as catalytic hydrocracking and refining of different crude-oil fractions often result in the discharges of huge amount of toxic and inorganic compounds of nitrogen and sulfide (in the form of ammonia ( $\text{NH}_3$ ) and hydrogen sulfide ( $\text{H}_2\text{S}$ ), respectively) into water bodies. In a petroleum refinery process, waste water (sour water) is generated during the start-up/cooling process. Purged water can be generated as well from hydro-desulphurization units (HDS), Liquefied Petroleum Gases (LPG), Fluidized Catalytic Crackers (FCC), and hydrocrackers units. In addition, Natural Gas (NG) and Liquefied Petroleum Gas (LPG) refining plants generate spent caustics containing high levels of sulfide compounds (El-Naas et al., 2009; Coelho et al., 2006). The refinery sulfidic spent caustic (RSC) is generated during the absorption process of sulfide compounds such as thiols and hydrogen sulfide ( $\text{H}_2\text{S}$ ) in caustic scrubber (Hariz et al., 2013).

Moreover,  $\text{H}_2\text{S}$  is formed naturally in many gas wells due to the desulfurization of petroleum stocks where the sulfur compounds are reduced to  $\text{H}_2\text{S}$  (aq) through refining process such as distillation, wash system, water from knockouts and amine systems (Zaman and Chakma, 1995; Reverberi et al., 2016). There are three forms of  $\text{H}_2\text{S}$  in waste water, namely sulfide ions ( $\text{S}^{2-}$ ), hydrosulfide ions ( $\text{HS}^-$ ) and hydrogen sulfide ( $\text{H}_2\text{S}$  (aq)) (Kalapala, 2014; Jacukowicz et al., 2015; Edathil et al., 2017).  $\text{H}_2\text{S}$  (aq) is one of the most toxic pollutants which causes environmental and economic damages (Vollertsen et al., 2008; Xu et al., 2017). The odour threshold for human has been reported to be 0.13 ppm and it is very harmful to health at concentrations greater than 13 ppm (Boumniel et al., 2016). Health issues such as respiratory problems that lead to difficulties in breathing are some of the effects of untreated  $\text{H}_2\text{S}$  (aq)-contaminated waste water.  $\text{H}_2\text{S}$  (aq) test can be



detected in water with concentration as low as 0.05 mg/L. The acceptable limit in waste water is 0.5 mg/L as recommended by Department of Environment (DOE), Malaysia, standard (A). Besides, process facilities are easily corroded due to the presence of dissolved  $\text{H}_2\text{S}$  (aq) in process water found in petroleum refinery. In addition, poisonings of many catalysts occur even at low  $\text{H}_2\text{S}$  (aq) concentration because of sulfur is present during the shift reaction, it attacks the catalyst surface and gets oxidized, thereby poisoning the catalyst (Pourzolfaghar et al., 2014). The environmental and economic damages stemming from the releases of these inorganic compounds of sulfur (major water pollutant) have attracted the attentions of many researchers.

Since the past decades, several measures have been proposed to manage the discharge of refinery waste water in order to protect the environment and to ensure human well-being. Several factors such as availability of space for construction of treatment facilities, reliability of process equipment as well as capital and operating costs are usually considered in the selection of waste water treatment process (Estrada et al., 2010). The main aim is to find a cost-effective and environmental friendly way to deal with these toxic pollutants. Several technological options such as stripping (Almasvandi et al., 2016), catalyst oxidation (Nguyen and Bandosz, 2005), biofiltration (Lestari et al., 2016), wet scrubbing (absorption) (Lien et al., 2014), and adsorption (Kazmierczak et al., 2015; Xu et al., 2014) have been explored to treat  $\text{H}_2\text{S}$  contaminated waste water.

Techniques such as the biological and chemical cleanings as well as the physicochemical sorption methods have been used for treating  $\text{H}_2\text{S}$ -contaminated waste water (Siefers et al., 2010). Although these techniques are somewhat efficient, they incur high operating cost and they are not environmentally friendly due to it is difficult to control during the removal of pollutant. Thus, some of undesired by-product might be occurred (White, 2010). Furthermore, the biological method is relatively slow and sensitive to operating conditions and contamination level (Lestari et al., 2016). Similarly, chemical treatment method is not preferred because the reactor vessels can be easily corroded due the presence of  $\text{H}_2\text{S}$  (aq). These drawbacks would lead to high operating costs (Couvert et al., 2008).

The removal of  $\text{H}_2\text{S}$  from waste water via adsorption is a promising method because this process is environmentally friendly due to can be easily operated and control during the adsorption process and it does not incur high operating cost (Bagreev, 2001;

Edathil et al., 2017). Adsorption process is straight forward and it is easy to maintain (Foo and Hameed, 2010; Jacukowicz et al., 2015). However, the treatment of waste water using adsorption requires the use of high quality adsorbent. Therefore, several materials such as silica and graphene oxide, alumina, zeolites and activated carbons have been extensively investigated for waste water treatment (Bae et al., 2009; Esmaeili et al., 2014; Sitthikhankaew et al., 2014; Ozekmekci et al., 2015). Among these adsorbents, activated carbon is the most popular adsorbent in waste water treatment because its surface properties can be easily modified using various physical and chemical methods. However, the use of activated carbon for waste water treatment is often limited by high preparation cost of raw material (Foo and Hameed, 2010). Hence, recent research works have been concentrating on developing low-cost adsorbents for treating waste water.

Raw materials such as those obtained from agricultural wastes can be employed to prepare low-cost activated carbon. These raw materials are abundant, inexpensive, rich in organic content and low in inorganic content. Hence, these raw materials can be easily activated (Bansaland Goyal, 2005). Low-cost adsorbents prepared from agricultural wastes are environmental friendly. Several types of low-cost adsorbents have been prepared by using agricultural products such as sugar canes (Rufford et al., 2010), nut shells (Yang and Qiu, 2010), fruit stones (Kazemipour et al., 2008), coconut shells (Yang et al., 2010), macadamia nut shells (Martins et al., 2015), fibres of oil palm empty fruit bunches (Farma et al., 2013), rice straws (Gao et al., 2011), sun flower straws (Foo and Hameed, 2011), cotton stalks (Deng et al., 2010; Chen et al., 2013), palm kernel shells (Jalani et al., 2016), wood saw dusts (Foo and Hameed, 2012) and date stones (Sekirifa et al., 2013).

All these adsorbents have shown different degree of performance in removing toxic pollutants from waste water. However, studies have shown that the performance of these adsorbents can further be enhanced by modifying their surface properties (Guijarro et al., 2011). Various studies have been conducted to enhance the surface chemistry of activated carbons (ACs) via impregnation. Specifically, in order to enhance the adsorption capacity, it is necessary to study the structure of raw materials and the proper activation agent prior to enhancing the surface chemistry of adsorbents. Different impregnated agents have been used to enhance the adsorption capacity of ACs in H<sub>2</sub>S (g) removal such as metal hydroxides and oxides (Li et al., 2008; Bashkova et al., 2009; Cui

et al., 2009), carbonates (Chen et al., 2010), and urea/melamine (Seredych and Bandosz, 2008). ACs can be also impregnated with metal oxides like graphite oxide (Mabayoje et al., 2012; Seredych et al., 2011), and Cu (II) (Liu et al., 2017).

Furthermore, studies on adsorption of H<sub>2</sub>S (g) using ACs derived from various sources such as oil palm shell (Guo et al., 2007), coffee industry waste materials (Kante et al., 2012), agricultural/forestry wastes (Shang et al., 2016) and petroleum coke (Mochizuki et al., 2016) have been reported. Many researchers have performed the removal of H<sub>2</sub>S (aq) using different materials such as carbonated steel slag (Asaoka et al., 2013), cupric oxide (CuO) and zinc oxide (ZnO) (Haimour et al., 2005), crushed oyster shell (Asaoka et al., 2009), Fe<sup>2+</sup> with Ca(OH)<sub>2</sub> (Altaş & Büyükgüngör, 2008) and ACs prepared from empty fruit bunch (EFB) (Amosa, 2016).

## 1.2 Problem Statement

The removal of H<sub>2</sub>S from waste stream (liquid or gaseous) is considered as one of the major problem in energy industries such as natural gas, liquefied petroleum gas, tail gas, fuel cells, transportation gases (e.g. diesel, gasoline), palm oil mill and jet fuels (Ozekmekci et al., 2015; Almasvandi et al., 2016). The traces of small concentrations of H<sub>2</sub>S (aq) in waste water could be detrimental to human and aquatic lives.

Many researchers have reported that humidity can enhance the removal efficiency (RE) of H<sub>2</sub>S (g) due to the dissociation of H<sub>2</sub>S (g) into its ionic form during the adsorption process (Xu et al., 2014; Sitthikhankaew et al., 2014). However, studies related to the removal of H<sub>2</sub>S (aq) from solution are limited. The main concern in treating contaminated waste water is to find an adsorbent that is easily available and efficient. To this end, activated carbons (ACs) have been employed for treating H<sub>2</sub>S (aq)-contaminated waste water because their physical and chemical properties can be easily modified. However, adsorption of pollutants using commercial activated carbon is costly and it is beyond the reach of most industries (Dabrowski et al., 2005 ; Ahmed et al., 2010). Hence, activated carbon derived from wastes is able to reduce the handling costs of these wastes.

By using steam activation (pyrolysis), Amosa (2015) obtained the activated carbon from empty fruit bunch (EFB) to remove H<sub>2</sub>S (aq) (at low concentration level 0.8 ppm) from bio-treated POME and the removal efficiency was found to be 90%. However, related studies for H<sub>2</sub>S (aq) at high concentration were not reported. Moreover, the use of

optimization tools for H<sub>2</sub>S (aq) removal from waste water with ACs and IACs using design of expert (DOE) has not been reported. Furthermore, there are many agricultural wastes such as coconut shell (CNS), palm kernel shell (PKS) and wood sawdust (WSD) that can be used to treat H<sub>2</sub>S (aq)-contaminated waste water. These agriculture wastes are cheap and abundance in Malaysia. The adsorption capacity of activated carbon can therefore be improved by impregnating using calcium. One of the good sources of calcium carbonate is egg shells (poultry waste) which can be easily obtained. So far, study detailing on the modification of surface properties of adsorbents using calcium carbonates extracted from egg shells for H<sub>2</sub>S (aq) removal has not been reported. Therefore, this research aims to bridge the knowledge gap by investigating the adsorption capacities and removal efficiencies of locally sourced adsorbents obtained from coconut shell, palm kernel shell and wood saw dust in removing H<sub>2</sub>S (aq) from refinery waste water.

### **1.3 Research Objectives**

The overall objective of this study is to investigate the removal of H<sub>2</sub>S (aq) from petroleum refinery waste water using locally-sourced adsorbents obtained from agricultural and industrial wastes. The following specific objectives will be used in achieving the overall objective.

- i. To prepare the activated carbons (ACs) and Impregnated Activated Carbons (IACs) from coconut shell (CNS), palm kernel shell (PKS) and wood saw dust (WSD) wastes.
- ii. To characterize ACs and IACs in the form of the chemical structure and physical properties to select the best adsorbent in terms of removal efficiency of H<sub>2</sub>S (aq) from simulated waste water.
- iii. To optimize the synthesis and operating conditions of selected adsorbent during the removal of H<sub>2</sub>S (aq) from simulated waste water using Response Surface Methodology (RSM).
- iv. To determine the mechanism of adsorption process through thermodynamic, isotherms and kinetics models for the selected adsorbent.

## 1.4 Scope of Study

The following scopes were used in achieving the above research objectives:

### Objective 1:

Three types of agriculture waste materials, Coconut shell (CNS), palm kernel shell (PKS) and Wood sawdust (WSD) will be used to prepare activated carbons (ACs). The ACs obtained from three different agriculture wastes was modified and impregnated with calcium (Ca) extracted from egg shells to produce impregnated activated carbon (IACs).

### Objective 2:

The chemical and physical properties of ACs and IACs will be investigated by characterizing the original and exhausted adsorbents using several analytical approaches such as Scanning electron microscope (SEM), Energy-dispersive X-ray spectroscopy (EDX), Brunauer–Emmett–Teller (BET), Fourier transform infrared spectroscopy (FTIR), Thermogravimetric analysis (TGA), pH of the adsorbent surface, X-ray powder diffraction (XRD) and X-ray Photoelectron Spectroscopy (XPS). The removal efficiency of ACs and IACs in removing  $\text{H}_2\text{S}$  (aq) from simulated waste water will be investigated and the adsorbent efficiencies of ACs and IACs adsorbents in removing  $\text{H}_2\text{S}$  (aq) will be compared. The condition of used include: Initial concentration of  $\text{H}_2\text{S}$  (aq) (500 mg/L), pH of solution (7), dosage (1 mg/L), agitation speed (150 rpm), and contact time (660 minutes).

### Objective 3:

The optimization of preparation conditions of selected adsorbent in removing  $\text{H}_2\text{S}$  (aq) from simulated waste water will be conducted by applying the response surface methodology (RSM). The optimization of operating conditions of selected adsorbent in removing  $\text{H}_2\text{S}$  (aq) from real waste water will be investigated by using response surface methodology (RSM). The range of value used during the optimization preparation conditions include: calcination temperature (800-1000 °C), calcium concentration (25-75 %v), and calcination contact time (30-90 min). In addition, the range of value used during the optimization of operating conditions include: initial  $\text{H}_2\text{S}$  (aq) concentration (300-700 mg/L), adsorption contact time (420-660 minutes), and adsorbent dosage (0.75- 1 g/L).

#### Objective 4:

The four isotherm adsorption models, namely Langmuir, Freundlich, Temkin, and Dubinin models and the thermodynamic will be applied for the selected adsorbent. The three adsorption kinetic models namely Pseudo-first order, Pseudo-second order, and Intra-particle diffusion models will be used for the selected adsorbent.

### 1.5 Significance of Study

The following are the significant of this study:

- i.  $\text{H}_2\text{S}$  (aq) is a very toxic and hazardous pollutant which is released from the petroleum refinery industries as contaminant. Finding a proper way to remove  $\text{H}_2\text{S}$  (aq) from waste water is an important task.
- ii. Adsorption process using adsorbents derived from local agricultural wastes is simple, cost-effective and less hazardous compared to chemical treatment method.
- iii. Applying an effective method to investigate the optimum removal efficiency of  $\text{H}_2\text{S}$  (aq) by using the design of expert approach.
- iv. The use of locally sourced materials such as (CNS, PKS, and WSD) in removing  $\text{H}_2\text{S}$  (aq) from petroleum refinery waste water is able to address problems associated with environmental impact, human health, safety and cost.
- v. This work is significant in terms of revealing the mechanisms of  $\text{H}_2\text{S}$  (aq) removal in waste water using adsorption method.
- vi. This research will act as a blueprint for the removal of  $\text{H}_2\text{S}$  (aq) laden waste water at high concentration. The optimization study on the other hand provided the optimum condition at which highly concentrated  $\text{H}_2\text{S}$  (aq) laden waste water can be treated.



## 1.6 Thesis Layout

This thesis is organized into five chapters. Chapter 1 explores the general introduction and the main goals of the current work. The research objectives, scope of the study and significant of the research are given as well.

Chapter 2 discusses the literatures related to the current work such as sources of H<sub>2</sub>S, toxicity, regulation recommendations, and the cleaning technology of H<sub>2</sub>S. Previous modelling strategies will be reported in this chapter as well.

Chapter 3 presents the methods and procedures performed to remove H<sub>2</sub>S (aq) from simulated waste water. The research methodology consists of six parts, i.e. descriptions of materials and chemicals employed, flow chart of the methodology, activation and impregnation processes of activated carbons (ACs) and impregnated activated carbons (IACs), preliminary studies on operating conditions for the removal of H<sub>2</sub>S (aq) from simulated water, characterization of ACs and IACs and the experimental procedures.

Chapter 4 presents the research findings. The preliminary study is firstly discussed, followed by the characterization, optimization and modelling of selected adsorbent. The reaction mechanism is also discussed in this chapter.

Chapter 5 concludes the current work and offers some recommendations for future work. The current research contributions are highlighted as well.

## CHAPTER 2

### LITERATURE REVIEW

#### 2.1 Introduction

This chapter entails the review of previous studies with the aim of identifying knowledge gap, novelty and their contributions. Under this chapter the sources of hydrogen sulfide ( $H_2S$ ) (liquid and gas form), toxicity, regulations, current removal technologies, various impregnated activated carbon, optimization studies, (response surface methodology), adsorption equilibrium, batch kinetic, isotherm and thermodynamic studies, were succinctly discussed.

#### 2.2 Sources and Discharge of $H_2S$

The discharged of  $H_2S$  is indirectly reliant on human activity. Thus, the natural gas processing, paper production, petroleum refining, coal gasification, petrochemical manufacturing are considered the central elements of anthropogenic activities. The discharged of  $H_2S$  in different sources of waste water are listed in Table 2.1.

Table 2.1 Different sources of  $H_2S$  (g)

Sources	Concentration of $H_2S$ (g) (ppm)	Reference
Petroleum refining process	-	Gao et al. (2012)
Sulfide reduced bacteria (SRB)	12000	Lee et al. (2006)
Volcanoes, hot springs and geothermal sources	-	Skrtic (2006)
Sewer network	54	Zhang et al. (2008)
Coal seams	500	Liu et al. (2012)

Most chemical plant releases  $H_2S$  (aq) as a by-product of sulfide within the range of 58 to 110 million tons of sulfur/year. Whereas it is produced from black sea around 30



to 170 million tons of sulfur/year. Moreover, above 60 million tons per year of toxic H<sub>2</sub>S is released from hydro-processing of petroleum, coal and minerals (Startsev et al., 2013).

Furthermore, H<sub>2</sub>S is found also in confined spaces of waste treatment systems such as landfills, digesters, and waste water collection systems. Natural sources such as volcano eruptions, thermal springs and bogs are other sources of sulfide discharge (D'Alessandro et al., 2008). Moreover, activities such as the decompositions of animals and dead plants in wet conditions with limited oxygen (e.g. swamps) produce H<sub>2</sub>S (Skrtic, 2006). Sulfate reducing bacteria (SRB) is considered as the main contributor to H<sub>2</sub>S gas emission when it is consumed and converted to sulfate (SO<sub>4</sub><sup>-2</sup>) under anaerobic conditions in landfills (Lee et al., 2006; Ko JH et al., 2015).

### **2.2.1 Petroleum Refinery Waste Water**

In the Petroleum refinery process a large volume of water is used-up in the process of getting useful product from crude oil. Typically, water is used in different units for generating the steam with many processes relying on the steam as a separating medium in distillation and hydrodesulphurization units. Figure 2.1 shows a schematic example of the typical water balance in a refinery. This water is used in different units. Mostly, it is used for producing the steam. Moreover, leakages and spills emanating from equipment during shutdown or start-up of equipment, condensate from steam-stripping operations, and waste water from storage tanks are considered as the major sources of these wastes (EcA, 2010).

It is thereafter condensed as aqueous phase and isolated as sour water. As the steam reduces in the existence of hydrocarbons which comprises the hydrocarbons comprising hydrogen sulfide (H<sub>2</sub>S) and ammonia (NH<sub>3</sub>) are typically absorbed into water that need treatment (EcA, 2010; Addington et al., 2011). The pH of sour water is elevated to 12, as temporary solution, to decrease the odour and corrosion effect until it moved to waste water treatment plant (striping). In addition, waste water in a refinery is created by strippers which use straight steam injection as a stripping medium (EcA, 2010). Table 2.2 shows the composition of sulfide in selected petroleum refinery effluents. Van Hamme et al. (2003) reported that gas streams are first scrubbed with an aqueous washing liquid, with dissolution of the sulfur components into an aqueous phase as seen in Equation 2.1) and (2.2).

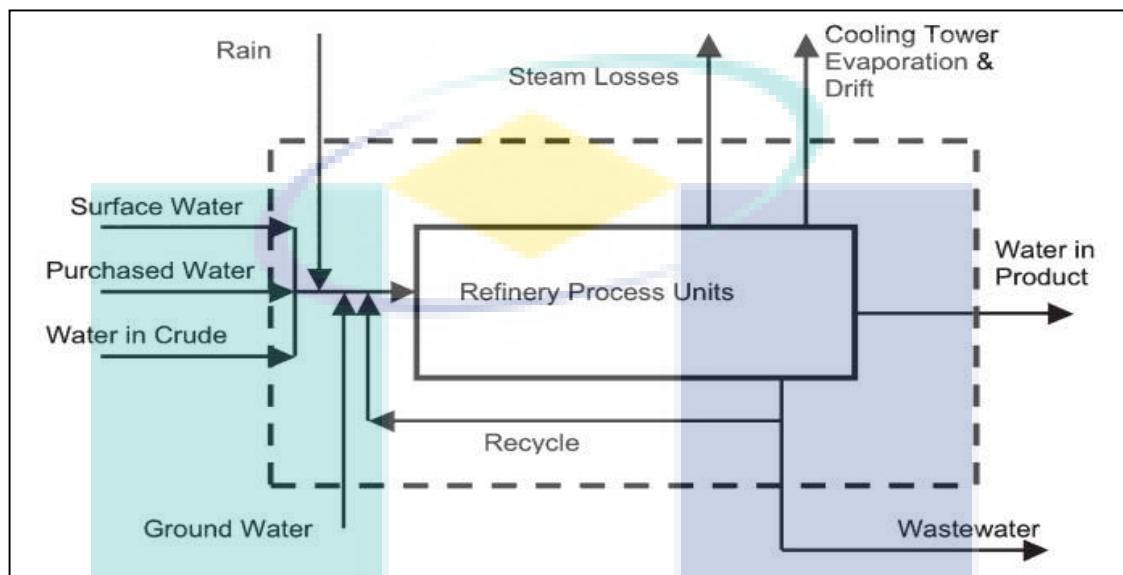


Figure 2.1 A schematic example of the typical water balance in a refinery

Source: EcA, (2010).

Table 2.2 Typical composition in selected petroleum refinery effluents

pH	Sulfide concentration (mg/L)	COD (mg/L)	Suspended solid (mg/L)	References
6.6	887	596	120	El-Naas et al. (2009)
8.0–8.2	15–23	850–1020	--	Coelho et al. (2006)
6.5–7.5	--	170–180	420–650	Saien and Nejati (2007)
8.44	22	216	--	Altas and Büyükgüngör (2008)
6.5–8.5	17	800	100	Demirci et al. (1997)
7–9	--	300–600	150	Ma et al. (2009)

### 2.2.2 Hydrogen Sulfide in Waste Water

Hydrogen sulfide ( $\text{H}_2\text{S}$ ) is very hazardous and a dangerous material (Boumniel et al., 2016). It causes respiratory problems, safety problems posed by its highly flammable nature as well as economic problems arising from corrosion of metals (Ozekmekci et al., 2015). Moreover, a part from metal corrosion due to  $\text{H}_2\text{S}$ , concrete surface would be corroded as well due to the gradual formation of sulfuric acid and

eventually causes damage on the sewer (Vollertsen et al., 2008). According to the Environmental Protection Agency (EPA), concrete waste water pipe corrodes (due to  $\text{H}_2\text{S}$  (aq)) at a rate of 3.6 mm/year. The rate of concrete corrosion in sewer pipes is 2.5–10 mm/year based on the data from 34 cities (US Environmental Protection Agency, 1991). Replacement of those corroded pipelines would incur a huge cost (Zhang et al., 2008). For instance, in Los Angeles, the cost incurred for the repair of these corroded sewer pipelines is ~\$400 million (Sydney et al., 1996). In Flanders (Belgium), approximately 10% of the total cost for waste water treatment is spent to replace the pipelines, amounting to ~€5 million per year (Vincke et al., 2002). In Germany, about €100 billion per annum is spent on the restoration of damaged sewer systems (Kaempfer and Berndt, 1998). Processing crude oil into useful products such as kerosene and gasoline was achieved by the numerous refinery configurations. During these processes, the petroleum waste water was produced in the units like Hydro-cracking, Hydro-skimmer flare, Hydro-cracker flare, Hydro-skimming, desalter and sour water (Aljuboury et al., 2017). They have reviewed the treatment of petroleum waste water by conventional and new technologies. Moreover, a treatment technologies for petroleum refinery effluents were reviewed by Diyauddien et al. (2011). Ma et al. (2009) studied the application of bioaugmentation to improve the activated sludge for treating petrochemical waste water. Table 2.3 shows concentration of  $\text{H}_2\text{S}$  and  $\text{S}^{2-}$  on different kind of waste water. It can be seen that tannery waste water discharged higher concentration of sulfide compared with another types. Moreover, concentration of  $\text{H}_2\text{S}$  (aq) is lower in black sea.

Table 2.3 Concentration of  $\text{H}_2\text{S}$  and  $\text{S}^{2-}$  on different kind of waste water

Source	Concentration (mg/L)	Forms	References
Black Sea	9.5	$\text{H}_2\text{S}$	Baykara et al. (2007)
Waste water, Kuwait	18 - 25	$\text{H}_2\text{S}$	Tomar & Mamta (1994)
Real spring water	0.06–22	$\text{H}_2\text{S}$	Čmelík et al. (2010)
Waste water, Brazil	5.59	$\text{H}_2\text{S}$	Santos et al. (2009)
Tannery waste water	250 - 525	$\text{S}^{2-}$	Wiemann et al. (1998)
Waste water paper mill	35-55	$\text{S}^{2-}$	Dutta et al. (2010)

### 2.2.2.1 Effect of pH on Hydrogen Sulfide Forms

The pH has a noticeable impact on  $\text{H}_2\text{S}$  forms.  $\text{H}_2\text{S}$  exists in three forms in aqueous systems, such as Hydrogen sulfide ( $\text{H}_2\text{S}$  (aq)), bisulfide ion ( $\text{HS}^-$ ), and sulfide ion ( $\text{S}^{2-}$ ).  $\text{H}_2\text{S}$  is a weak acid. It presents in the reactive molecular form of  $\text{H}_2\text{S}$  (aq) at low

the pH value (Kalapala, 2014; Jacukowicz et al., 2015) according to the following equations:



It can be seen from Figure 2.2 that the pH ranging from 8 to 11, the bisulfide (HS<sup>-</sup>) is the prevalent form and it is the most reactive ion in the free radical chain reaction. Below pH 7, H<sub>2</sub>S (aq) is prevalent. At pH 7, the reduced sulfur species in aqueous solution is equally separated between the dissolved bisulfide (HS<sup>-</sup>) and the hydrogen sulfide (H<sub>2</sub>S (aq)). Sulfide (S<sup>2-</sup>) dominates at pH >11 (Thompson et al., 1995).

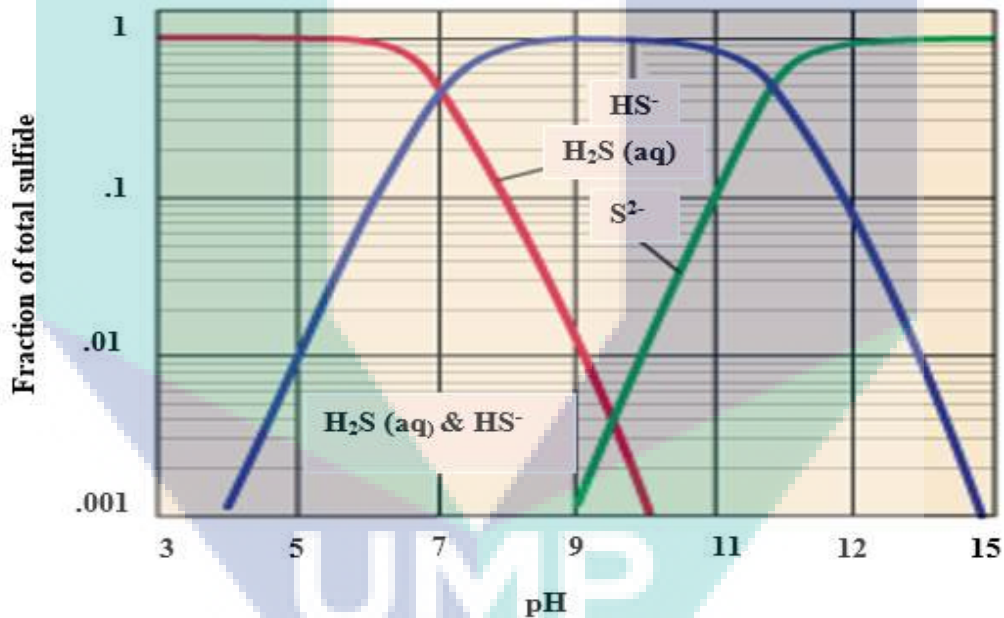


Figure 2.2 Distribution of three sulfide species in water

Source: Thompson et al. (1995).

### 2.2.2.2 Toxicity of H<sub>2</sub>S

The concentration of H<sub>2</sub>S (aq) in ground water is a significant problem in various areas. The presence of H<sub>2</sub>S (aq) in water is hazardous due to the ability of human to detect even at concentration as low (0.003-0.2 ppm). Therefore, a high degree of treatment is needed to render the water drinkable (EPA, 2003). Drinking water contaminated with

sulfide can be fatal at higher dosage (10-15g). Ingestion of sulfides through drinking water can result in stomach discomfort, nausea and vomiting (Edwards et al., 2011). In addition,  $\text{H}_2\text{S}$  (aq) in blood is rapidly oxidized by molecular oxygen and thus reduces the oxidation power of haemoglobin. Unoxidized  $\text{H}_2\text{S}$  (aq) can act upon the central nervous system and cause either paralysis or respiratory failure (Edwards et al., 2011). It can be detected by smell at a level of  $11\ \mu\text{g m}^{-3}$ , it numbs a person's sense of smell at a level of  $140\ \text{mg m}^{-3}$  and above  $700\ \text{mg m}^{-3}$  inhalation can very quickly be fatal (Selene and Chou, 2003). It is, therefore, desirable to have a very low concentration of  $\text{H}_2\text{S}$  in water because of its high toxicity to animals and humans and corrosively problems.

$\text{H}_2\text{S}$  (g) is a harmful and putrid gaseous compound, detectable by human nose at a low concentration level of 0.5 ppb (Skrtic, 2006). Other adverse health effect of  $\text{H}_2\text{S}$  (g) include coma, irritation to the eyes and respiratory system. Excessive exposure to  $\text{H}_2\text{S}$  (g) might cause both chronic and acute ramifications as reported by Lambert et al., (2006). According to the recommendation made by Agency for Toxic Substances and Disease Registry (ATSDR), the minimum  $\text{H}_2\text{S}$  inhalation risk level is 0.02 ppm. The concentration of  $\text{H}_2\text{S}$  equals or greater than 500-1000 ppm might threaten human life and lead to imminent impairment on the human physique (Wiheeb et al., 2013). The Occupational Safety and Health Administration (OSHA) has therefore regulated the exposure limit of 20 ppm for general industrial workday to safeguard the employees health (Kazmierczak et al., 2015). The maximum level of 50 ppm is permissible for a maximum duration of 10 minutes. Moreover,  $\text{H}_2\text{S}$  has been known to primarily target the neural system and major organs such as liver and kidney (Guidotti, 1994). Exposure to higher level of  $\text{H}_2\text{S}$  (g) can cause death (Hendrickson et al., 2004). Therefore, due to its acute and chronic toxicity, an oral reference dose (RFD) of 0.003 mg/kg/day and an inhalation reference concentration (RFC) of  $0.001\ \text{mg/m}^3$  have been recommended by the EPA. It is worth to mention here that  $\text{H}_2\text{S}$  (g) concentration above 700 ppm can lead to loss of consciousness, while sudden loss of consciousness/death happens if the concentration ranges from 1000 to 2000 ppm is detected (Kazmierczak et al., 2015). Janoszka et al. (2013) reported in U.S the maximum admissible concentration is 10 ppm and the maximum admissible ceiling concentration is 20 ppm. Lambert et al. (2006) notified the eye irritation as the first symptom that manifest at low  $\text{H}_2\text{S}$  (g) concentration. On the other hand, enzymes in the body could detoxify  $\text{H}_2\text{S}$  through oxidation to form the safe compound such as sulfate. The human body is therefore able to tolerate low level of

H<sub>2</sub>S (g) (Ramasamy et al., 2006). H<sub>2</sub>S (g) is detrimental to the human nervous system and respiratory tract from which human can be exposed to it via inhalation route and drinking water. The standard concentration level of H<sub>2</sub>S (aq) in drinking water is 0.05 mg/L as reported by the US National Interim Secondary Drinking Water Regulations (NISDWR). There are wide ranges of health effects according to the duration of workers' exposure to H<sub>2</sub>S (g) and the concentration of this fatal gas. Case reports, occupational studies, and community studies are the sources of information on the toxicity of H<sub>2</sub>S (g) in humans. For the concentration of H<sub>2</sub>S (g) of 4000 ppm, a several fatal cases of H<sub>2</sub>S (g) poisoning have been found in Talvivaara, Finland (Heinonen, 2012) and Japan (Kage et al., 2004; Asakura, 2015).

### 2.2.2.3 Safety Regulations and Recommendations

The Occupational Safety and Health Administration (OSHA), Food and Drug Administration (FDA), and Environmental Protection Agency (EPA) are the agencies that implemented rules, recommendations and laws. The Nova Scotia Department of Health sets the maximum allowable concentration of H<sub>2</sub>S (aq) in drinking water at 0.05 ppm (NSDH, 2009). According to Malaysia's Environmental Law, the effluent of waste water discharge standards A and B is shows in Table 2.4. It shows the guidelines for Environmental Quality (Sewage and Industrial Effluents) regulations 2009, Malaysia: It selected parameter limits of effluent of Standards A and B (Department of Environment, DOE, Malaysia) (Tumin et al., 2008).

Table 2.4 Selected parameter limits of effluent of Standards A and B (Department of Environment, DOE, Malaysia 2009)

Parameters	Unit	Standard A	Standard B
Temperature	°C	40	40
pH Value		6.0 – 9.0	5.5 – 9.0
BOD at 20 C	mg/L	20	50
Sulfide	mg/L	0.5	0.5
COD	mg/L	80	200
Suspended Solids	mg/L	50	100

Source: Tumin et al. (2008).

Moreover, the Agency for Toxic Substances and National Institute for Disease Registry (ATSDR), and Occupational Safety and Health (NIOSH) are also recommended some guideline for exposure to H<sub>2</sub>S as given in Table 2.5. Furthermore, The American Conference of Governmental Industrial Hygienists (ACGIH) is implemented and



recommended the level of exposure to H<sub>2</sub>S. For example, the ACGIH is recommended the H<sub>2</sub>S standard are 15 ppm for the Threshold Limit Value - short term exposure limit (TLV-STEL) and 10 ppm for the Threshold-Limit Value-Time Weighted Average (TLV-TWA). The TVL-TWA is the time-weighted average concentration to which workers can be routinely and consistently exposed over an 8 h workday and 40 h workweek without adverse effect. The TVL-STEL is the concentration to which workers can be exposed for short periods of time without suffering adverse health effects (Skrtic, 2006). In the 1970s, OSHA is started implemented standards for workers exposure to toxic materials. It has an occupational exposure limit of 10 parts per million (ppm) for 8 h exposure (Sen et al., 2008). It is important to note that OSHA standards apply only to workplaces and not to domestic situations or residences. Table 2.5 demonstrates some of regulations guidelines for exposure to H<sub>2</sub>S. Thus, Jacukowicz et al. (2015) reported that the sulfide concentration in waste water disposal to environment reservoirs has to be kept at a very low level (e.g. below 0.2 mg/L). In the US EPA has proposed a reduction of sulfur in gasoline from 30 ppm to 10 ppm by 2017 (Gupta et al., 2016). Human may experience discomfort on eyes if the H<sub>2</sub>S concentration is ranging between 10 and 20 ppm. Therefore, efforts leading to efficient H<sub>2</sub>S removal are indeed necessary due to its harmful effects on the environment and human beings if its emission is not properly monitored (Gupta et al., 2016).

Table 2.5 Guidelines for Occupational Exposure to H<sub>2</sub>S (g)

[H <sub>2</sub> S] (ppm)	Agency	Duration
0.1	AIHA	1 hour
10	OSHA	8hr/day, 40hr/week
10	ACGIH	TLV-TWA 8hr/day, 40hr/week
15	ACGIH	TVL-STEL
20	OSHA	Ceiling
27	EPA	1 hour
30	AIHA	1 hour
32	EPA	30 minutes
37	EPA	4 hours
41	EPA	10 minutes
50	OSHA	10 minutes ceiling
50	EPA	1 hour
76	EPA	30 minutes
100	AIHA	1 hour

Source: Skrtic (2006).

### 2.3 Current Removal Technologies for H<sub>2</sub>S

There are several techniques for removing H<sub>2</sub>S (aq) from water including aeration, ozonation, ion exchange, biological treatment and chemical oxidation and adsorption (Edwards et al., 2011). These technologies can be generally classified into biological, electrochemical, chemical, and physicochemical methods. This study therefore reviews different types of removal technologies of H<sub>2</sub>S from downstream as seen in Figure 2.3.

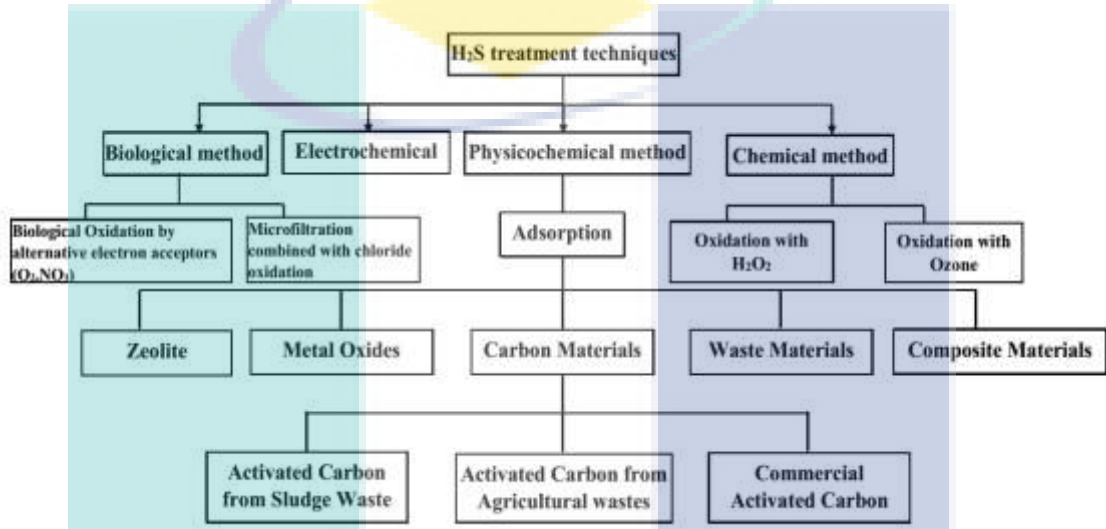


Figure 2.3 Cleaning technologies methods of H<sub>2</sub>S from down stream

Table 2.6 summarizes the method used for the removal of H<sub>2</sub>S (aq) from waste water and some of the inherent drawback. It can be seen that the adsorption process is widely used and does not incur high operation cost. Biological method is relatively slow and sensitive. Moreover, chemical and electrochemical methods are required a high energy and costly.

Table 2.6 Categories of Methods used for H<sub>2</sub>S (aq) removal

Methods	Materials	Advantage and disadvantage	References
Biological	Biotrickling filter	It is not completely removed the H <sub>2</sub> S concentration and slow.	Tsang et al. (2015)
Electrochemical	Pt/Ir and Ta/Ir coated titanium	Required a high energy and costly.	Pikaar et al. (2012)
Chemical	Fe <sup>+2</sup> and Fe <sup>+3</sup> ions	It is not completely removed H <sub>2</sub> S (aq) and caused technical problem.	Altaş and Büyüküngör (2008)
Physicochemical	Adsorption	It is environmentally friendly and it does not incur high operating cost, effective method and widely used.	Edathil et al. (2017)



### 2.3.1 Biological Treatment Method

Biological method was carried out using fixed-film bioreactor with carbon in order to convert dissolved  $H_2S$  (aq) to elemental sulfur as reported by Henshaw (2001). Thompson et al. (1995) investigated the effectiveness of using microfiltration and this could be used in combination with chloride oxidation for  $H_2S$  (aq) removal. Different biological processes have been employed by researchers such as biofilters (Rehman et al., 2010) and microorganisms supported on activated carbon (AC) (Kennedy et al., 2004). Despite the limitations of biofiltration, such as being sensitive to operating conditions/contamination and its relatively slow, it is still widely used for  $H_2S$  removal (Lestari et al., 2016).

The most common process for removing  $H_2S$  (g) in the biogas industry is the biological desulfurization. For instance, Ward et al. (2008), studied the biological desulfurization using bacteria *sulfobacter oxydans* present inside the digester. Approximately 2-5% of air is firstly injected into the raw biogas residing in the headspace of the digester to convert  $H_2S$  into elemental sulfur and sulfurous acid (via bacteria *Sulfobacter oxydans*).

Gadekar et al. (2006) reported that, biological oxidation of  $H_2S$  (aq) could take place at the sewer surfaces exposed to the sewer atmosphere. The aerobic and autotrophic *Thiobacillus* sp. growing on the moist surface can oxidize  $H_2S$  to sulfuric acid. On the other hand, Lestari et al (2016) investigated the removal of  $H_2S$  using salak fruit seeds packed in the bed reactor with sulfur oxidizing bacteria acting as biofilm with removal efficiency of 97.15%. Also, pure culture of various sulfide oxidizing bacteria such as *Thiobacillus*, *Pseudomonas* and *Xanthomonas* has the capacity to metabolize  $H_2S$  effectively due to its fast oxidation rate and low acid production in ACs (Ward et al., 2008; Gadekar et al., 2006; Rattanapan et al., 2010). Rattanapan et al. (2010) used the granular AC biofiltration to study the  $H_2S$  removal efficiency. Furthermore, the removal of  $H_2S$  in a biotrickling filter was studied by Tsang et al. (2015). The disadvantage of biological desulfurization methods is that it cannot completely removed the  $H_2S$ . Also, the presence of air increases the corrosion activity of biogas and the air must be removed if the natural gas pipeline is used (White, 2010).

Figure 2.4 illustrates chemical and biological for H<sub>2</sub>S (aq) emission control in sewer system modified. It shows the method of inhabitation and elimination of H<sub>2</sub>S form by using chemical and biological method for H<sub>2</sub>S emission control in sewer system. The figure is modified by De Lomas et al. (2006) and Zhanget al. (2008). Vaiopoulou et al. (2005) studied the removal of hydrogen sulfide from oil-refining waste water using autotrophic de-nitrification in a multi-stage treatment plant as an alternative flowchart for the biological method. Tong et al. (2013) used activated sludge process coupled with an immobilized biological filter to treat of heavy oil waste water. Shokrollahzadeh et al. (2008) studied the biodegradation potential and bacterial diversity of a petrochemical waste water treatment plant.

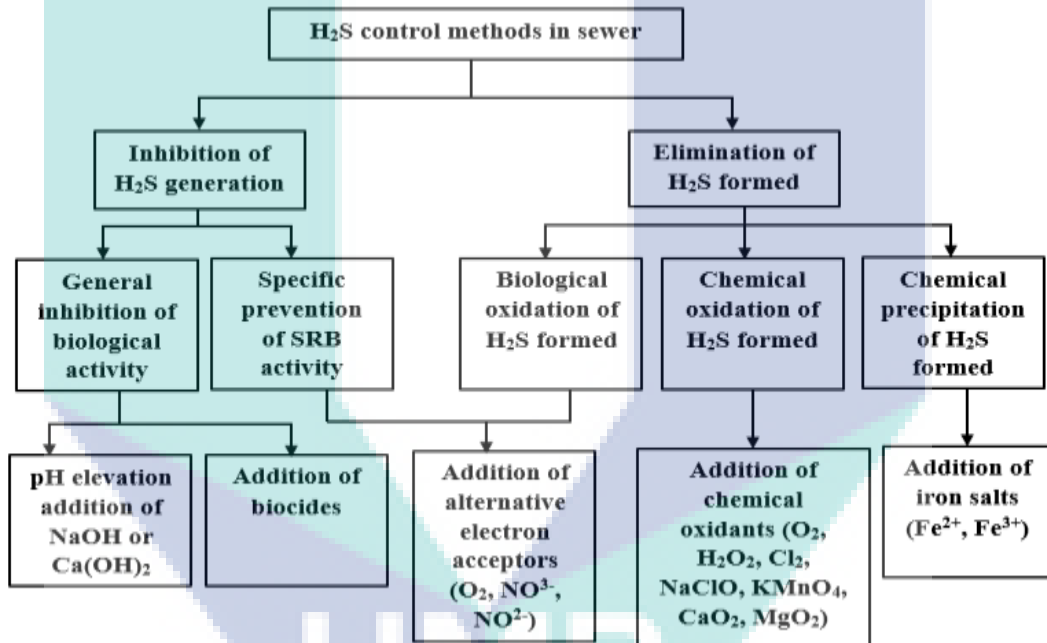


Figure 2.4 Chemical and biological process for H<sub>2</sub>S emission control in sewer system

Source: Zhanget al. (2008).

### 2.3.2 Electrochemical Methods

Electrochemical method can be used to remove H<sub>2</sub>S (aq) from aqueous solutions using a lab scale fuel cell. Dutta et al. (2008) reported that at ambient temperature and neutral pH conditions, sulfide was removed continuously for 2 months at a rate of 0.62 kg S/m<sup>3</sup>/d of net anodic compartment of 0.28 kg S/m<sup>3</sup>/d of total anodic compartment. The sulfur element was produced during the oxidation process and deposited on the anode,

while potassium ferricyanide was used as cathodic electron acceptor. In addition, the removal of sulfide from paper mill using the electrochemical method was studied by Dutta et al. (2010). The results found that the concentration of sulfide in the effluent was 44 mg/L and it was reduced to 8 mg/L. Moreover, Pikaar et al (2012) studied the electrochemical method which was effective to reduce the sulfide concentration to below normal level utilizing Pt/Ir and Ta/Ir coated titanium electrodes under the simulated sewer conditions during field trials. The results suggested that the electrochemical method could prevent sewer corrosion.

The electrochemical method is effective for removing low concentrations in domestic waste water. Recently, the electrochemical method was used to remove sulfide from spend caustic downstream waste water. Lin et al. (2016) tested the low-cost electrode materials such as stainless steel and carbon cloth. They have been used in anaerobic digestion for sulfide removal using electrochemical method. Complete removal of sulfide within 2 days on this electrode materials at 3 V.

### **2.3.3 Chemical Method**

The absorption process is considered as the main way to remove  $\text{H}_2\text{S}$  (aq) from mixture. However, absorption of  $\text{H}_2\text{S}$  (aq) from the solution by stripping process is not an effective way due to the odour released (Chaudhuri, 2004).  $\text{H}_2\text{S}$  could be removed using  $\text{Fe}^{+2}$  and  $\text{Fe}^{+3}$  ions, as well as by hydro oxidation method which involved the addition of solid oxidants such as magnesium peroxide ( $\text{MgO}_2$ ) (Altaş and Büyükgüngör, 2008; Chang et al., 2007). In addition, oxidation is a very popular chemical process involving oxidants such as hydrogen peroxide, oxygen, chlorine, hypochlorite, and potassium permanganate (Poulton et al., 2002). The removal of  $\text{H}_2\text{S}$  using alkaline was studied by Boumnijel et al. (2016). They have been analysed the absorption of  $\text{H}_2\text{S}$  in a chlorinated seawater solution under alkaline condition. Taheri et al. (2016) studied the simultaneous absorption of  $\text{H}_2\text{S}$  from a gas mixture using amine-based nanofluid in a wetted wall column. The results showed that  $\text{SiO}_2$ -ethylenediamine nanofluid has deteriorating effects on the  $\text{H}_2\text{S}$  absorption. Several industrial water-based techniques for removing  $\text{H}_2\text{S}$  (g) from the gas stream have been reviewed by Renee et al. (2012).  $\text{H}_2\text{S}$  absorption capabilities of silica and exfoliated GO in a bubble column were studied by Esmaili et al. (2014).

### 2.3.4 Physiochemical Sorption (Adsorption)

Adsorption is the process by which compounds in liquid or gas state are separated and adsorbed onto a solid surface. The materials have an extremely porous structure and large surface area could be designed to adsorb liquids or gases onto their surface by various mechanisms. Adsorption is a common process which employs physisorption and chemisorption processes for the cleansing of natural air and water, leading to the final removal of adsorbed material in the form of adsorbate. It is popular in pollutant removal due to its exceptional pollutant removal efficiency and its ease of operation. It has been widely applied in removing organic materials from aqueous media as it has a strong affinity for attaching organic substances even at low concentrations. The removal of H<sub>2</sub>S from gas phase by adsorption process has been studied by Lemos et al. (2012).

Chemisorption and physisorption adsorption processes are the main processes that enhanced the adsorption of H<sub>2</sub>S (aq) from downstream. The connection and bonding between the adsorbent surface and the adsorbate molecular could be either chemisorption (chemical adsorption) or physisorption (physical adsorption) (Thommes et al., 2015). Chemisorption and physisorption differ in the origins and magnitude of the interacting forces. In chemisorption, the binding energy is about 1 eV. Moreover, the equilibrium distance between the surface adsorbent and adsorbate is 1–3 Å. On the other hand, the binding energy of physisorption is below 0.25 eV, and the distance between the adsorbent surface and adsorbate is much higher than that in chemical adsorption about 3–10Å. As a result, physical adsorption is reversible (Feng et al.,2005). Table 2.7 shows the differences between physical adsorption and chemical adsorption. Moreover, physical adsorption is the process that occurred due to physical forces such as Van Der Waals forces which enforce the molecules to attach the surface of adsorbent. While, the chemical adsorption is the process that could make a strong interaction with the surface of adsorbent. During the adsorption process, heat is released as the molecules are attached to the surface of adsorbent which means it is an exothermic process.

Table 2.7 Differences between physical and chemical adsorption

	<b>Physisorption</b>	<b>Chemisorption</b>
Bonding Nature	Weak interaction through van der Waals forces.	Strong Chemical bond, with loss/gain or share of electrons
Bonding Strength	Potential well 0.25 eV or less	Potential well greater than 0.25 eV
Reversibility	Reversible	Irreversible
Number of Layers	Can be multi-layer	Normally monolayer
Heat	Exothermic	Exothermic or endothermic, depends on the reaction

Sources: Feng et al. (2005).

Researchers have investigated on the removal of gaseous H<sub>2</sub>S using different adsorbents such as ACs (Elsayed et al., 2009), alumina (Bae et al., 2009), silica (Belmabkhout et al., 2009) and zeolite (Alonso et al., 2010). Over the past three decades, adsorption technology by activated carbons (ACs) has been widely adopted in petrochemical industries, production of industrial gases as well as air and water purification (Zhou, 2005). ACs derived from carbonaceous wastes is easily available and it can be considered as an effective method to remove pollutants from water and air by adsorption. So, ACs are very attractive for purification of water (Foo and Hameed, 2011) and gases (Nowicki et al., 2013). Seemingly, the current research focussed mainly on finding the most cost-effective adsorbent of removing H<sub>2</sub>S (aq) from waste water. Waste materials, composite adsorbents, zeolite, metal oxide and activated carbons are the most common adsorbents that used for the removal of H<sub>2</sub>S contaminated waste water.

## 2.4 Adsorption of H<sub>2</sub>S

### 2.4.1 Adsorption of H<sub>2</sub>S Using Waste Materials

Many researchers have utilized waste materials as adsorbents to remove H<sub>2</sub>S (g) from waste water. For instance, Wanget al.(2013) have been used Fine Rubber Particle Media (FRPM) as an adsorbent to remove of H<sub>2</sub>S (g). They have found that the adsorption capacity was 0.12 mg H<sub>2</sub>S/g FRPM, which was very low due to the fact that naturally, FRPM particulate does not have enough surface area and possesses limited porosity in supporting a pure physical adsorption. Moreover, Pham et al. (2015) have been studied the calcium carbonate-based solid wastes for the treatment of H<sub>2</sub>S (g) from the gas phase.

In addition, the removal H<sub>2</sub>S (aq) from waste water using waste materials was reported by some researchers. Take for instance, Wang and Pei (2012) studied the

adsorption of H<sub>2</sub>S (aq) using ferric and alum water treatment residuals (FAR). They concluded that FARs have higher adsorption capacity at pH 7 rather than in those of higher pH (e.g. pH 8–10). Asaoka et al. (2013) used the Carbonated Steel Slags as adsorbent to remove H<sub>2</sub>S (aq). They found out that the maximum adsorption of H<sub>2</sub>S (aq) onto the carbon steel slag is 7.5 mg.g<sup>-1</sup>. The specific surface area of the carbonated steel slag used is 14.4 m<sup>2</sup>.g<sup>-1</sup>. The large amount of calcium (from carbon steel slags) dissolved into seawater triggers a rapid increase of pH. Therefore, the seawater pH increases up to 12.3. On the other hand, Asaoka et al. (2009) have shown that the crushed oyster shells (dominated by CaCO<sub>3</sub>) have the ability to adsorb the low concentration of dissolved H<sub>2</sub>S (aq) from the sediment pore sea water. The first-order equation correlates well with the Langmuir plot in describing the adsorption behaviour by using batch experiment that shows removal kinetics of H<sub>2</sub>S (aq) with the maximum adsorption of 12 mg-S g<sup>-1</sup>. Although the crushed oyster shell is able to remediate the organically enriched sediments in eutrophic coastal seas, its preparation cost is high and its calcium contents would dissolve in water leading to increase of pH. Moreover, it has limited surface area of merely 0.25 m<sup>2</sup> g<sup>-1</sup>. Table 2.8 shows the adsorbents derived from wastes materials which used for removal of H<sub>2</sub>S from mixture as an aqueous and gas form as clearly stated the phase of H<sub>2</sub>S in Table 2.8.

Table 2.8 Adsorbents derived from wastes materials

Adsorbents	Breakthrough H <sub>2</sub> S (mg/g)	BET (m <sup>2</sup> /g)	Phase of H <sub>2</sub> S	References
FRPM	0.12	0.3	g	Wang et al. (2013)
Crushed oyster shell	12	0.25	L	Asaoka et al. (2009)
Red mud	17	31.7	g	Sahu et al. (2011)
Ferric and alum water		80.96	L	Wang and Pei (2012)
Sewage sludge	87.1	82	g	Ortiz et al. (2014)
Mineral wool waste			g	Bergersen and Haarstad (2014)

#### 2.4.2 Adsorption of H<sub>2</sub>S on Metal Oxide and Zeolite Materials

Recently, refined zeolite compounds have been used as an adsorbent/oxidant of H<sub>2</sub>S (g). Natural zeolites exhibited better properties than the simulated ones in commercial separation (Ozekmekci et al., 2015). The H<sub>2</sub>S (g) removal efficiency of virgin zeolite (for palm oil mill effluent (POME) biogas desulfurization) was investigated by Pourzolfaghar and Ismail (2013) at ambient temperature and pressure. In addition,



Yaşyerli et al. (2002) have been tested the capacity of H<sub>2</sub>S removal using the natural zeolite which was about 94% removal efficiency. Moreover, the performances of zinox and zeolite materials as adsorbents to remove H<sub>2</sub>S from natural gas has been evaluated by Melo et al. (2006). The surface area of zeolite 13X was 16.15 m<sup>2</sup>/g and the maximum adsorption capacity was 53 mg H<sub>2</sub>S/g at 25 °C. Their results correlated well with those of the Toth's model. Both Zeolite 13X and Zinox 380 could be used as adsorbents to remove H<sub>2</sub>S (g) from natural gas, and Zeolite 13X gives better adsorption of H<sub>2</sub>S (g) than Zinox. However, Zinox 380 has higher surface area compared to Zeolite 13X (34.54 m<sup>2</sup>/g). In fact, the functional groups play a significant role in the adsorption processes of Zinox 380 and Zeolite 13X. Calcium oxide, hydroxyls, and ZnO<sub>4</sub> were observed as functional groups on the surface of Zinox 380 by FTIR test. For zeolite 3X, hydroxyls, SiO<sub>4</sub> and AlO<sub>2</sub> tetrahedral were active groups that contributed to the adsorption process. Furthermore, there is a few literatures related to removal H<sub>2</sub>S (aq) from solution. Haimour et al. (2005) studied of using a metal oxides such as CuO and ZnO to remove H<sub>2</sub>S (aq) from solution.

#### **2.4.3 Adsorption of H<sub>2</sub>S (g) on Composite Materials**

A series of hydroxide composites or metal oxide with graphite oxide (GO) have been proposed as the H<sub>2</sub>S (g) removal media (Mabayoje et al., 2012; Seredych et al., 2011). Surface chemistry of the carbonaceous adsorbents can also be enhanced by adding some transition metals. For example, ACs with metal containing bentonite binders was studied by Nguyen and Bandosz (2005). They investigated the effects of bentonite clay binders containing copper, zinc or iron in the interlayer spaces on the performances of adsorbents in H<sub>2</sub>S (g) removal. As reported, modification with copper-containing binder could enhance the capacity of carbon adsorbents, thereby indicating that surface oxygenated groups play an important role in the adsorption process. The modification of ACs with bentonite binder decreased the micropore volume and the surface area due to the accumulation of metals in small pores. But, the adsorption capacity of ACs increased because the copper appeared in the small pores acted as an oxygen activator that would promote the oxidation process.

In contrast, Mabayoje et al. (2012) studied the effective of using cobalt (hydr)oxide/GO composites to remove of H<sub>2</sub>S (g) and the results clearly demonstrated the ability of composite material cobalt(hydr)oxide/GO in improving the adsorption capacity. The results also indicated that the adsorption capacity of adsorbent improved when the

ratio of GO in the composite decreased. The removal efficiency of H<sub>2</sub>S (g) is higher in a humid environment due to H<sub>2</sub>S (g) oxidation to form elemental sulfur and H<sub>2</sub>S (g) dissociation. Bagreev and Bandosz (2005) reported that the basic pH enhances the dissociation of H<sub>2</sub>S (g) via oxidation. In the presence of 70% relative humidity, the adsorbed H<sub>2</sub>S (g) dissolve in water and dissociate to HS<sup>-</sup> and H<sup>+</sup> (as shown in equation 2.3. In addition, KOH can absorb water vapor easily and the basic property of KOH leads to the acid–base reaction (Xu et al., 2014; Sitthikhankaew et al., 2014).



As reported by many researchers, adsorption capacity increases with respect to the relative humidity, signifying the importance of oxygenated group of GO (Xu et al., 2014). Mabayoje et al. (2013) examined of using visible light photoactive zinc (hydro)oxide/GO and zinc (hydro)oxychloride/GO composites to remove of H<sub>2</sub>S (g). They have found that highly energetic adsorption centres were formed on the composite surfaces and exposure to visible light would decrease the H<sub>2</sub>S (g) adsorption capacity. These processes involved active centres and OH<sup>-</sup> groups that react with H<sub>2</sub>S. However, in dark environment, the oxidation of H<sub>2</sub>S (g) was limited and the terminal groups played an important role in the removal process. The adsorption capacities of these composite materials ranged from 40 to 155 mg/g. Apart from that, the performance of nano-sized zinc oxide/reduced graphene oxide composite (ZnO/rGO) at ambient condition was investigated by Song et al. (2013). Moreover, Li et al. (2015) have concluded that the ACs coated with CeO<sub>2</sub>-NiAl-LDHs was promising in aqueous SO<sub>2</sub> and H<sub>2</sub>S (g) removals. Table 2.9 summaries the H<sub>2</sub>S (g) adsorption efficiencies for some composite materials. Figure 2.5 compares the H<sub>2</sub>S (g) adsorption capacities of some composite materials.

Table 2.9 The literatures of adsorption process based on composite materials

Adsorbents	Adsorption capacity (mg/g)	SBET (m <sup>2</sup> /g)	Reference
Bentonite binders/AC	47.0	1410	Nguyen and Bandosz (2005)
Zr(OH) <sub>4</sub> /GO	52.8	210	Seredychet al. (2011)
Cd/GO	80.4	50	Florent et al. (2015)
ZnO/rGO	113.5	--	Song et al. (2013)
Co(hydr)oxide/GO	120.3	121	Mabayoje et al. (2012)
Zn(OH) <sub>2</sub> /GO	155.0	47	Mabayoje et al. (2013)



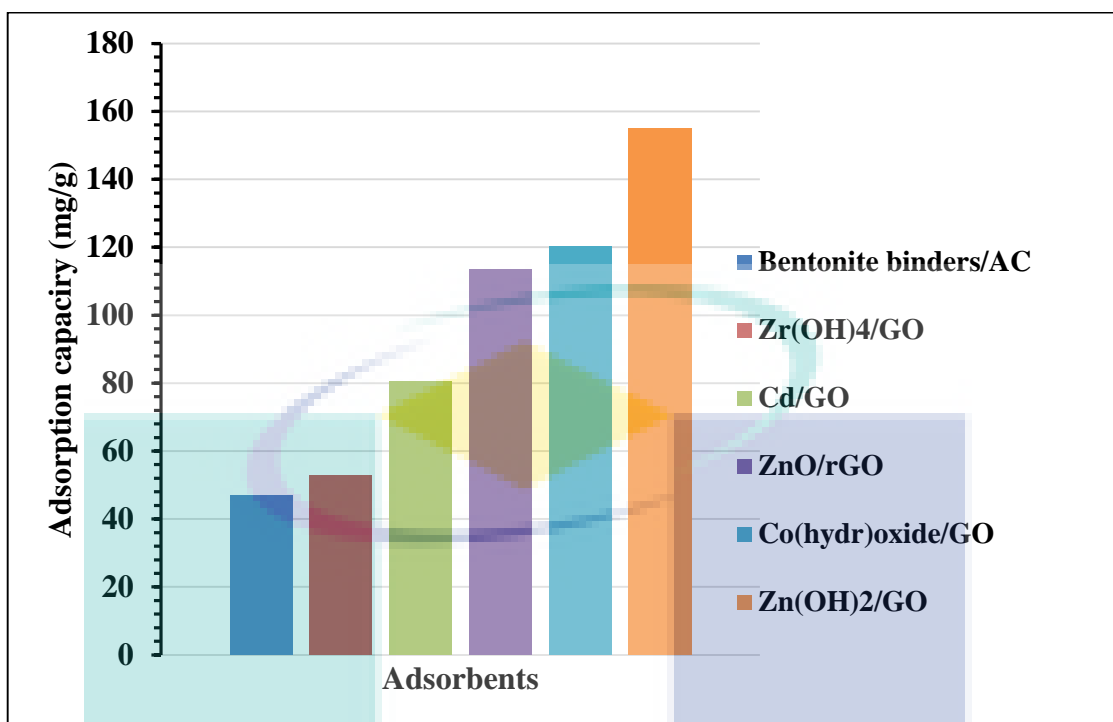


Figure 2.5 H<sub>2</sub>S (g) adsorption capacities of some composite materials

#### 2.4.4 Adsorption of H<sub>2</sub>S on Activated Carbons

Activated Carbons (ACs) are solid, porous and black carbonaceous material. They can be produced from any carbonaceous solid precursor, either in the simulated or natural standpoint. For instance, ACs could be prepared from a large number of sources such as agricultural wastes, peats, black ashes, charcoals, lignite, bituminous coals, petroleum cokes, which are materials with low inorganic components and high carbon content. The two common forms of activated carbons (ACs) are granular (GAC) with sizes ranging from 0.5 to 2.5 mm; these are used in adsorption and columns. While Powdered Activated Carbons (PACs) forms with a size predominantly less than 0.15 mm are used in batch adsorption followed by filtration (Allen and Koumanova, 2005; Dabrowski et al., 2005).

Furthermore, few studies reported the removal of H<sub>2</sub>S (aq) using activated carbon as an adsorbent. For instance, Amosa (2015) investigated the effectiveness of ACs prepared from empty fruit bunch (EFB) for removing a very low concentration of H<sub>2</sub>S (aq) from palm oil mill effluent waste water. The activated sludge was used to remove low concentration of H<sub>2</sub>S (aq) which was conducted by Pang et al. (2017). Furthermore, studies on adsorption of H<sub>2</sub>S (aq) by biochars derived from pyrolysis of different agricultural/forestry wastes have been conducted by Shang et al. (2016). According to

their findings, the sorption capacity of the biochar is related to the pyrolysis temperature and the surface pH.

The early 19th century, the first Powdered Activated Carbons (PACs) was produced commercially in Europe. Moreover, ACs has high internal surface area and pore volume, making it attractive to be used as adsorbent, or catalyst in gas and liquid phase processes for purification and chemical recovery (Radovic et al., 2001). An effective method developed for the removal of pollutants from water and air is therefore adsorption using the activated carbons (Bansal and Goyal, 2005). Availability, cost, low inorganic matter content, low degradation during storage and ease of activation are the criteria needed in the selection of the precursors for adsorption process (Dabrowski et al., 2005). Physical and chemical activation methods are normally used for activation of the chosen precursor. Physical activation is considered one of the method used in activating the precursor thereby enhancing the materials porosity, area and surface chemistry. Two steps are involved in these include thermal carbonization and activation. The purpose of carbonization of the raw materials under high temperature is to increase the carbon content and reduced the other component in the materials used. The activation process is conducted under a gasified condition using an oxidizing agent (mostly steam or carbon dioxide) to enhance the porosity, surface area and functional groups characteristics. However, chemical activation is conducted for raw materials using a considerable amounts of chemical agent such as alkaline hydroxides, zinc chloride, or phosphoric acid, and followed by carbonization under inert gas and high temperature. The chemical agents used for impregnation process. After impregnation process, the remaining agent on the surface of materials should be washed to remove excess chemical agent (Zhang et al., 2011).

Recently, adsorption on ACs from organic components can be regarded as the most effective way in removing pollutants from waste water which could be due to its cost effectiveness. Activated carbons (ACs) have been used by many researcher to remove H<sub>2</sub>S from gas mixture and liquid. Moreover, many factors determine the capacity of adsorbents during the adsorption process which include, porosity, surface area, functional groups, activation method and adsorbate conditions. The structure of raw materials and the proper activation agent are the important factors that enhance the adsorption capacity and functional groups characteristics of the adsorbent surface.

Different impregnated agents have been used to enhance the adsorption capacity of ACs in  $\text{H}_2\text{S}$  (g) removal and these include metal hydroxides and oxides (Li et al., 2008; Bashkova et al., 2009; Cui et al., 2009), carbonates (Chen et al., 2010), and nitrogen groups using urea or melamine (Seredych and Bandosz, 2008).

ACs could be obtained either commercially or from waste materials, the latter will be discussed here in details. Guo et al. (2007) used oil palm shell to remove  $\text{H}_2\text{S}$  (g) from mixture gas. Different activation methods such as thermal and chemical methods were tested. The result obtained revealed that treated with strong acid possesses better dynamic adsorption performance. However, there might be an inherent hazard using a fixed bed self-ignition which could be due to the extreme heat released from the reaction and a significant decrease in adsorption capacity due to blockage of pore entrance. From the results obtained it was indicated that the chemical activation of palm shell ACs using  $\text{H}_2\text{SO}_4$  or KOH activation gave a better performance than when  $\text{CO}_2$  was used for thermal activation. The mechanisms of  $\text{H}_2\text{S}$  (g) removal using the palm shell ACs include chemisorption, physisorption, and/or  $\text{H}_2\text{S}$  oxidation. Their finding was buttressed by the Boehm titration and Fourier transform infrared spectroscopy (FTIR) which showed that alkaline groups of pyrones (cyclic ketone) and other keto-derivatives of pyran were the main surface functional groups on the KOH-impregnated adsorbent. While phenols, carboxylic acids and carbonyl groups were the main surface functional groups on the  $\text{H}_2\text{SO}_4$  impregnation with only carbonyl groups and phenol detected for thermally activated ACs. However, effect of humidity on adsorption process was part of the consideration from previous investigation conducted by Guo et al. (2007). Xu et al. (2014), addressed this limitation by focusing on the effects of relative humidity and pH on the adsorption capacities in sewage sludge and pig manure. It deduced that the non-humidified pig manure biochar had higher capacity (59.6 mg/g) than the sewage sludge biochar (43.9 mg/g). This could be possibly as a result of the effectiveness of functional groups from the adsorption process. It was also reported that, as the biochar was humidified at 25 wt%, the saturation time increased to 200 and 180 minutes. The removal capacities for pig manure biochar and sewage sludge biochar therefore increased by ~10 and ~8.3%, respectively, relative to those of non-humidification controls. Both pig manure biochar and sewage sludge biochar have high pH values. The alkaline working condition is only favourable for the dissociation of  $\text{H}_2\text{S}$  (g) at the biochar surface, followed by the removal of  $\text{H}_2\text{S}$  (g) via the oxidation of dissociated  $\text{HS}^-$ .

Seredych et al. (2008) applied fly ash on sewage sludge-based material to remove H<sub>2</sub>S from biogas and air. Adsorbents were packed in a glass column (length 370 mm, internal diameter 9 mm, bed volume 6 cm<sup>3</sup>). H<sub>2</sub>S (g) (1000 ppm dry) was passed through the column of adsorbent with a flow rate of 0.15 L/minute. The results showed that the addition of nonporous ashes to sewage sludge decreased the surface area and the porosity (where sulfur can be stored as H<sub>2</sub>S (g) oxidation product). The active surface area is more influential than the micro porosity in the process. Another study conducted by Phooratsamee et al. (2014) indicated that the adsorption of H<sub>2</sub>S lead to 50% decrease in the volume of micropores (with a 50% decrease in surface area). Parameters such as surface area, total pore volume and microspore volume was investigated. ACs derived from palm oil shell and impregnated with NaOH and K<sub>2</sub>CO<sub>3</sub> was used to remove H<sub>2</sub>S (g). They compared the performances of impregnated ACs and commercial ACs and found out that the surface area, total pore volume and microspore volume increased with respect to the char product to chemical agent ratio (1:1 to 1:3).

Moreover, the ACs derived from alkaline impregnated coconut shell was adopted to remove H<sub>2</sub>S from gas stream. The fresh adsorbent was impregnated with NaOH, KOH and K<sub>2</sub>CO<sub>3</sub> using wet impregnation method. The adsorbent was successfully impregnated with three types of alkaline and findings showed that K<sub>2</sub>CO<sub>3</sub> provided the best impregnation with the highest adsorption capacity. However, the adsorption capacity decreased when NaOH impregnated ACs ratio increased (Choo et al., 2013).

Kante et al. (2012) investigated the use of carbonaceous adsorbents from coffee industry waste materials to remove the H<sub>2</sub>S (g). The materials obtained were used as media for separating H<sub>2</sub>S from air at ambient conditions. They discovered that the porous surface of carbons governed the separation process. The adsorption capacities of ACs was therefore dependent on surface pH value and ash content, ranging from 20 to 127 mg/g. The chars and ACs were packed into a glass column (internal diameter 9 mm, bed volume 3 cm<sup>3</sup>). Dry or wet air with 0.1% of H<sub>2</sub>S (g) was passed through the dry bed of the adsorbent at 450 cm<sup>3</sup>/minute. From the appropriate choice of pyrolysis condition and activation procedure, it is possible to obtain adsorbents with high removal capacity of H<sub>2</sub>S (g) (281.5 mg H<sub>2</sub>S/gads). Nowicki et al. (2014) studied the effective of ACs activated with carbon dioxide with a very large sorption capacity towards H<sub>2</sub>S (g) and the wet condition is ideal for adsorption capacity. Kazmierczak et al. (2015) reported that the

adsorption capacities of ACs towards  $\text{H}_2\text{S}$  (g) were dependent on the activation temperature and adsorbent conditions.  $\text{H}_2\text{S}$  (g) adsorption capacity of ACs or IACs increased with respect to the relative humidity. However, the role of humidity was not clearly understood in the removal of  $\text{H}_2\text{S}$  (g) from gas mixture as concluded by Xiao et al. (2008). Impregnation was conducted by mixing 50 g of carbon with 25 mL of 6%  $\text{Na}_2\text{CO}_3$  solution for 30 minutes. The mixed gases (100–1000 ppm) of  $\text{H}_2\text{S}$  passed through the adsorbent bed at a flow rate of about 120 mL/minute. They found out that the roles of water and  $\text{Na}_2\text{CO}_3$  in the process were not clearly understood and increasing temperature would reduce the  $\text{H}_2\text{S}$  (g) adsorption capacity of IACs. Bagreev et al. (2004) studied the ACs obtained from bituminous coal for the removal of  $\text{H}_2\text{S}$  (g). They found out that the modification of bituminous coal-based ACs with melamine and melamine with urea followed by heat treatment at  $850^\circ\text{C}$  produced more efficient adsorbents. The performance of melamine has been reported to be two times higher than that of melamine with urea at low char temperature ( $600^\circ\text{C}$ ). The sorption of  $\text{H}_2\text{S}$  (g) on virgin and oxidized ACs was investigated (Bagreev and Bandosz, 2000).

Yuan and Bandosz (2007) reported that the adsorption of  $\text{H}_2\text{S}$  (g) on ACs might be affected by the chemical and physical properties of the adsorbent (i.e. surface area, porosity, and surface chemistry). Zhang et al. (2016) examined the ACs prepared from flue gas precipitated lignin by means of steam activation. The results showed a large specific surface area of  $1010\text{ m}^2/\text{g}$  with an excellent removal of  $\text{H}_2\text{S}$  from the gas stream. The physisorption using ACs at ambient temperature and pressure was found to be economical and cost-effective for  $\text{H}_2\text{S}$  removal from the gas stream. Furthermore,  $\text{H}_2\text{S}$  (g) adsorption on KOH impregnated ACs was investigated by Sitthikhankaew et al. (2014).

Recently, the adsorption of  $\text{H}_2\text{S}$  on ACs prepared from petroleum coke by KOH chemical activation was studied by Mochizuki et al. (2016). The results showed that increased activation temperature and KOH/petcoke weight ratio would enhance the pore structure. Kazmierczak et al. (2016) tested the ACs activated by microwave radiation (physical activation) to remove toxic gases. The surface area and the pore volume of final product were obtained to be  $377\text{ m}^2/\text{g}$  and  $0.24\text{ cm}^3/\text{g}$ , respectively, which were higher than those of the chemically activated ACs. Table 2.10 reported different adsorbent types

and their corresponding H<sub>2</sub>S adsorption capacities. Figure 2.6 shows the linear relation ( $R^2 = 0.9534$ ) between the adsorption capacity and the adsorbent surface area.

Table 2.10 The literatures of some types of adsorbent and their adsorption capacity

Adsorbents	Uptake (mg/g)	S <sub>BET</sub> (m <sup>2</sup> /g)	References
ACs from sawdust pellets	6.2	426	Kazmierczak et al. (2015)
IACs under anaerobic conditions	9.4	732	Xiao et al. (2008)
Graphite derived materials	30.5	192	Seredych and Bandosz (2009)
ACs from oil-palm shell	76	1062	Guo et al. (2007)
Sewage sludge/fish waste mixture	87.1	80	Ortiz et al. (2014)
N <sub>2</sub> modified carbide-derived carbons	90.5	1297	Seredych et al. (2009)
Adsorption/oxidation on ACs	112	1063	Bagreev and Bandosz (2001)

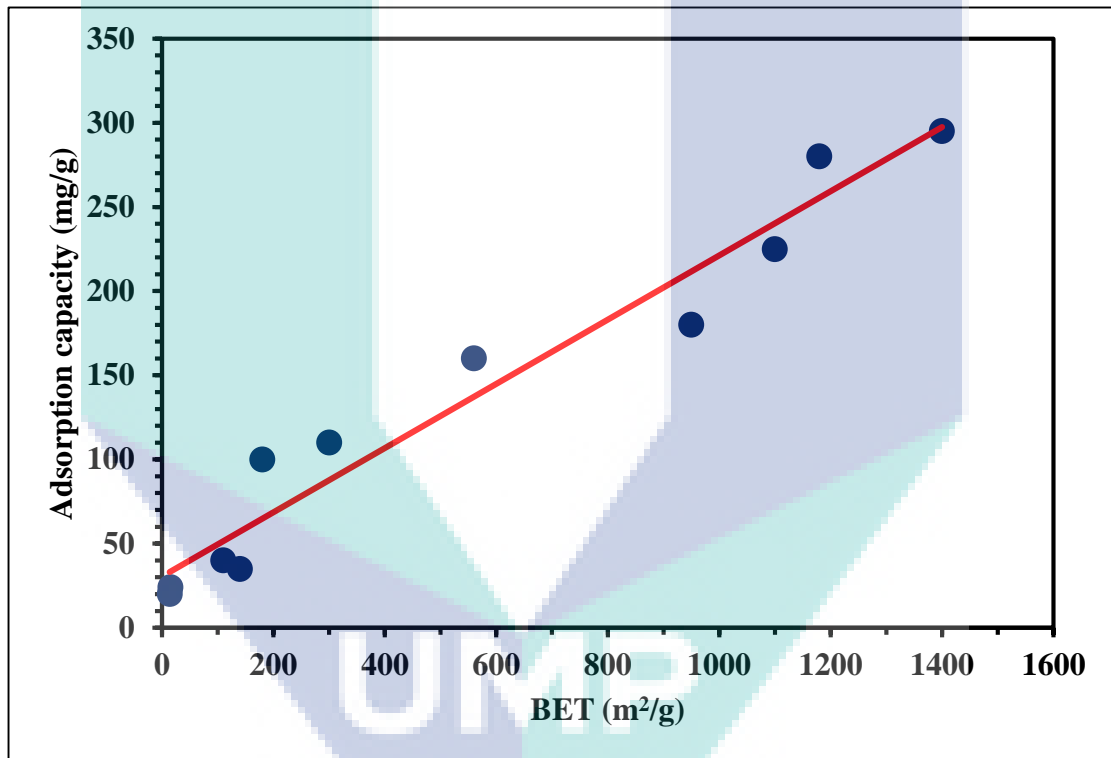


Figure 2.6 Linear dependence of H<sub>2</sub>S adsorption capacity of some carbon based materials on the adsorbent surface area (solid line is the linear fitting)



#### 2.4.4.1 Structure Properties and Functional Groups of ACs

The chemical nature of ACs surface is very important to determine the removal efficiency (adsorption capacity) and the textural properties of ACs. The activated carbon surface is heterogeneous, consisting multiple faces/edges and layers of graphite sheets. The hydrogen, nitrogen, particularly oxygen and halogen are mainly located on the edges and consist of the chemisorbed foreign heteroatom (El-Sayed and Bandosz, 2004). The edge sites seem to be more reactive than the atoms residing in the interior of the graphite sheets. Oxygen in the surface oxides is bounded in the form of various types of functional groups. Precursor, activation process, post chemical treatment and heat treatment formed the surface chemical functional groups (Moreno, 2004; Derylo et al., 2008). The surface functional groups are seen in Figure 2.7. Various functional groups exist in organic chemistry. Most of them are carbon-based compounds. Some of the functional groups form a single bond with most of the hetero-atoms such as oxygen, iodine, and nitrogen. Figure 2.7 shows two types of functional groups that can be observed on the activated carbons surface such as acidic and basic functional groups.



UMP

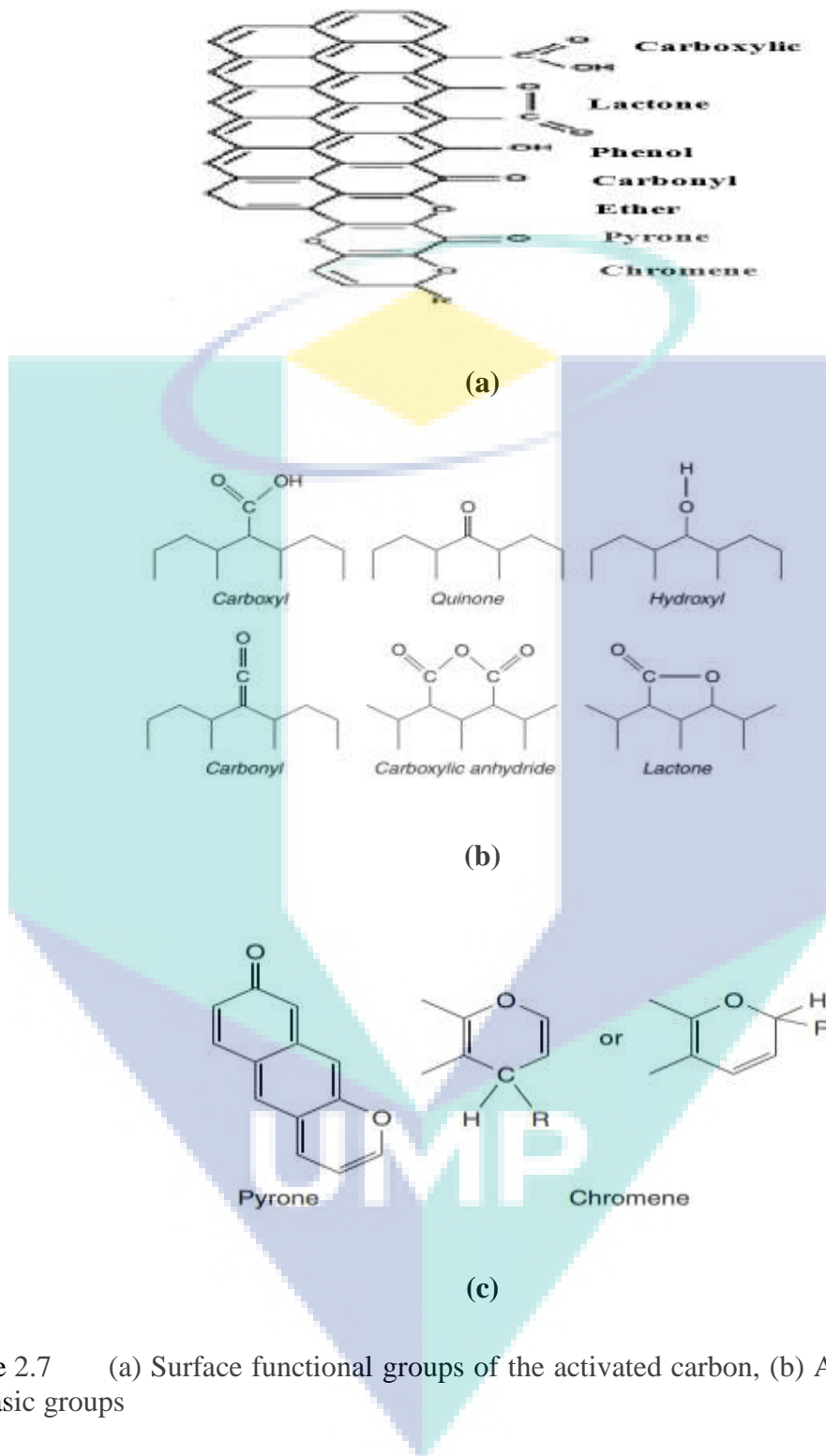


Figure 2.7 (a) Surface functional groups of the activated carbon, (b) Acidic groups, (c) Basic groups

Source: Mohamed (2011).



### 2.4.4.2 Physical Properties of the ACs

The pore structure and the specific surface area are the most important property of adsorbent. Pore structures of the activated carbons (ACs) and Impregnated activated carbon (IACs) can be obtained from nitrogen adsorption-desorption isotherms. The adsorption capacity can be effected by physical properties such as size, shape and number of pores. The International Union of Pure and Applied Chemistry (IUPAC) is defined the range of pore sizes as summarized in Table 2.11. The specific surface area is considered as an important property which determines the adsorbent usage and its capacity. Reports have shown that the total surface area of an activated carbon ranges from 500 to 2000 m<sup>2</sup>. g<sup>-1</sup> (Carrott and Carrott, 2007). For instance, from Figure 2.8, mesopores and macropores are mostly found in the external surface while the micropores dominate the internal surface of the activated carbon and contributes the most to the total pore volume.

Table 2.11 IUPAC classification of pore sizes

Pores	Pore width ( W; nm)
Ultramicropores	$W < 0.7\text{nm}$
Super micro pores	$0.7 < W < 2\text{nm}$
Micropores	$W < 2$
Mesopores	2-50
Macropores	$W > 50$

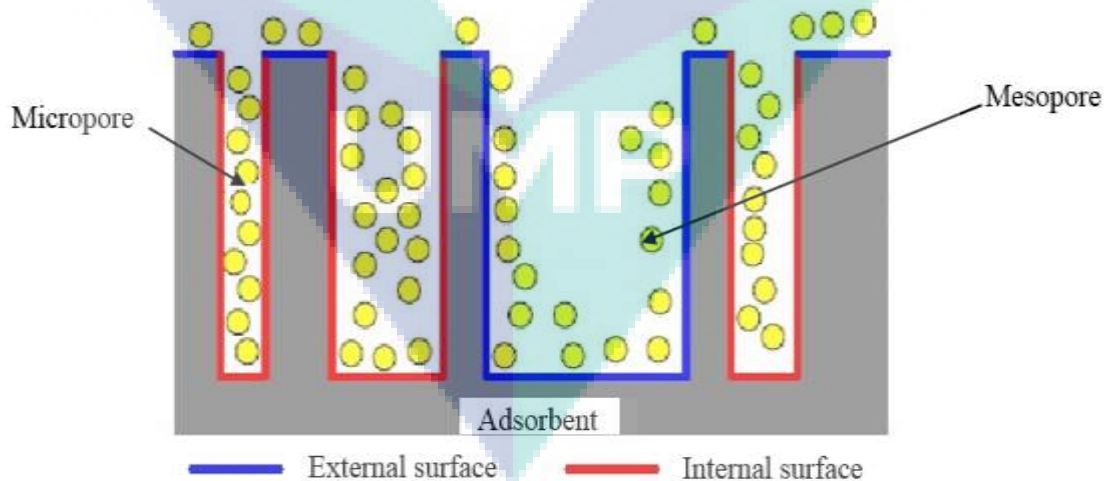


Figure 2.8 Schematic representation of external and internal adsorbent surface

Source: Mohamed (2011).

## 2.5 Impregnation of Activated Carbons (IACs)

The caustic carbon surface could help to immobilize the  $\text{H}_2\text{S}$  (aq) species on the adsorbent surface and allow for greater removal efficiency due to the fact that  $\text{H}_2\text{S}$  (g) is acidic in nature. The caustic materials such as NaOH or KOH is capable of improving the pH level from the carbon surface and this result in attraction of the adsorbent towards the  $\text{H}_2\text{S}$ . Other materials, such as KI,  $\text{Na}_2\text{CO}_3$ ,  $\text{K}_2\text{CO}_3$  and  $\text{KMnO}_4$  are also utilized for impregnation during gas desulfurization. For instance, Xiao et al. (2008) reported that the impregnation with  $\text{Na}_2\text{CO}_3$  could enhance the total removal capacity as much as about 40-60times that of the unmodified carbons. In addition, alkali and metal hydroxides, oxides or carbonates, or nitrogen groups using urea or melamine are employed to the impregnation of carbons (Bandosz, 2006). There is a difference between impregnated carbon and unmodified carbon in the adsorption mechanisms. For example, the chemical reaction with  $\text{H}_2\text{S}$  (g) is irreversible with impregnated carbon. Impregnation using caustic materials also escalates the selectivity towards sulfur formation (Bandosz, 2006). However, there is lack of enough scientific research which investigated the impregnation of activated carbons with metal oxide derived from wastes such as calcium derived from egg shells.

### 2.5.1 Dispersion of Calcium on Activated Carbon

One of the most common methods used for removal of low-concentration gaseous contaminants from air is adsorption on activated carbons (Bastani et al., 2010; Réguer et al., 2011). Air purification systems employing hybrid sorbents, i.e., porous solids loaded with chemicals that react with the target gas, are available commercially and are continuously being developed (Miyawaki et al., 2012). For example, activated carbons impregnated with chemicals of a strong basic character such as hydroxides or carbonates, is a highly efficient material for removing acidic gases from air (Bagreev and Bandosz, 2002). The mineral used for preparations mainly consisted of  $\text{CaCO}_3$ , which is a salt that decomposes thermally at  $800\text{ }^\circ\text{C}$  to  $\text{CaO}$  and  $\text{CO}_2$ . Muñoz et al. (1997) used calcium-containing carbons as low-temperature sorbents for  $\text{SO}_2$ . The particles of  $\text{CaO}$  dispersed on carbon were prepared by thermal decomposition of calcium acetate. They have studied the use of carbon as support to afford fine  $\text{CaO}$  particles, which in turn will provide high-surface-area  $\text{CaO}$  to increase the retention capacity of the calcium-based sorbent to remove  $\text{SO}_2$ .

Przepiórski et al. (2013) investigated the use of CaO-loaded carbon to efficiently remove  $\text{CO}_2$  and  $\text{SO}_2$  from air. Also, Zhenet et al. (2008) reported that CaO has the capacity to react with acidic gases. Nikulshina et al. (2009) have concluded that  $\text{Ca}(\text{OH})_2$  reacts with aforementioned acidic gases. There are many sources of  $\text{CaCO}_3$  such as limestone (53.16 %) (Marroccoli et al., 2010), oyster shell (36.4 %) (Pizzolante et al., 2011), and egg shells (96 %) (Laca et al., 2017). However, egg shells have more amount of calcium (Ca). Thus, the waste of egg shells are implemented in this study as a source of calcium (Olgun et al., 2015).

### **2.5.2 Sources of Calcium**

There are many sources of calcium from natural materials. Calcium can be extracted from calcium carbonate which is abundant in nature. Egg shells, oyster shells, and limestone are the major sources of calcium carbonate. For instance, egg shells contained around 96 % of calcium carbonate (Laca et al., 2017). Moreover, oyster shells have a percentage of calcium carbonate of 36.4 % (Pizzolante et al., 2011) and limestone of 53.16 % (Marroccoli et al., 2010). Calcium can easily be extracted from nature shells contained calcium carbonate due to in an acidic solution, calcium carbonate dissolves readily which can provide calcium.

#### **2.5.2.1 Components of Egg Shells**

Egg shells consist of about 94 to 96% calcium carbonate (Laca et al., 2017). An egg shell is a cost-effective and easily available. Huge amounts of egg shells are produced as a by-product because hen's eggs are one of the most common traditional foods and utilized universally, and egg shells represent approximately 11% of the total egg weight (Stadelman, 2000). Pundir et al. (2009) reported that the by-product egg shells from these breaking operations are conventionally deemed useless and a major waste for the processor. The egg waste is commonly thrown away and ends up in a landfill without any pre-treatment and causes environmental impact (Tsai et al., 2006). Due to the odour from biodegradation, this approach is a less preferred choice (Poland and Sheldon, 2001). In addition, due to properties such as high amounts of minerals and amino acids (Tsai et al., 2006); high porosity, antibacterial or anti-inflammatory characteristics (Pundir et al., 2009); and excellent adsorbent properties (Tsai et al., 2008), egg shells membranes

have multiple applications in therapeutic, nutraceutical, metallurgy or bioremediation areas, either as such or after processing (Pundir et al., 2009).

Researchers have shifted their focus onto natural porous materials in the last couple of years. The egg shells are impressive in that it is made up of five structurally different layers. The shells membranes, mammillary layer, palisade layer, vertical crystal layer, and the cuticle. The mammillary layer which is the first mineralized layer is thought to contain randomly orientated calcite ( $\text{CaCO}_3$ ) crystals (Ferguson, 1982; Moreno et al., 2014). Various researches have been conducted to evaluate the adsorption ability of egg shells as a low cost adsorbent, in artificial waste water with mono or multi components. Researchers in their studies have demonstrated the effectiveness of this adsorbent in the removal of heavy metals (Chojnacka, 2005), phenolic compounds (Koumanova et al., 2002), dyes (Tsai et al., 2008) and pesticides (Elwakeel and Yousif, 2010).

#### **2.5.2.2 Oyster Shells**

The oyster shells have a high percentage of calcium carbonate. Several studies have been conducted for other applications of oyster shells as catalyst (Nakatani et al., 2009), filtering medium (Park and Polprasert, 2008), and adsorption (Asaoka et al., 2009). The disadvantages of using the oyster shells for preparation of calcium as an impregnated agent due to difficult to prepare because it need to left soaking in seawater for 1–2 years to remove any remnants of oyster meat, dried in the field for 3–4 months to remove moisture and salts and high energy to dried in an oven at  $400^\circ\text{C}$ . Furthermore, very fine grain oyster shells are no suitable due to it become viscid and muddy when they are mixed together (Asaoka et al., 2009). Therefore, current study choose to use the egg shells as a source of calcium.

### **2.6 Adsorption of Dissolved $\text{H}_2\text{S}$**

There are some interactions affecting the adsorption process of  $\text{H}_2\text{S}$  (aq) from waste water. These are (i) Adsorbent (ACs & IACs)/adsorbate (dissolved  $\text{H}_2\text{S}$  (aq)) interaction which is controlled by the molecular structures of the adsorbate, the solution chemistry and the physicochemical properties of the adsorbents, (ii) Water/adsorbate (dissolved  $\text{H}_2\text{S}$  (aq)) interaction which is related to the chemical compatibility between water and  $\text{H}_2\text{S}$  (aq) molecules. (iii) Water/adsorbent (ACs & IACs) interaction which depends on the polarity of the adsorbents (Kose, 2010).

### 2.6.1 Factors Affecting the Adsorbent/Adsorbate Interactions

It is known that the adsorption capacity of activated carbon (ACs) for the liquid adsorption depends on the nature of the adsorbate such as polarity, aqueous solubility, molecular size and weight as well as nature of the adsorbent (its pore structure, functional groups, surface area, and ash content) (Terzyk, 2004; Zhang et al., 2006). In addition, operating conditions for adsorption such as pH of the solution, and temperature have implications on the adsorbent/adsorbate interactions (Al-Degs et al., 2008). Effect of electron donor/acceptor substituent groups, molecular size, solubility, hydrophobicity and polarity of adsorbate are the factors that affect the adsorption process. Several studies have showed that adsorption of H<sub>2</sub>S by ACs and IACs increases with increasing solubility and/or decreasing hydrophobicity in the water because of the dissociation of H<sub>2</sub>S (aq) to S<sup>2-</sup> and HS<sup>-</sup> that become easily to adsorbed the adsorbate (Nowicki et al., 2014). H<sub>2</sub>S (aq) could be a water soluble (4-6 g/L) (Heinonen, 2012; Pourzolfaghar et al., 2014).

The main parameters that determines water – adsorbate (dissolved H<sub>2</sub>S (aq)) interactions is the chemical compatibility between water and H<sub>2</sub>S ions. The hydrophobic and hydrophilic characteristic of a molecules is the driving force for the ions to the interfaces between solvent and solute. The nonpolar compounds are retained due to dispersive forces, the adsorption of polar compounds includes specific interactions via oxygen, nitrogen and other species on the surface. While polarity of pollutant molecules results from the difference in the electro-negativities among the various atoms, which causes an unequal distribution of electron density (Ania et al. 2008). The H<sub>2</sub>S (aq) is considered a polar molecule. Thus, the solubility of a H<sub>2</sub>S (aq) compound increased with decreasing difference between its polarity and the polarity of the solvent. Therefore, adsorption of a H<sub>2</sub>S (aq) by AC increased.

### 2.7 Optimization Studies of Removal Efficiency of H<sub>2</sub>S (aq)

The conventional and classical methods of studying a process by changing one variable at a time and maintaining other factors of the process at a constant level does not depict the combined effect of all the factors involved. This method is also time consuming and requires large number of experiments to determine optimum levels, which are unreliable. Therefore, optimization studies technique are conducted to determine the optimum conditions for the process variables under consideration and to find the



interactions between factors. The optimization study has been conducted using design of expert version 10.

### **2.7.1 Design of Expert (DoE)**

Design Expert (version 10) as a statistical tool which helps in optimizing adsorption conditions for H<sub>2</sub>S (aq) removal from waste water using response surface methodology (RSM). The response surface methodology (RSM), was first described by Box and Wilson (Box and Wilson, 1992). It is an experimental approach used in identifying the optimum conditions for a multivariable system. It is a collection of mathematical and statistical techniques useful for developing, improving and optimizing processes and can be used to evaluate the relative significance of several affecting factors even in the presence of complex interactions (Hamsaveni et al., 2001). Response surface methodology (RSM) is a statistical experimental design that solved all the limitations of a classical method (Elibol, 2002). The main objective of RSM is to determine the optimum operational conditions for the system or to determine a region that satisfies the operating specifications. In this work, response surface methodology was employed for the optimization of H<sub>2</sub>S (aq) removal factors to enhance the removal efficiency (RE).

In the last few decades, evaluated and optimized interactive effects of independent factors have been studied using response surface methodology (RSM). This has been conducted on numerous biochemical and chemical processes. Ahmad et al. (2009) studied the optimization of disperse dye removal from aqueous solution using waste-derived activated carbon. They have investigated the optimal preparation conditions for activated carbons prepared from rattan sawdust (RSAC) using central composite design (CCD) under RSM technique. The optimization application of preparation conditions of activated carbons was investigated. These applications have been investigated such as in the preparation of activated carbons sewage sludge (Rio et al., 2005) olive-waste cakes (Baçaoui et al., 2001), and Turkish lignite (Karacan et al., 2007). The Central Composite Design (CCD) was employed to study the optimized condition, interaction between factors and the effect of factors toward their responses. CCD was used to develop the correlation between the response surface and factors. Central Composite Design (CCD) is widely used by researchers due to its wide applicability in industries. The CCD technique is suitable for investigating the relationship between factors and optimization which can be performed with lesser experimental runs.

Recently, Bagheri et al. (2016) investigated the optimization of adsorption conditions on dyes removal efficiency based on central composite design (CCD) along with response surface methodology (RSM). Dehghani et al. (2017) also investigated the effect of interaction factors using response surface methodology (RSM) named central composite design (CCD) in order to optimize adsorption conditions of removing Reactive Red 120 and 196 using chitosan/zeolite composite from aqueous. However, there is no literature reported on the use of RSM for optimizing the operating conditions of removal  $\text{H}_2\text{S}$  (aq) from waste water. Therefore, this study addressed this limitation in the literatures by investigating the optimum conditions of removal of  $\text{H}_2\text{S}$  (aq) from petroleum waste water.

### **2.7.2 Statistical and Graphical Analysis.**

Significance of the model equations and their terms were evaluated using statistical tools such as coefficient of determination ( $R$ -squared), Fisher value ( $F$ -value), probability ( $P$  value), and residual (Hassani et al., 2014; Roy et al., 2014). Graphs were employed to analyse the combined effect of factors on responses using 3D plots and to also analyse the predicted versus actual value plots of the response variables.

### **2.8 Adsorption Isotherm Models**

Adsorption isotherm is a curve obtained by plotting at constant temperature the quantity of adsorbate against the concentration of the substance in the original gas or solution. The equilibrium and isotherm models are also conducted to explore the adsorption behaviour and screening scale before proceeding to actual industry. In the current study, the four well-known isotherm models, namely Langmuir, Freundlich, Temkin and Dubinin–Radushkevich models are described correlation between the adsorbent and the adsorbate at equilibrium status (Foo and Hameed 2010). Many studies have been conducted in describing the adsorption process for removing different pollutants from solutions. Dehghani et al. (2017) have been used the adsorption isotherm models to investigate the behaviour of adsorption process of removing Reactive Red 120 and 196 using chitosan/zeolite composite from aqueous.

However, it was very less studies on adsorption isotherm models on removing of  $\text{H}_2\text{S}$  (aq) from solution. Haimour et al. (2005) have been studied the adsorption isotherm models for removing low concentration of  $\text{H}_2\text{S}$  (aq) on CuO and ZnO. Asaoka et al.

(2009) studied the adsorption isotherm models to investigate the behaviour of adsorption  $\text{H}_2\text{S}$  (aq) on oyster shell wastes. Wang and Pei (2012) studied adsorption capacity of ferric and alum water treatment residuals for removing  $\text{H}_2\text{S}$  (aq) using Thomas and Yan models.

Recently, the adsorption capacity of activated carbon from empty fruit bunches have for removing very low concentration of  $\text{H}_2\text{S}$  (aq) been investigated by Amosa (2015) using Langmuir and Freundlich isotherm models. Still lack of literatures on investigation of adsorption capacity of activated carbons derived from palm kernel shells and its composite with calcium extracted from egg shells using adsorption isotherm models on removal of high concentration of  $\text{H}_2\text{S}$  (aq). Therefore, this study is implemented the well-known four models such as Langmuir, Freundlich, Temkin, and Dubinin to investigate the behaviour of adsorption process of  $\text{H}_2\text{S}$  (aq) from waste water. Adsorption isotherms are commonly categorized into five types which are shown in Figure 2.9 (Thommes et al., 2015) including Type H1 loop is found in materials which exhibit a narrow range of uniform mesopores. This is also called the Langmuir isotherm and is used to describe monolayer adsorption.

Hysteresis loops of Type H2: These isotherms are used to describe multilayer physical adsorption on macropores structure. Hysteresis loops of Type H2 are given by more complex pore structures in which network effects are important. It can be characterize to H2 (a) loops and H2 (b) loops. H2 (a) loops can be attributed either to pore-blocking/percolation in a narrow range of pore necks or to cavitation-induced evaporation. The Type H2 (b) loop is also associated with pore blocking, but the size distribution of neck widths is now much larger. Solids with mixed micro- and mesoporosity show Type H2 isotherms.

Isotherms (type H3 and H4 loops) are found with microporous and mesoporous adsorbents. These are favoured by weak and strong interactions between adsorbate - adsorbent systems and the adsorbate molecules which lead to multilayer formation.

Although the Type H5 loop is unusual, it has a distinctive form associated with certain pore structures containing both open and partially blocked mesopores. These type of isotherms are commonly observed for mesoporous materials.



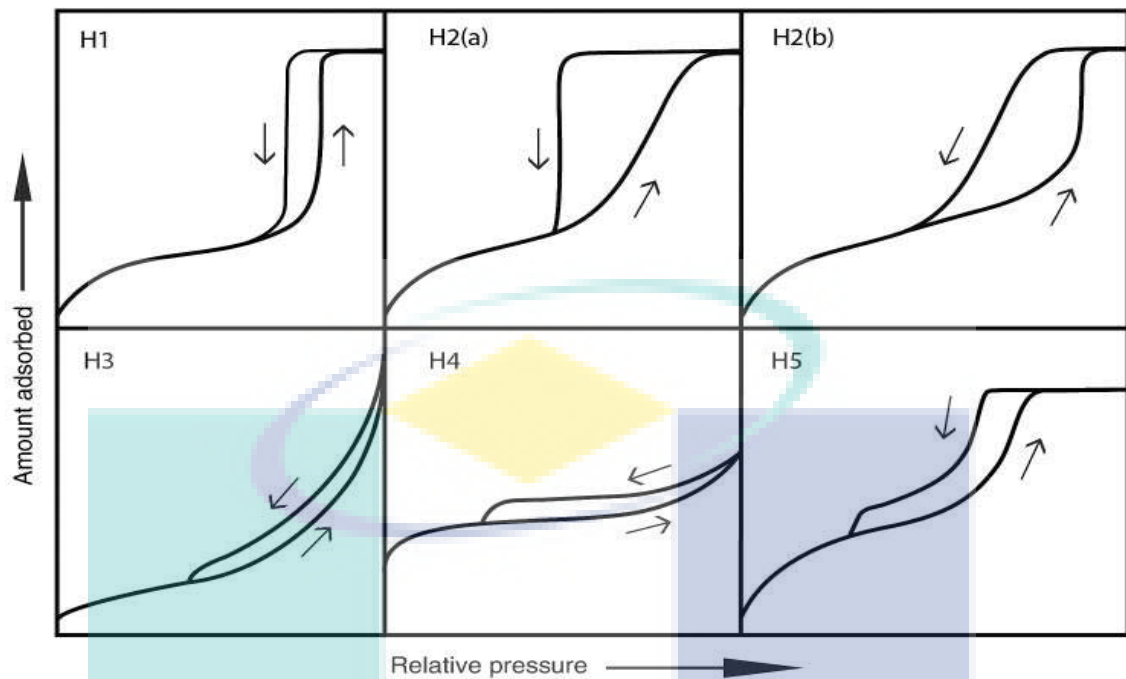


Figure 2.9 Classification of adsorption isotherm

Source: Thommes et al. (2015).

### 2.8.1 Langmuir Isotherm

Langmuir adsorption isotherm, firstly implemented to describe gas–solid-phase adsorption onto activated carbon. This empirical model assumes monolayer adsorption and it takes place at adsorption sites. This process is commonly known as homogeneous adsorption (Abdel et al., 2015). The linear forms of Langmuir’s isotherm model a can be represented in equation 2.6.

$$\frac{C_e}{q_e} = \frac{1}{Q_m b} + \left(\frac{1}{Q_m}\right) C_e \quad 2.6$$

Where  $C_e$  is the equilibrium concentration of the adsorbate ( $\text{H}_2\text{S}$ ) ( $\text{mg/L}$ ),  $Q_m$  is maximum monolayer coverage capacities ( $\text{mg g}^{-1}$ ),  $b$  is Langmuir constants ( $\text{L/mg}$ ), and  $q_e$  is the amount of adsorbate adsorbed per unit mass of adsorbent at equilibrium ( $\text{mg g}^{-1}$ ). The main characteristics of the Langmuir isotherm can be expressed in terms of the dimensionless equilibrium parameter separation factor ( $R_L$ ), which shows in equation 2.7.

$$R_L = \frac{1}{1 + bC_0} \quad 2.7$$

Where  $C_0$  is the initial concentration of  $H_2S$  ( $mg L^{-1}$ ) and  $b$  is the Langmuir constant. According to Foo (Foo and Hameed, 2010), the value of  $R_L$  indicates the shape of the isotherm to be either unfavourable ( $R_L > 1$ ), favourable ( $0 < R_L < 1$ ), linear ( $R_L = 1$ ) or irreversible ( $R_L = 0$ ).

### 2.8.2 Freundlich Isotherm

The Freundlich isotherm is the earliest known relationship describing the non-ideal and reversible adsorption. This empirical model can be applied to multilayer adsorption, with non-uniform distribution of adsorption heat and affinities over the heterogeneous surface (Foo and Hameed, 2010). This empirical assumes heterogeneous surface energies. Freundlich isotherm is widely conducted in heterogeneous systems especially, for highly interactive species or organic compounds on molecular sieves and activated carbon. The adsorption intensity or surface heterogeneity is measured by the slope ranges between 0 and 1, as its value gets closer to zero, it is becoming more heterogeneous. While, a value below unity implies chemisorption's process where  $1/n$  above one is an indicative of cooperative adsorption (Abdel et al., 2015). The correlation coefficient ( $R^2$ ) indicates the fitting error. The equation 2.8) represents the linear form of Freundlich equation.

$$\log q_e = \log K_F + \left(\frac{1}{n}\right) \log C_e \quad 2.8$$

Where  $q_e$  is the adsorption capacity at equilibrium ( $mg.g^{-1}$ ),  $C_e$  is the equilibrium concentration of the adsorbate ( $H_2S$ ) and  $K_F$  ( $mg/g$ ) ( $L/mg$ ) $^{1/n}$  and  $n$  are Freundlich constants which represent the adsorption capacity and adsorption intensity respectively.

### 2.8.3 Temkin Isotherm Model

Temkin isotherm is the early model describing the adsorption of hydrogen onto platinum electrodes within the acidic solutions. The indirect interactions between the adsorbent and the adsorbate molecules on adsorption isotherms is assumed by Temkin

isotherm. The heat of adsorption of all the molecules in the layer would decrease linearly (instead of logarithmically) due to the interactions and the adsorption is characterized by a uniform distribution of binding energies, up to some maximum binding energy (Hosseini et al., 2003; Angin, 2014). The Temkin isotherm is examined by using equation 2.9 (Demiral & Güngör, 2016).

$$q_e = \frac{RT}{b_T} \ln K_T + \left( \frac{RT}{b_T} \right) \ln C_e \quad 2.9$$

Where  $RT/b_T = B$ ,  $R$  is the gas constant (8.314 J/mol K) and  $T$  is the absolute temperature in K,  $b_T$  is the Temkin isotherm constant and  $B$  is related to the heat of adsorption (J/mol).  $K_T$  is the equilibrium binding constant (L/g).

#### 2.8.4 Dubinin–Radushkevich Isotherm

Dubinin and Radushkevich isotherm model is generally applied to express the adsorption mechanism on heterogeneous surface. It has been used to describe the liquid phase adsorption and estimated the adsorption energy from D-R equation depending on the assumption that the monolayer adsorption occurs on micropores surface based on the potential theory (Günay et al., 2007). The equation 2.10 represents Dubinin and Radushkevich linear form equation (Demiral & Güngör, 2016).

$$\ln(q_e) = \ln(q_s) - B_{DR} \varepsilon^2 \quad 2.10$$

Where  $\varepsilon$  is related to the equilibrium concentration and can be correlated as:

$$\varepsilon = RT \ln \left[ 1 + \frac{1}{C_e} \right] \quad 2.11$$

Here,  $q_s$  is the D-R monolayer adsorption capacity (mg/g) and  $B_{DR}$  ( $\text{mol}^2 \text{Kj}^{-2}$ ) is the constant related to the adsorption energy and  $E$  is the energy of adsorption (kJ/mol). The constant  $B_{DR}$  gives the mean free energy  $E$  of sorption per molecule of the sorbate when it is transferred to the surface of the solid from the solution.  $E$  can be computed by using the relationship:

$$E = \frac{1}{\sqrt{2B_{DR}}} \quad 2.12$$

## 2.9 Batch Kinetic Models Studies

Adsorption kinetics models can be used to simulate the uptake of H<sub>2</sub>S (aq) by the adsorbents. The adsorption kinetic models are conducted in many adsorption process studies. Aмоса (2015) studied kinetic models in the removal of low concentration (0.8 ppm) of H<sub>2</sub>S (aq) on activated carbon. The kinetic study involved in the removal low concentration of H<sub>2</sub>S (aq) on activated sludge was conducted by Pang et al. (2017). However, there is no enough scientific research on adsorption kinetic study using palm kernel shells based activated carbon and impregnated with calcium extracted from egg shells on the removal of high concentration of H<sub>2</sub>S (aq) from waste water. In order to fill-up this knowledge gaps, the adsorption of kinetic models studies are conducted using the Pseudo-first-order, Pseudo-second order and Intra-particle diffusion kinetic models.

### 2.9.1 Pseudo-First-Order Kinetic Model

Typically, the pseudo-first-order kinetic model is applied for predicting adsorption kinetics. This model assumes that the rate of change of solute uptake with time is directly proportional to the difference in saturation concentration. The rate constant for adsorption is determined from the pseudo-first-order equation as given by Agarwal et al. (2016).

$$\log(q_e - q_t) = \log q_e - \frac{k_1}{2.303} t \quad 2.13$$

Where,  $q_e$  and  $q_t$  are the amounts of adsorbed H<sub>2</sub>S (mg/g) at equilibrium and at time  $t$ , respectively, and  $k_1$  is the rate constant of adsorption ( $h^{-1}$ ). The  $k_1$  values were calculated from the plots of  $\log(q_e - q_t)$  versus  $t$  for different H<sub>2</sub>S concentrations.

### 2.9.2 Pseudo-Second-Order Kinetic Model

The pseudo-second-order equation based on equilibrium adsorption is expressed as follows (Agarwal et al., 2016):

$$\frac{1}{q_t} = \frac{1}{k_2 q_e^2} + \frac{1}{q_e} t \quad 2.14$$

where,  $k_2$  (g/mg h) is the rate constant for second-order adsorption.

### 2.9.3 Intra-particle Diffusion Model

Depending on the theory proposed by Weber and Morris, the intra-particle diffusion model was tested to identify the diffusion mechanism (Agarwal et al., 2016). It is an empirical functional relationship, common to a majority of the adsorption processes, where uptake varies almost proportionally with  $t^{1/2}$  rather than with the contact time  $t$ . According to this theory.

$$q_t = k_{ip} t^{1/2} + C \quad 2.15$$

Where,  $k_{ip}$  (mg/g h<sup>1/2</sup>) is the intra-particle diffusion rate constant.

### 2.10 Thermodynamics of Adsorption Equilibrium

The study of thermodynamic parameters could provide an in-depth information regarding the structural changes and the inherent energy after adsorption. Thermodynamic parameters can be calculated, when the adsorption phenomenon reaches equilibrium. These parameters comprise the Gibbs free energy change ( $\Delta G^\circ$ ), standard enthalpy change ( $\Delta H^\circ$ ) and the standard entropy change ( $\Delta S^\circ$ ). Gupta et al. (2003) investigated the adsorption process using activated slag and activated carbon to adsorb basic red dye. The results revealed that the positive entropy indicated an increased in randomness after the adsorption of basic red on activated carbon and activated slag. The negative values of Gibbs free energy change ( $\Delta G^\circ$ ) showed the spontaneous nature of basic red adsorption on both adsorbents. The positive values of enthalpy change ( $\Delta H^\circ$ ) indicated the endothermic nature of the adsorption process. Ramesh et al. (2005) investigated the thermodynamic parameters for the removal of heavy metal and dyes from waste water, using a low cost adsorbent. They found out that when adsorption capacity increased with temperature, the process was claimed to be endothermic, and vice versa. It can therefore be concluded that, there is no literature reporting the thermodynamics on an activated carbon derived from palm kernel shell which is impregnated with calcium extracted from egg shells to remove of high concentration of H<sub>2</sub>S (aq) from waste water.

## 2.11 Knowledge Gap

The previous works on adsorption process of removal of H<sub>2</sub>S (aq) from solution were reviewed in this study. Various parameters were compared and summarized in Table 2.12. It can be seen from Table 2.12, there was few investigations conducted on the adsorption of H<sub>2</sub>S (aq) from waste water. For instances, Haimour et al. (2005) studied the adsorption of low concentration H<sub>2</sub>S (aq) on CuO and ZnO. The waste materials of crushed oyster shell was used by Asaoka et al. (2009). Recently, Pang et al. (2017) investigated the possibility of using activated sludge to remove low concentration of H<sub>2</sub>S (aq) from solution. Only a single study was conducted to investigate the activated carbon derived from agriculture wastes to remove of H<sub>2</sub>S (aq) (Amosa, 2015). He investigated the removal of low concentration (0.8 ppm) of H<sub>2</sub>S (aq) from oil mill effluent using empty fruit bunches based activated carbon. He studied the optimization of preparation conditions using 2-level full factorial approach. However, there is no present literature on the possibility of using abundant agriculture wastes materials in Malaysia such as coconut shell, palm kernel shell, and wood saw dust. The possibility to convert this wastes materials to activated carbons (ACs) and investigate their removal efficiency at high concentration (100- 1000 mg/L) of H<sub>2</sub>S (aq) were conducted in the present work. In addition, the enhancement of the adsorption capacity through the modification of the surface chemistry of activated carbons with calcium extracted from egg shells to produce calcium impregnated activated carbons (IACs) was also not mentioned in the literatures. Therefore, the impregnation, optimization, modelling, and thermodynamic study of the selected adsorbents were conducted to cover these gaps as presented in Table 2.12.

Table 2.12 Literature summary on adsorption of aqueous H<sub>2</sub>S (aq) using different adsorbents

Conc. (mg/L)	Types of adsorbent	Activation method	Impregnation method	Optimization of		Parameters studied	Adsorp. isotherm	Kinetic models	Thermo dynamic	References
				preparation condition	operating condition					
5	CuO and ZnO	-	-	-	-	Time, conc.	Langmuir, Freundlich, Redlich-Peterson	-	-	Haimour et al. (2005)
5-800	Crushed oyster shell	-	-	-	-	Time, conc.	Langmuir, Freundlich, Henry	-	-	Asaoka et al. (2009)
200-800	Ferric and alum water	-	-	-	-	Time, conc., pH	Thomas, Yan	-	-	Wang and Pei (2012)
10-100	Carbonated steel slag	-	-	-	-	Time, conc.	-	✓	-	Asaoka et al. (2013)
30	Activated sludge	-	-	-	-	Time, conc.	Langmuir, Freundlich,	✓	-	Pang et al. (2017)
0.8	ACs from empty fruit bunch (EFB)	Physical activation (steam)	-	-	2 level factorial	Time, conc.	Langmuir, Freundlich,	✓	-	Amosa (2015)

## CHAPTER 3

### RESEARCH METHODOLOGY

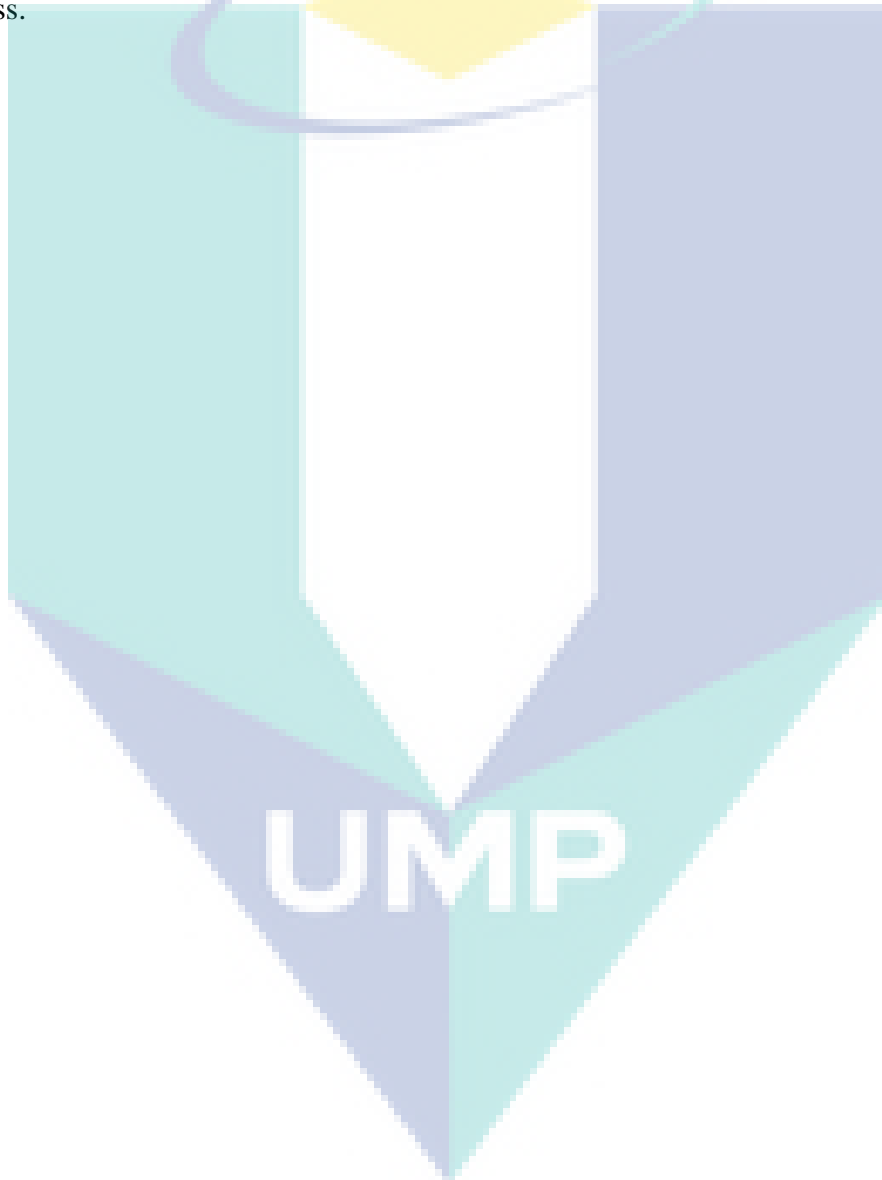
#### 3.1 Introduction

This chapter consists of six sections. The first section presents the detailed descriptions of materials and chemicals employed in this study. The overall methodology was explained using flowchart in section 2. In Section 3, preparation, carbonization, and activation process of activated carbons (ACs) were demonstrated along with impregnation of activated carbons (IACs) with calcium extracted from egg shells. While, section 4 was discussed the characterization techniques used for characterizing ACs and IACs. Preliminary studies on operating conditions for the removal of H<sub>2</sub>S (aq) from simulated waste water was presented in Section 5. Section 6 was explained the steps and procedures followed to conduct the experiments, processes, optimizing and modelling.

The research methodology employed in this study involve collection and preparation of raw biomass materials as illustrated in Figure3.1. The first stage involves the collection and preparation of raw biomass materials. The material preparation was followed by activation process, screening, and optimization of the precursors such as coconut shell (CNS), palm kernel shell (PKS), and wood saw dust (WSD). Chemical activation method was employed to produce activated carbons as adsorbents and labelled as follows: palm kernel shell based activated carbon (ACPKS), coconut shell based activated carbon (ACCNS), and wood saw dust based activated carbon (ACWSD). Thereafter, the activated carbons were modified (impregnation) with calcium extracted from egg shells to produce impregnated activated carbon (IACs) as adsorbents. The IACs were labelled as following: calcium impregnated activated carbon (Ca-ACCNS, Ca-ACPKS and Ca-ACWSD). Subsequently, the prepared adsorbents were characterized by SEM/EDX, BET, FTIR, TGA, XRD and XPS.



$\text{H}_2\text{S}$  (aq) solution (simulated waste water) was prepared for subsequent studies. Investigation and determination the removal (the efficiency) of the ACs and IACs toward dissolved  $\text{H}_2\text{S}$  (aq) from solutions carried out. The effective adsorbent was selected. The optimization of the preparation conditions of the selected adsorbent was also performed. Furthermore, the operating conditions of removal of  $\text{H}_2\text{S}$  (aq) from actual waste water were screened and optimized. Finally, the thermodynamic, isotherm and kinetic models studies were conducted for the selected adsorbent to clarify the behaviour of adsorption process.



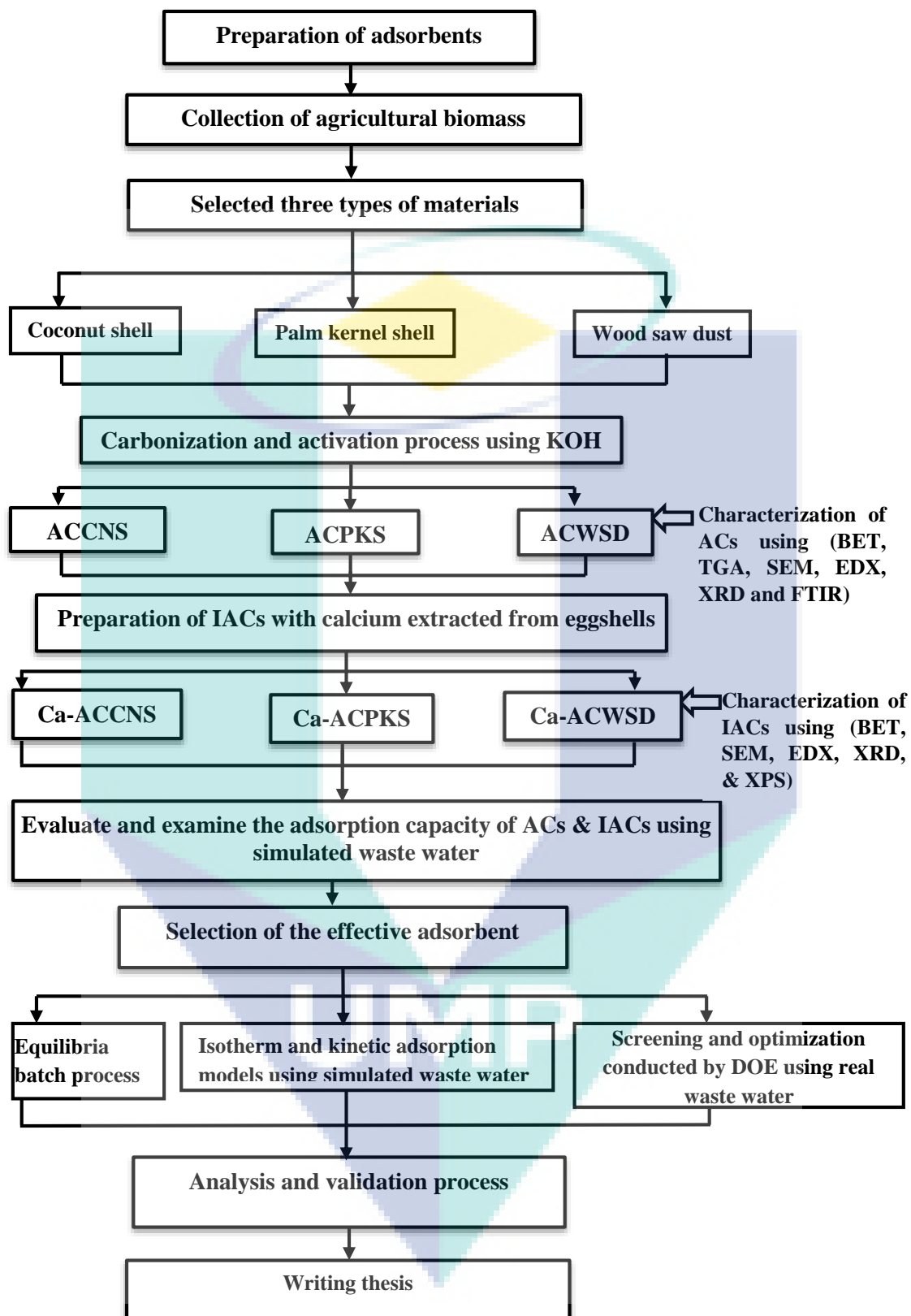


Figure3.1 Overall methodology flowchart

### 3.2 Synthesis of ACs from Agricultural Wastes

The detailed description of the steps involved in the preparation of the ACs from agricultural wastes materials was explained in this section. The three precursors used for the preparation of the ACs were coconut shell (CNS), palm kernel shell (PKS), and residual wood sawdust (WSD) and they were locally sourced as agriculture wastes as seen in Figure 3.2. The coconut shell (CNS) was collected from plantation. In addition, palm kernel shell (PKS) was collected from United Palm Oil Mill, Malaysia. While residual wood sawdust (WSD) was collected from local sawmill shop in Kuantan, Malaysia. Moreover, egg shells wastes were used as precursor for calcium (Ca) in this study for the modification of the ACs which was collected from local restaurant. Each material was thoroughly cleaned to remove moistures and subsequently dried in an oven at 110°C. Dried samples were grinded in different particle size (0.5-1) mm and stored in a sealed container. While the egg shells were grinded to a powdery form (0.25-0.3) mm. The resulting precursors were stored in sealed containers.



Figure 3.2 Raw materials for preparation of activated carbons from (a) coconut shell, (b) palm kernel shell, (c) wood saw dust

#### 3.2.1 Carbonization Process of ACs

The sample of CNS, PKS, and WSD were carbonized at 700 °C at heating rate of 10 °C/min (first pyrolysis) for 2 h in an inert atmosphere (N<sub>2</sub> flow of 150 mL/min) in a horizontal tubular furnace placed in a tube furnace (Nabertherm GmbH, Germany). The carbon produced was then drenched in potassium hydroxide (KOH) solution (molarity of 0.2304 mol/L) with an impregnation proportion of 4:1 for 24 h (Stavropoulos and

Zabaniotou, 2005). The impregnation ratio with activating agent proportion (IR) was estimated from Equation 3.1).

$$IR = \frac{M_{KOH}}{M_{carbon}} \quad 3.1$$

Where  $M_{KOH}$  is the mass of KOH pallets (g) and  $M_c$  is the mass of carbon (g). The schematic representation of the detail procedure of the carbonizations and activation process of the precursors shows in Figure 3.3.

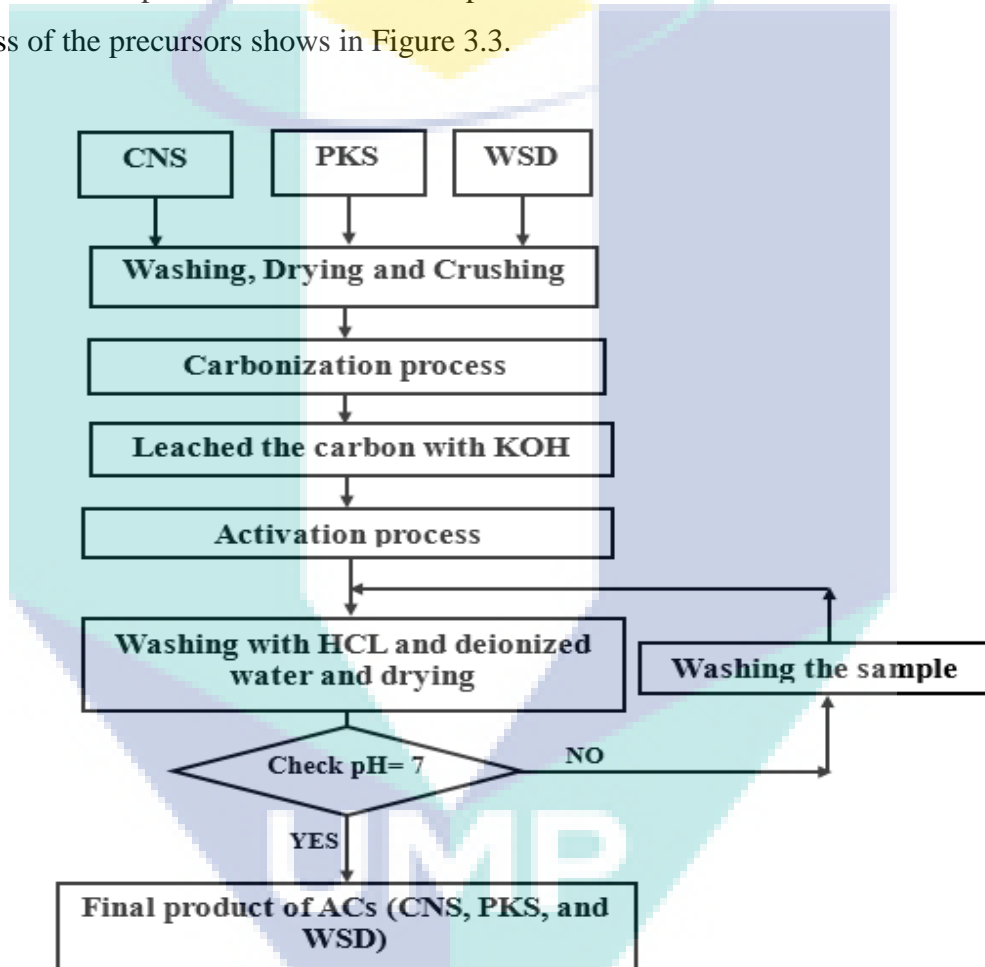


Figure 3.3 Carbonization and activation process of ACs

### 3.2.2 Activation Process of ACs

After carbonization, the resulting treated carbon materials were placed in a tubular horizontal furnace (Nabertherm, GmbH, Germany 212080 /R 50/500/12) and gradually heated with inert gas ( $N_2$  flow of 150 mL/min) until the maximum temperature of 750 °C was attained. Then, the  $N_2$  gas was replaced with  $CO_2$  gas for 2 h (Kazmierczak et al., 2015; Jiang et al., 2016). Activated carbons (ACs) produced were cooled and washed

using deionized water with HCl (0.1 M) three times to remove the residual KOH. The acid-washed samples were further washed with distilled water until neutral pH was obtained. The final product was dried in an oven at 110 °C for 24 h and coded as ACCNS, ACPKS, and ACWSD. The yield of the carbon materials produce were estimated using equation 3.2).

$$\text{Yield (\%)} = \frac{W_c}{W_o} \times 100 \quad 3.2$$

Where,  $W_c$  and  $W_o$  are the dry weight of the final sample and the dry weight of precursor, respectively.

### 3.3 Modification and Impregnation Process of ACs

#### 3.3.1 Extraction of Calcium from Egg Shells

The egg shells thoroughly washed with deionized water to remove any trace of impurities. After that, it dried in oven at 110 °C. The resulting dried egg shells were grind to powdery form. The stripped inner membrane of egg shells soaked in acetic acid solution (25-100 %v) to obtain calcium solution with different concentrations (Treviño et al., 2013). In this stage, a ratio of 0.05 g of egg shells per mL of acetic acid with different concentration range (25-100 %v) was used.

The membrane of egg shells separated from the solution by filtering since the membrane was insoluble in acetic acid. A temperature controlled shaker was used to shake the mixture (*i e*, egg shells and acetic acid) at 150 rpm for 5 h. The Atomic Absorption Spectrometer (AAS) was used to measure the concentration of calcium from the solution. Finally, the obtained calcium solution with concentration of 72.5 mg/L was utilized for the impregnation of the ACs. While the concentration of calcium from oyster shells was 64.6 mg/L. Thus, egg shells were preferred as an impregnation agent. Three samples were measured and the mean of results are calculated. The details results of measuring calcium concentration shows in Appendix D.

### 3.3.2 Synthesis Process of IACs

The modification of the ACs was done in accordance with the method reported by Guijarro et al. (2011). The calcium solution extracted from egg shells was used to modify the surface chemistry of ACs. A proportion of 0.2 g of activated carbons per mL of calcium solution concentration of 72.5 mg/L was utilized for the impregnation of ACs. This impregnation process was performed under constant stirring (150 rpm) and at 30 °C for 4 h. The solution was evaporated at 66 °C and then the sample was dried at 100 °C for 15 h. Finally, the impregnated activated carbons (IACs) were heated at a desired temperature (800-1000 °C) for 1.5 h in a tubular horizontal furnace (Nabertherm, GmbH, Germany 212080/R 50/500/12). The IACs were washed with deionized water until neutral pH was constant and finally dried at 100 °C for 24 h. The IACs such as Ca-ACCNS, Ca-ACPKS and Ca-ACWSD were stored in a sealed flask and kept in a desiccator until it was used for characterizations and adsorption tests. The whole procedure of the modification process is shown in Figure 3.4.

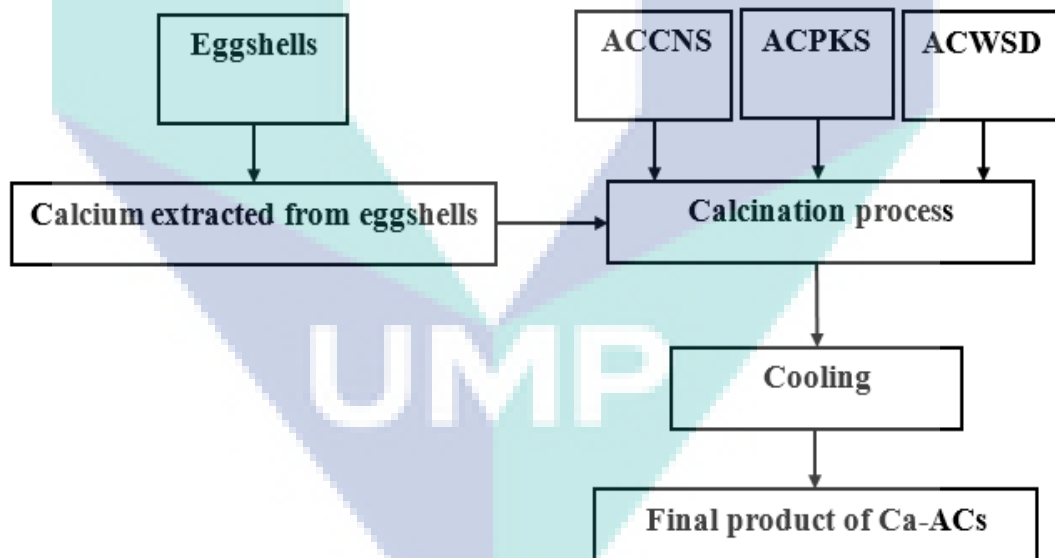


Figure 3.4 Preparation and modification of surface chemistry of IACs with calcium extracted from egg shells

### 3.4 Characterization of the ACs and IACs

Various analytical techniques employed in this study to determine the morphology, surface chemistry, and the structure of the optimally prepared ACs and IACs. All the adsorbents (ACs & IACs) properties and conditions investigated and characterized. The names of equipment, brand and models for characterizations study shows in Table 3.1. The analytical approaches used are represented in Figure 3.5.

Table 3.1 Equipment employed for characterization study

Brand S/N	Equipment	Specification/model
Toledo AG	PH meter (Mettler-Toledo AG (8603))	Mettler-Toledo AG (8603)
Hitachi 3030	Scanning electron microscope (SEM)	Hitachi 3030 plus, Japan
Hitachi 3030	Energy Dispersive X Ray Test (EDX)	Hitachi 3030 plus, Japan
ASAP 2020	Sorption of Nitrogen	ASAP 2020 Micromeritics, USA.
JASCO-480	Fourier transform infrared spectroscopy	JASCO-480 Plus, Japan
Q500.0617	Thermal gravimetric analysis (TGA)	TGA Q 500
RIGAKU	X-ray diffraction (XRD)	RIGAKU Miniflex II
PHI5000	X-ray photoelectron spectroscopy (XPS)	PHI5000VersaProbeII

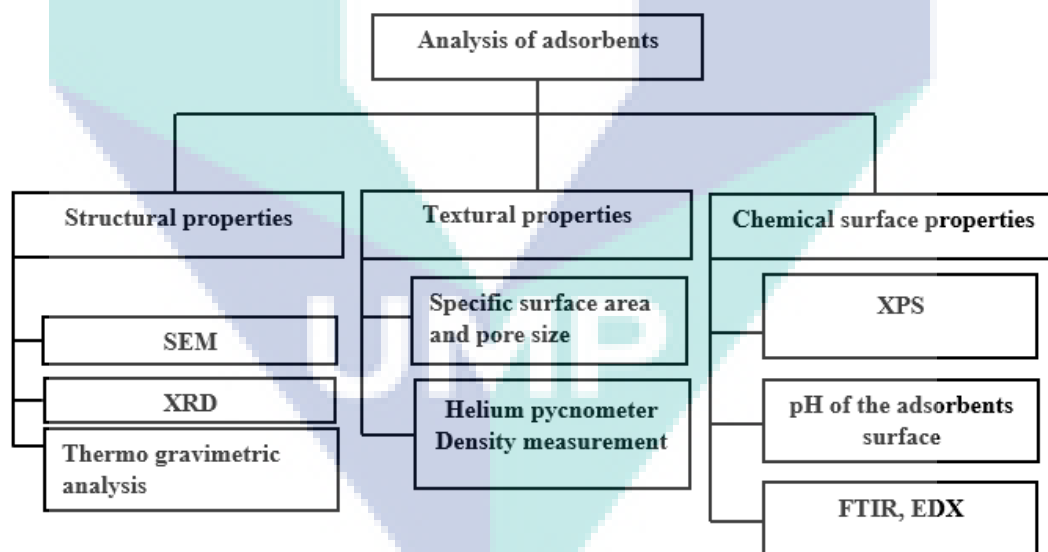


Figure 3.5 Different techniques of analysis for adsorbents characterization

#### 3.4.1 Scanning Electron Microscope (SEM)

SEM used to measure the morphology of the adsorbent surface. It is an electron microscope used for scanning a sample with a focused beam of electrons to produce images. The working principle was based on the interaction of the electrons with atoms



in the particle sample resulting in many signals that contain information about the sample's composition and surface topography. Observation was made through a scanning electron microscope (SEM) and the porous material analysed to determine if the porous properties were elucidated. The SEM ran at 20kV accelerating potential on a Hitachi TM 3030 Plus, Japan.

#### **3.4.2 Energy Dispersive X-Ray Test (EDX)**

Elemental analysis of the samples was conducted using Energy-Dispersive X-ray spectroscopy (EDX) Hitachi TM 3030 Plus, Japan. EDX was a useful tool to investigate the composite elements on the surface of adsorbents. It investigated an interaction of some source of X-ray excitation on the sample. Its characterization capabilities depend mainly on the basic principle that every individual element possesses a unique atomic structure, which allows a specific set of peaks on its X-ray spectrum. A high-energy beam of charged particles such as protons or electrons, or a beam of X-rays, was concentrated on the sample to generate the emission of characteristic X-rays from a specimen.

#### **3.4.3 pH Measurement of Adsorbent Surface and Solution**

The test was conducted to all six adsorbents. A sample of 0.4 g of dry carbon powder was added to 20 mL of water, and the suspension were stirred overnight to mixed solution. Then the sample filtered, and the pH of the solution measured using a pH meter (Mettler-Toledo AG (8603)). The obtained result was considered as the pH value of the adsorbent surface. The pH of solution was also measured before and after adsorption process.

#### **3.4.4 Sorption of Nitrogen**

The pore structures of the adsorbents particles, related to surface area, pore volume, and pore size distribution, were obtained by measuring N<sub>2</sub> adsorption-desorption isotherms at -196 °C using an ASAP 2020 apparatus (Micromeritics Co., USA). At the beginning of the experimental, the samples were heated at 120 °C and then outgassed at this temperature under a vacuum of 10<sup>-5</sup> Torr to constant pressure. Brunauer-Emmett-Teller (BET) and Barrett-Joyner-Halenda (BJH) methods were used to estimate the specific surface area (S<sub>BET</sub>, m<sup>2</sup>/g) and total pore volume (V<sub>t</sub>, cm<sup>3</sup>/g at STP) of the adsorbent from the adsorption and the desorption isotherms. The actual density (ρ<sub>s</sub>) of the

sample was measured by the helium displacement method using an AccuPyc II 1340 pycnometer (Micromeritics Co., USA).

#### **3.4.5 Fourier Transform Infrared Spectroscopy (FTIR)**

Fourier transform infrared spectroscopy (FTIR) mainly employed as a qualitative technique for evaluating the chemical structure of carbon materials. It considered as a helpful tool to observe the functional groups on the surface of the solid materials. Different functional groups absorbed infrared light at distinct wavelengths. The FTIR spectra of ACs were measured over the frequency range 4000 to 400  $\text{cm}^{-1}$  at resolution of 4  $\text{cm}^{-1}$ . FTIR analysis was performed using JASCO-480 Plus, Japan.

#### **3.4.6 Thermal Gravimetric Analysis (TGA)**

Thermogravimetric analysis (TGA) was conducted using (TGA Q 500) to find the thermal stability of materials during the carbonization and activation process. The percentage of weight loss was displayed the effect of temperature on the materials. The sample was maintained at 120  $^{\circ}\text{C}$  for 2 h and then heated to 900  $^{\circ}\text{C}$  with a heating rate of 10  $^{\circ}\text{C}/\text{min}$  in a high purity nitrogen atmosphere.

#### **3.4.7 X-Ray Diffraction (XRD)**

The position and intensities of XRD peaks provided information about the shape of the crystalline structure. The XRD patterns were recorded using X-ray diffractometer (RIGAKU Miniflex II) operating at 40 Kv and 40 mA with Cu  $\text{K}\alpha$  radiation ( $\lambda = 1.5406 \text{ \AA}$ ). The  $2\theta$  ranging from 5 to 80 degree with a scanning rate of 0.02 degree/min was recorded at room temperature (23  $^{\circ}\text{C}$ ). The X-ray diffractometer was operated with  $1^{\circ}$  diverging and a continuous scan was carried out with a step size of  $0.015^{\circ}$  and a step time of 0.2 second.

#### **3.4.8 X-ray Photoelectron Spectroscopy (XPS)**

X-ray photoelectron spectroscopy (XPS) is a spectroscopic technique and a surface-sensitive quantitative that measures the composition of elemental at the parts per thousand range, chemical state, empirical formula and electronic state of the elements that exist within a material. The surface chemistry of a material could be analysed using XPS. It showed all elements on the surface of the sample and the quantification table indicating

all elements observed, their atomic percentages and binding energies. X-ray photoelectron spectroscopy (XPS) was the useful technique that used to measure the chemical states of elements composition on the surface. It could be utilized to analyse the surface chemistry of a material such as inorganic compounds, metal alloys, polymers, elements, catalysts, glasses, ceramics, and woods.

### 3.5 Preparation of Simulated and Some of Real Waste Water

#### 3.5.1 Preparation of Simulated Waste Water

The simulated waste water containing  $\text{H}_2\text{S}$  (aq) solution were prepared by adapting the procedure used by Asaoka et al. (2009). Sodium sulfide ( $\text{Na}_2\text{S}\cdot 9\text{H}_2\text{O}$ ) dissolved in distillate water was purged with  $\text{N}_2$  gas to avoid oxidation of sulfide to get various concentration of  $\text{H}_2\text{S}$  (aq) as seen in Table 3.2 (Edathil et al., 2017). The theoretical calculations of  $\text{H}_2\text{S}$  (aq) are showed in appendix C. The pH of the solution was reduced from pH value of 11.5 to neutral value using 0.1 M of HCl.

Table 3.2 Preparation of different concentration of dissolved  $\text{H}_2\text{S}$  (aq) and the weight of  $\text{Na}_2\text{S}\cdot 9\text{H}_2\text{O}$

Preparation sample of waste water	Concentrations of dissolved $\text{H}_2\text{S}$ (aq) (mg/L)	Weight of $\text{Na}_2\text{S}\cdot 9\text{H}_2\text{O}$ (g/L)
Simulated waste water	200	1.5
	400	3.0
	600	4.5
	800	6.0
	1000	7.5

#### 3.5.2 Real Waste Water

The real petrochemical waste water was taken from a petrochemical industry in the East Coast region of Malaysia. A 5 liter of actual waste water has been used for optimization process of the operating conditions using Design of Expert (DOE). The characteristics of real waste water is below in Table 3.3. The characteristic of petrochemical waste water was conducted in the lab. In this study, the real waste water was used to investigate the optimum conditions that can remove the  $\text{H}_2\text{S}$  (aq) in the same conditions with simulated one to validate the optimization process.

Table 3.3 Characteristics of petrochemical waste water

Parameters	Value	Regulations standard (A)	Regulations standard (B)
Concentration of H <sub>2</sub> S (aq) (mg/L)	1000	0.5	0.5
COD (mg/L)	1665	80	200
pH	7	6.0-9.0	5.5-9.0

### 3.6 Batch Equilibrium Studies of H<sub>2</sub>S (aq) Adsorption by ACs

Batch adsorption experiments were conducted in a set of 250 mL Erlenmeyer flasks containing 0.1 g adsorbent and 100 mL of H<sub>2</sub>S (aq) solutions at various initial concentrations (100 to 1000 mg/L) were investigated. This range was selected based on the current study scope which targeted the high concentration of H<sub>2</sub>S (aq) due to lack of literatures. The flasks were agitated in a thermostatic orbital shaker at 150 rpm and 30 °C until the equilibrium was reached. The pH of the solution was controlled to neutral by using a diluted solutions of 0.1 M HCl.

#### 3.6.1 Analysis of H<sub>2</sub>S (aq) Concentration

The concentrations of H<sub>2</sub>S (aq) in the simulated and actual waste water were measured by using spectrophotometer HACH DR2800 which conducted using sulfide reagent 1&2 (Method: Methyl Blue) (Edathil et al., 2017). The procedure that used to measure the H<sub>2</sub>S (aq) concentration as a followed. Firstly, the blank sample was prepared by fill a sample cell with 10 mL deionized water. Then a 0.5 mL sulfide reagent 1 was added to sample cell. The mixture was swirl to mix. After that, a 0.5 sulfide reagent 2 was added to sample cell. Secondly, the spectrophotometers and started the instrument timer. A 5-minute reaction time were started. When the timer expired, the blank inserted into the cell holder and pushed zero. The display was showed 0 mg/L. Finally, the prepared sample was inserted into the cell holder then pushed read. The results showed in mg/L. The solution shows pink and then blue if sulfide is in the sample. The adsorption capacity ( $q_e$ , mg/g) was calculated by equation 3.3). Subsequently, the initial and final concentrations were measured after the suspensions were filtered.

$$q_e = \frac{(C_0 - C_e)V}{m} \quad 3.3$$

Where  $V$  is the solution volume (L),  $m$  is the adsorbent amount (g) and  $C_0$  and  $C_e$  are the initial and final  $H_2S$  (aq) concentrations, respectively. All adsorption experiments were repeated at same conditions with a deviation of 5 %. All measurements and experiments were conducted in a fume hood since  $H_2S$  is a harmful gas. The removal efficiency (RE) was defined as:

$$RE = \frac{C_0 - C_e}{C_0} \times 100\% \quad 3.4$$

Where  $C_0$  is initial concentration of solute (mg/L),  $C_e$  is equilibrium concentration of solute (mg/L),  $V$  is volume of solution (L) and  $m$  is mass of activated carbon used (g). The adsorbent sample yield can be calculated using the equation 3.2).

### 3.6.2 Preliminary Study of the Parameters

Preliminary study was done to investigate the best process conditions and ranges for removal of  $H_2S$  (aq) from waste water. In this study, initial concentration (mg/L), contact time (min), amount of adsorbent (dosage (g)), agitation speed (rpm), and pH were investigated. The experimental equipment employed in this study shows in Table 3.4.

Table 3.4 The experimental rig employed in this study

Brand S/N	Equipment	Specification/model
DR2800	Spectrophotometer	HACH DR2800
SI-100D	Shaker Incubator	SI-100D
212080	Furnace (Nabertherm, GmbH, Germany)	R 50/500/12

The concentration parameter was considered as one of the important factors that could significantly influence the removal efficiency (RE) of the pollutant from waste water. The ranges of initial concentrations investigated were as follows: 200, 400, 600, 800 and 1000 mg/L. The initial concentrations used in this study was in accordance with that reported by Hariz and Monser, (2014). The other parameters were constant during the investigation of the effect of the initial concentration on RE of  $H_2S$  (aq). For instance, contact time (min) (Fang et al., 2013), dosage (g) (Asaoka et al., 2013), solution pH (Haimour et al., 2005; Wang and Pei, 2012), and agitation speed (rpm) were constant with values of (540 min, 1 g/L, 7, & 150 rpm) respectively. Table 3.5 shows the various concentration ranges and others constant factors.

The effect of contact time was important factor. To investigate the effect of contact time, 0.1 g of the adsorbent was added to 100 ml of solution concentration of 200 mg/L of H<sub>2</sub>S (aq) in vital flask size 250 ml. The batch container was sealed tightly and subsequently shaken at 150 rpm. The solution of H<sub>2</sub>S (aq) was neutral. All the details information shows in Table 3.5.

The amount of adsorbent used was investigated as shows in Table 3.5. It was important to study the dosage to know the adsorption capacity of adsorbent. In addition, the results have been agreed with other work that studied by Asaoka et al. (2013). Table 3.5 shows the variations of the pH of solution keeping the other factors constant. The pH was investigated from value of 5 to 9. The results were supported by other researchers reported in elsewhere study (Haimour et al., 2005; Wang and Pei, 2012). The agitation speed was an important factor that contributed on removal efficiency of H<sub>2</sub>S (aq). The variety of agitation speed with constant other factors demonstrate in Table 3.5.

Table 3.5 Preliminary study of operating condition parameters

Concentrations (mg/L)	Contact time (h)	Dosage (g)	Solution pH	Agitation speed (rpm)
200	1	0.1	5	0
400	3	0.2	6	50
600	5	0.3	7	100
800	7	0.4	8	150
1000	9		9	200

### 3.6.3 Comparison Study between the Adsorbents

The six adsorbents were subjected to comparison study toward the RE of H<sub>2</sub>S (aq) from simulated waste water. The optimization of preparation conditions of selected adsorbent were investigated using simulated waste water. Moreover, the operating conditions of the removal of H<sub>2</sub>S (aq) from actual petroleum waste water for selected adsorbent were conducted. The selected adsorbent was also subjected to isotherm, and kinetic adsorption models and thermodynamic studies.

### 3.7 Optimization of Adsorption Process

The flow chart of optimization of adsorption process using Design of Expert version (DX10 USA) shows in Figure 3.6. In this study, two optimization process were conducted. Firstly, the significant factors of preparation conditions for the selected



adsorbent were optimized using response surface methodology (RSM). Response surface methodology (RSM) was a statistical experimental design that solved all these limitations of a classical method process. The central composite design (CCD) was employed to study optimization, interaction between factors and the effect of factors toward their responses. It used to develop the correlation between the response surface and factors. The optimum preparation conditions of selected adsorbent investigated. Secondly, the screening and optimization process of operating conditions of H<sub>2</sub>S (aq) from actual petroleum waste water using selected adsorbent conducted. For screening study, the 2 level factorial design used to investigate the significant of factors on the responses during the adsorption process of dissolved H<sub>2</sub>S (aq) from waste water. While, Response surface methodology (RSM) with central composite design (CCD) employed to study optimization, interaction between operating conditions and the effect of factors toward their responses (Bagheri et al., 2016). Analysis of variance (ANOVA) was conducted to determine the regression and graphical analysis with statistical significance. ANOVA was subsequently performed to explore and indicate the significant of the models. Optimization strategy utilized to decide the optimum preparation and operation conditions for the procedure factors under consideration. To accomplish this, objectives were set with requirements. For each of the variables, goal was set “in range” with limitations. For the responses surface, the objective for RE and selected adsorbent yield were set “maximize”. Moreover, model validation was carried out by conducting batch experiment under optimum preparation conditions. In order to evaluate the validity of the model, experimental values got were compared with the model predicted values. The batch equilibrium studies using (DOE) demonstrates in Figure 3.6.



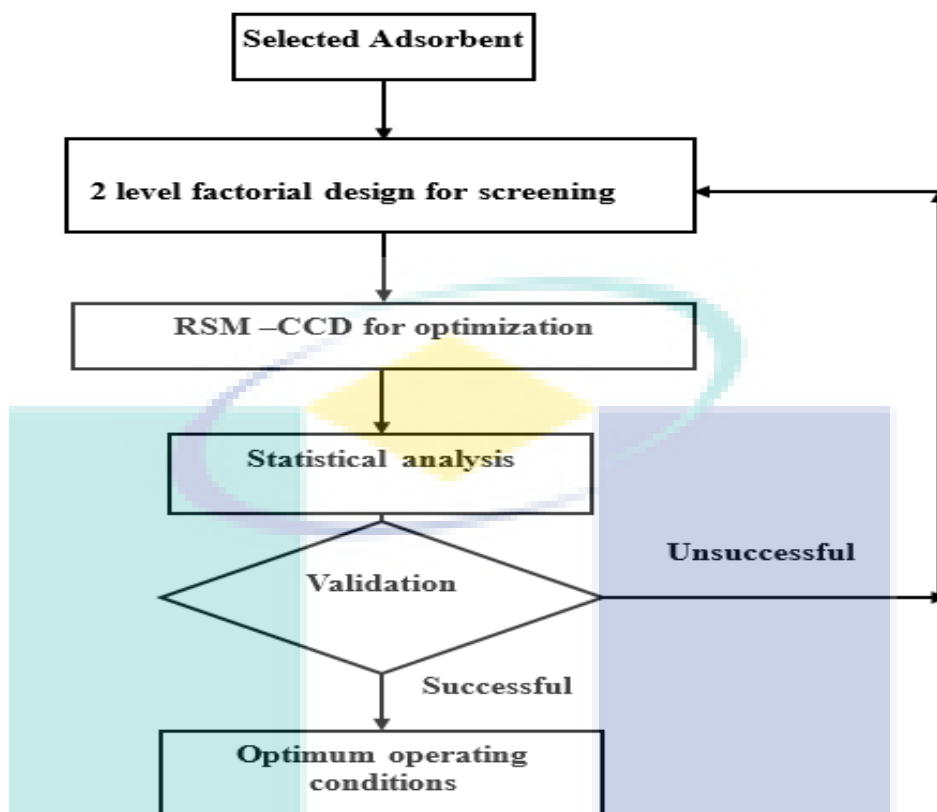


Figure 3.6 Batch equilibrium studies using (DOE)

### 3.7.1 Optimization of Preparation Conditions of Selected Adsorbent

The modification method of surface chemistry of selected adsorbent was done according to procedure conducted by Guijarro et al. (2011). The calcium solution extracted from egg shells was used to modify the surface chemistry of selected adsorbent. The details explanation of the process was provided in section (3.3.2). Finally, the selected adsorbent was heated at desired temperature for a period of time as suggested by CCD software. The three parameters investigated were calcination temperature (°C); concentration of calcium solution (%v) for impregnation; and calcination contact time (min) with the responses are RE (Y1) and selected adsorbent yield (Y2). The variables of preparation conditions of selected adsorbent for optimization study shows in Table 3.6.

Table 3.6 Independent parameters, ranges and dependent responses for ptimization of preparation conditions of selected adsorbent

Factors	Unit	Coded variable levels				
		- $\alpha$	-1	0	+1	+ $\alpha$
Calcination temperature	°C	731	800	900	1000	1068
Calcium concentration	V%	8	25	50	75	92
Calcination contact time	min	10	30	60	90	110

### 3.7.2 Optimization of Operating Conditions for Adsorption Process

The DOE technique was implemented in the study of screening and optimization of operating conditions of removal of H<sub>2</sub>S (aq) from actual petroleum waste water. The 2 level factorial design has been used for screening purpose of the effecting factors. While the response surface methodology (RSM) was used for optimizing significant and related factors by using CCD approach. The Effect of initial H<sub>2</sub>S (aq) concentration (ppm), adsorption contact time (min), dosage of adsorbent (g), pH, and agitation speed were investigated. At the beginning, the screening approach were conducted using factorial design. The factors of initial H<sub>2</sub>S (aq) concentration, adsorption contact time, adsorbent dosage, pH, and agitation speed were investigated as shown in Table 3.7. All the ranges were chosen based on the preliminary studies. For example, the dosage of 0.75-1 g/L could be adsorbed the target concentration. Moreover, the effect of dosage was not significant to the removal efficiency of H<sub>2</sub>S (aq).

Table 3.7 Screening removal factors of H<sub>2</sub>S (aq) on selected adsorbent (2 level factorials design)

<b>Name</b>	<b>Unit</b>	<b>Type</b>	<b>Low</b>	<b>High</b>
Initial H <sub>2</sub> S (aq) concentration	mg/L	Numeric	500	700
Adsorption contact time	min	Numeric	420	540
Adsorbent dosage	g/L	Numeric	0.75	1
pH	-	Numeric	2	12
Agitation speed	rpm	Numeric	100	200

The optimization process of significant factors were important to determine the optimum operation conditions of significant factors for removal of dissolved H<sub>2</sub>S (aq) from waste water. The significant factors after screening stage were initial H<sub>2</sub>S (aq) concentration, adsorption contact time and adsorbent dosage. The factors, unit and ranges all together presents in Table 3.8. Analysis of variance (ANOVA) was subsequently performed to explore and indicate the significant of the models and to show the interaction between factors. The validation study was conducted after optimization process to investigate the optimal removal operation conditions. The experiment values compared well with predicted values to calculate the percentage error of the model. Table 3.8 was design depending on the optimum conditions from screening process. The optimum conditions were used as a centre point of optimization study.

Table 3.8 Optimization of significant factors of adsorption of H<sub>2</sub>S (aq) on the selected adsorbents using (RSM)

Factors	Unit	Coded variable levels				
		- $\alpha$	-1	0	+1	+ $\alpha$
Initial H <sub>2</sub> S (aq) concentration	mg/L	163	300	500	700	836
Adsorption contact time	min	338	420	540	660	742
Adsorbent dosage	g	0.579	0.75	1	1.25	1.42

### 3.8 Batch Kinetic and Thermodynamic Study

The adsorption modelling study were important to investigate the adsorption behaviour of the adsorption process and to show the type of adsorption process. It was combined of adsorption isotherm and kinetic models and thermodynamic study.

#### 3.8.1 Adsorption Isotherm Models

Adsorption isotherms were basically important for describing the manner in which solutes interact with adsorbents. Moreover, it also demonstrated the manner in which adsorbed molecules distributed between the solid and liquid phases and the time taken to reach an equilibrium state. Generally, isotherms models were very important to understand the adsorption mechanisms. The analysis of the data by different isotherm models fitting was an important step for finding a suitable model that can be used for describing the adsorption process (Demiral & Güngör, 2016). Adsorption isotherm models provided a fundamental and useful information for design process of full scale operation unit stream (Amosa, 2015). Equilibrium data were then fitted using four different adsorption isotherm models: Langmuir, Freundlich, Temkin, and Dubinin–Radushkevich models, which were considered to be well-known equilibrium adsorption isotherm models. All the isotherms models equations were appeared on Table 3.9 (Foo and Hameed, 2010). However, the whole procedure of the process of the isotherm models shows in Figure 3.7.

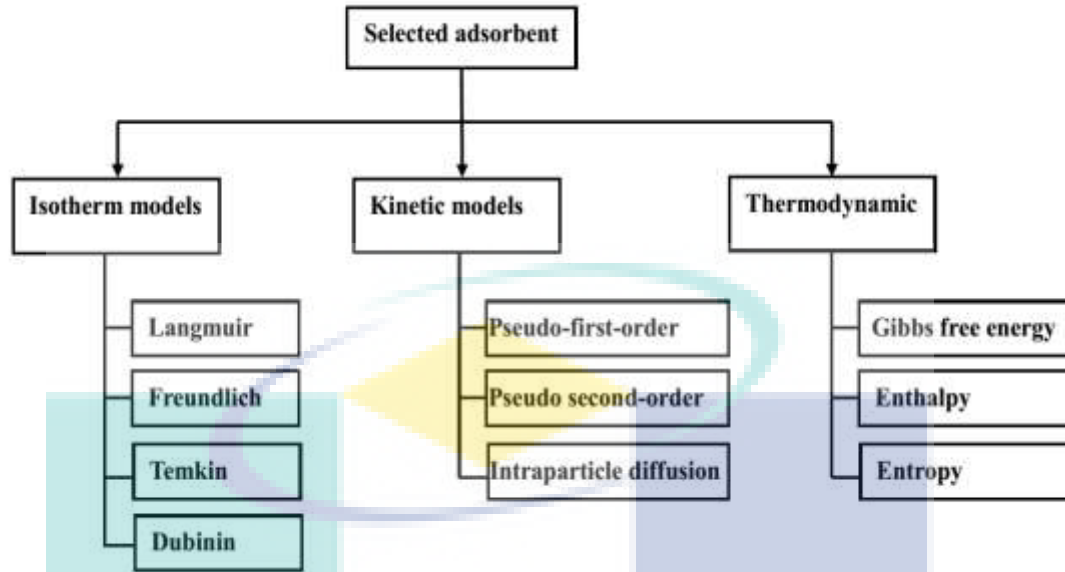


Figure 3.7 Batch equilibrium thermodynamic, isotherm and kinetic modeling studies

Table 3.9 List of adsorption isotherms models

Isotherm	Nonlinear form	Linear form	Plot
Langmuir	$q_e = \frac{Q_m b C_e}{1 + b C_e}$	$\frac{C_e}{q_e} = \frac{1}{Q_m b} + \left(\frac{1}{Q_m}\right) C_e$	$\frac{C_e}{q_e} vs C_e$
Freundlich	$q_e = K_F C_e^{1/n}$	$\log q_e = \log K_F + (1/n) \log C_e$	$\log q_e vs \log C_e$
Dubinin	$q_e = q_s \exp(-B \Sigma^2)$	$\ln(q_e) = \ln(q_s) - B \Sigma^2$	$\ln(q_e) vs \Sigma^2$
Temkin	$q_e = \frac{RT}{b_T} \ln K_T C_e$	$q_e = \frac{RT}{b_T} \ln K_T + \left(\frac{RT}{b_T}\right) \ln C_e$	$q_e vs \ln C_e$

### 3.8.2 Batch Kinetic Studies

In addition to isotherm studies, adsorption kinetics are carried out for simulating the adsorption of H<sub>2</sub>S (aq) by adsorbents. For investigating the adsorption kinetics of H<sub>2</sub>S (aq) on selected adsorbents, the pseudo-first-order, pseudo second-order, and intra-particle diffusion models were employed for simulating experimental data. All the kinetics models equations states in Table 3.10 (Foo and Hameed, 2010). The linear and nonlinear questions of pseudo-first-order and pseudo second-order models are shown in Table 3.10. The experimental results were simulated using the three kinetic models. The parameters were calculated from the pseudo-first-order, pseudo second-order, and intra-particle diffusion models linear equations as seen in Table 3.10.

### 3.8.3 Adsorption Thermodynamics

The thermodynamic study was important to investigate the effect of temperature on the transport/kinetic process of H<sub>2</sub>S (aq) adsorption in the solution. Therefore, the parameters such as changes in enthalpy ( $\Delta H^\circ$ ), entropy ( $\Delta S^\circ$ ) and Gibbs free energy ( $\Delta G^\circ$ ) were investigated. The values of the enthalpy of adsorption ( $\Delta H^\circ$ ) and the entropy of adsorption ( $\Delta S^\circ$ ) were determined from the slope and intercept of the linear plot of  $\log(q_e/C_e)$  versus  $1/T$  as seen in Table 3.10. Once enthalpy and entropy were obtained, Gibbs free energy was determined from equation 3.5 (Errais et al., 2011).

$$\Delta G^\circ = \Delta H^\circ - T\Delta S^\circ \quad 3.5$$

Table 3.10 List of adsorption kinetic models and thermodynamic equations

Isotherm	Linear form	Nonlinear form	Plot
Pseudo first-order	$\log(q_e - q_t) = \log q_e - \frac{K_1}{2.303} t$	$q_t = q_e(1 - e^{-kt})$	$\log(q_e - q_t) vs t$
Pseudo second-order	$t/q_t = 1/k_2 q_e^2 + (1/q_e) t$	$q_t = \frac{k_2 q_e^2 t}{1 + k_2 q_e t}$	$t/q_t vs t$
Intraparticle diffusion	$q_t = k_p t^{1/2} + C$		$q_t vs t^{1/2}$
Thermodynamic	$\log \frac{q_e}{C_e} = \frac{\Delta S^\circ}{2.303 R} - \frac{\Delta H^\circ}{2.303 RT}$		$\log(q_e / C_e) vs 1/T$

## CHAPTER 4

### RESULTS AND DISCUSSION

#### 4.1 Introduction

This chapter is made up of three sections which include the characterization, optimization and adsorption modeling. The first section demonstrated the mechanism of the adsorption process in ACs and IACs using a set of physicochemical characterization. The preliminary studies on different activated carbons (ACs) were succinctly discussed under this section. Additionally, the effects of ACs and IACs on the removal efficiency (RE) of H<sub>2</sub>S (aq) (from simulated waste water) was investigated in order to select the best adsorbent. In section two, the optimum conditions in the preparation of selected adsorbent was determined with the aid of Design of Expert®. The operating conditions for the removal of H<sub>2</sub>S (aq) from real petroleum waste water using the selected adsorbent were carefully screened and optimized, accordingly. Moreover, the third section, discussed the thermodynamic, isotherm and kinetic adsorption models for selected adsorbent in order to reveal their behaviour during adsorption process.

#### 4.2 Characterizations of Adsorbents

The physical and chemical properties of ACs and IACs were characterized using various analytical techniques such as Scanning Electron Microscope (SEM), Energy Dispersive X Ray Test (EDX), pH measurement, sorption of nitrogen for surface area and pore size distribution, Fourier Transform Infrared Spectroscopy (FTIR), Thermal Gravimetric Analysis (TGA), X-Ray Diffraction (XRD) and X-Ray Photoelectron Spectroscopy (XPS).

## 4.2.1 Morphological Characterization Test

### 4.2.1.1 Morphological Characterization for the ACs

The following activated carbons (ACs) were used as adsorbents; namely, ACCNS, ACPKS, and ACWSD. They were subjected to the scanning electron microscopy (SEM) coupled with an electron dispersive unit (EDX) with the latter used mainly to identify the elemental composition in the adsorbent. Figure 4.1 (a, b) shows the morphologies of ACCNS before and after the adsorption process. The precipitation of elemental sulfur was observed on the surface of ACCNS at the post-adsorption regime as illustrated in the EDX result (Table 4.1). This is similar to the image morphology reported by Khalid et al. (2016). They used a coconut shell as a source of carbon. They used chemical activation method with KOH to activate the carbon. It was almost the same method with current study.

Table 4.1 The components of ACs for fresh and spent adsorbent

Element	ACCNS		ACPKS		ACWSD	
	Fresh (w%)	Spent (w%)	Fresh (w%)	Spent (w%)	Fresh (w%)	Spent (w%)
Carbon (C)	76.648	73.244	79.66	78.94	86.135	77.10
Oxygen (O)	19.995	25.646	18.81	17.91	12.195	22.02
Potassium (K)	3.227	0.724	1.518	0.25	1.670	0.706
Sulfur (S)	Not detected	0.385	Not detected	2.90	Not detected	0.240

Figure 4.1 (c, d) shows the EDX test results for ACCNS before and after the adsorption process. Before the adsorption process began, the elemental carbon (C), oxygen (O), and potassium (K) were the main elements in ACCNS (Figure 4.1 (c)). However, after the adsorption process, elemental sulfur (S) content was detected at 0.385 w % as presented in Table 4.1. After adsorption, the amount of K decreases from 3.227 % to 0.724%, and this is attributed to its reaction with the dissolved  $H_2S$  (aq) in simulated waste water as presented in Table 4.1. Since the boiling point of potassium (K) is  $780^\circ C$ , it therefore remained on the surface of carbon which could subsequently increase the cation ( $K^+$ ) on its surface as seen from the EDX results. This occurred due to the activation temperature of ACs was  $750^\circ C$ . Therefore, the high activation temperature led to an increase in the cation ( $K^+$ ) on the adsorbent surface. During the adsorption process, the cation has the ability to attract the anion ( $HS^-$ ) from solution (Tseng et al., 2008; Mopoung et al., 2015).



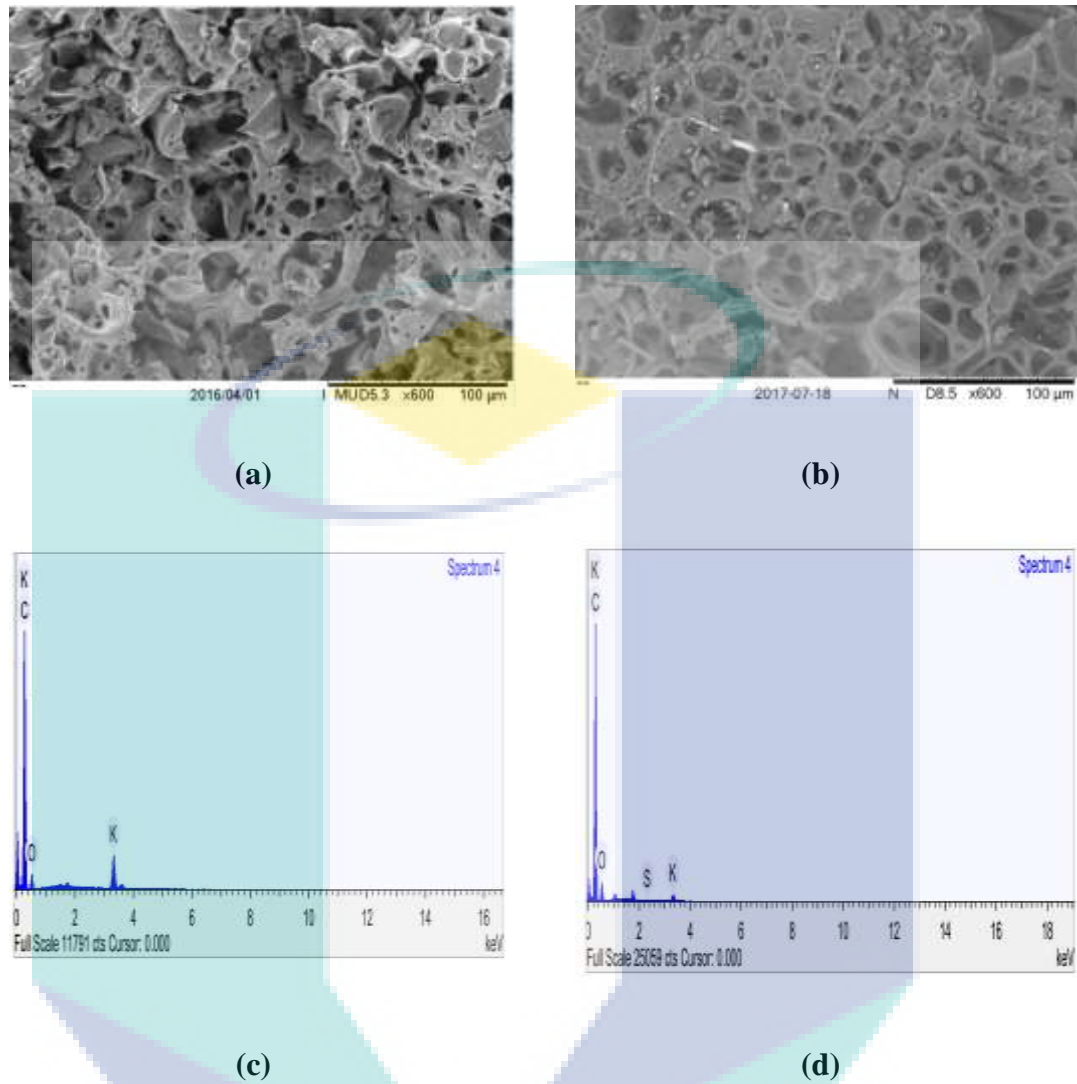


Figure 4.1 SEM images (a, b) before and after adsorption process for ACCNS.EDX test (c, d) before and after adsorption process for ACCNS, respectively

Figure 4.2 (a, b) shows the morphologies of ACPKS before and after adsorption process. Figure 4.2 (a) displays the morphological structure of the fresh ACPKS. From the results obtained from the SEM-monograph, several pores were observed on the surface of ACPKS. However, upon the adsorption, these pores were filled by small particles as lesser porosity was observed (Figure 4.2 (b)). This observation is consistent with the report made by Abechi et al. (2013) and Joshi and Pokharel (2014). Palm kernel shell was used as a source of carbon by Abechi et al. (2013). They were used chemical activation method as well during the activation process to produce activated carbons Table 4.1 shows the elemental compositions of ACPKS adsorbent. The components peaks of element in the ACPKS adsorbent before and after the adsorption process were presented in Figure 4.2 (c, d). The EDX test performed on the fresh ACPKS adsorbents

(before adsorption) revealed the existences of elemental C, O and K elements. Additional peaks were observed upon adsorption which confirmed the presence of elemental sulphur (S).

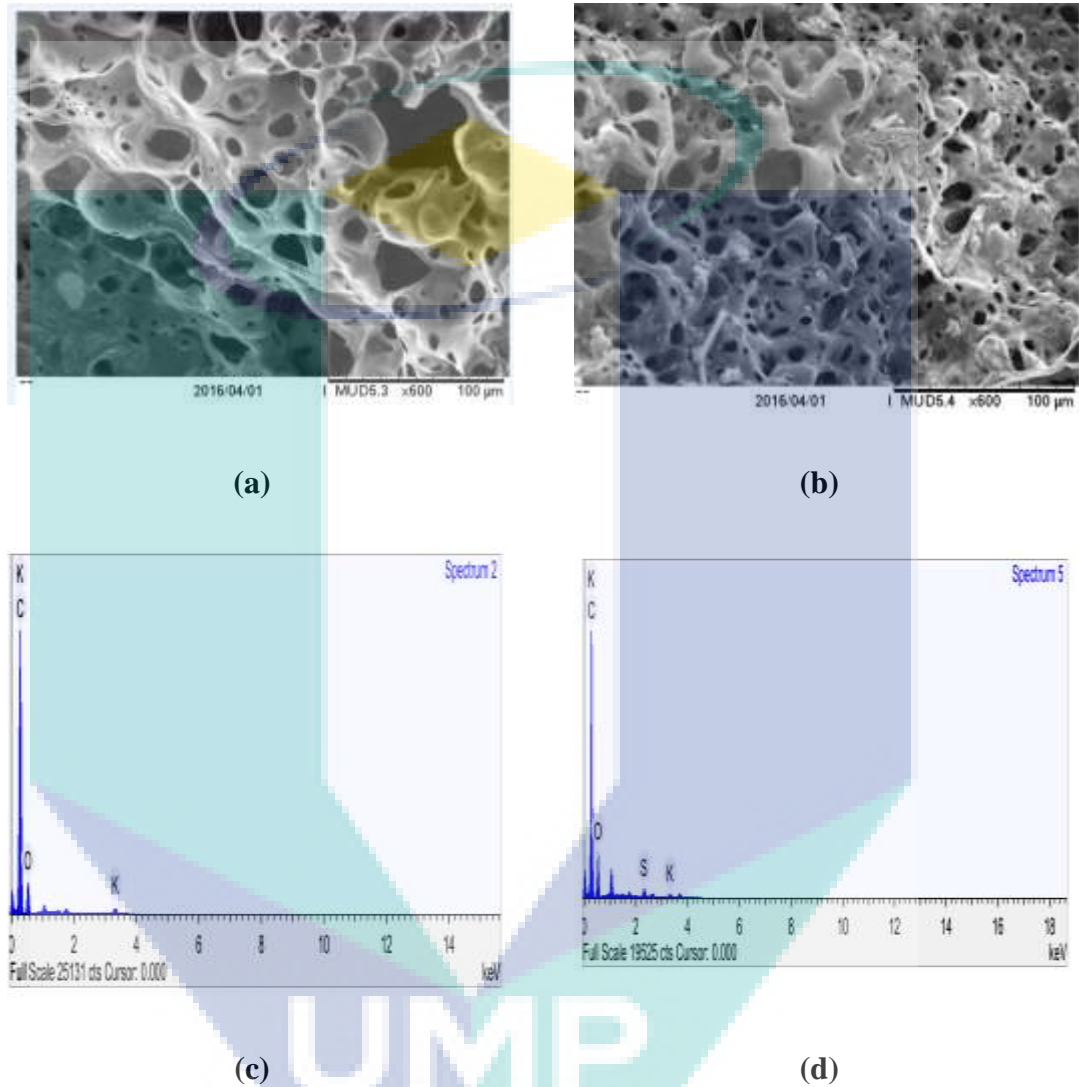


Figure 4.2 SEM images (a, b) before and after adsorption process for ACPKS. EDX test (c, d) before and after adsorption process for ACPKS, respectively

Figure 4.3 (a, b) shows the SEM-monograph of ACWSD before and after the adsorption process. It can be deduced from Figure 4.3 (a), that the chemical activation process with KOH was effective in creating a pores on the surfaces of the ACs (huge porous structure is observed). Similar observations were reported for ACs prepared from the waste woodceramics (Taoet al., 2016) and the plant precursors (Gottipati and Mishra, 2010). Upon adsorption, the pores were blocked by small particles (Figure 4.3 (b)) as reported also in the investigation conducted by Banerjee and Chattopadhyaya (2017).

Figure 4.3 (c, d) shows the results from EDX test for the ACWSD, before and after the adsorption process. Before the adsorption process, the peaks related to the elemental C, O and K were visibly evident. Upon adsorption, Figure 4.3 (d) shows an additional peak which is related to the elemental sulfur (S).

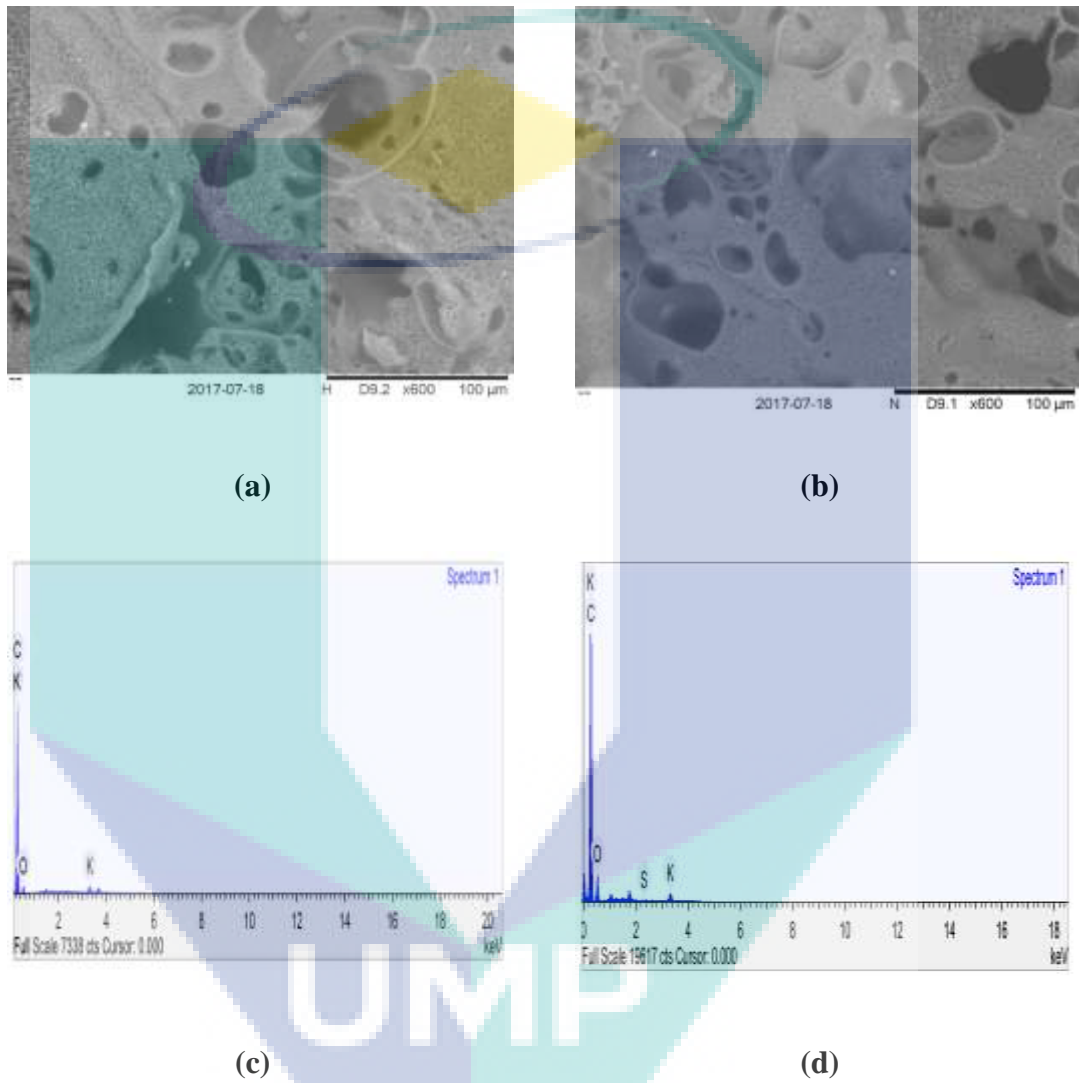


Figure 4.3 SEM images (a, b) before and after adsorption process for ACWSD.EDX test (c, d) before and after adsorption process for ACWSD, respectively

From the results obtained, the development of pore structures in ACs was due to the release of volatile components and the breakdown materials occasioned by thermal expansion during the chemical activation. The reaction between the elemental carbon atom (C) and the activation agent (KOH) at high temperature resulted in the formation of pores of various sizes (Li et al., 2017). Moreover, the pores (hence effective surface area) depends on activation temperature, activation contact time and impregnation ratio (Li et

al., 2017). From the EDX result in Table 4.1, all the ACs developed were able to remove the dissolved  $\text{H}_2\text{S}$  (aq) from waste water.

#### 4.2.1.2 Morphological Characterization for the IACs

The SEM test results for Ca-ACCNS adsorbent are shown in Figure 4.4 (a, b). Figure 4.4 (a) shows the surface morphology of fresh adsorbent Ca-ACCNS before adsorption. From the monograph obtained from SEM, a large number of pores were observed on the adsorbent which indicated the effectiveness of the current carbonization and activation processes. The surface morphologies of spent Ca-ACCNS (after adsorption) are shown in Figure 4.4 (b).

Figure 4.4 (c, d) shows the EDX elemental peaks from fresh and spent Ca-ACCNS adsorbents. Several white particles (i.e. calcium (Ca)) were observed on the surface of Ca-ACCNS as seen in Figure 4.4 (b). In fact, these particles affected the porosity and surface area as they occupied the pores. In other way round, these particles enhanced the surface chemistry of the adsorbent due to the presence of  $\text{Ca}^+$  that acts as a cation to attract anion ( $\text{HS}^-$ ). Table 4.2 presents the percentages of chemical elements from both the fresh and spent IACs adsorbents. Generally, it can be observed that the percentages of chemical elements on IACs decreased after the adsorption process and this is attributed to the oxidation reactions which occurred between the elements (on the adsorbent surface) and the  $\text{H}_2\text{S}$  (aq) (in the solution) which give up sulfur as seen in Table 4.2. As seen from Table 4.2 and Table 4.1, the Ca-ACCNS and Ca ACPKS have higher carbon content compared to ACCNS and ACPKS. This is due to the carbonization temperature for Ca-ACCNS and Ca ACPKS was higher compared with ACCNS and ACPKS carbonization temperature. Moreover, Table 4.2 shows the EDX test of the elements on the surface of Ca-ACCNS, Ca-ACPKS, and Ca-ACWSD for fresh and spent adsorbents.

Table 4.2 The components of IACs for fresh and spent adsorbent

Elements	Ca-ACCNS		Ca-ACPKS		Ca-ACWSD	
	Fresh (w%)	Spent (w%)	Fresh (w%)	Spent (w%)	Fresh (w%)	Spent (w%)
Carbon (C)	88.639	83.16	87.57	85.67	80.105	86.9
Oxygen (O)	9.156	13.02	10.61	9.93	15.55	12.13
Potassium (K)	0.916	0.029	0.60	0.04	2.239	0.049
Sulfur (S)	Not detected	3.241	Not detected	3.65	Not detected	0.167
Calcium (Ca)	1.289	0.543	1.22	0.71	2.1	0.685

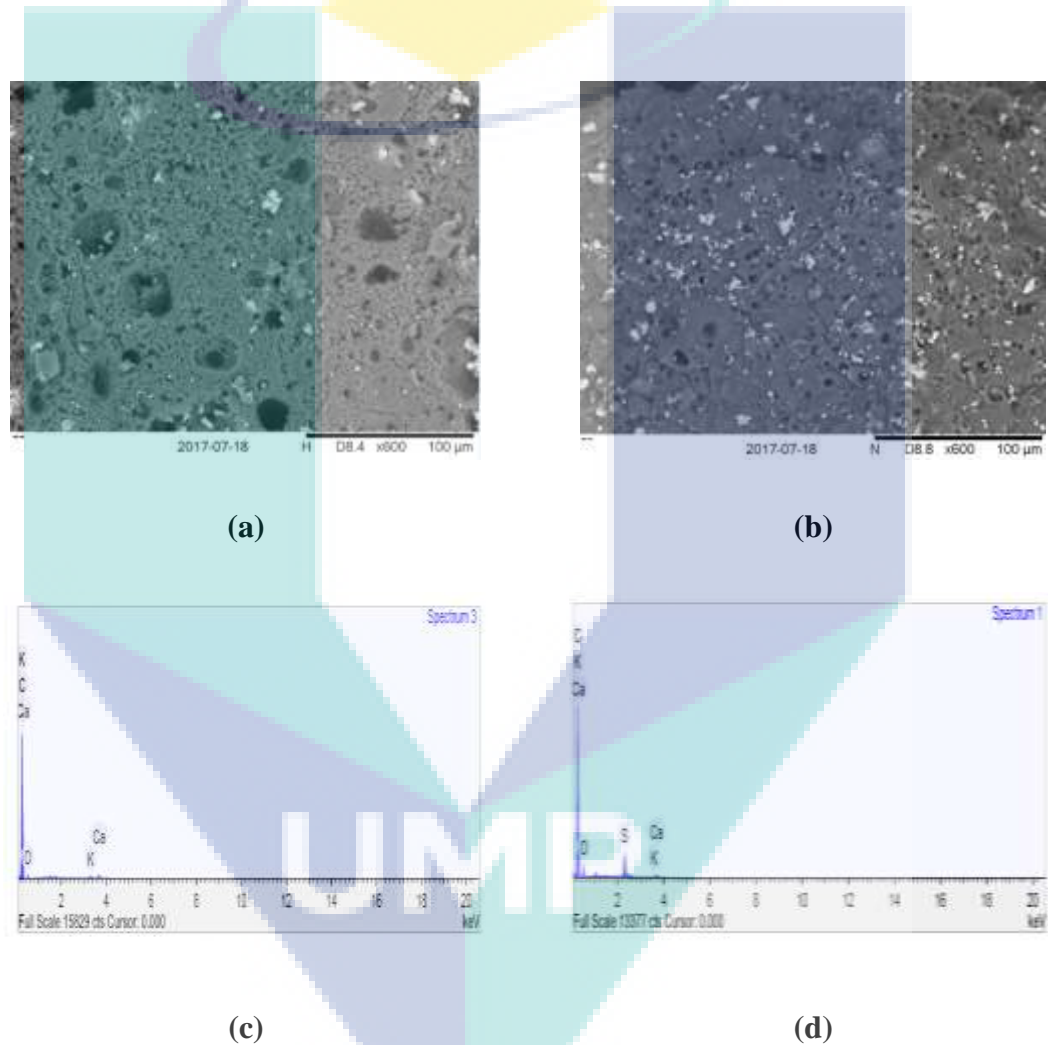


Figure 4.4 SEM images (a, b) before and after adsorption process for Ca-ACCNS. EDX test (c, d) before and after adsorption process for Ca-ACCNS, respectively

Figure 4.5 (a, b) shows the SEM-images for the fresh and spent Ca-ACPKS adsorbents. The fresh Ca-ACPKS adsorbent exhibited a highly porous carbon structure which are beneficial for adsorption process. Calcium (small white particles) was loaded from the calcium solution as shown in the SEM image (Figure 4.5 (a)). Figure 4.5 (b)



shows the SEM image of spent adsorbent (after adsorption process). Dark aggregates (from the adsorbed materials) were observed on the surface of Ca-ACPKS and this is similar to images as reported by Kundu et al. (2015). They were prepared activated carbon from palm kernel shell using chemical activation method. Figure 4.5 (c, d) illustrates the EDX test results from Ca-ACPKS before and after the adsorption process. The formation of many dark aggregates on the surface of Ca-ACPKS was observed from the EDX test results. The elemental composition of the fresh adsorbent were C, O, Ca and K with Sulfur(S) detected after the adsorption process as shown in Table 4.2.

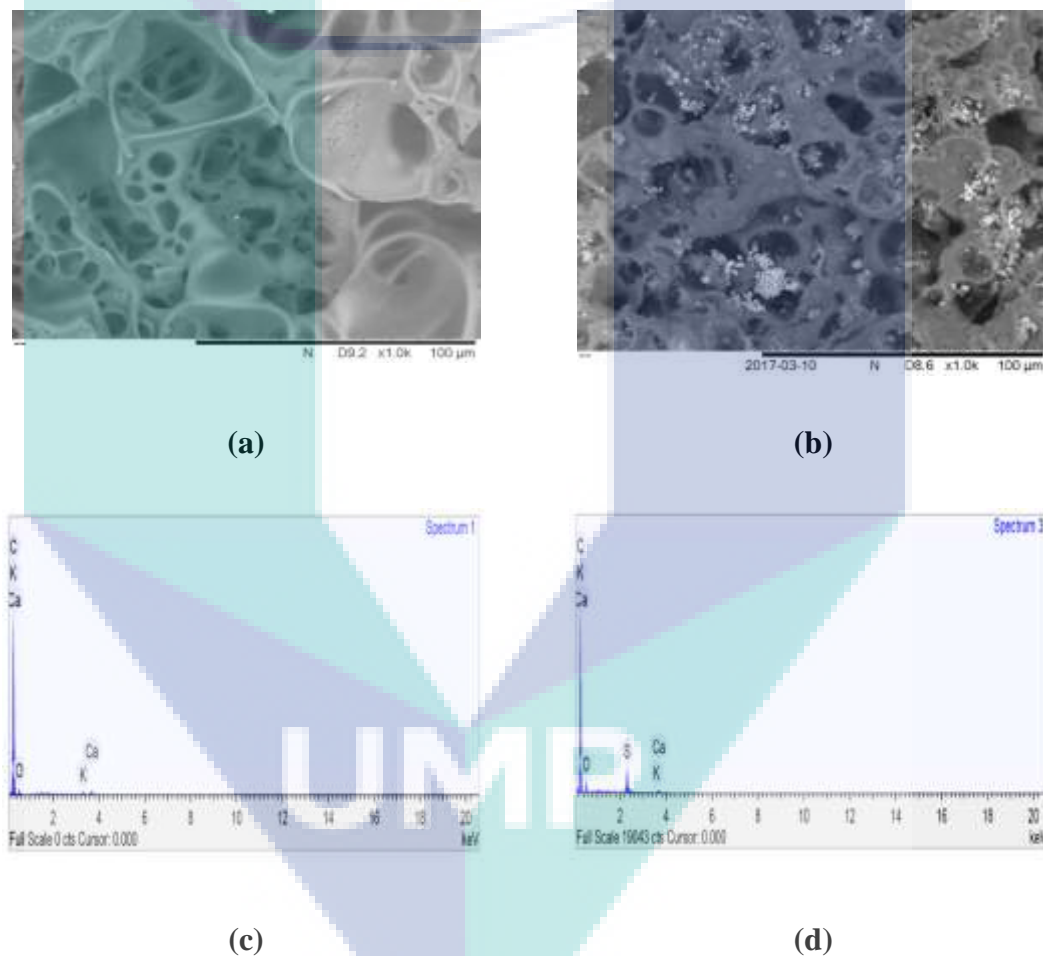


Figure 4.5 SEM images (a, b) before and after adsorption process for Ca-ACPKS. EDX test (c, d) before and after adsorption process for Ca-ACPKS, respectively

The images of fresh and spent Ca-ACWSD adsorbents are shown in Figure 4.6 (a, b). The EDX analyses for Ca-ACWSD before and after the adsorption process were demonstrated in Figure 4.6 (c, d). Treviño et al. (2013) were reported that the presence of element Ca helping in the enhancement of the adsorption capacity of the adsorbent.

Figure 4.6 (b) shows the image of the spent Ca-ACWSD adsorbent. It can be seen that the pores was effected from the adsorption process and most of the pores and layers destroyed. While the spent Ca-ACPKS image shows a strong pores as seen in Figure 4.5 (b).

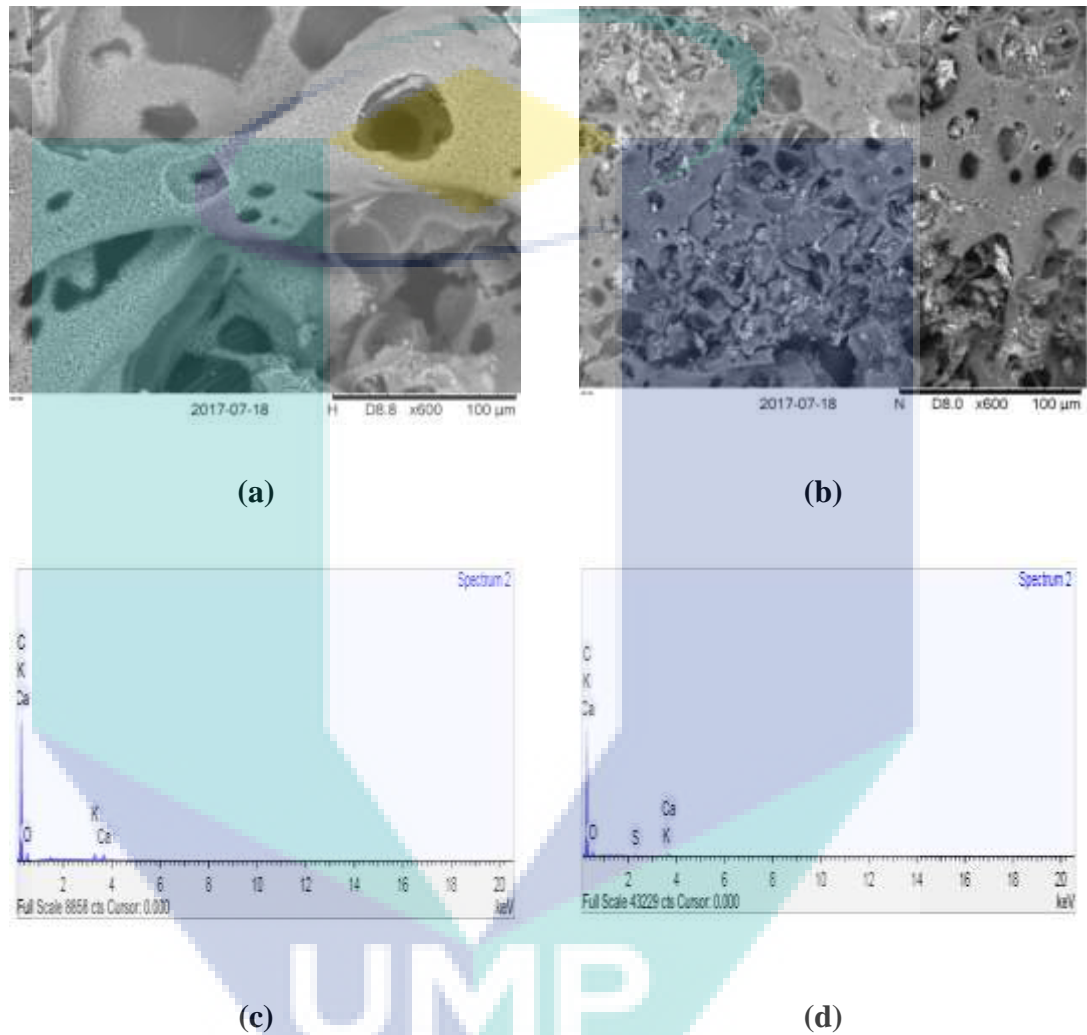


Figure 4.6 SEM images (a, b) before and after adsorption process for Ca-ACWSD. EDX test (c, d) before and after adsorption process for Ca-ACWSD, respectively



#### 4.2.2 pH Measurement

Table 4.3 shows the pH values of the adsorbents surface and simulated waste water before and after adsorption process. The results obtained revealed a decrease in the pH values for the fresh adsorbents after the adsorption process and this is due to the reaction between the H<sub>2</sub>S (aq) and elements on the adsorbents surface. The pH value of the adsorbent therefore plays an important role in the dissociation rate of H<sub>2</sub>S (aq) in forming ions in the pores. Previous study reported the basic adsorbents ability in the enhancement of RE in H<sub>2</sub>S (aq) due to the chemisorption process. For acidic adsorbent, however, only physical adsorption happens (Bandosz, 2002). Activated carbons (ACs) possesses active sites with positively charged cation (K<sup>+</sup>). These cations would interact with the anions (HS<sup>-</sup>) in the chemisorption adsorption process as seen in equation 4.1). The pH values obtained for the IACs adsorbents and the simulated solution were reported in Table 4.3. It can be observed that all fresh IACs have pH > 7 due to the presence of Ca (upon impregnation). Upon adsorption, the pH was closer to 7 as seen in Table 4.3 and this is due to the reaction between the basic species (Ca<sup>2+</sup>) and the species of HS<sup>-</sup> as seen from Equation 4.2). Similar observations was reported by (Jacukowicz et al., 2015).



The pH value of adsorbents surfaces were measured using pH meter (Mettler-Toledo AG (8603)). The amount of 0.4 g of dry carbon powder was added to 20 mL of water, and the suspension were stirred overnight to mixed solution. Then the sample filtered, and the pH of the solution measured. The obtained results were considered the value of pH of the adsorbents surfaces as seen in Table 4.3.

Table 4.3 The values of pH of the solutions and surfaces of adsorbents

Adsorbents	Adsorbents surfaces		Adsorbate solution		
	Fresh	spent	Before	After	% RE
ACCNS	7.9	7.1	7	6.9	89
ACPKS	8.3	6.9	7	6.7	93.7
ACWSD	7.6	7.3	7	7.1	68
Ca-ACCNS	8.7	7.7	7	7.4	94
Ca-ACPKS	9.6	7.2	7	6.9	99.2
Ca-ACWSD	8.1	7.9	7	7.6	85

### 4.2.3 Analysis of Nitrogen Sorption

The pore structures of the adsorbents particles, related to surface area, pore volume, and pore size distribution, were obtained by measuring N<sub>2</sub> adsorption–desorption isotherms at –196 °C using an ASAP 2020 apparatus (Micromeritics Co., USA). At the beginning of the experimental, the samples were heated at 120 °C and then outgassed at this temperature under a vacuum of 10<sup>-5</sup> Torr to constant pressure. Brunauer–Emmett–Teller (BET) and Barrett-Joyner-Halenda (BJH) methods were used to estimate the specific surface area (S<sub>BET</sub>, m<sup>2</sup>/g) and total pore volume (V<sub>t</sub>, cm<sup>3</sup>/g at STP) of the adsorbent from the adsorption and the desorption isotherms.

The specific surface area (S<sub>BET</sub>) of the fresh ACCNS adsorbent was obtained as 1093.4 m<sup>2</sup>/g. The pore volume and average pore diameter obtained were 0.402 cm<sup>3</sup>/g and 3.2 nm, respectively. These properties are analogous to those of a mesoporous material. The adsorption–desorption plot for ACs and IACs were displayed in Figure 4.7. The adsorption–desorption plot of ACCNS exhibited a type I characteristics with a hysteresis loop at 0.4 < p/p<sub>0</sub> < 0.9 in accordance with the classification by International Union of Pure and Applied Chemistry (IUPAC). The result therefore confirmed the presence of mesopores with strong absorbing surfaces (Sevilla & Fuertes, 2013) which had been reported from similar investigation reported by Khalid et al.,(2016) and Edathil et al. (2017). Consequently, the void fraction or porosity (ε) can be calculated using Equation 4.3) as shown in Table 4.4:

$$\varepsilon = V_p / (V_p + \frac{1}{\rho}) \quad 4.3$$

Moreover, the N<sub>2</sub> adsorption-desorption isotherm of ACPKS showed a type I isotherm, thus indicating the presence of mesopores on the carbon surface. The surface area of micropores was 309.3 m<sup>2</sup>/g and the pore volume was 0.162 cm<sup>3</sup>/g. The total pore volume of ACPKS was 0.34 cm<sup>3</sup>/g, and the average pore diameter was 3.9 nm. The porosity (ε) and other parameters are presented in Table 4.4.

Table 4.4 Specific surface area and other related parameters of ACs and IACs

Adsorbents	Surface Area ( $\text{m}^2 \text{g}^{-1}$ )		Pore volume ( $\text{cm}^3/\text{g}$ )				
	$S_{\text{BET}}^{\text{a}}$	$S_{\text{ext}}^{\text{b}}$	$V_{\text{t}}^{\text{c}}$	$V_{\text{mic}}^{\text{d}}$	$P_{\text{d}}^{\text{(e)}}(\text{nm})$	$P_{\text{w}}^{\text{(f)}}(\text{nm})$	$\epsilon^{\text{(g)}}$
ACCNS	1093.4	136	0.402	0.316	3.2	2.17	0.515
ACPKS	776.4	207	0.342	0.162	3.99	2.64	0.431
ACWSD	458.7	78	0.247	0.200	3.3	2.15	0.364
Ca-ACCNS	581.7	223.6	0.334	0.19	3.5	2.3	0.446
Ca-ACPKS	322.4	58.4	0.175	0.130	3.4	2.1	0.275
Ca-ACWSD	292.6	51	0.170	0.127	2.2	2.3	0.282

Notes: <sup>(a)</sup> The specific surface area obtained from BET; <sup>(b)</sup> the external surface area; <sup>(c)</sup> the total pore volume; <sup>(d)</sup> the micropores volume; <sup>(e)</sup> Average pore diameter; <sup>(f)</sup> Average pore width; <sup>(g)</sup> porosity.

The theory behind the formation of porosity and surface area are attributed to the chemical and physical activations with the aid of KOH and CO<sub>2</sub>. The reaction between KOH–carbon and CO<sub>2</sub>–carbon could possibly create more pores on the surface of adsorbents. Pore generation resulted from the dehydration of KOH to form K<sub>2</sub>O, which then reacted with CO<sub>2</sub> produced by the water–shift reaction to produce K<sub>2</sub>CO<sub>3</sub>. This process promotes the diffusion of KOH and CO<sub>2</sub> molecules into the pores, thereby increasing porosity as shown in Equation 4.6) (Stavropoulos & Zabaniotou, 2005). C<sub>f</sub> represents the active site on the ACs surface and its reaction with KOH are presented in Equation (4.4), (4.5) and (4.6). As reported by Tseng et al. (2008) and Mopoung et al. (2015).

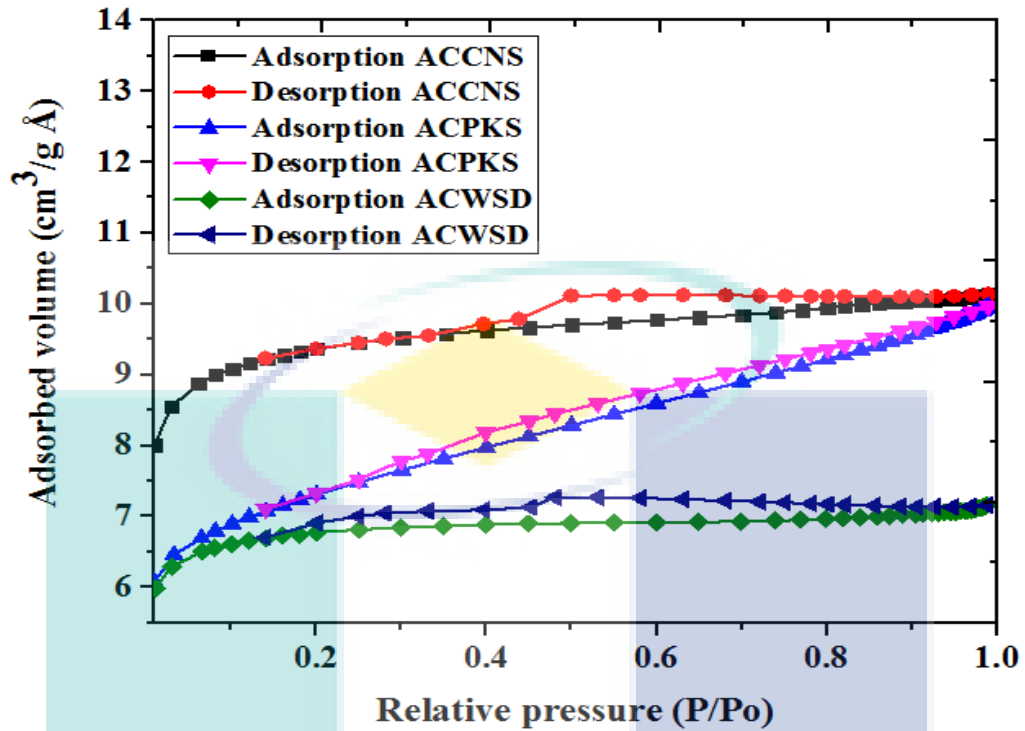
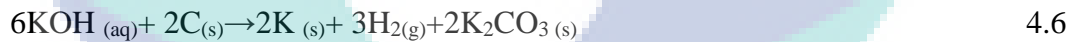


Figure 4.7  $N_2$  adsorption–desorption isotherm of ACs



In addition, adsorbents with large portions of mesopores promote the formation of water film, thereby facilitating the chemisorption of  $\text{H}_2\text{S}_{(aq)}$ . Moreover, the metallic potassium (K) appeared to be responsible for the drastic increase in the carbon material, resulting in pore formation and increased pore volume. The enhancement of porosity is associated with gasification process (Foo and Hameed, 2011). Furthermore, the  $N_2$  adsorption–desorption of ACWSD adsorbent exhibited a Type I characteristics with a hysteresis loop at  $0.2 < p/p_0 < 0.1$  as illustrated in Figure 4.7. Hence, ACWSD showed a low specific surface area and pore volume as presented in Table 4.4.

Comparing all the IACs, the Ca-ACCNS has the higher specific surface area and total pore volume (with lesser  $V_{mic}$ ) while Ca-ACPKS has a higher value for  $V_{mic}$  with lower value of average pore diameter (i.e. 3.4 nm). In addition, Ca-ACPKS exhibited a lower average pore width ( $P_w$ ) of 2.1 nm when compared with other adsorbents. The

results for the surface area and pore volume are reported in Table 4.4, with Ca-ACWSD having the lowest value among all. This would definitely affect the adsorption capacity of Ca-ACWSD. Ca-ACCNS showed a type IV characteristics with a hysteresis loop at  $0.1 < p/p_0 < 0.1$  (based on the classification of IUPAC). The  $N_2$  adsorption-desorption isotherm of Ca-ACPKS displayed a type I isotherm, indicating the presence of mesopores and micropores on the carbon surface. The adsorption-desorption isotherm of Ca-ACWSD showed a type IV isotherm as seen in Figure 4.8 which is similar to the results obtained by Li et al. (2017). They were prepared activated carbon from gulfweed using chemical activation method with KOH.

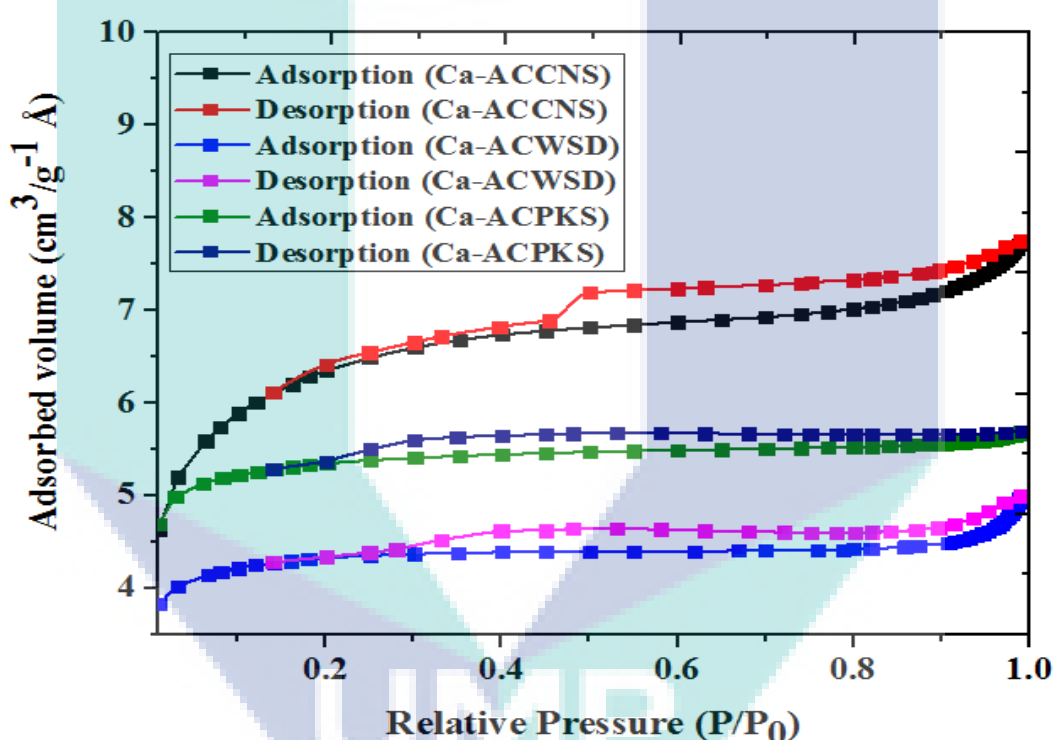


Figure 4.8  $N_2$  adsorption-desorption isotherm of IACs

#### 4.2.4 FTIR Test

Figure 4.9 shows the results obtained from Fourier Transform Infrared (FTIR) analysis of ACCNS. The fresh ACCNS adsorbent (before adsorption) exhibited the following band:  $2000\text{ cm}^{-1}$  for C=N nitriles groups and  $2156\text{ cm}^{-1}$  for C, C triple bond acetylene. Table 4.5 shows that the following bands of  $1716$ ,  $850$ , and  $717$  disappeared after adsorption process. The observation band at  $1716\text{ cm}^{-1}$  was attributed to the C=O stretching vibration of nonaromatic carboxyl groups and the band at  $1475\text{ cm}^{-1}$  was

attributed to the C=C bond (Li et al., 2017). Upon adsorption, the FTIR test result shows additional band at 910  $\text{cm}^{-1}$  which was related to the C-S-O bond stretching (Kar et al., 2012).

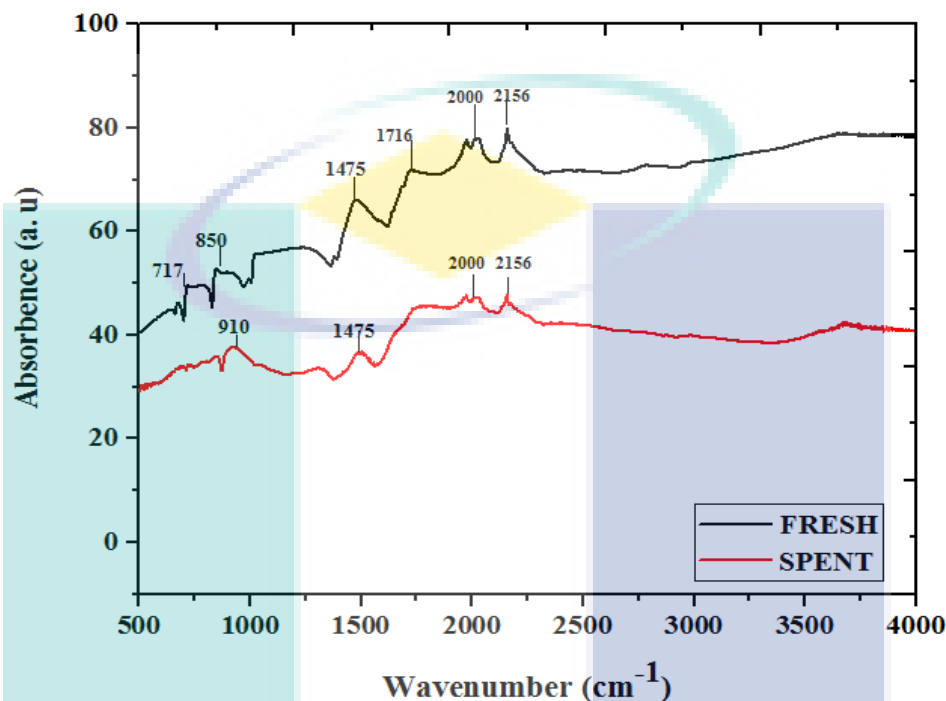


Figure 4.9 FTIR spectrum test for ACCNS fresh and spent

Table 4.5 The functional group list of ACCNS (fresh and spent)

Functional group		Molecular Motion		Wavenumber ( $\text{cm}^{-1}$ )		References
Fresh	Spent	Fresh	Spent	Fresh	Spent	
Alkynes	Alkynes	C,C Triple bond stretch	C,C triple bond stretch	2156	2156	Theivandran et al. (2015)
Nitriles	Nitriles	C=N Stretch	C=N Stretch	2000	2000	Ghosh et al. (2009)
Ketones	--	C=O Stretch	--	1716	--	Sahira et al. (2013)
Aromatics	Aromatics	C=C Stretch	C=C Stretch	1475	1475	Kanjanarong et al. (2017)
Aromatics	--	C-H Bend	--	850	--	Kanjanarong et al. (2017)
Alkanes	--	CH <sub>2</sub> Bend	--	717	--	Kanjanarong et al. (2017)
--	Alkenes , sulfonates	--	S-O, C-H Bend	--	910	Kar et al. (2012)

The Fourier Transform Infrared (FTIR) spectra of ACPKS (before and after adsorption) were presented in Figure 4.10 with visible peaks observed at the wavenumbers of  $2976\text{cm}^{-1}$ ,  $2158\text{ cm}^{-1}$ , and  $1650\text{cm}^{-1}$ , which are corresponding to the O–H, C,C Triple bond, and  $\text{R}_2\text{C}=\text{N-R}$  stretching, respectively (Das et al., 2015). Chemical activation using KOH as an activation agent could possibly increase the basic groups due to the increase in a strongly basic hydroxyl group ( $\text{OH}^-$ ) on the surface (Lee et al., 2006). Also, the primary amine group ( $\text{R-NH}_2$ ) was observed at peak  $1650\text{ cm}^{-1}$  before adsorption. Upon adsorption, the amine group disappeared completely as indicated in Figure 4.10 and Table 4.6. This is because of its interaction with sulfides during the adsorption process (Pang et al., 2017). The band of  $1090\text{ cm}^{-1}$  was attributed to the C-O stretch of carbonyl. Lu et al. (2010) reported that the chemical activation with KOH yields mainly phenolic or alcoholic components. Upon adsorption, additional band was formed at  $911\text{ cm}^{-1}$ , which was associated with the C–S-O bond stretching (Kar et al., 2012). This indicated that elemental sulfur S was accumulated and bonded to the carbon surface as presented in Table 4.6.

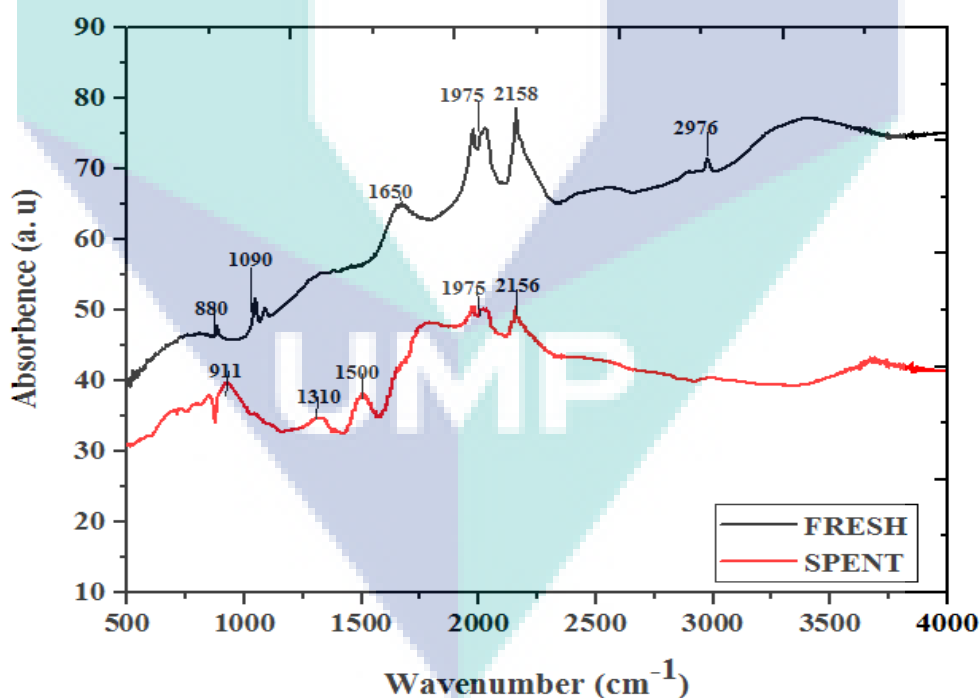


Figure 4.10 FTIR spectrum test for ACPKS fresh and spent



Table 4.6 The functional group list of ACPKS (fresh and spent)

Functional group		Molecular Motion		Wavenumber (cm <sup>-1</sup> )		References
Fresh	Spent	Fresh	Spent	Fresh	Spent	
Hydroxyl	--	O-H Stretch	--	2976	--	Lee et al. (2006)
Alkynes	Alkynes	C,C Triple bond	C,C triple	2158	2156	Ghosh et al. (2009)
Amines	--	R <sub>2</sub> C=N-R Stretch	--	1650	--	Kundu et al. (2015)
--	Sulfonates	--	S-O	--	1310	Kanjanarong et al. (2017)
Carbonyl	--	C-O Stretch	--	1090	--	Kanjanarong et al. (2017)
--	Alkenes , Sulfonates	--	S-O, C-H Bend	--	911	Kar et al. (2012)
Aromatics	--	C-H Bend	--	850	--	Sahira et al. (2013)

The FTIR spectra for the ACWSD are presented in Figure 4.11 with the graph showing information about different peaks with 880 cm<sup>-1</sup> attributed to C–H stretching, 1640 cm<sup>-1</sup> attributed to R<sub>2</sub>C=N-R Stretch (amine), and 2000 cm<sup>-1</sup> attributed to C=N Stretch. The FTIR spectra agreed with those reported by (Li et al., 2016). Kanjanarong et al. (2017) argued that hydroxide radical and carboxylic groups contributed mostly to the H<sub>2</sub>S sorption. Pang et al. (2017), reported that the peak observed at 875 cm<sup>-1</sup> corresponds to the S-O bond as presented in Table 4.7.

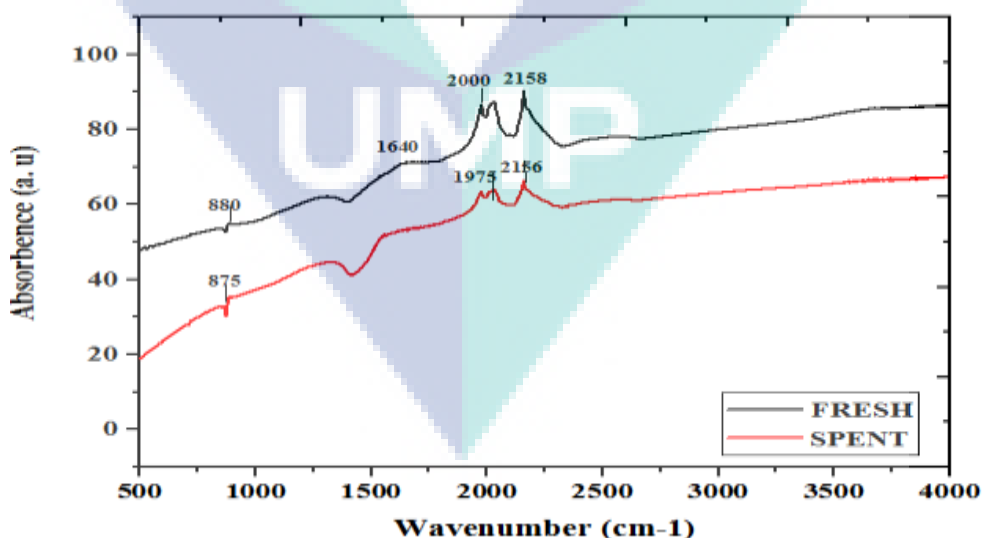


Figure 4.11 FTIR spectrum test for ACWSD fresh and spent

Table 4.7 The functional group list of ACWSD (fresh and spent)

Functional group		Molecular Motion		Wavenumber (cm <sup>-1</sup> )		References
Fresh	Spent	Fresh	Spent	Fresh	Spent	
Alkynes	Alkynes	C,C Triple bond stretch	C,C triple bond stretch	2158	2156	Ghosh et al. (2009)
Nitriles	--	C=N Stretch	--	2000	--	Ghosh et al. (2009)
Amines	--	R <sub>2</sub> C=N-R Stretch	--	1640	--	Kundu et al. (2015)
Aromatics	--	C-H Bend	--	880	--	Sahira et al. (2013)
--	Sulfonates	--	S-O Stretch	--	875	Kar et al. (2012)

#### 4.2.5 Thermal Gravimetric Analysis

Figure 4.12 shows the result of TGA of the precursor of ACCNS sample. The effect of carbonization temperature was investigated using TGA test. The carbonization temperature ranged from 50 °C – 800 °C. From the TGA curve, the weight loss process can be divided into three stages. The first stage occurred at temperature below 200 °C involving weight loss of 7.210 %, which was attributed to evaporation of moisture content, solvents of low molecular weight and gas desorption from the precursor surface. The second stage occurs at temperature ranging from 200°C -350 °C and involved the weight loss of 28.5 %. The weight loss in this stage was attributed to the evaporation of volatile materials. The final stage occurs at 400°C -700 °C that involved the carbonization of hydrocarbonated compounds. The residuals formed were ashes. The sample demonstrates high thermal stability at temperature of 700°C with similar result reported by Zhi et al. (2017). They were used bean residue carbons as an adsorbent and their TGA result is similar to current result. The effect of temperature and weight loss summarized in Table 4.8.

Table 4.8 Thermal analysis of the materials used to prepare ACs and IACs

Materials	Temperature °C	Weight loss (mg)	Weight loss (%)
CNS	50-150	0.402	7.21
	300-350	1.59	28.54
	350-700	2.185	39.15
PKS	50-100	0.322	10.44
	300-350	0.88	28.74
	350-700	1.152	37.72
WSD	50-150	0.298	10.65
	35--700	1.738	61.54
Ca-ACCNS	50-100	0.583	10.31
	200-700	0.440	7.78
Ca-ACPKS	50-100	0.601	9.4
	600-700	0.443	6.9
Ca-ACWSD	50-100	0.0687	5.891
	200-500	0.1797	12.21
	600-800	0.114	7.7

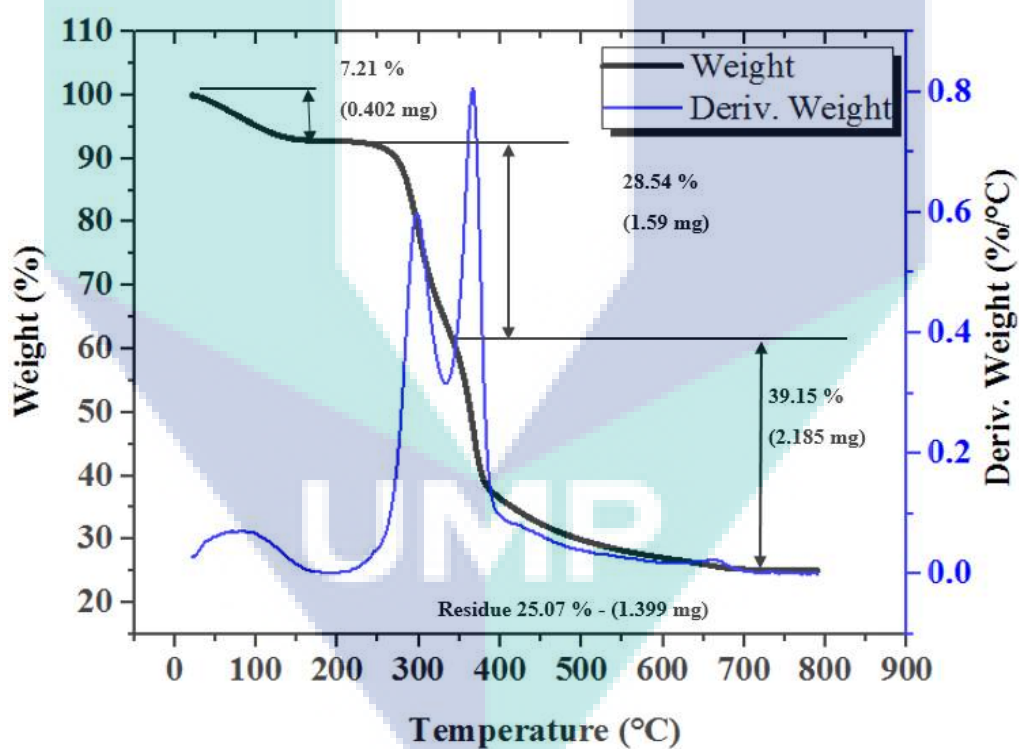


Figure 4.12 TGA curves of ACCNS

Figure 4.13 presents the TGA test result for Ca-ACCNS. The thermal impregnated conditions can be categorized based on the gradual weight loss occurred at temperature ranging from 25 °C – 900 °C. These three stages of weight loss were shown in Figure 4.13. The first stage occurred at temperature (< 200 °C), and this is associated with weight loss of 10.31 % (due to evaporation of moisture/solvents of low molecular weight and gas desorption from the precursor surface). The second stage occurs at 600°C -700 °C, which is associated with weight loss of 7.786 % (due to O<sub>2</sub> decomposition). The final stage of the thermo-analysis occurs at temperature ranging from 700°C.-900 °C. Carbon dioxide was emitted due to the calcination process of egg shells (conversion of CaCO<sub>3</sub> to CaO). The final residuals were calcium oxide, calcium, and ashes.

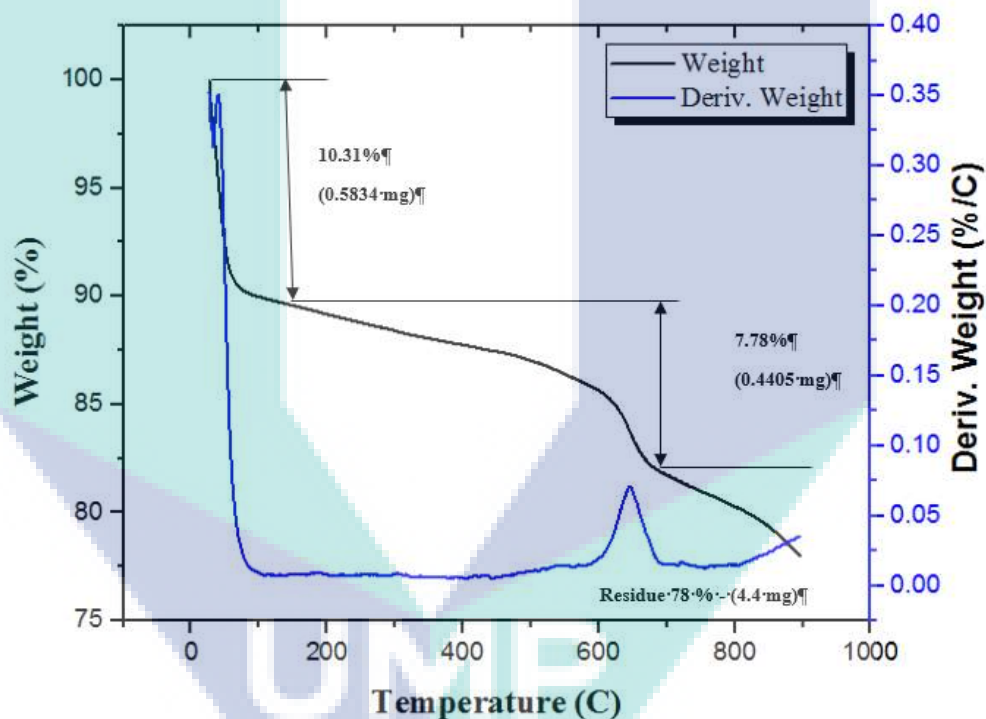


Figure 4.13 TGA curves of Ca-ACCNS

A thermal analysis of the precursor of ACPKS was performed in order to choose a suitable carbonization temperature. The corresponding TGA test result is shown in Figure 4.14. The first stage of weight loss (10.44 %) occurred at temperature ranging from 25°C -250°C and this was due to the removal of adsorbed surface water or gases. However, at temperature ranging from 250°C -300°C, higher weight loss was recorded at 28.74 % because CO<sub>2</sub> and other materials have been removed (Das et al., 2015; Pongener et al., 2015). Between 650 °C and 800 °C, a thermally stable carbon structure existed in ACPKS.

Therefore, 700 °C was chosen as carbonization temperature. Similar result has been reported by Zhi et al. (2017).

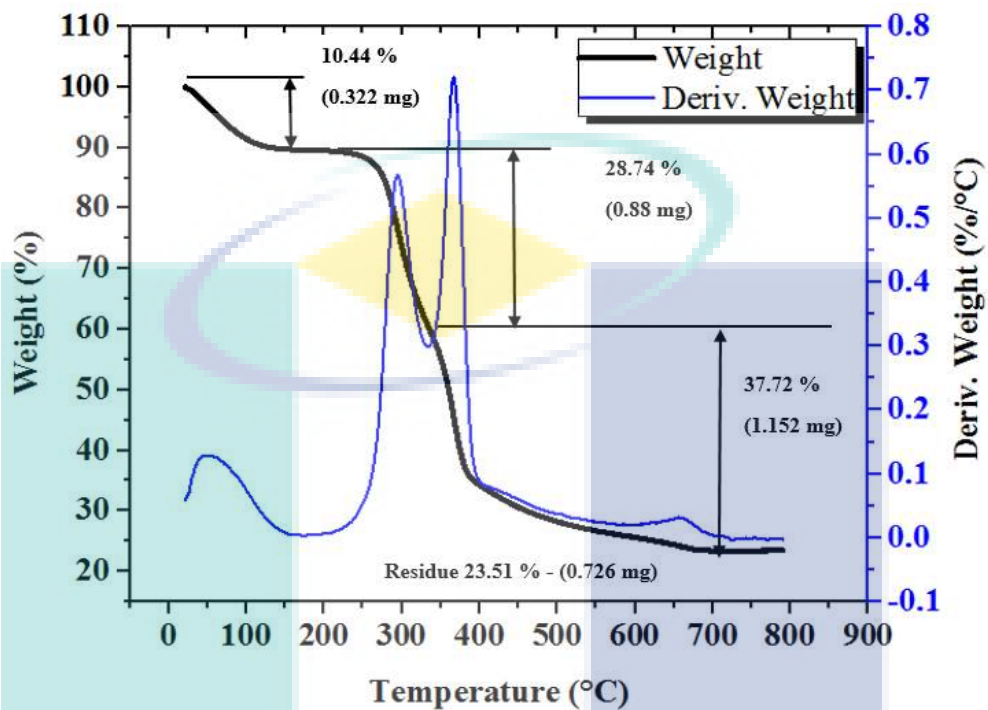


Figure 4.14 TGA curves of ACPKS

The TGA result of the modified Ca-ACPKS is displayed in Figure 4.15. Three distinct mass drops can be seen in the TGA curve. It showed the mass loss of 9.40% at 100 °C was due to the removal of physically adsorbed water and other volatile matters. After the dehydroxylation process of the  $\text{Ca}(\text{OH})_2$  phase, the calcium carbonate ( $\text{CaCO}_3$ ) is converted to  $\text{CaO}$  and  $\text{CO}_2$  is released. Interestingly, the weight loss represented by the peaks between 200 °C and 900 °C can be correlated with the amount of carbonaceous phase in each composite. At 500 °C, it showed the other weight loss of 6.92% due to the removal of  $\text{CO}_2$ . Between 750 °C and 900 °C, the weight loss was 4.39% and this is attributed to the calcination process as reported by the investigation made on green coconut shell (Das et al., 2015).

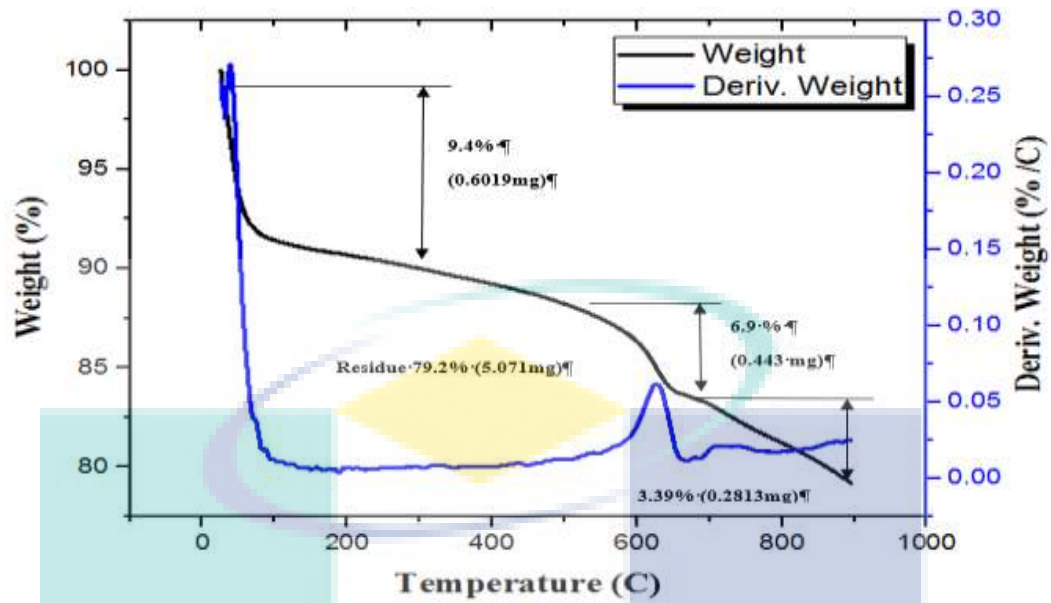


Figure 4.15 TGA curves of Ca-ACPKS

Figure 4.16 shows the TGA result of the precursor of ACWSD. At temperature ranging from 300°C and 600 °C, the weight loss was quite significant (61.54 %). The residual content was 22.56 % and this is attributed to the formation of ashes. The curve suggested the thermal stability more pronounced at temperature between 700°C and this explains why it was chosen as the carbonization temperature.

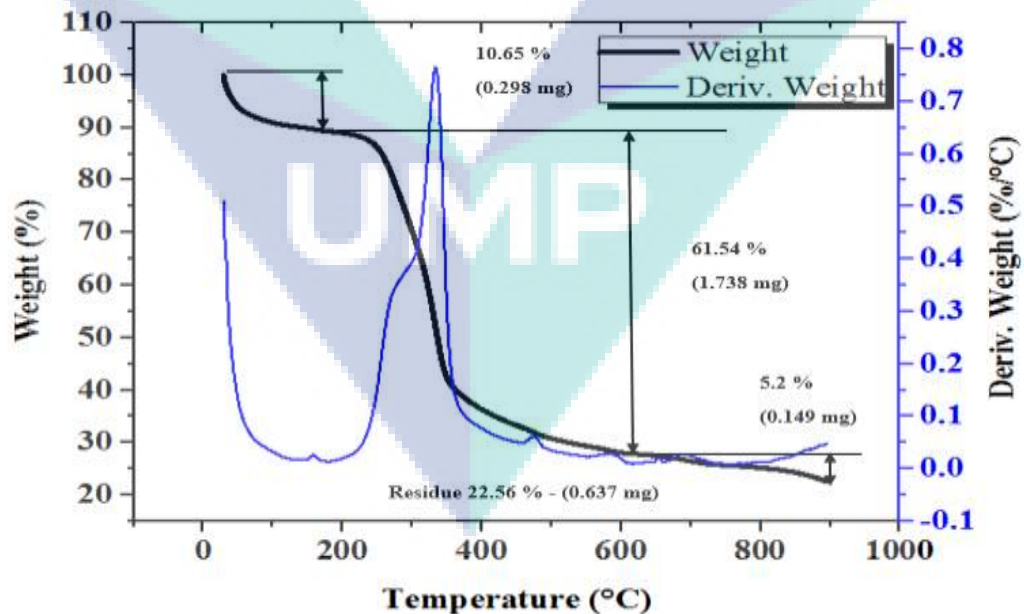


Figure 4.16 TGA curves of ACWSD



Figure 4.17 shows the TGA of the calcination process of Ca-ACWSD. It can be observed that the weight loss was 5.8 % at temperature below 200°C and this could be traced to the removal of moisture with the adsorbed gases. The residual content after the thermal process was recorded as 73 % and this is attributed to the formation of ashes.

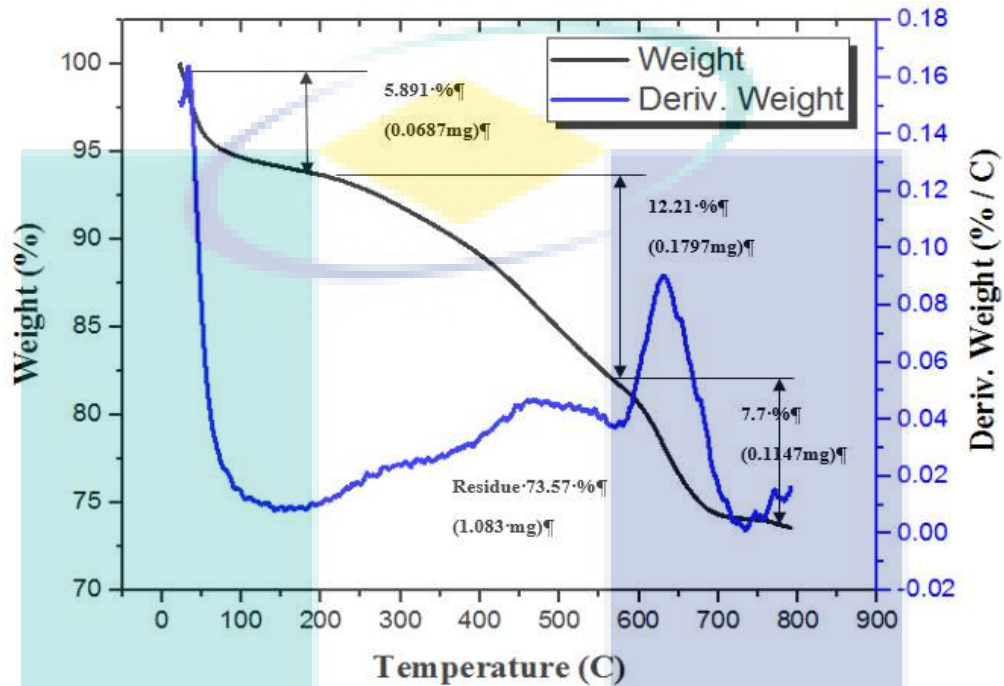


Figure 4.17 TGA curves of Ca-ACWSD

#### 4.2.6 X-Ray Diffraction (XRD)

The positions and intensities of XRD peaks provided information about the shape of a crystalline structure. Figure 4.18 shows the XRD patterns of ACCNS and modified Ca-ACCNS (fresh & spent). It can be clearly seen that the modified Ca-ACCNS XRD pattern exhibited more peaks than ACCNS. The XRD results for ACCNS revealed the presence of two peaks at  $2\theta = 24^\circ$  and  $42^\circ$ . The peak observed at  $24^\circ$  correspond to  $K_2O$ . On the other hand, the peaks corresponding to K metal appear at  $29^\circ$  and  $42^\circ$  (Mopoung et al., 2015). The modified Ca-ACCNS is expected to increase the adsorption properties due to surface complexation reactions. Peaks related to calcite ( $CaCO_3$ ) are observed at  $2\theta = 23.1^\circ, 29.5^\circ, 36^\circ, 39.4^\circ, 43.1^\circ, 47.5^\circ, 57.4^\circ, 60.7^\circ$  and  $64.6^\circ$ . The peaks of lime ( $CaO$ ) are visible at  $2\theta = 36^\circ$ , and  $64.6^\circ$ . Carbon (C) is observed at  $2\theta = 29.2^\circ, 43.1^\circ$  and  $47.4^\circ$ . The XRD test result for spent adsorbent (Ca-ACCNS) showed different peaks. Peaks related to carbon sulfide ( $CS_2$ ) are observed at  $2\theta = 29.8^\circ, 36.9^\circ, 39.8^\circ, 47.5^\circ, 57.5^\circ, 65.9^\circ, 69.6^\circ$  and  $70.5^\circ$ . Sulfide (S) was visible at  $2\theta = 47.9^\circ$  and  $56.9^\circ$ . The peak of



diamond was visible at  $2\theta = 43.6^\circ$ . The calcium sulfide was observed at  $2\theta = 36.4^\circ$  as well. It can be concluded that all active sites on carbon surface and calcium consumed during the adsorption process were clearly seen in Figure 4.18. The type of crystalline was hexagonal. It can be seen from Figure 4.18 that the shape of Ca-ACCNS spent changed. This indicated that some of pores was destroyed after adsorption process.

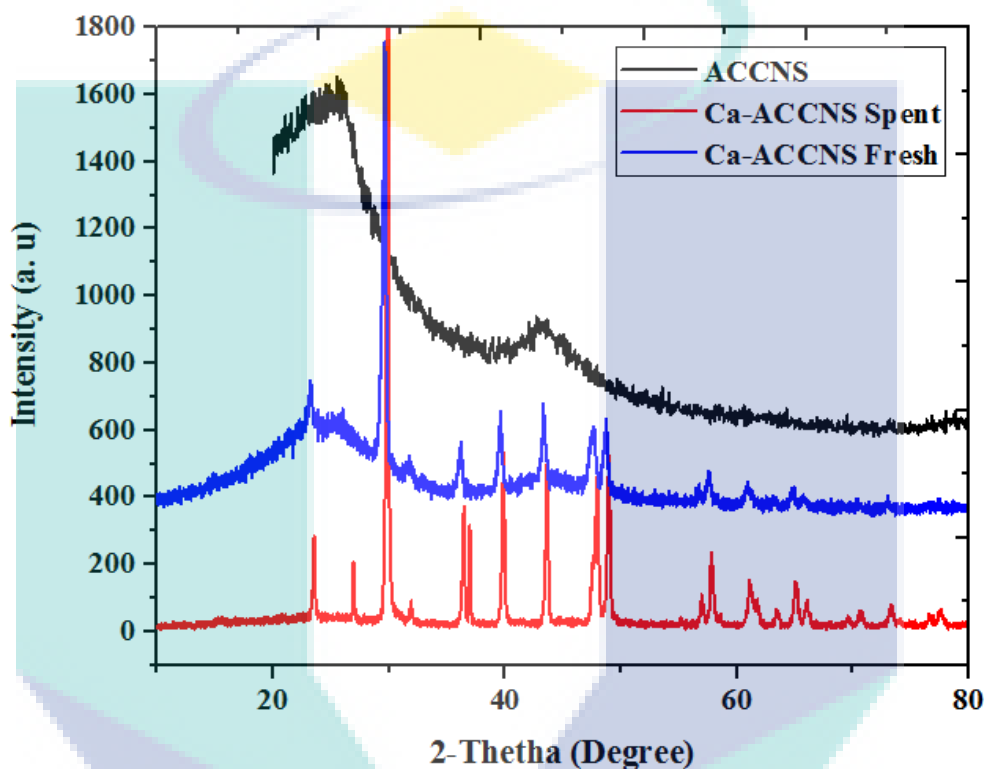


Figure 4.18 The XRD pattern of the ACCNS (fresh) and Ca-ACCNS (fresh and spent)

Figure 4.19 represents the XRD patterns of ACPKS and modified Ca-ACPKS (fresh and spent). It showed a hexagonal crystalline type. ACPKS exhibits many small peaks at around  $2\theta = 24^\circ, 30^\circ, 32^\circ, 34^\circ, 39^\circ$  and  $40^\circ$  which were related to  $H_2O$ ,  $K_2CO_3$ , K,  $K_2O$  and KOH, respectively. These components are produced after the activation process as shown in Equations 4.4). Similar observation has been reported by Liu et al. (2017) with the fresh Ca-ACPKS contains elements such as diamond (C), calcium carbide ( $CaC_2$ ), calcium peroxide ( $CaO_2$ ) and calcite ( $CaCO_3$ ). The peaks was obtained at  $2\theta = 29.6^\circ, 36.03^\circ, 43.1^\circ$  and  $64.5^\circ$ , respectively. The sulfur (S) content in the spent Ca-ACPKS sample peaks at  $2\theta = 26.6^\circ$ . Similar findings were reported for other commercial carbons impregnated with egg shells by (Guijarroet al., 2011). The curve revealed that Ca-ACPKS exhibited more crystalline structures than other adsorbents. The crystalline

structure of spent Ca-ACPKS was never affected after the adsorption process as shown in Figure 4.19.

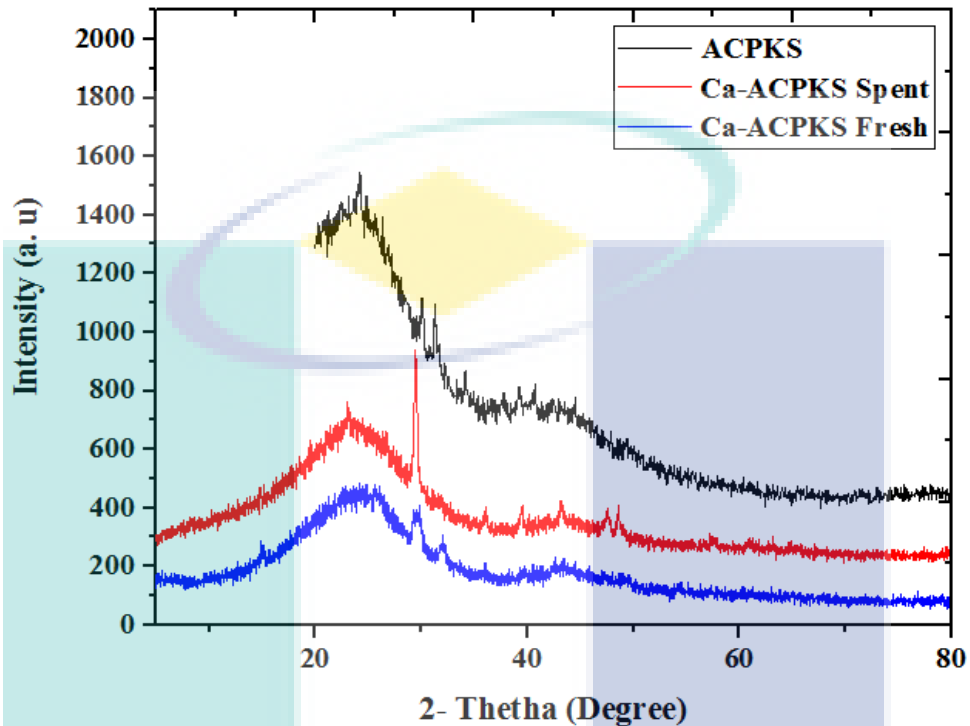


Figure 4.19 The XRD pattern of the ACPKS (fresh) and Ca-ACPKS (fresh and spent)

The XRD pattern of ACWSD and Ca-ACWSD was depicted in Figure 4.20. The XRD test result for ACWSD revealed the presence of two peaks. The sharp peak at  $2\theta = 29^\circ$  correspond to K and the peak at  $24^\circ$  correspond to  $K_2O$ . The untreated Ca-ACWSD revealed diffraction peaks at  $2\theta = 23.49^\circ, 29.84^\circ, 36.43^\circ, 39.85^\circ, 43.58^\circ, 47.95^\circ, 48.97^\circ, 56.96^\circ, 61.01^\circ, 63.36^\circ,$  and  $65.04^\circ$ . These were attributed to the cubic structure of  $CaCO_3$  (indicates the presence of Ca). In addition, the diffraction peaks at  $2\theta = 39.85^\circ$  and  $57.81^\circ$  which were attributed to the cubic structure of CaO which confirmed the presence of elemental Ca in the adsorbent. The elemental carbon (C) was confirmed from the diffraction peak at  $2\theta = 43.58^\circ$ . The XRD pattern of Ca-ACWSD corroborated the EDX analysis. According to the XRD analysis reported by Kanjanarong et al. (2017), the presences of two strong peaks at  $2\theta = 25^\circ$  and  $28^\circ$  indicate the formation of elemental S.

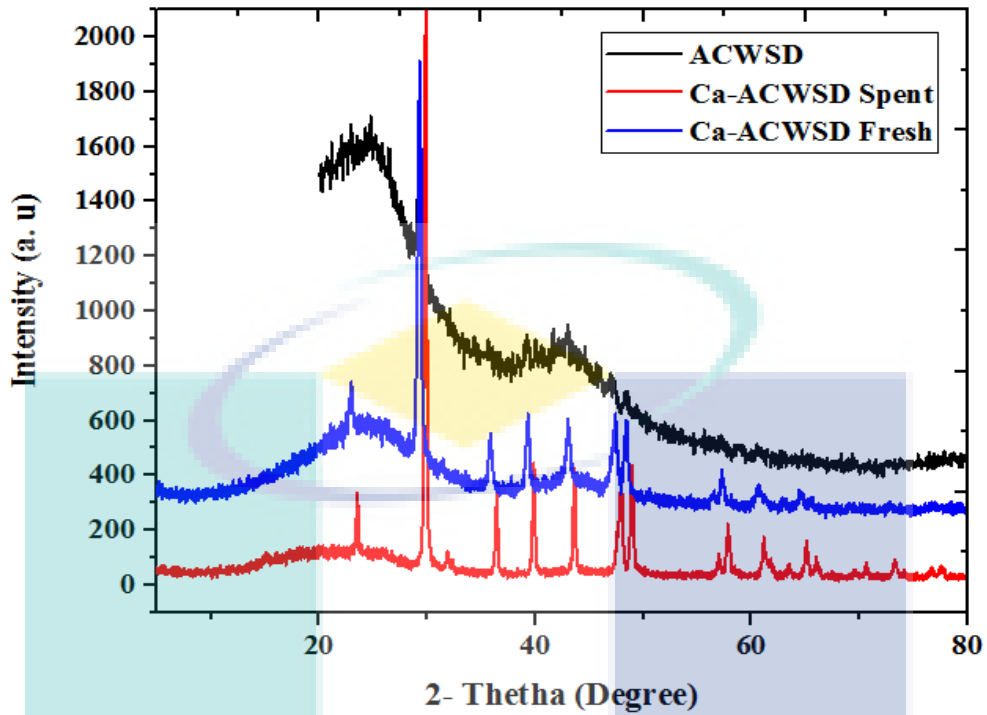


Figure 4.20 The XRD pattern of the ACWSD (fresh) and Ca-ACWSD (fresh and spent)

#### 4.2.7 X-ray Photoelectron Spectroscopy

The XPS test was conducted for ACs and IACs samples to investigate the chemical states of elemental compositions on the surface. Figure 4.21 shows the peaks of the chemical states of composite elements on the surfaces of ACCNS and Ca-ACCNS adsorbents. It can be clearly seen that both adsorbents exhibited the highest peaks of carbon (C1s) and oxygen (O1s) atoms. However, the extra peaks of Ca2p3 and Ca2p1 appeared on the surface of modified activated carbon adsorbent (Ca-ACCNS) were associated with the binding energies (BE) of 455eV and 250.13 eV, respectively as illustrated in Figure 4.21.

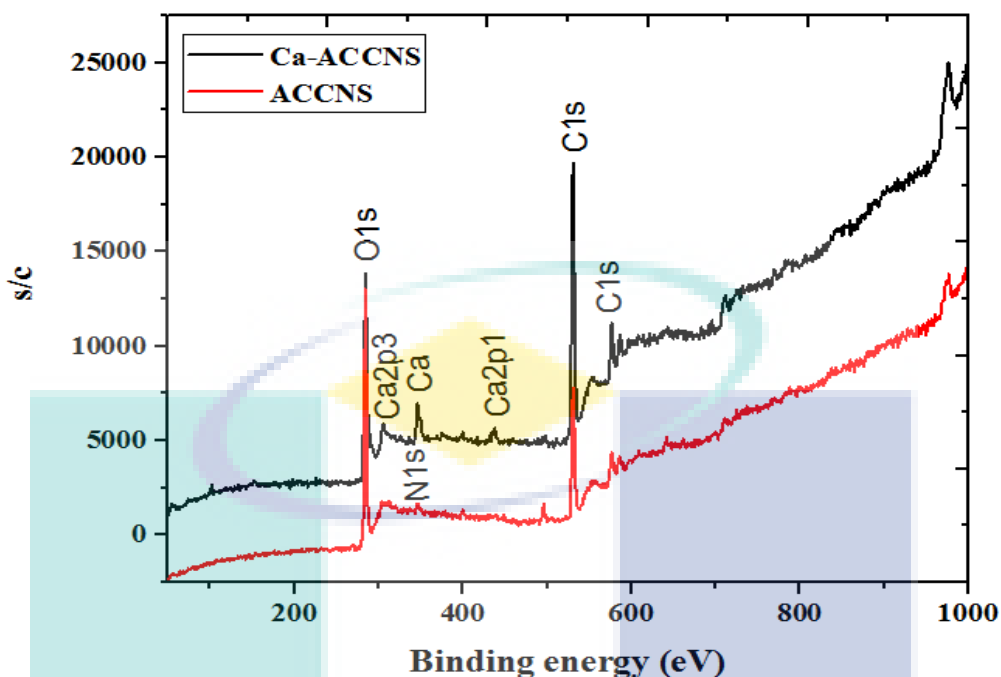


Figure 4.21 X-ray photoelectron spectroscopy (XPS) test for the ACCNS (fresh) and Ca-ACCNS (fresh)

Figure 4.22 shows the binding energy plots of ACPKS and Ca-ACPKS before and after the adsorption process. The carbon (C1s) and oxygen (O1s) atoms exhibited the highest peaks. Also, the fresh Ca-ACPKS adsorbent showed the peaks of calcium (Ca2s, Ca2p3 and Ca3p1) atoms. Meanwhile, the spent Ca-ACPKS showed two additional peaks for sulfur (S2s, S2p) and sodium (Na2s) atoms. The XPS test result revealed that the chemisorption adsorption may occur during the adsorption process. The elemental sulfur interacted well with a metal or an oxygen atom by transferring electrons from  $\text{H}_2\text{S}(\text{aq})$  orbitals into those unoccupied orbitals of the metals as reported by Song et al. (2013). Therefore, CaS was produced from the reaction of CaO with  $\text{H}_2\text{S}(\text{aq})$  as presented in Equation 4.21). This observation was consistent with the XRD test result in Figure 4.20. The peaks of Ca2s, Ca2p3 and Ca3p1 for Ca-ACPKS (fresh) adsorbent indicated that the oxidation state of calcium was actually  $\text{Ca}^{2+}$ . Also, the active sites of IACs for  $\text{H}_2\text{S}(\text{aq})$  adsorption are  $\text{Ca}^{2+}$  and CaO. In addition, the binding energy (BE) of Ca2s decreases slightly after the adsorption process. This indicates that the active site (CaO) on the adsorbent surface is chemically converted to CaS. Moreover, it is evident that only the spent adsorbent contains S2s spectrum. Therefore, it is obvious that the fresh active  $\text{Ca}^{2+}$  in the adsorbent surface is chemically reacted with  $\text{H}_2\text{S}(\text{aq})$  to form CaS.

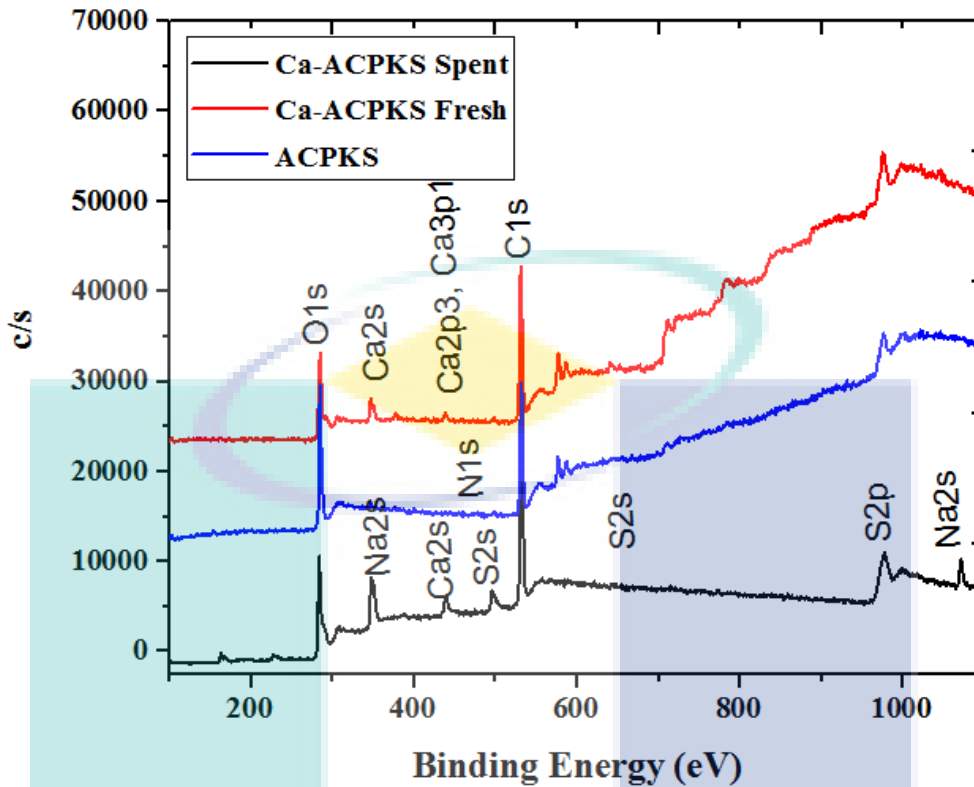


Figure 4.22 X-ray photoelectron spectroscopy (XPS) test for the ACPKS (fresh) and Ca-ACPKS (fresh and spent)

Figure 4.23 demonstrates the chemical states of composite elements on the surfaces of ACWSD and Ca-ACWSD. It can be seen that the XPS test results conform to those of XRD and FTIR tests. All the characterizations have indicated the success of the current impregnation process of ACs which could enhance the RE of  $H_2S$  (aq) from petroleum waste water.

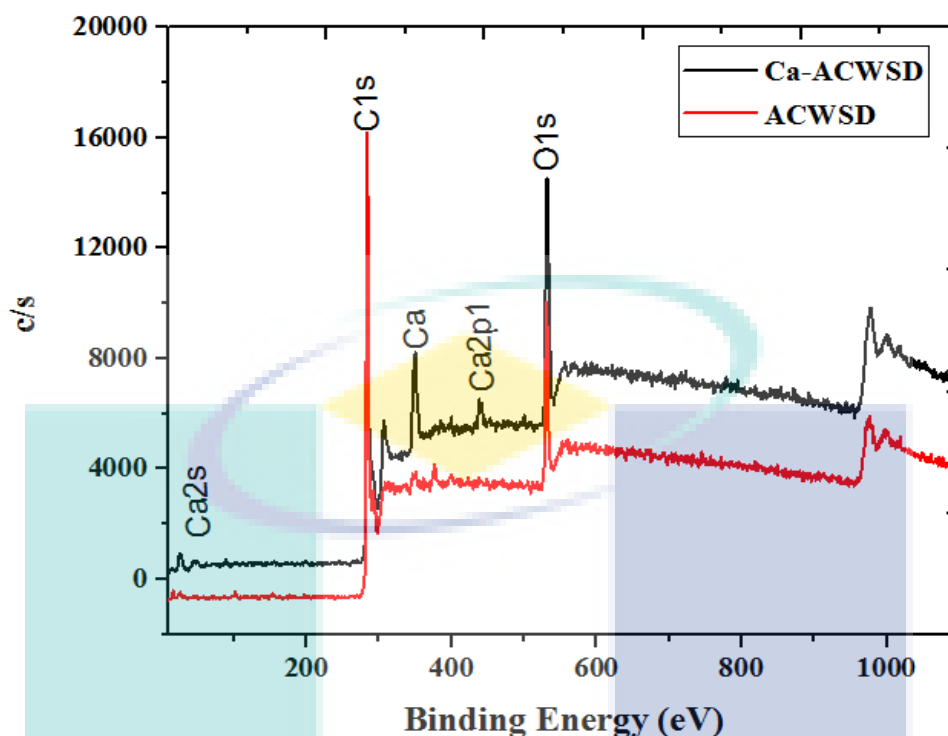


Figure 4.23 X-ray photoelectron spectroscopy (XPS) test for ACWSD (fresh) and Ca-ACWSD (fresh)

### 4.3 Batch Adsorption Studies

The adsorption experiments were conducted in a batch mode. The details of batch adsorption process were explained. Subsequently, the initial and final concentrations were measured after the suspensions were filtered. The adsorption studies using One Factors At Time (OFAT) were conducted. Parameters such as initial concentrations of  $\text{H}_2\text{S}$  (aq) (mg/L), adsorption contact time (h), dosage (g), pH of solution and agitation speed (rpm) were determined.

#### 4.3.1 Effect of Initial $\text{H}_2\text{S}$ (aq) Concentration

Initial  $\text{H}_2\text{S}$  (aq) concentration is an important factor that affects the RE of  $\text{H}_2\text{S}$  (aq). It is related to the amount of mass transfer between adsorbent and adsorbate (Ouaisif et al., 2013). Figure 4.24 shows the impact of initial concentration on % RE of  $\text{H}_2\text{S}$  (aq) by using ACs adsorbents. Low  $\text{H}_2\text{S}$  (aq) concentration (i.e. 200-600 mg/L) results in higher RE of because the number of active sites on an adsorbent surface is analogous to the number of  $\text{H}_2\text{S}$  (aq) ions in the solution. The higher RE is observed in concentration of 200 mg/L with value of 95.3 %, 89 %, and 75% for ACPKS, ACCNS and ACWSD

adsorbents respectively. However, at high  $H_2S$  (aq) concentration (i.e. 800-1000 mg/L), the availability of active sites is lesser than the  $H_2S$  ions. Therefore, RE decreases as the initial  $H_2S$  (aq) concentration increases. The lower % RE of  $H_2S$  (aq) was observed in concentration of 1000 mg/L with values of 70 %, 50 %, and 35 % for ACPKS, ACCNS and ACWSD adsorbents respectively. As recommended by DOE for industrial effluent, this values are not environmentally acceptable and need more purification before discharge it to the environment. Similar observation have been reported by Edathilet al. (2017) and Jacukowicz et al. (2015). It is observed that ACPKS gives higher RE at all initial  $H_2S$  (aq) concentrations. The effect of initial concentration for all ACs have negative effect as concentration increased the RE% was decreased.

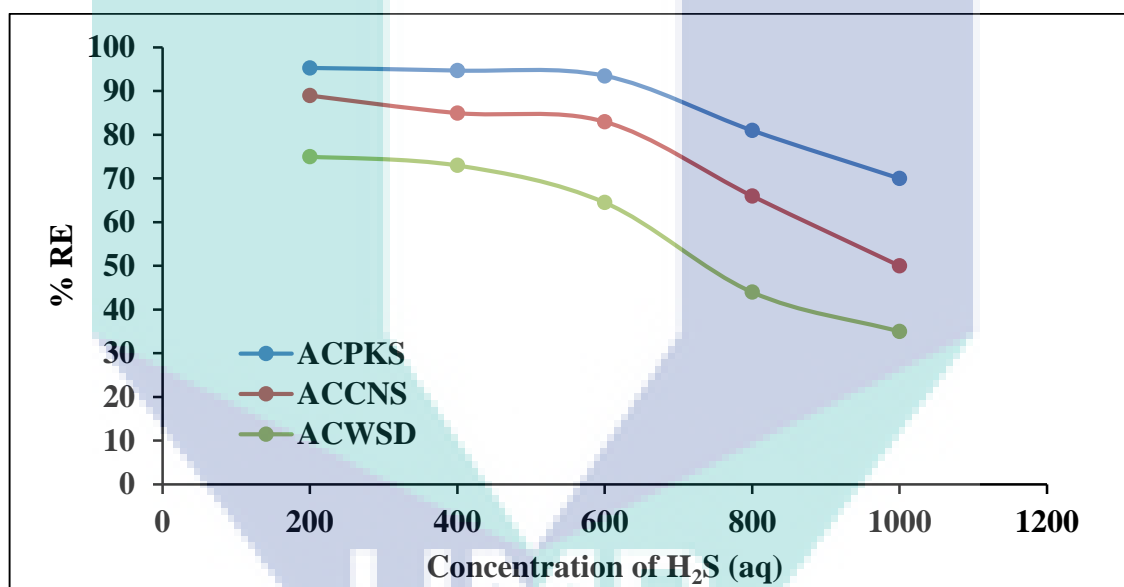


Figure 4.24 Effect of initial concentration of  $H_2S$  (aq) on % RE

#### 4.3.2 Effect of Adsorption Contact Time

The effect of adsorption contact time on the RE of 500 mg/L of  $H_2S$  (aq) were examined as detailed in Table 3.5. The influence of adsorption contact time (using ACs) on the RE of  $H_2S$  (aq) was presented in Figure 4.25. From the result obtained, it is clearly evident that ACPKS gave the highest RE than other adsorbents with ACPKS requiring a lower contact time at ~ 9 h in order to reach the equilibrium state, while ACCNS and ACWSD required 11 h to reach the equilibrium state as succinctly illustrated in Figure 4.25. In fact, the adsorption process was executed for more than 17 h in order to



ensure that complete equilibrium was achieved. All ACs adsorbents revealed that the amount of sorption increased with the increasing adsorption contact time. At the beginning of adsorption process, the adsorbent possessed a larger number of empty active sites. The available number of active sites decreased and the molecule diffusion resistance increased as adsorption was taking place; therefore, the % RE of H<sub>2</sub>S (aq) decreases. Hence, the contact time affects the adsorption process significantly.

In general, the adsorption of H<sub>2</sub>S (aq) ions on the surface of ACs occurred in two stages. In the first stage, adsorption rate was more rapid due to the abundance of vacant active sites on the mesopores surface of the adsorbent. In the second stage, however, the uptake rate decreased due to the required sufficient time to diffuse of H<sub>2</sub>S (aq) ions inside the microporous structure (Zhi et al., 2017). This same trend was observed by Edathil et al. (2017) in their investigation.

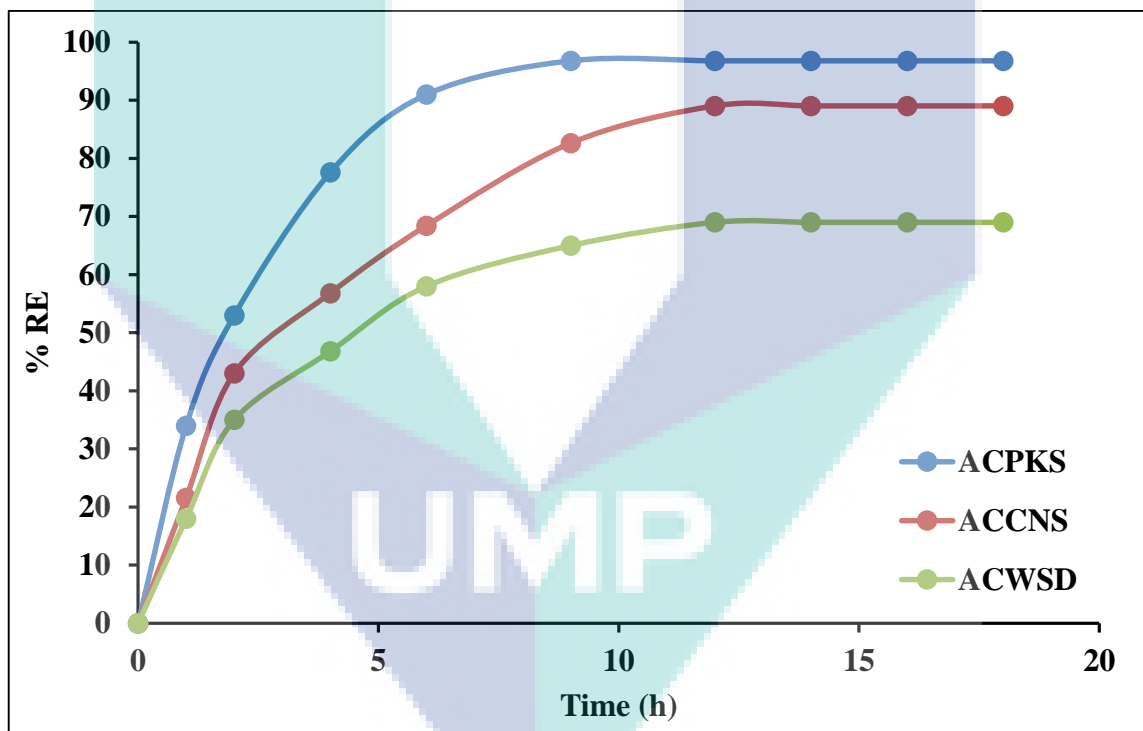


Figure 4.25 Effect of adsorption contact time on % RE

### 4.3.3 Effect of Adsorbent Dosage

Figure 4.26 shows the effect of adsorbent dosage on RE of 500 mg/L of H<sub>2</sub>S (aq). In general, RE increased as the amount of ACs increases. In fact, as the amount of adsorbents increased, the number of active sites increases also. Therefore, the RE for the

H<sub>2</sub>S (aq) was greatly enhanced with similar trend reported by Anbia and Haqshenas (2015). The effect of amount of adsorbents (dosage) were not significant compared with effect of contact time and initial concentration as clearly seen in Figure 4.26.

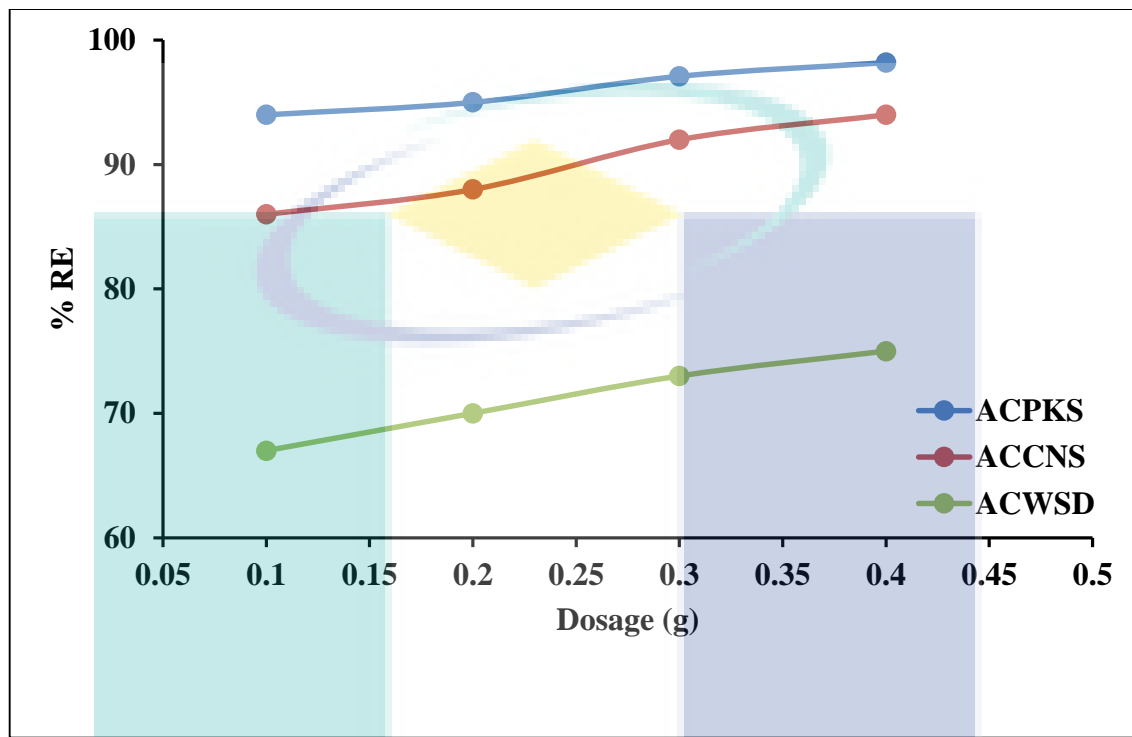


Figure 4.26 Effect of amount of adsorbent on % RE

#### 4.3.4 Effect of Initial Solution pH

Removal efficiency of 500 mg/L of H<sub>2</sub>S (aq) can be affected by several factors such as competitive effects of hydrogen ions with dissolved H<sub>2</sub>S (aq) ions. The changes in the ionic forms for the functional groups on the adsorbent surface and speciation form of H<sub>2</sub>S (aq) in solution. Therefore, it is necessary to investigate the effect of pH while keeping other variables constant. The effect of initial pH on RE is shown in Figure 4.27 with ACPKS exhibiting higher RE of H<sub>2</sub>S (aq). Hence, as the initial solution pH increases, the RE increases until pH 7 was attained. However, RE experienced a decrease thereafter which is due to the fact that the concentration of hydrogen ions (H<sup>+</sup>) was very high at a very low pH which could result in it competing with H<sub>2</sub>S (aq) ions for any available active sites. Thus, as the initial solution pH increases, the number of hydrogen ions (H<sup>+</sup>) decreases also. Therefore, the competition between ions (H<sup>+</sup>) and dissolved H<sub>2</sub>S (aq) ions on the available active sites experienced a decreased.

The state of hydrogen sulfide becomes unstable which could easily be converted to either liquid or gaseous form, as illustrated in Equation 2.1). As the pH increases,  $H_2S$  (g) was converted to  $H_2S$  (aq) and dissociated to ions such as bisulfide ( $HS^-$ ) and sulfide ( $S^{2-}$ ) as shown in Equations 2.3) and 2.4), respectively. At pH = 7, both  $H_2S$  (aq) and  $HS^-$  ions are dominant as seen in Figure 2.2. Thus, RE experienced an increase at this particular pH value. Thereafter, the solution turned to basic (interacts with  $HS^-$  and  $S^{2-}$  ions). Therefore, RE decrease was due to the basic ACs surfaces as reported by Kalapala, (2014). As a result, pH 7 gave higher RE for the  $H_2S$  (aq) as shown in Figure 4.27. The pH has significant effect for ACPKS compared with other adsorbents. The result was consistent with those reported by Haimour et al., (2005) and Wang and Pei (2012).

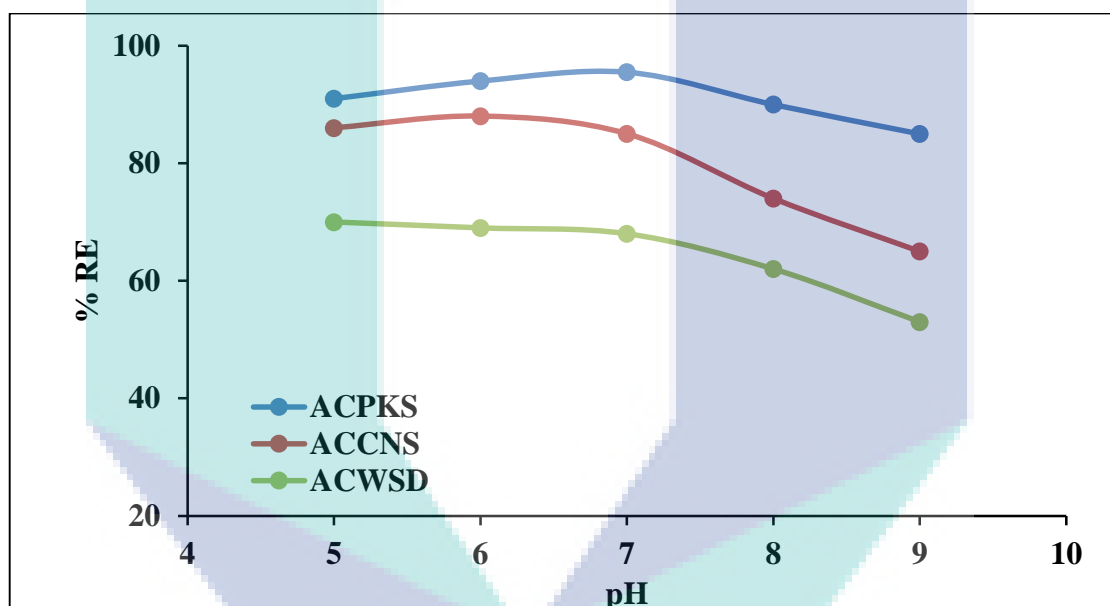


Figure 4.27 Effect of initial solution pH on % RE

#### 4.3.5 Effect of Agitation Speed

Figure 4.28 shows the influence of agitation speed on RE of 500 mg/L of  $H_2S$  (aq) using various ACs adsorbents. For all the ACs, RE increased with respect to the agitation speed. The highest RE was attained at the agitation speed of 150 rpm, which is attributed to the increased solute (dissolved  $H_2S$  (aq)) transport from the bulk solution to the ACs active sites (Roy et al., 2014). The agitation speed of more than 150 rpm might transform  $H_2S$  (aq) from adsorbent surface to the solution. Therefore, the agitation speed of 150 rpm is more suitable with similar observation reported by Roy et al. (2014).

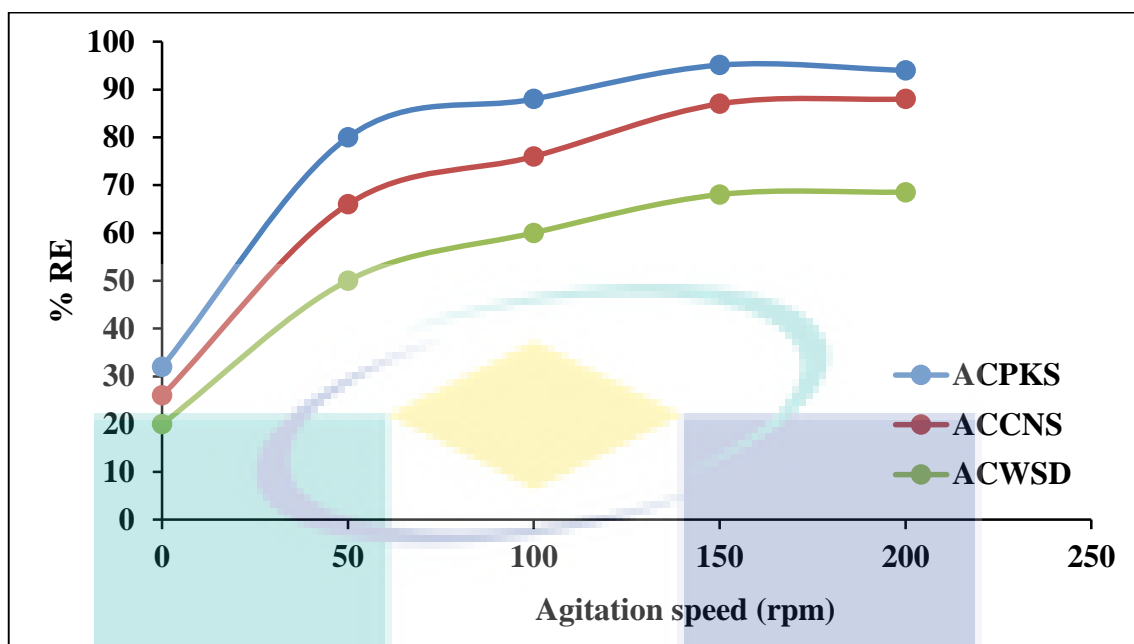


Figure 4.28 Effect of agitation speed on % RE

#### 4.4 Adsorption of H<sub>2</sub>S (aq) on IACs adsorbents

##### 4.4.1 Effect of Preparation Factors on Removal Efficiency

The effect of calcination contact time on IACs type is shown in Figure 4.29. The result showed that at contact time of 90 min a better performance was achieved. This is sufficient to provide a complete reaction between the impregnation agent (egg shells compounds) and carbons during the calcination process. In addition, the removal of all undesired materials such as carbon dioxide and ashes during the calcination process was made possible. In fact, longer contact time has the capacity to increase the amount of calcium oxide (thermally converted from calcium carbonate) upon the calcination process. Hence, Ca-ACPKS showed a better performance in terms of RE of H<sub>2</sub>S (aq) when compared with other IACs.

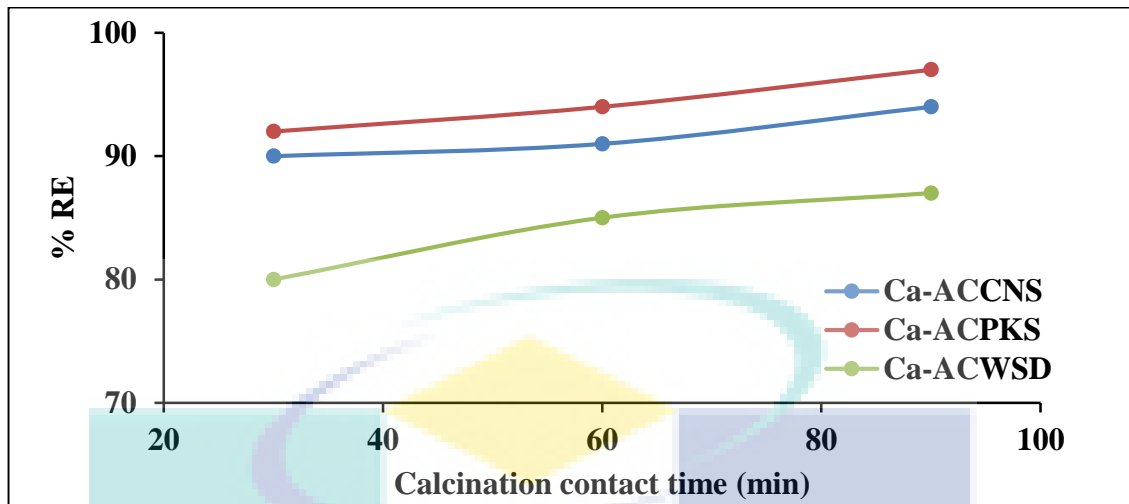


Figure 4.29 Effect of the calcination contact time and types of IACs on RE

Figure 4.30 demonstrates the effect between IACs types and calcination temperature on the RE. Better performances were attained for all the IACs at 900 °C. At 900 °C, with almost all the calcium carbonates ( $\text{CaCO}_3$ ) converted to calcium oxide ( $\text{CaO}$ ) (He et al., 2017). In addition, a thermally stable temperature was witnessed from the TGA result obtained. Increasing the calcination temperature above 900 °C would destroy the bridge layers and structures of carbon. Therefore, the porosity of the IACs adsorbents was affected which lead to decrease in RE. It can be clearly seen that Ca-ACPKS exhibited a higher RE compared with other adsorbents.

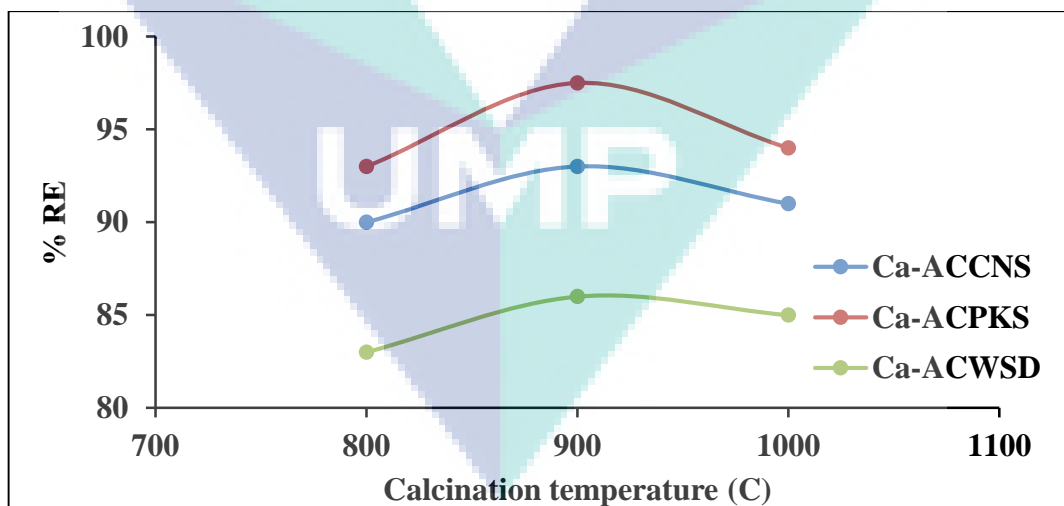


Figure 4.30 Effect of the calcination temperature and types of IACs on RE

Figure 4.31 shows the effect between the calcium concentration and IACs types on RE. It was evident that as the calcium concentration increased the RE degraded accordingly. This degradation is attributed to the blocking of pores by the elemental

calcium, thereby reducing the external surface area of carbon as presented in Table 4.4. However, the concentration of calcium helped in the enhancement on the surface of IACs, as a result to increase RE. From these observations, it can therefore be concluded that the preparation conditions of IACs have a significant effect on the performances of IACs in terms of RE of H<sub>2</sub>S (aq) with Ca-ACPKS having the highest RE amongst other adsorbents.

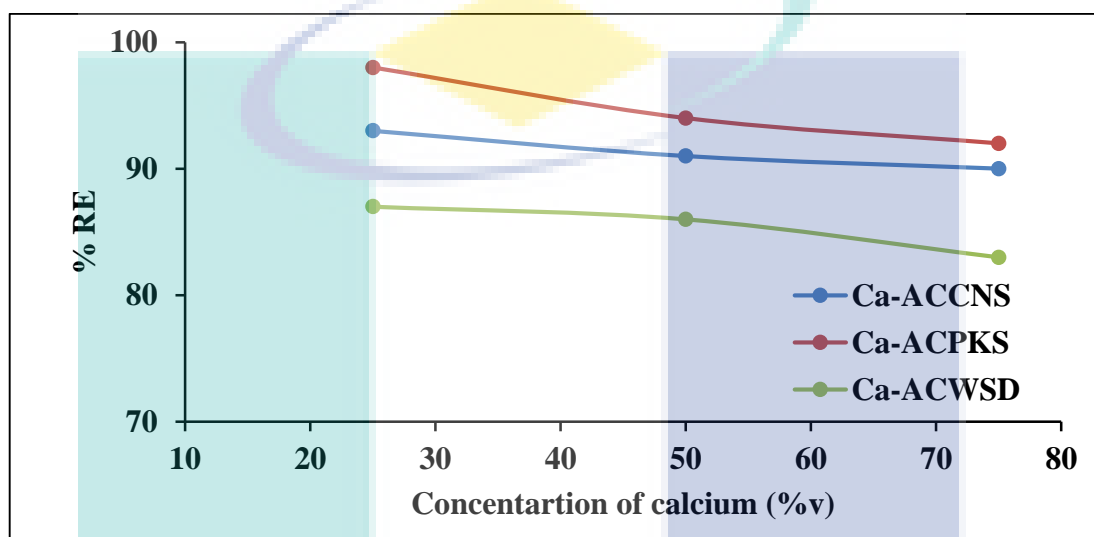


Figure 4.31 Effect of the concentration of calcium and types of IACs on RE

#### 4.4.2 Selection of Effective Adsorbent

Figure 4.32 shows the comparative study of different types of adsorbents with Ca-ACPKS seemingly giving the highest RE. For all the IACs adsorbents, the calcium oxide and the calcium carbonate components derived from egg shells impacted significantly on the RE. Specifically, the SEM image result indicated that Ca-ACPKS possessed more regular morphology and more developed pores. This gave considerable spaces for calcium oxide and calcium carbonate to become deposited on the external surface of the adsorbent, thus enhancing the surface chemistry of Ca-ACPKS. Therefore, the adsorption capacity of Ca-ACPKS was greatly improved.

The EDX result further confirmed that Ca-ACPKS performed better (higher RE) than other adsorbents as presented in Table 4.2. The XRD test result showed that Ca-ACPKS exhibited more crystalline structures compared to other adsorbents. The crystalline structure of spent Ca-ACPKS was not affected after the adsorption process as shown in Figure 4.19. Ca-ACPKS gave the highest RE. Thereafter the preparation

conditions of Ca-ACPKS were optimized using RSM. Additionally, the operating conditions for removing  $H_2S$  (aq) from actual waste water using Ca-ACPKS was also optimized. The associated isotherms, kinetics models and thermodynamic properties of Ca-ACPKS were adequately investigated.

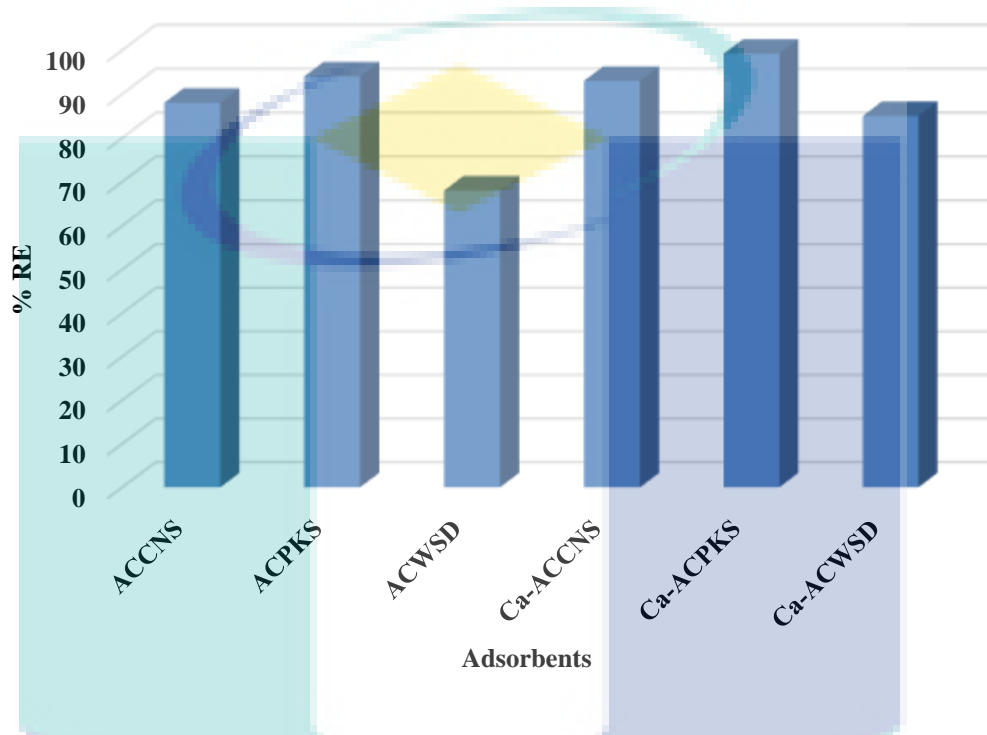


Figure 4.32 Comparison between adsorbents

#### 4.5 Optimization of Preparation Conditions of Ca-ACPKS

The Design of Expert (DOE) (version DX10 USA) software was employed to conduct this study. The preparation conditions of Ca-ACPKS was optimized using RSM. The studied variables are calcination temperature, concentration of calcium solution, and calcination contact time. The responses are RE of  $H_2S$  (aq) and Ca-ACPKS yield. Both responses are listed in Appendix (C). The RE of  $H_2S$  (aq) on Ca-ACPKS was calculated through a batch adsorption test. The details of factors, codes, unites and ranges are shown in Table 3.6.

##### 4.5.1 Analysis of Variance Test

From the ANOVA result in Table 4.9, the quadratic model has the  $F$ -value of 338.56 and the  $P$  value of 0.0001, indicating that the model was significant (Basu et al., 2012). Hence, the significant model terms were A, B, C, AB, AC, BC,  $A^2$ ,  $B^2$  and  $C^2$ .



Table 4.10 shows the result for ANOVA and the lack-of-fit for IACs yield. The *F*-value and p-values were obtained as 147.91 and 0.0001, respectively. This indicated that the model is significant. Moreover, some factors such as A, B, C, A<sup>2</sup>, B<sup>2</sup> and C<sup>2</sup> were significant as well. However, factors such as AB, AC, and BC were insignificant. From the statistical results, it can be concluded that the above models were sufficient to predict the RE and the yield within the ranges of the examined factors. The residual and the lack of fit for both responses were very low, indicating the accuracy of the current model (see Table 4.9).

Table 4.9 Analysis of variance and lack-of-fit test for RE using Ca-ACPCKS

Sources	Sum of squares	df	Mean square	F-value	P-value	Comment
Model	321.17	9	35.69	338.56	<0.0001	significant
A: calcination temperature of Ca-ACPCKS	7.73	1	7.73	73.35	<0.0001	
B: concentration of calcium solution	1.36	1	1.36	12.91	0.0015	
C: calcination contact time	0.48	1	0.48	4.51	0.0441	
AB	1.05	1	1.05	9.97	0.0043	
AC	3.71	1	3.71	35.16	<0.0001	
BC	2.64	1	2.64	25.05	<0.0001	
A <sup>2</sup>	199.53	1	199.53	1893.01	<0.0001	
B <sup>2</sup>	130.86	1	130.86	1241.52	<0.0001	
C <sup>2</sup>	148.72	1	148.72	1410.91	<0.0001	
Residual	2.53	24	0.11			
Lack of Fit	0.69	5	0.14	1.41	0.2638	not significant

Table 4.10 Analysis of variance and lack-of-fit test for Ca-ACPCKS yield

Sources	Sum of squares	df	Mean square	F-value	P-value	Comment
Model	331.25	9	36.81	147.91	<0.0001	Significant
A: calcination temperature of Ca-ACPCKS	215.20	1	215.20	864.83	<0.0001	
B: concentration of calcium solution	4.95	1	4.95	19.88	0.0002	
C: calcination contact time	18.69	1	18.69	75.12	<0.0001	
AB	0.36	1	0.36	1.45	0.2408	
AC	0.42	1	0.42	1.70	0.2049	
BC	0.64	1	0.64	2.57	0.1219	
A <sup>2</sup>	89.99	1	89.99	361.63	<0.0001	
B <sup>2</sup>	6.78	1	6.78	27.23	<0.0001	
C <sup>2</sup>	3.41	1	3.41	13.72	0.0011	
Residual	5.97	24	0.25			
Lack of Fit	4.80	5	0.96	15.54	<0.0001	Significant

Table 4.11 shows the results of regression statistics models for both yield and RE. For RE at equilibrium, the quadratic model was suggested with R<sup>2</sup> and standard deviation of 0.992 and 0.32, respectively. The cubic model was aliased. In addition, Table 4.11 shows the regression statistics for Ca-ACP<sub>KS</sub> yield. The quadratic model was used as well with R<sup>2</sup> and standard deviation values of 0.982 and 0.5, respectively. This suggested that the quadratic model could be utilized to represent the relationship between the interacting factors and the responses.

Table 4.11 Regression statistics for RE and yield at equilibrium using Ca-ACP<sub>KS</sub>

Response	Source	Standard deviation	R <sup>2</sup>	Adjusted R <sup>2</sup>	Predicted R <sup>2</sup>	Comment
RE	Linear	3.24	0.0296	0.0675	0.0888	
	2FI	3.37	0.0524	0.1582	0.1563	
	Quadratic	0.32	0.9922	0.9893	0.9853	Suggested
	Cubic	0.32	0.9939	0.9899	0.9852	Aliased
Ca-ACP <sub>KS</sub> yield	Linear	1.81	0.7083	0.6791	0.6372	
	2FI	1.90	0.7125	0.6486	0.6095	
	Quadratic	0.50	0.9823	0.9756	0.9635	Suggested
	Cubic	0.48	0.9864	0.9776	0.9579	Aliased

Centre Composite Design (CCD) was used to determine the correlation between the response surface and the input variables. Relationship coefficient and standard deviation were utilized to assess the wellness of the models developed. The quadratic models suggested by the software for RE and yield were presented in Equation 4.7) and 4.8).

$$\text{RE} = 98.42 + 0.53A + 0.22B + 0.13C + 0.26AB - 0.48AC - 0.41BC - 2.97A^2 - 2.41B^2 - 2.57C^2 \quad 4.7$$

$$\text{Yield} = 35.26 - 2.81A - 0.43B - 0.83C - 0.15AB - 0.16AC + 0.20BC - 2.00A^2 - 0.55B^2 - 0.39C^2 \quad 4.8$$

Figure 4.33 (a, b) is the plot of the predicted and actual plots with the normal plot of residual for RE. From Figure 4.33 (a), the predicted values were closer to the actual ones, thus validating the current models. Moreover, the residual error was very lower as indicated in Figure 4.33 (b). The predicted and actual plot and the normal plot of residual for IACs yield were shown in Figure 4.34 (a, b), respectively. Both predicted and actual values showed good agreement with the residual values having a relatively low value.

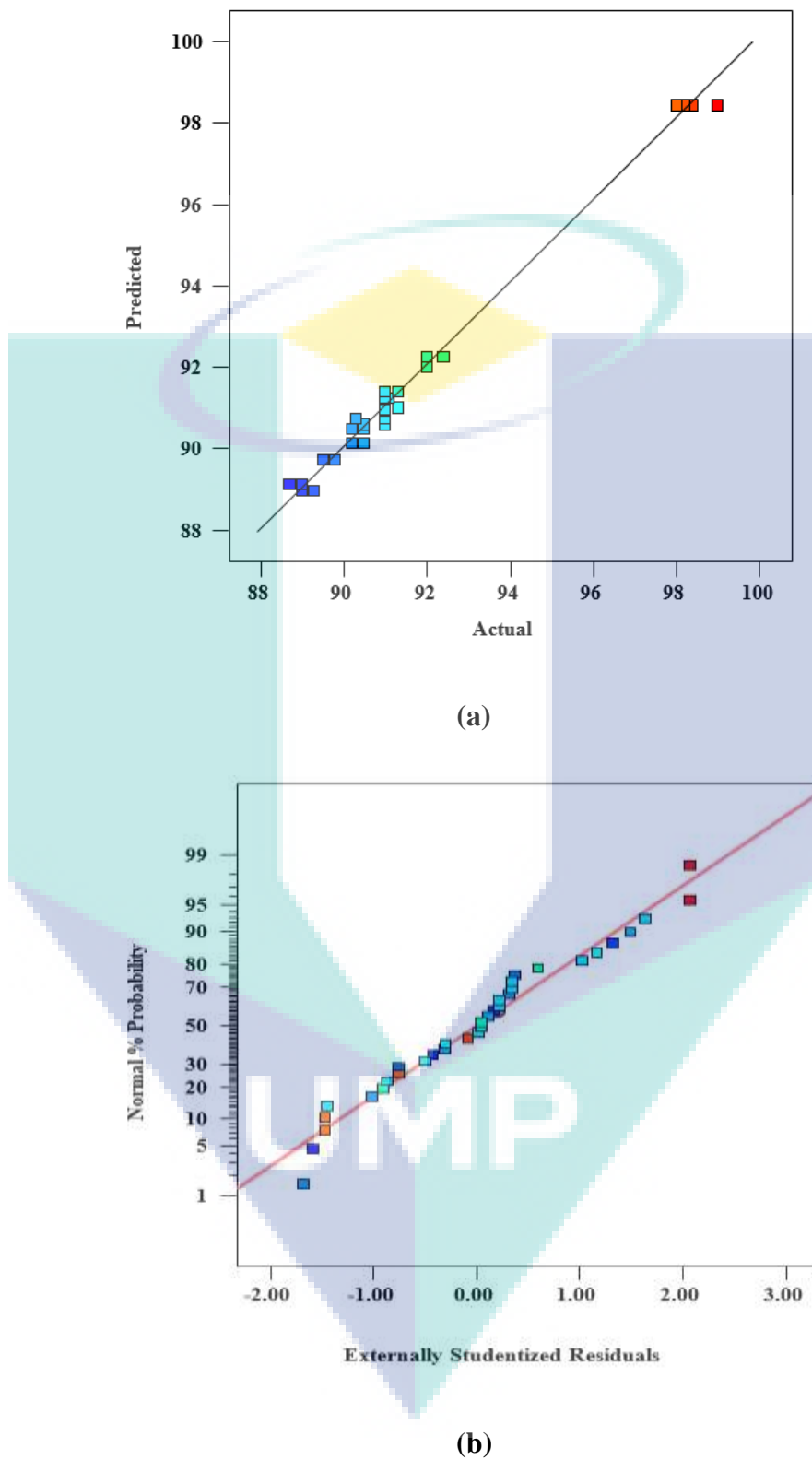
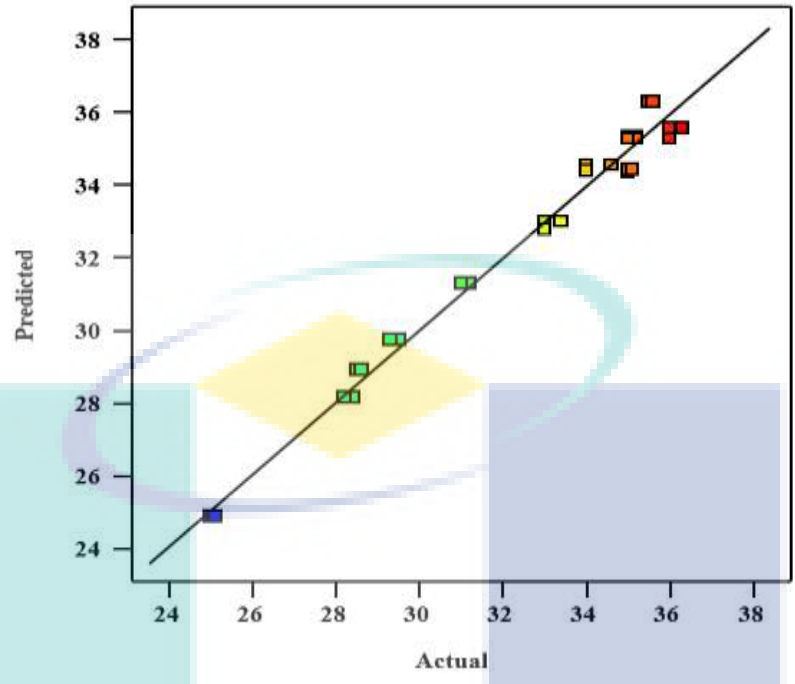
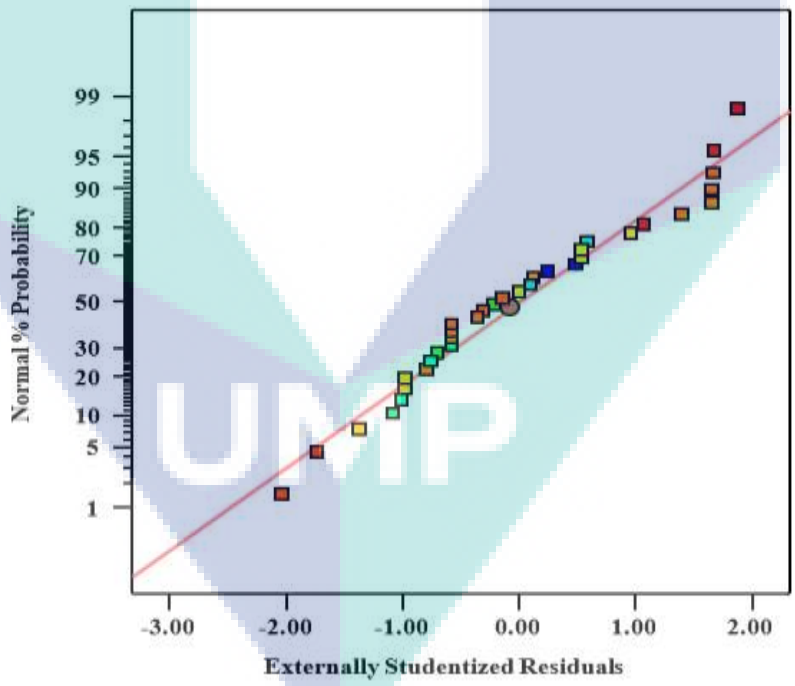


Figure 4.33 (a) The predicted and actual values, (b) Normal plot residual for RE using Ca-ACPES



(a)



(b)

Figure 4.34 (a) The predicted and actual values, (b) Normal plot residual for the yield of Ca-ACPES

#### 4.5.2 Combined Effect of 3D Plot on Removal Efficiency

Figure 4.35 shows the interactions between two independent variables, (i.e. calcination temperature and concentration of calcium solution) on RE while fixing the calcination contact time. As seen, the interaction between these two factors was clear. The calcination temperature range of 800 °C to 1000 °C and the calcium concentration range of 25 v % -75v% imposed a significant influence on the RE. It can be clearly seen that the effect of calcination temperature on RE was more significant. With the calcination temperature of ~800°C, the value of RE was estimated to be 89.7%. Thereafter, the RE increased with calcination temperature increment. The concentration of calcium therefore imposed a direct impact on the RE. In general higher concentration gave a higher RE. However, excessive level of concentration of calcium had a negative impact on the RE.

The melting point of calcium was 842 °C, thus, the elemental calcium (Ca) was evaporated, leaving behind a huge amount of calcium vapour deposits on the carbon layers and original pores between carbon atoms. At 900 °C, most of the calcium carbonate were converted to calcium oxide, thereby increasing the compound of metal oxide between carbon layers and pore structures. Therefore, the removal of H<sub>2</sub>S (aq) was adequately enhanced.

The interactions of time and calcination temperature of Ca-ACP<sub>KS</sub> on RE are shown in Figure 4.36. It can be seen that the effect of calcination temperature on RE was more significant. The calcination contact time, however, had less contribution on RE. Figure 4.37 shows the interactions between calcination contact time and calcium concentration. The effect of contact time was less significant than that of calcium concentration.

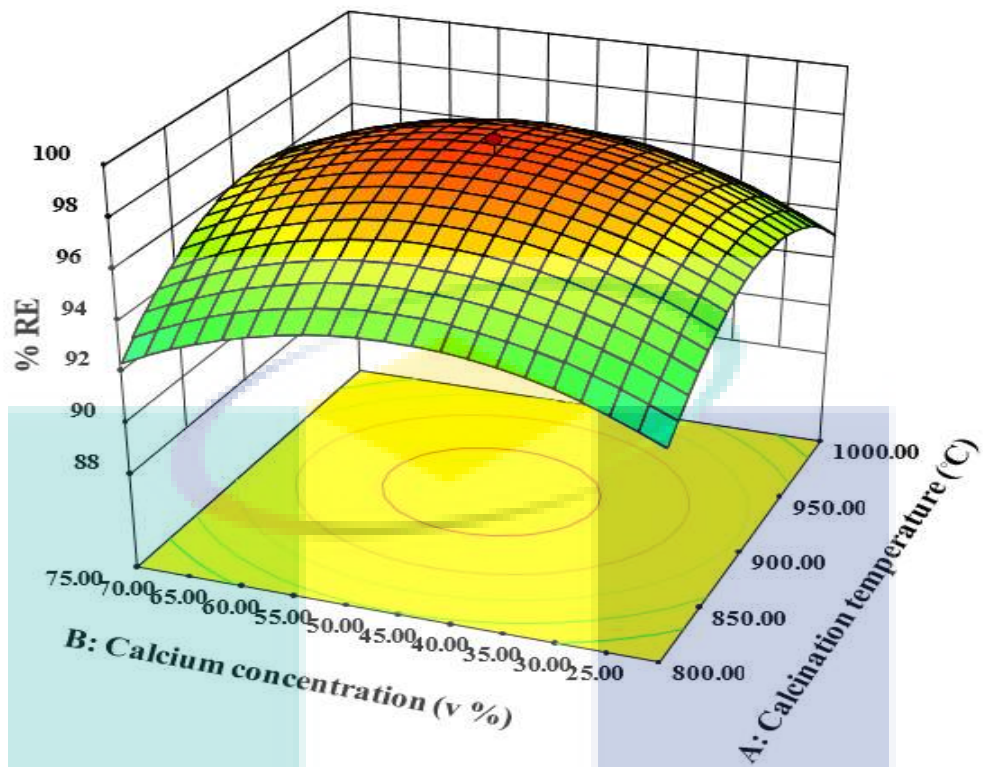


Figure 4.35 The combined effect of calcination temperature and calcium solution concentration on RE

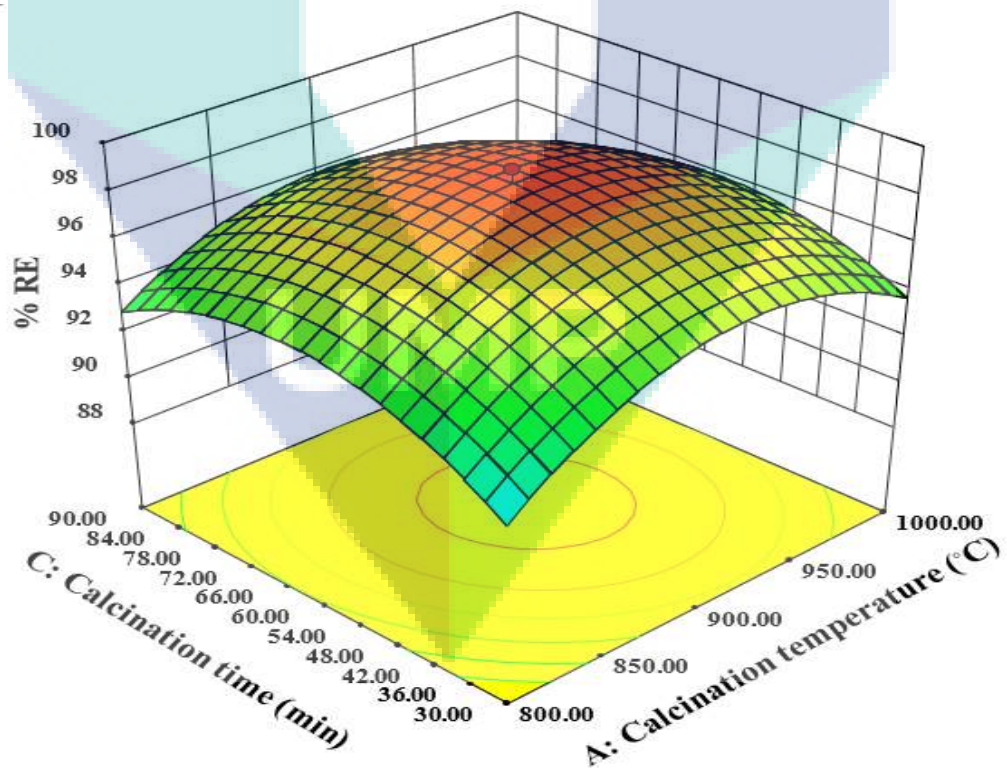


Figure 4.36 The influence of combined the calcination temperature and calcination contact time on RE



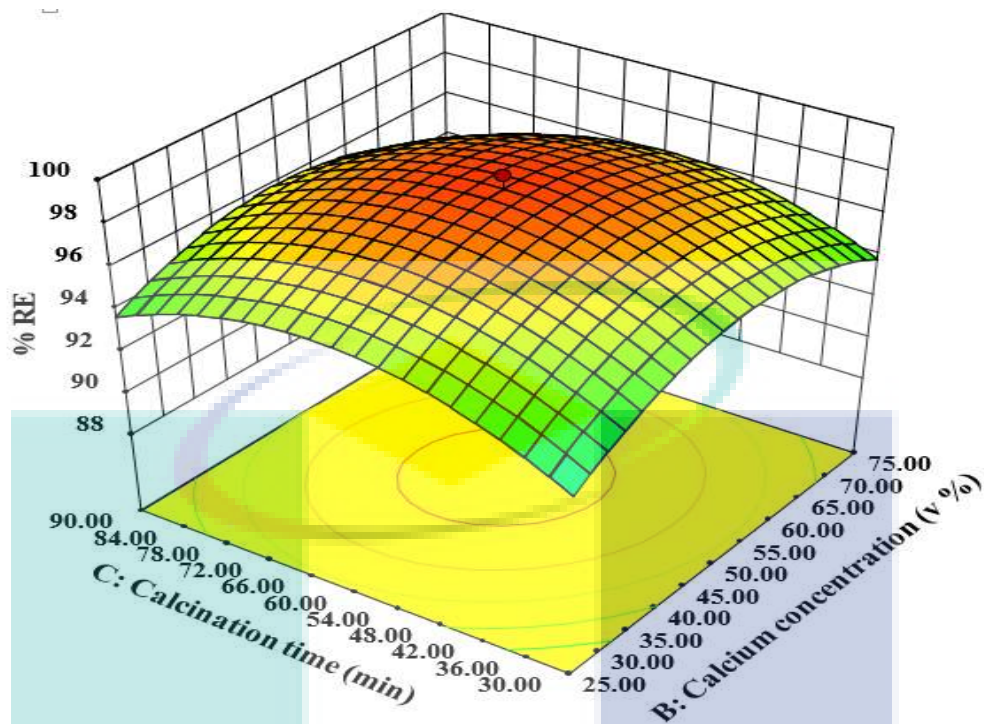


Figure 4.37 The influence of combined of calcium concentration and calcination contact time on RE

#### 4.5.3 Combined Effect of 3D Plot on Ca-ACP<sub>2</sub> Yield

The combined effect of calcination temperature and concentration of calcium on Ca-ACP<sub>2</sub> yield is shown in Figure 4.38. The effect of calcination temperature on Ca-ACP<sub>2</sub> yield was more significant than that of calcium concentration. There was a relative decrease in the yield as both calcination temperature and concentration of calcium increased. Figure 4.39 shows the 3D plot of combined effect of calcination contact time and calcination temperature on yield. It indicated that the effect of calcination temperature on yield was more significant than that of calcination contact time. Figure 4.40 shows the 3D plot of combined effect of calcination contact time and concentration of calcium on yield. Both calcination contact time and concentration of calcium almost the same effect on the yield. It can therefore be clearly seen that a very low yield was obtained at contact time of 120 min and calcium concentration of 90 %v.



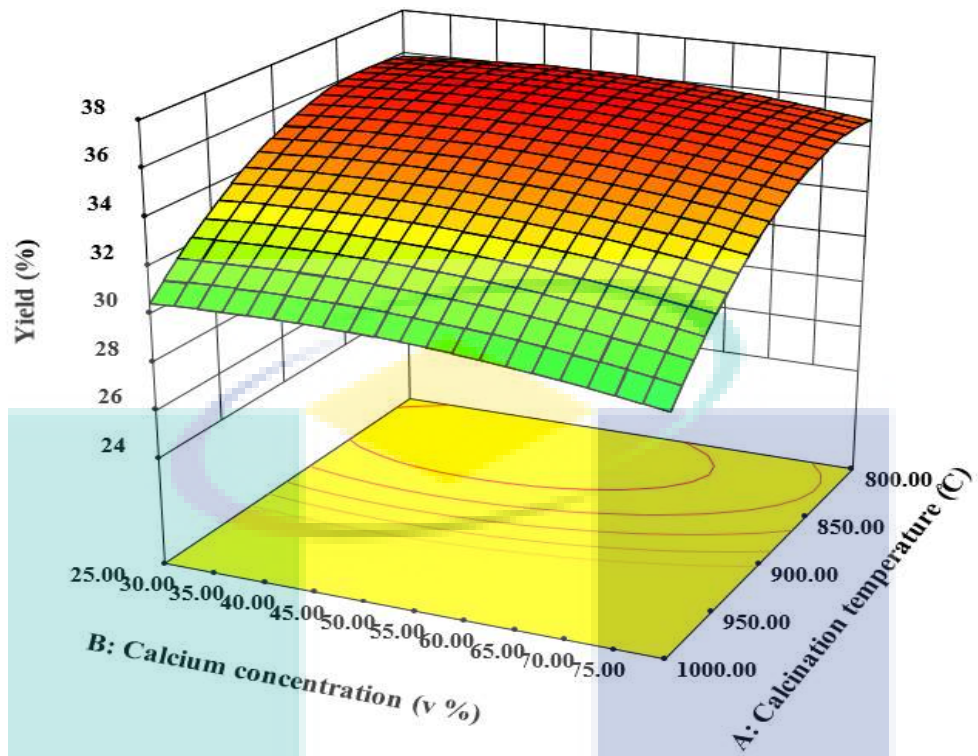


Figure 4.38 The influence of combined the calcination temperature and calcium concentration on the yield of Ca-ACPKS

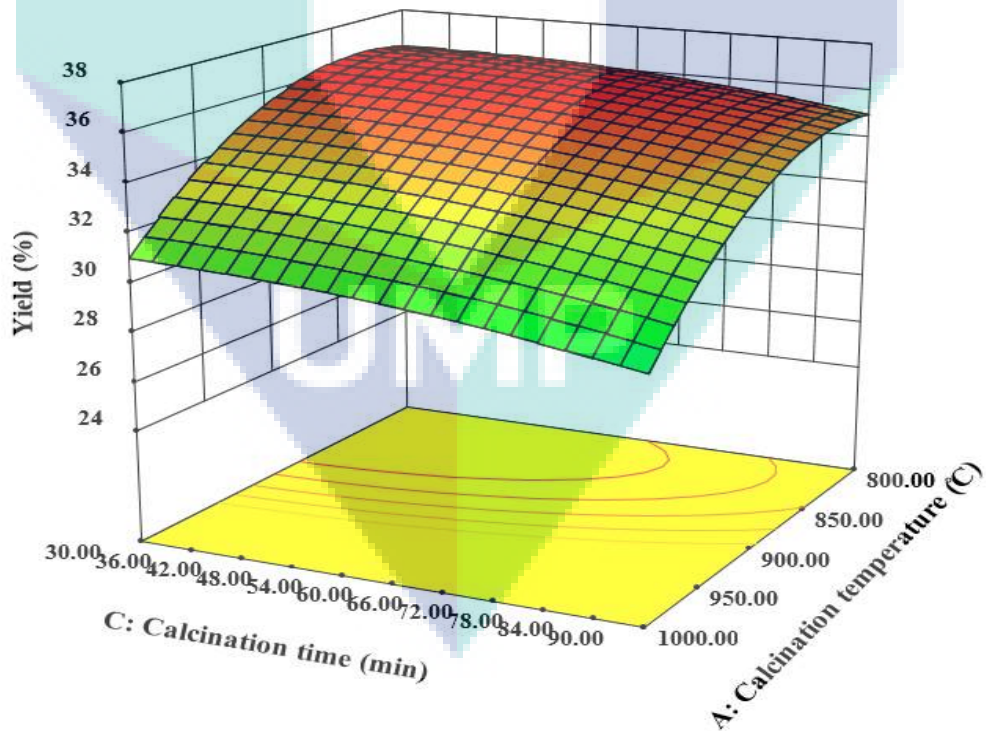


Figure 4.39 The influence of combined the calcination temperature and calcination time on the yield of Ca-ACPKS

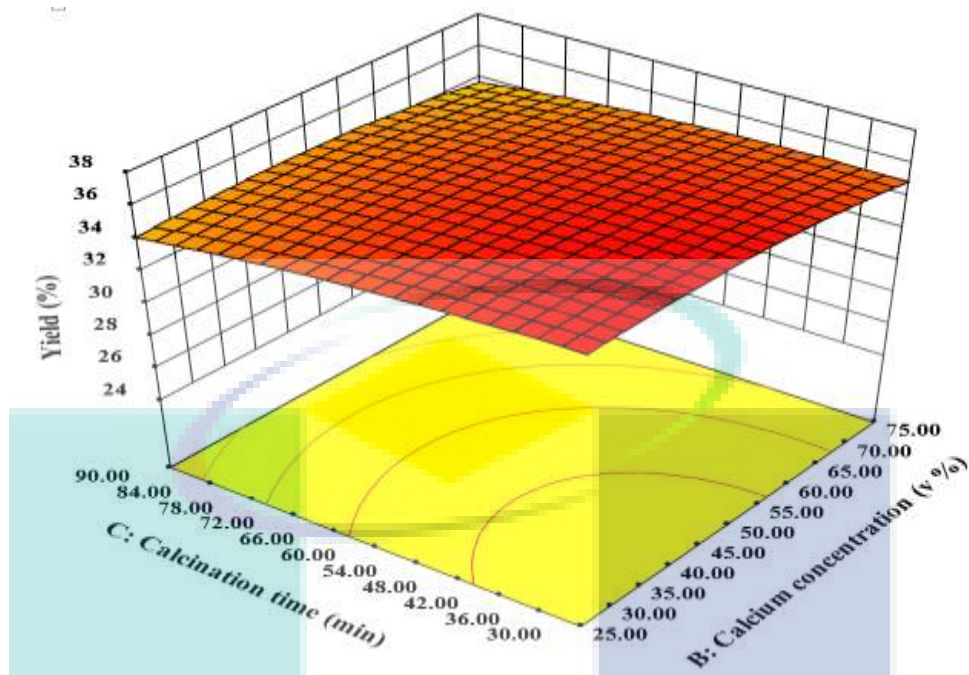


Figure 4.40 The influence of combined the concentration of calcium and calcination time on the yield of Ca-ACPKS

#### 4.5.4 Validation of preparation conditions of Ca-ACPKS

The optimum conditions are shown in Figure 4.41. The desirability was 0.937, which is relatively high. The validation results of the current RSM model are reported in Table 4.12. It was discovered that the experimental results compared well with the RSM values. Therefore, the model equation suggested by RSM was valid.

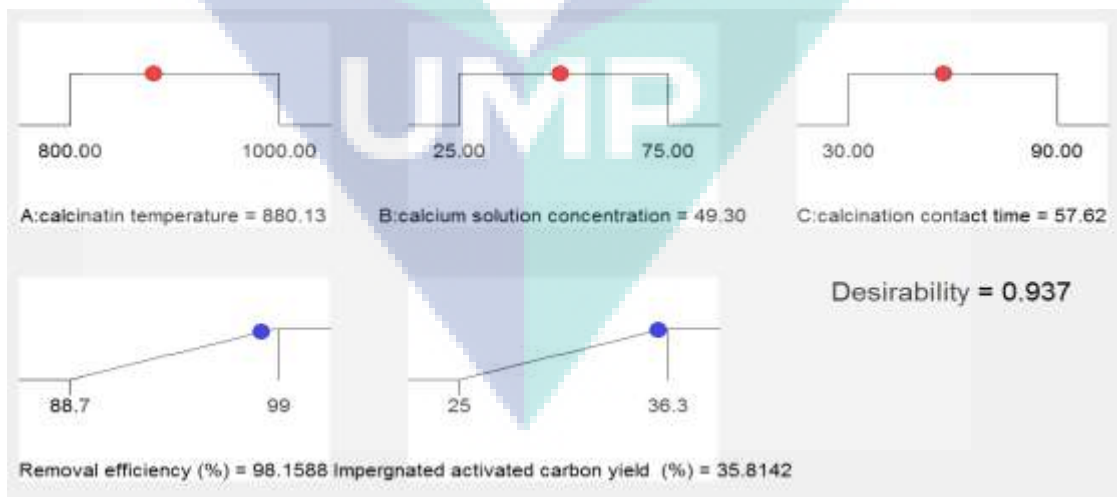


Figure 4.41 The optimum of the preparation conditions and desirability of Ca-ACPKS

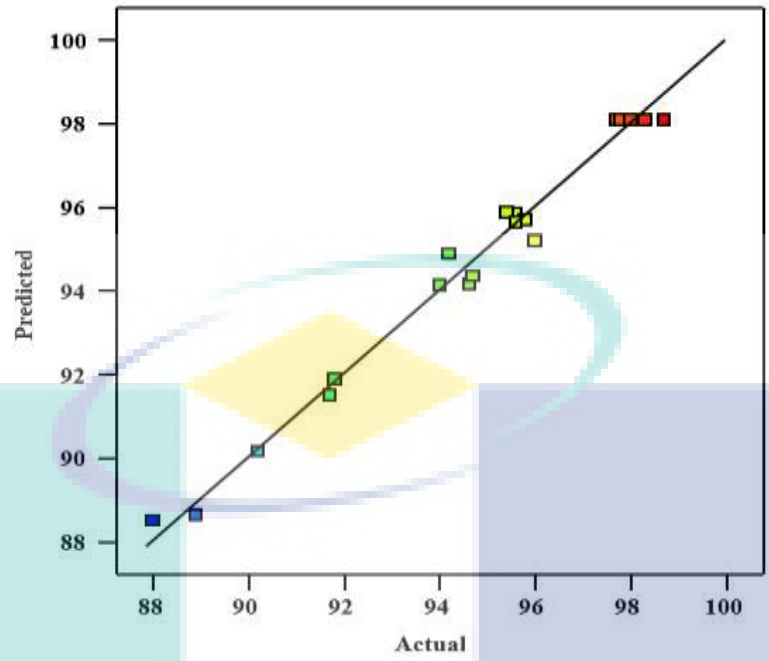
Table 4.12 Model validation of preparation conditions of Ca-ACPKS

Variables			Theoretical		Experimental		
Calcination temp. (°C)	Calcium concentration (v %)	Calcination time (min)	Yield	RE	Yield	RE	Error
880	49.3	57.5	35.8	98.2	33.8	99.2	0.99

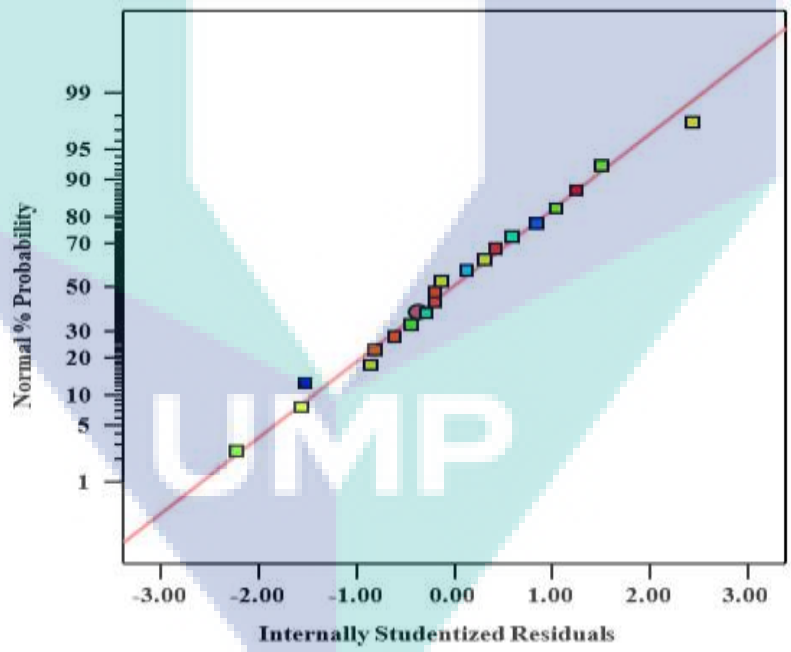
#### 4.6 Optimization of Adsorption Process of Ca-ACPKS

Factors such as initial concentration of H<sub>2</sub>S (aq) (mg/L), adsorption contact time (min), dosage of adsorbent (g), pH and agitation speed (rpm) were adequately screened. The ranges of these factors were reported in Table 3.7. The ANOVA test was conducted to show the significance of model and factors. The details of the statistical analysis are shown in Appendix (C). It can be observed that the model was significant with R<sup>2</sup> of 0.998. The results revealed that initial H<sub>2</sub>S (aq) concentration, adsorption contact time, adsorbent dosage have significant impacts on the RE of H<sub>2</sub>S (aq). However, factors such as pH and agitation speed are insignificant. The best operating conditions were, the initial H<sub>2</sub>S (aq) concentration of 500 mg/L, adsorption contact time of 540 min and amount of adsorbent of 1 g/L. The insignificant factors such as pH and agitation speed are 7 and 150 rpm, respectively. The best conditions of the screening process were used in the subsequent optimization study.

The factors, units and ranges for all significant factors were reported in Table 3.8. Figure 4.42 (a, b) shows the predicted and actual plots and normal plot of residual for RE. It can be deduced from Figure 4.42 (a) that the predicted values were very close to the actual ones. Figure 4.42 (b) shows that the residual errors were low as well, and this indicated the effectiveness of the current second-order model. As observed from Figure 4.42 (a), most of the values were closer to standard line (indicating low residual error). Meanwhile, the experimental values were quite close to the predicted values, indicating that the model developed was good (Figure 4.42 (b)).



(a)



(b)

Figure 4.42 (a) The predicted vs actual values, (b) Normal plot of residuals for optimization of operating conditions of RE using Ca-ACPKS

#### 4.6.1 Analysis of Variance Test

ANOVA was subsequently performed to explore and indicate the significance level of the model. The ANOVA test results are listed in Table 4.13. From the F-value (74.19) and p-value (<0.0001), the quadratic model was significant (Basu et al., 2012). Moreover, the value of lack of fit is very low with the variables such as A, B, C AB, BC, A<sup>2</sup>, B<sup>2</sup>, and C<sup>2</sup> taking up significant functions. The AC term, however, was insignificant. The low levels of residual and pure error indicated the fitness of the current model. It can be concluded that the effect of adsorption contact time was more significant than those of other variables (Table 4.13).

Table 4.13 Analysis of variance (ANOVA) and lack-of-fit test for RE using Ca-ACPKS

Sources	Sum of squares	df	Mean square	F-value	P-value	Comment
Model	188.42	9	20.94	74.19	<0.0001	significant
A-Initial H <sub>2</sub> S concentration	21.22	1	21.22	75.22	<0.0001	
B-Adsorption contact time	53.87	1	53.87	190.92	<0.0001	
C-Adsorbent dosage	2.01	1	2.01	7.14	0.0234	
AB	2.57	1	2.57	9.09	0.0130	
AC	0.29	1	0.29	1.04	0.3325	
BC	2.57	1	2.57	9.09	0.0130	
A <sup>2</sup>	36.41	1	36.41	129.03	<0.0001	
B <sup>2</sup>	70.27	1	70.27	249.04	<0.0001	
C <sup>2</sup>	17.26	1	17.26	61.18	<0.0001	
Residual	2.82	10	0.28			
Lack of Fit	2.15	5	0.43	3.22	0.1125	not significant

The regression statistics models for operating conditions are presented in Table 4.14. The model suggested by the software is a quadratic model with R<sup>2</sup> and standard deviation of 0.9852 and 0.53, respectively. The result obtained showed that the cubic model is aliased. Moreover, the predicted R<sup>2</sup> was 0.9852, which agreed reasonably well with the adjusted R<sup>2</sup> of 0.9720 due to the difference less than 0.2 (Pamnani et al., 2015; Kumar et al., 2016). The quadratic model suggested by the software is shown in Equation 4.9). The Adeq precision was used to measure the signal to noise ratio. The predicted R<sup>2</sup> showed how well the developed model can be used to predict the response. The negative sign indicated that the term promoted a decrease in RE and vice-versa (Junior et al., 2014).



$$RE = 98.09 - 1.25A + 1.99B + 0.38C + 0.57AB - 0.19AC - 0.57BC - 1.59A^2 - 2.21B^2 - 1.09C^2$$

4.9

Table 4.14 Regression statistics for operating conditions of RE using Ca-ACPKS

Response	Source	Standard deviation	R <sup>2</sup>	Adjusted R <sup>2</sup>	Predicted R <sup>2</sup>	Comment
RE	Linear	2.67	0.4032	0.2913	0.1569	Suggested Aliased
	2FI	2.89	0.4316	0.1692	-0.5175	
	Quadratic	0.53	0.9852	0.9720	0.9071	
	Cubic	0.39	0.9953	0.9850	0.7223	

#### 4.6.2 Combined Effect of 3D Plot on Removal Efficiency

The 3D plot of the combined effect of initial concentration of H<sub>2</sub>S (aq) and adsorption contact time on RE is shown in Figure 4.43. As seen, the effect of adsorption contact time on RE was more significant. The lowest RE was attained at adsorption contact time of 420 min and initial concentration of H<sub>2</sub>S (aq) of 700 mg/L. This was due to the fact that the adsorbate molecules were competing intensively in order to occupy the active site. Therefore, more time was needed during the period of competition. In general, the RE of H<sub>2</sub>S (aq) increased as the adsorption contact time increased and the H<sub>2</sub>S (aq) initial concentration decreased as shown in Figure 4.43. The optimum RE of 99.5 % was attained at contact time of ~585 min with concentration of 440 mg/L. A similar 3D plot was reported by Sohrabi et al. (2016).

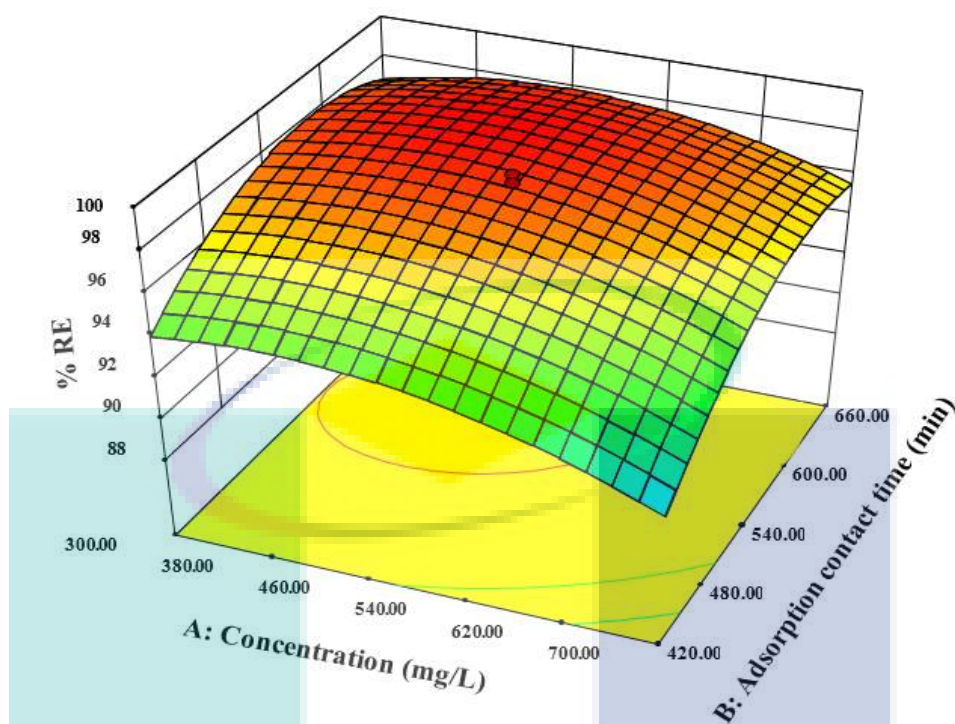


Figure 4.43 Combined effect of initial concentration of  $H_2S(aq)$  and contact time on RE using Ca-ACPKS

Figure 4.44 shows the 3D plot of the combined impact of initial concentration of  $H_2S(aq)$  and dosage used. Seemingly, the effect of dosage was less significant. The initial concentration of 700 mg/L and the Ca-ACPKS amount of 0.75 g gave the lowest value of RE. This was because the low amount of Ca-ACPKS has less number of unoccupied active sites and the competition between ions at higher concentration lead to the reduction of RE. Thus, adsorption was more ineffective due to insufficient active sites (low adsorbent dosage). As the amount of Ca-ACPKS increased and the initial concentration decreased the RE increased correspondingly. Moreover, the initial concentration showed more contribution to the RE compared with Ca-ACPKS dosage. From the results, dosage of 1 g can remove  $\sim 440$  mg/L of  $H_2S(aq)$ . Similar trend has been noticed by Sahu et al. (2009).



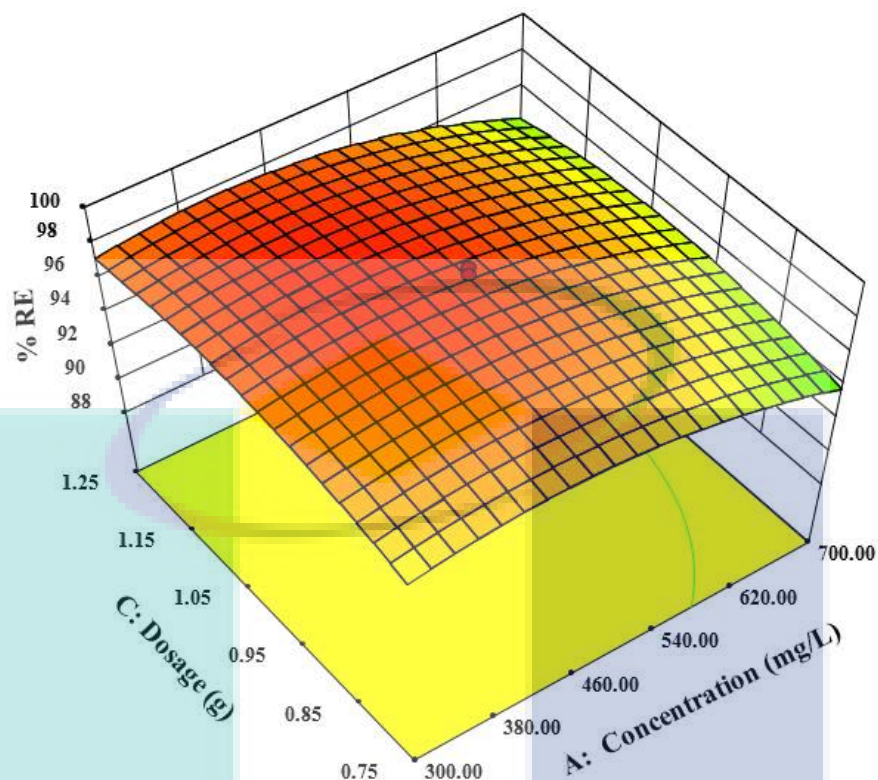


Figure 4.44 Combined effect of initial concentration of  $H_2S$  (aq) and dosage on RE using Ca-ACPKS

The combined influence of dosage and adsorption contact time is presented in Figure 4.45. It can be seen that the effect of adsorption contact time on RE was more significant. An increase in the contact time resulted in a corresponding increase in RE. The effect of adsorption contact time on RE was therefore significant and this is largely due to the fact that the dissolved  $H_2S$  (aq) ions require a sufficient time to transport from the bulk solution to the Ca-ACPKS surface film. Then, cross the film to reach the unoccupied active site in the external micropores. The highest RE was attained with the contact time around 585 min. The dosage of Ca-ACPKS, however, recorded a less effect on RE. This was as a result of Ca-ACPKS having more porosity and active site and even the low amount of Ca-ACPKS could be occupied the dissolved  $H_2S$  (aq). Thus, the increasing of Ca-ACPKS amount recorded a low effect on RE as reported by Roosta et al. (2015).

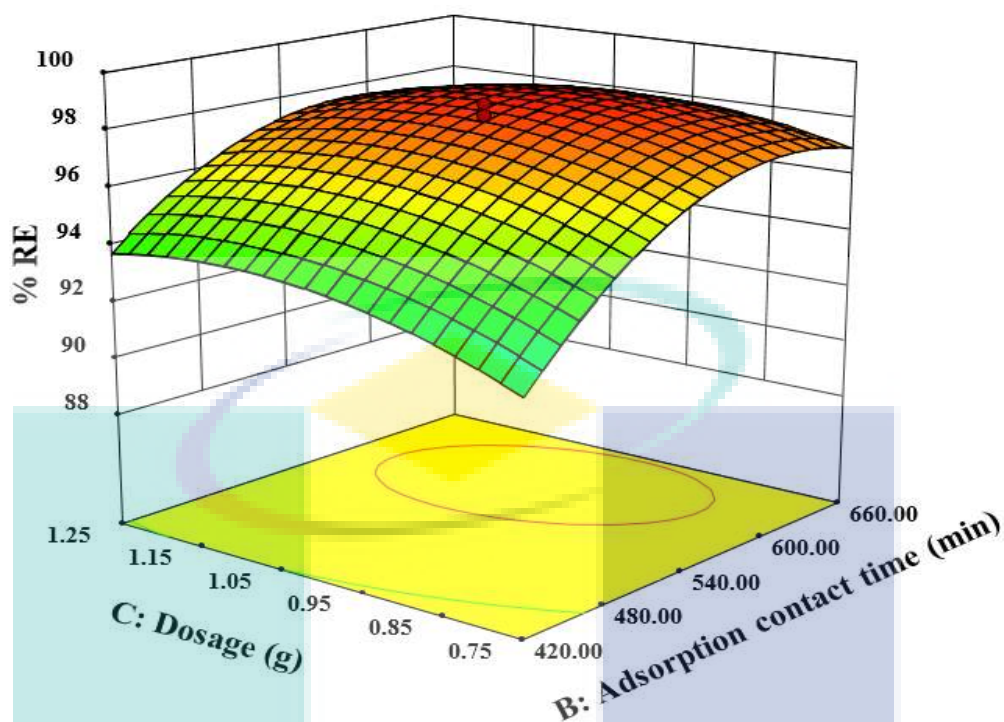


Figure 4.45 Combined effect of dosage and contact time on RE using Ca-ACPKS

### 4.6.3 Validation of Operating Conditions

The optimum operating conditions of Ca-ACPKS were all summarized in Table 4.15. The experimental values compared well with the predicted ones as shown in Figure 4.46. Therefore, the model equation suggested by RSM was valid.

Table 4.15 Validation of operating conditions of RE of H<sub>2</sub>S(aq) using Ca-ACPKS

Variables			Theoretical	Experimental	
Concentration of H <sub>2</sub> S (mg/L)	Contact time (min)	Adsorbent dosage	RE	RE	Error
440	585	1.05	98.7	99.5	0.8

Figure 4.46 presents the validation between predicted and actual results. The predicted values were obtained from Equation 4.9) which are in close agreement with the actual ones as seen in Figure 4.46.

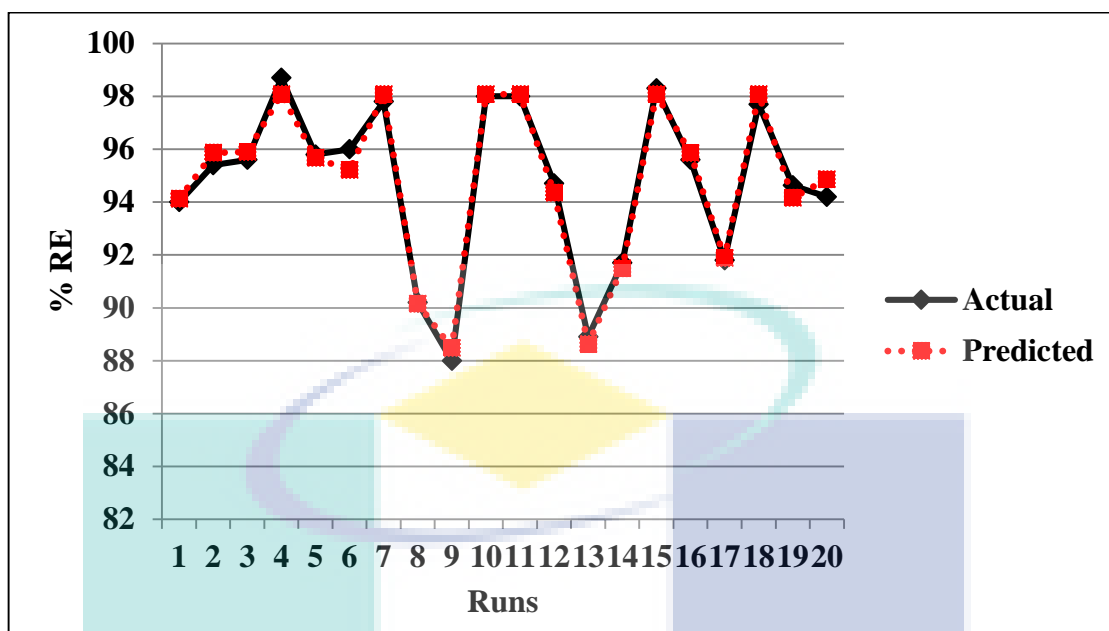


Figure 4.46 Validation between actual and predicted results of operating conditions of RE using Ca-ACPES

#### 4.7 Equilibrium, Isotherm, and Kinetic Study of Ca-ACPES

##### 4.7.1 Effect of Contact Time and Initial Concentration

The batched adsorption mode was conducted by adding 0.1 mg of Ca-ACPES adsorbent to 250 mL volume of conical flasks containing solution of 100 mL. The initial concentration of the dissolved  $H_2S$  ( $C_0$ ) is ranging from 100 mg/L -500 mg/L. Detail of batch adsorption process were carefully discussed in Section 3.6. The adsorption capacity ( $q_e$ , mg/g) was calculated using Equation 3.3). Subsequently, the initial and final concentrations were measured after the suspensions were filtered. The RE can then be determined using Equation 3.4). Figure 4.47 shows the plots of RE versus time at various initial  $H_2S$  (aq) concentrations. The temperature was fixed at 30 °C. From Figure 4.47, the initial amount of  $H_2S$  (aq) adsorbed onto the carbon surface increases rapidly. However, the adsorption rate decelerates upon reaching a critical point as the amount of  $H_2S$  (aq) desorbed from the adsorbent was equivalent to the amount of  $H_2S$  (aq) adsorbed onto the adsorbent. Initially, the solution pH was neutral before gradually decreasing due to the oxidation of  $H_2S$  (aq). On the overall, at concentrations of 100 mg/L and 200 mg/L, the equilibrium times were very short due to the abundance of many empty sites. At the neutral condition, the dominating forms of sulfide were  $H_2S$  (aq) and bisulfide ( $HS^-$ ). The ion exchange reaction was likely to occur due to the diffusion of sulfide anions and

calcium cations to the active site to produce calcium sulfide (CaS). CaS exists on the surface of adsorbent as white crystallized materials. In fact, the solution changes from yellow colour to colourless at the equilibrium state. The removal of H<sub>2</sub>S (aq) can then be summarised based on the colour change. At the first stage (yellow colour), the gaseous H<sub>2</sub>S (g) dissolved to aqueous H<sub>2</sub>S (aq) and HS<sup>-</sup> as shown in Equations 2.1) and 2.3), respectively. Then, during the adsorption process (after 3-4 h), the solution colour was white due to the formations of calcium sulfide (CaS) and sulfur as shown in equations 4.21) and 4.24). At the final stage, the solution became colourless due to the precipitation of metal sulfide, sulfur and salts on the pores. The carboxylic functional group (-COOH) obtained from the calcium acetate (Ca (C<sub>2</sub>H<sub>3</sub>O<sub>2</sub>)<sub>2</sub>) composite and ACs gave the best chemisorption capacity towards H<sub>2</sub>S (aq). At low pH, the removal of H<sub>2</sub>S (aq) was lower due to high affinity of carboxylic functional groups toward H<sup>+</sup>. At the initial stage of the adsorption process; calcium sulfide (CaS) was formed as shown in Equation 4.21). In summary, most of the adsorption processes exhibited chemisorption. Similar observation was reported by Jacukowicz et al. (2015). They were used a hybrid materials containing iron oxide for removal of sulfides from water.

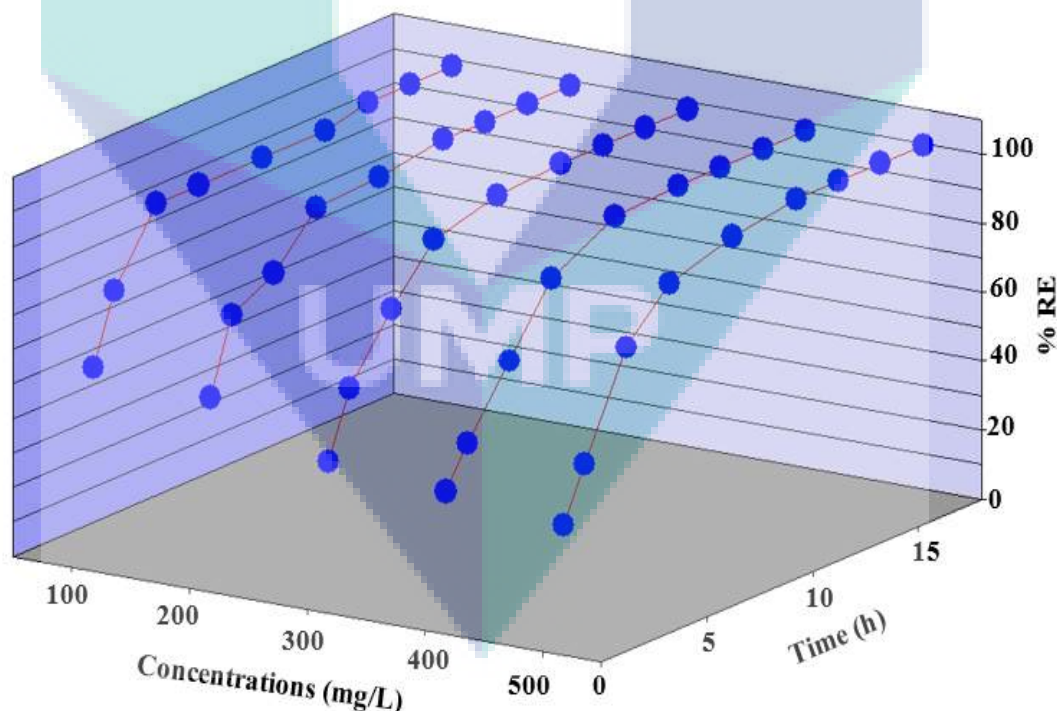


Figure 4.47 The effect of adsorption time with various initial H<sub>2</sub>S (aq) concentration on RE using Ca-ACPKS

#### 4.7.2 Adsorption Isotherms Model

The four adsorption isotherm models such as Langmuir, Freundlich, Temkin and Dubinin–Radushkevich were applied to describe the behaviour of the adsorption process. The Langmuir adsorption isotherm model (linear plot of  $C_e/q_e$  against  $C_e$ ) was used to determine the Langmuir parameters as shown in Figure 4.48 (a). The Langmuir parameters such as  $Q_{max}$  were determined from the slope and the intercept respectively using Equation 2.6). The correlation coefficients ( $R^2$ ) and parameters are reported in Table 4.16. The  $R^2$  value was 0.939 and the Langmuir isotherm constant parameters were negative, and this indicated that the Langmuir isotherm model was inadequate to adequately elucidate the adsorption process (Köse et al., 2011). Also, the value of  $R_L$  was obtained as 3.68, which indicated that the Langmuir isotherm was unfavourable in analysing the current adsorption process using Ca-ACPES.

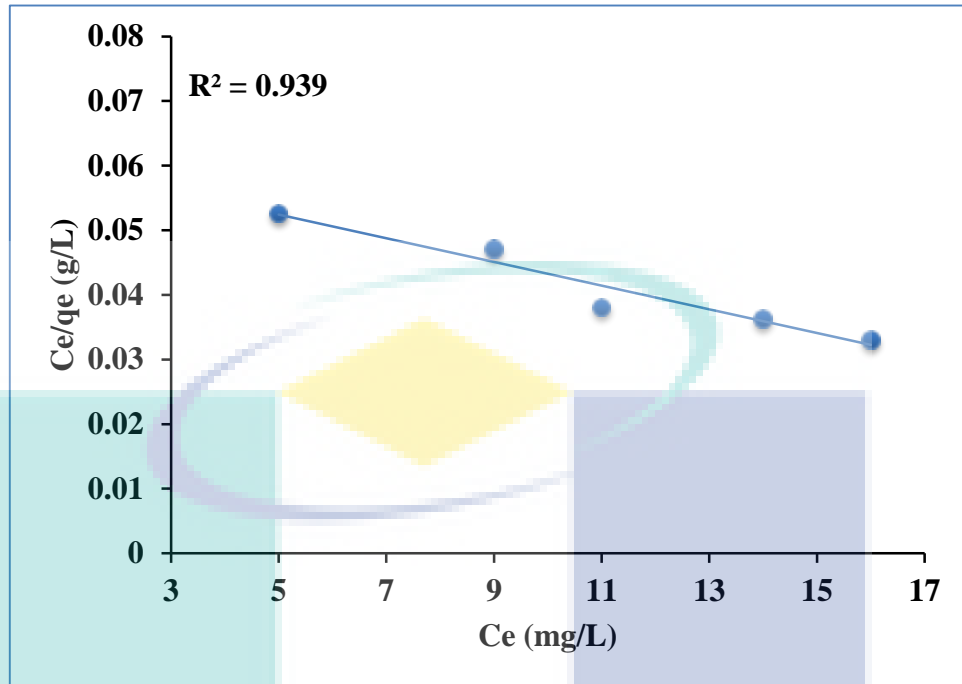
Table 4.16 Isotherm models parameters and correlation coefficients for adsorption of H<sub>2</sub>S on Ca-ACPES

Isotherm models	Parameters		$R^2$
Langmuir	$Q_{max}$ (mg/g)	543.47	0.939
	b (L/mg)	0.03	
Freundlich	$K_F$ (mg/g)(L/mg) <sup>1/n</sup>	9.574	0.9926
	1/n	1.4	
Temkin	$K_T$ (L/g)	4.170	0.9185
	$b_T$	7.79	
Dubinin–Radushkevich	$q_s$ (mg/g)	456.7	0.8922
	B (mol <sup>2</sup> /J <sup>2</sup> )	7.86x10 <sup>-6</sup>	
	E (J/mol)	252.2	

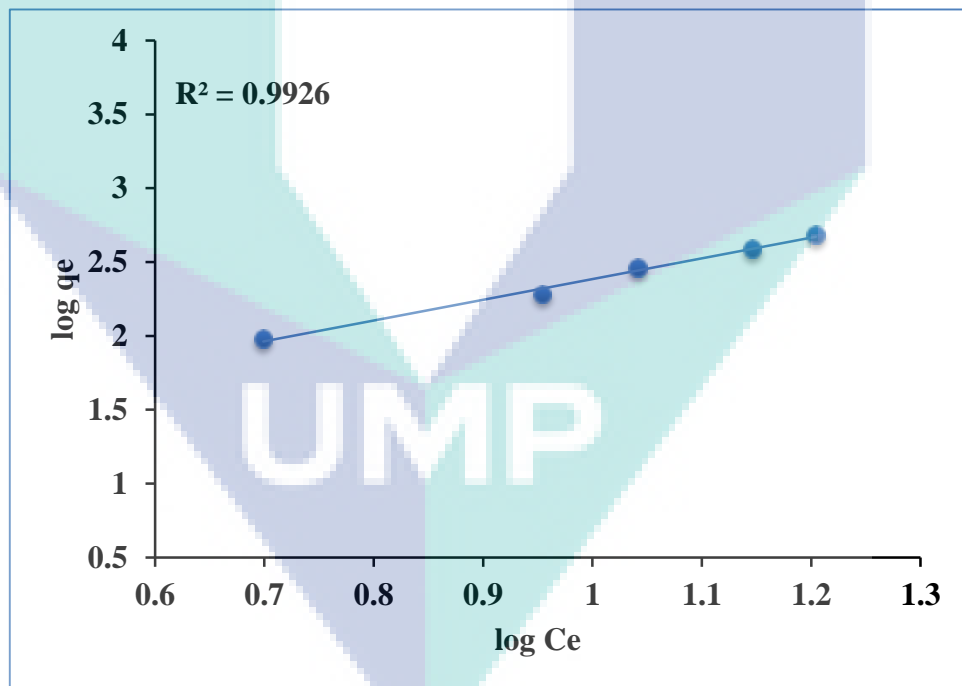
Freundlich isotherm (a straight line with a slope of  $1/n = 1.4$ ) was obtained by plotting  $\log q_e$  versus  $\log C_e$  as shown in Figure 4.48 (b). The value of  $R^2$  is 0.9926, indicating that the adsorption data were well fitted on the Freundlich model. The adsorption process occurred at specific heterogeneous sites on the surface of adsorbent. The initial concentration provides the driving force to overcome the mass transfer resistance between solution (solute) and solid phase. The Freundlich constants  $K_F$  and  $n$  were calculated from equation 2.8) and listed in Table 4.16.  $n < 1$  indicates favourable adsorption of pollutant on the Ca-ACPES (Anbia & Haqshenas, 2015; Demiral & Güngör, 2016). On the other hand, Temkin model was obtained by plotting  $q_e$  against  $\log C_e$  as shown in Figure 4.48 (c). The fitting parameters ( $K_T$  &  $b_T$ ) are shown in Table 4.16. However, the value of  $R^2$  for Temkin model was 0.9185, and this indicated that the



adsorption data of H<sub>2</sub>S (aq) on ACPKS was less fitted as compared to the Freundlich model. However, the adsorption was characterized by a uniform distribution of binding energies (Angin, 2014). The Dubinin–Radushkevich isotherm was also used in describing the adsorption process. A straight line was obtained from the plot of ln q<sub>e</sub> versus ε<sup>2</sup> (Appendix E (d)). From the intercept and the slope of plot ln q<sub>e</sub> vs ε<sup>2</sup>, the isotherm constants q<sub>s</sub> and B can be obtained respectively (Figure 4.48 (d)). A smaller R<sup>2</sup> value of 0.8922 was obtained for the Dubinin–Radushkevich isotherm. The constants q<sub>s</sub> and E was determined using the linear equation shown in Table 4.16. The value of E can be used to estimate the type of adsorption process. The physical adsorption process is happening if E < 8 kJ mol<sup>-1</sup> (Köse et al., 2011; Demiral& Güngör, 2016). Therefore, the adsorption process of H<sub>2</sub>S (aq) on the Ca-ACPKS surface is mostly described by the physisorption adsorption process. While still there was some adsorption process that occurred under chemisorption as confirmed by XPS and FTIR test. This is because the adsorption process is a complex process and could be occurred in many stages. In general, the Freundlich isotherm model is the best fitting model. The adsorption takes place at specific heterogeneous sites with further adsorption taking place when all the active sites are occupied by pollutant as a multilayers.

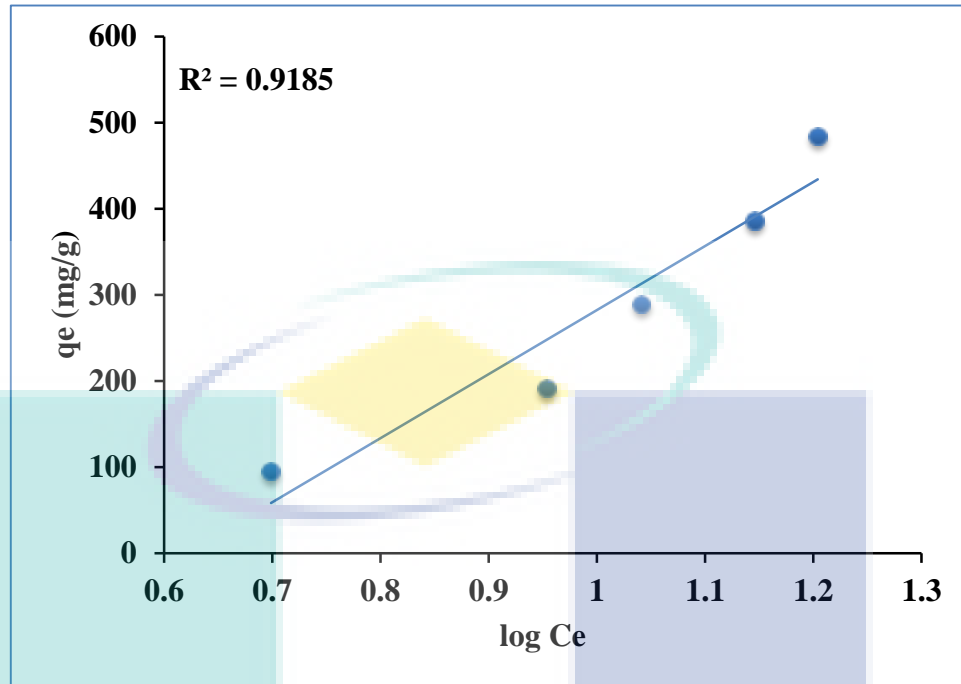


(a)

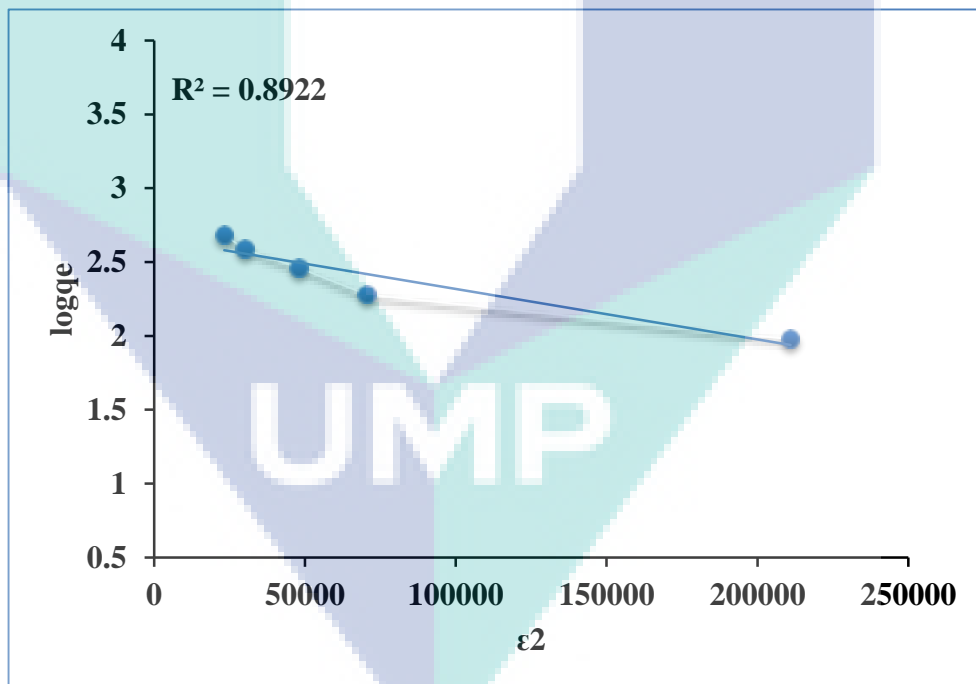


(b)





(c)



(d)

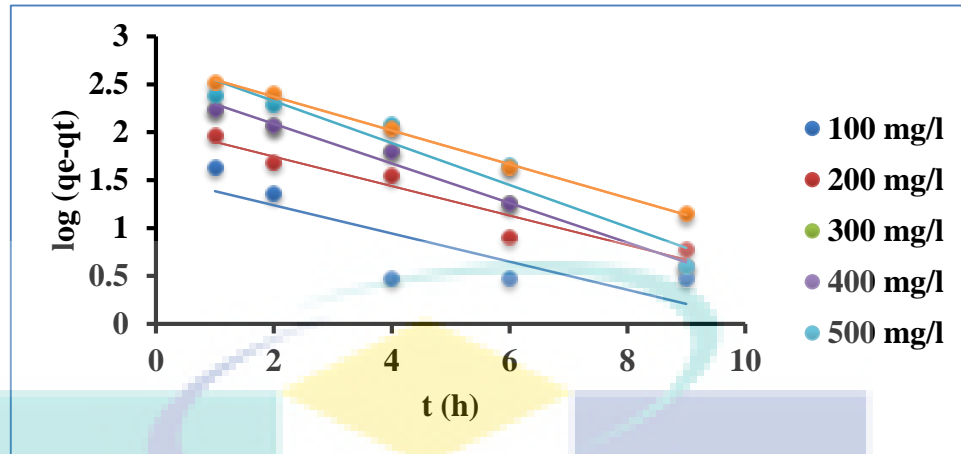
Figure 4.48 Langmuir (a), Freundlich (b), Temkin (c) and Dubinin–Radushkevich (d) adsorption isotherms of H<sub>2</sub>S (aq) on Ca-ACP<sub>KS</sub> at 30 °C

### 4.7.3 Kinetics of Adsorption

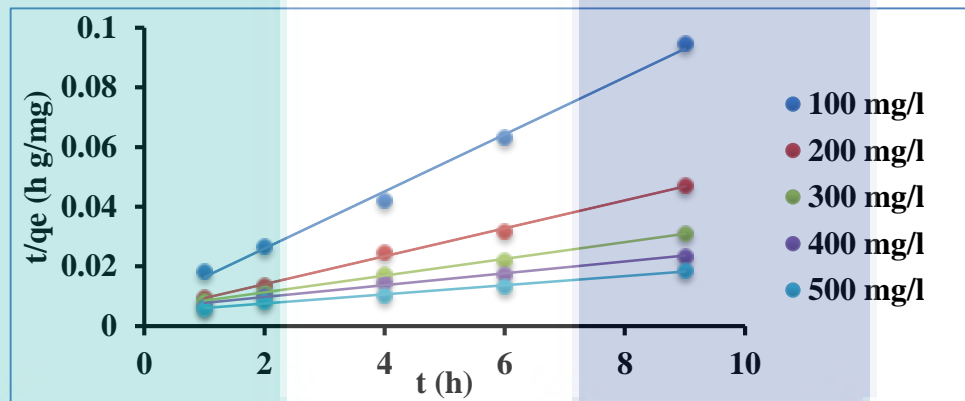
In this study, three kinetic adsorption models were applied, namely pseudo-first-order model, pseudo-second-order model and intra-particle diffusion model. For the pseudo-first-order kinetic model, straight lines were obtained by plotting  $\log (q_e - q_t)$  versus  $t$ . The slopes of the linear plots are shown in Figure 4.49 (a). The correlation coefficient and  $k_1$  values were obtained from the slopes listed in Table 4.17. However, the experimental  $q_e$  values do not match with the calculated values from the pseudo-first-order equation. When the pseudo-second-order kinetic model is applied, the plot of  $t/q_t$  versus  $t$  becomes linear.  $q_e$  and  $k_2$  can then be determined from the slope and the intercept of the plot, respectively. This procedure is more effective in predicting the behaviour over the whole range of adsorption. The linear plot of  $t/q_t$  versus  $t$  is shown in Figure 4.49 (b). The agreement between the experimental and the calculated  $q_e$  values was promising (Table 4.17). Besides, the  $R^2$  values for the second-order kinetic model are greater than 0.96 for all  $H_2S$  concentrations. The intra-particle diffusion model rate constant,  $K_p$  was obtained from the slope of  $q_t$  versus  $t^{1/2}$  plot (Figure 4.49 (c)). The  $R^2$  values obtained were shown in Table 4.17 and the result revealed a lower value than those obtained from the pseudo-second-order model. The results found that the adsorption of  $H_2S$  on Ca-ACPES is best described by the second-order kinetic model (Angin 2014; Demiral and Gungör, 2016).

Table 4.17 Kinetic models parameters for adsorption of  $H_2S$  (aq) on Ca-ACPES

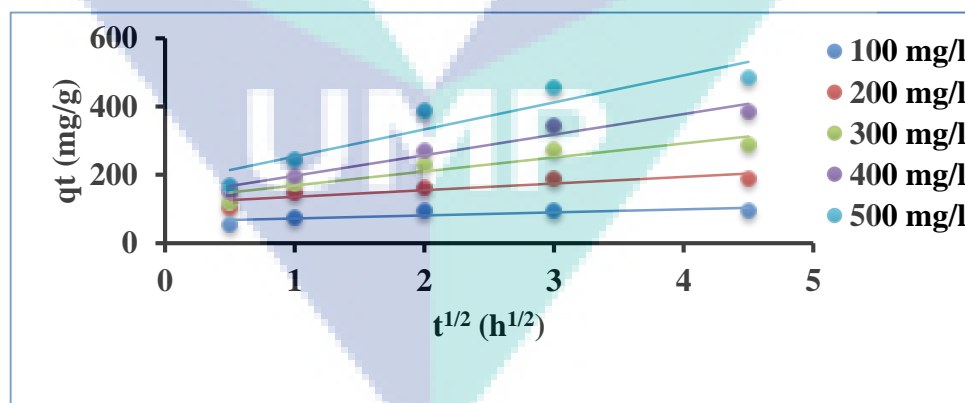
Kinetic Model	Parameter	Initial $H_2S$ (aq) Concentration (mg/L)				
		100	200	300	400	500
Pseudo-first-order	$K_1$ (1/h)	0.338	0.3536	0.475	0.5033	0.4053
	$R^2$	0.6916	0.9221	0.9884	0.933	0.9971
Pseudo-second-order	$K_2$ (g/mg h)	0.0115	4.727	1.290	6.6448	4.414
	$R^2$	0.9982	0.9982	0.985	0.9634	0.9607
Intraparticle diffusion	$K_3$ (1/h)	9.33	18.83	40.514	59.495	78.174
	$R^2$	0.7271	0.8211	0.9329	0.9807	0.9824



(a)



(b)



(c)

Figure 4.49 Pseudo-first-order (a), pseudo-second-order (b) and intra-particle diffusion (c) kinetic models for the adsorption of H<sub>2</sub>S (aq) on Ca-ACPKS

#### 4.7.4 Thermodynamic Study

The thermodynamic study was then performed to investigate the effect of temperature on the adsorption process. The thermodynamic parameters such as  $\Delta H^\circ$ ,  $\Delta S^\circ$  and  $\Delta G^\circ$  of the adsorption process were studied. The values for  $\Delta H^\circ$  and  $\Delta S^\circ$  were calculated from the slope and intercept from the plot shown in Figure 4.50. The calculated values for  $\Delta H^\circ$ ,  $\Delta S^\circ$  and  $\Delta G^\circ$  were listed in Table 4.18. The negative value of  $\Delta H^\circ$  indicated the exothermic nature of the current adsorption interaction. The positive value of  $\Delta S^\circ$  reflected the affinity of Ca-ACPKS for  $H_2S$  and increasing randomness at the solid–solution interface during the adsorption process. The negative value of  $\Delta G^\circ$  indicated the feasibility and the spontaneous nature of the current adsorption process.

Table 4.18 Thermodynamic parameters of  $H_2S(aq)$  adsorption on Ca-ACPKS

$\Delta H^\circ$ (kJ/mol)	$\Delta S^\circ$ (J/mol K)	$\Delta G^\circ$ (kJ/mol)			
		303 K	308 K	313 K	318 K
-91.512	328.93	-191.19	-192.83	-194.47	-196.12

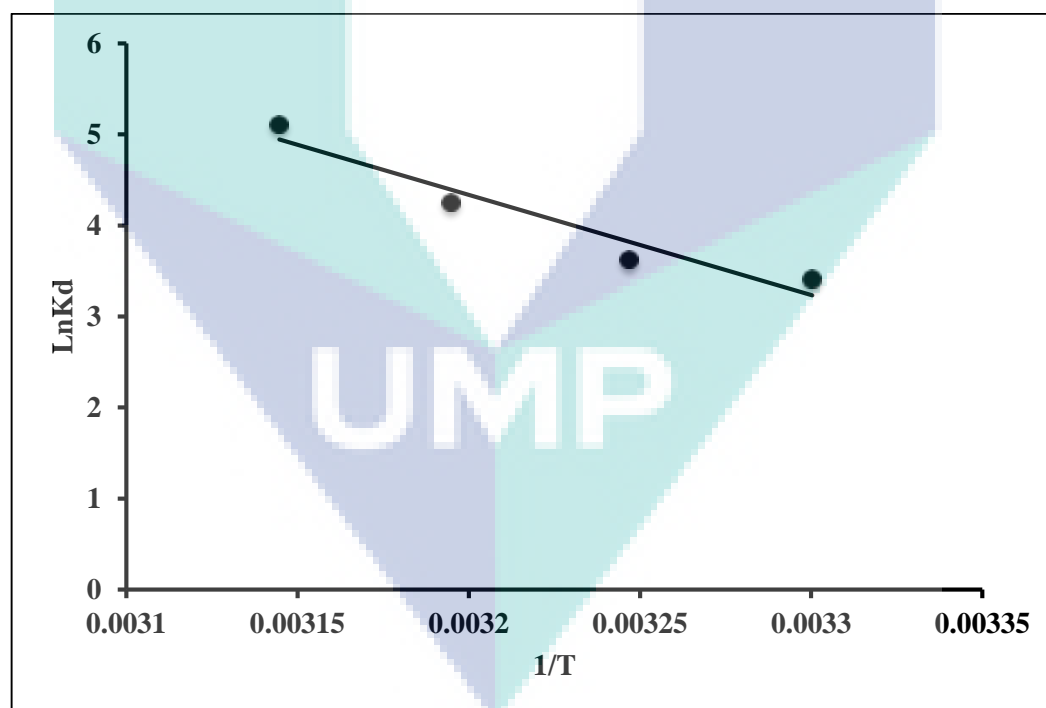


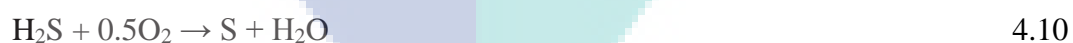
Figure 4.50 Thermodynamic study of the adsorption of  $H_2S$  (aq) on Ca-ACPKS

#### 4.7.5 Reaction Mechanisms of Adsorption

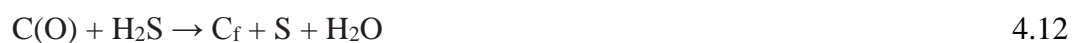
The physisorption and chemisorption occurred during adsorption processes. Physisorption process was attributed to Van der Waals force of attraction which involves a weaker electrical force responsible for the attraction of molecules in the domain. However, chemisorption is a chemically bounded process between molecules. The adsorption of H<sub>2</sub>S (aq) on ACs and IACs are mainly due to the emergences of oxygenated functional groups on the adsorbent surface which has the capacity to enhance the RE of H<sub>2</sub>S (aq).

The carbons were activated using potassium hydroxide (KOH) which could enhance the porosity of ACs by increasing the active sites as shown in Equations 4.4. The boiling point of potassium (K) is 780 °C and the activation temperature was 750 °C. The K metals remaining on the carbon surface could increase the cation (K<sup>+</sup>) on the surface. These cations (K<sup>+</sup>) could attract anion such as bisulfide (HS<sup>-</sup>) from the solution during the adsorption process (Tseng et al., 2008; Mopoung et al., 2015). Abechi et al.(2013) have reported that KOH could enhance the porosity of ACs.

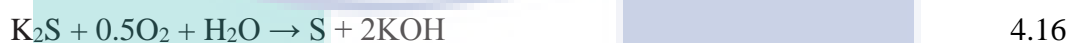
As indicated from the FTIR result, the surface functional groups such as the carboxylic, phenolic, or carbonyl groups existed on the ACs surface. The dissolved H<sub>2</sub>S (g) in the solution was converted to H<sub>2</sub>S (aq) as shown in Equation 2.1). Then, the presence of KOH on the external surface of adsorbent could dissociate H<sub>2</sub>S (aq) to ions as shown in Equation 2.3). Therefore, reaction probably occurs between KOH and H<sub>2</sub>S (aq) bisulfide (HS<sup>-</sup>) as reported by Nowicki et al. (2014). The following equation presented the possible reaction:



Depending on the activity of the carbon surface, the following reaction might occur:



Where C(O) is chemisorbed oxygen and C<sub>f</sub> is a free active site of carbon for oxygen chemisorption. Moreover, KOH (on the surface of activated carbon) contributed to the oxidation of H<sub>2</sub>S (g) as well (Bagreev & Bandosz, 2002). Kanjanarong et al. (2017) reported that under alkaline condition, it catalysed the oxidation of HS<sup>-</sup> to elemental sulfur until the base was completely exhausted as shown in Equations 4.14) to 4.16).



From the FTIR results, for the ACs adsorbents; it can be clearly seen that the primary amine group (R-NH<sub>2</sub>) was represented by a peak at 1650 cm<sup>-1</sup> for the fresh adsorbent. This peak vanished after the adsorption process (Figure 4.10). This is because the amine group was consumed by sulfides. Therefore, one of the radical groups for the bonding of sulfides on adsorbent surface was R-NH<sub>2</sub> as shown in Equations 4.17), 4.18) and 4.19).



ACs can be enhanced with calcium extracted from egg shells in order to increase the RE of H<sub>2</sub>S (aq) as explained earlier. The possible reactions that might occur during the adsorption process of H<sub>2</sub>S (aq) on IACs were investigated. The reaction in equation 4.20) might occur due to the oxygen content that supporting the carbonization process of the material. However, the dissociation of calcium oxide in water as outlined in Equation 4.22) formed calcium hydroxide (Ca(OH)<sub>2</sub>) on the surfaces of IACs adsorbents. This could further attract the acidic pollutant such as H<sub>2</sub>S (aq) via the active sites. Moreover, in Equation 4.23), the OH<sup>-</sup> from Ca(OH)<sub>2</sub> reacted with H<sub>2</sub>S (aq) to form Ca(HS)<sub>2</sub> which is then converted to elemental S as demonstrated in Equation 4.24) (Altaş & Büyükgüngör, 2008).



The overall enhancement in RE of  $\text{H}_2\text{S}_{(\text{aq})}$  could be demonstrated by the following mechanisms using calcium oxide (as a heterogeneous oxidant). The first stage involved the formation of calcium-sulfide surface complexes (Davies et al., 2007):



The S free radical was then released from the surface complex with the presence of the  $\text{HS}^-$  free radical more probable than the S radical due to the solution pH is adjusted to 7 as shown in the Equation (4.26) (Jacukowicz et al., 2015).



The presence of new active sites and the release of free radicals were accompanied by the dissolution of  $\text{Ca}^{2+}$  that caused the presence of carboxylic functional groups (in the  $\text{H}^+$  form) on the surface of adsorbent:



Dissolution of  $\text{Ca}^{2+}$  ions created new active sites on the calcium oxide. Meanwhile, the S free radicals has the ability to react with the active sites on CaO and release  $\text{Ca}^{2+}$  that could precipitate in the form of CaS as a results of its reaction with sulfides:





## CHAPTER 5

### CONCLUSION AND FUTURE WORK

#### 5.1 Overall Conclusion

Generally, this study was conducted to investigate the effectiveness of using locally sourced materials and its potential in lab toward removal of  $\text{H}_2\text{S}$  (aq) from waste water. Laboratory batch kinetic studies were conducted to evaluate these waste materials. The preparation, characterization, optimization and modelling studies are conducted to investigate the effect of factors and conditions on the adsorption process. Comparison studies have been conducted between the ACs and IACs adsorbents. The present research investigated the RE of three different locally sourced waste materials as a green and economic adsorbents for the removal of  $\text{H}_2\text{S}$  (aq) from petroleum refinery waste water.

The objectives of this work have been largely achieved and the results showed a good correlation among all the results obtained for the ACs and IACs adsorbents from the preparation, characterization, optimization and modelling studies as summarized below in accordance with the research objectives and scopes. From the overall objective of this study the removal of  $\text{H}_2\text{S}$  (aq) from petroleum refinery waste water was investigated using locally-sourced adsorbents obtained from agricultural and industrial wastes. The following specific objectives of this research achieved the following:

**Objective 1:** Activated carbons (ACs) and Impregnated Activated Carbons (IACs) were prepared from coconut shell (CNS), palm kernel shell (PKS) and wood saw dust (WSD) wastes. These materials were used as precursors to produce the activated carbon (ACs). The three ACs namely (ACCNS, ACPKS, and ACWSD) were prepared and modified (impregnated) to enhance the surface chemistry of the adsorbents using calcium extracted from egg shells wastes. The three impregnated activated carbon (IACs) prepared (i.e. Ca-ACCNS, Ca-ACPKS and Ca-ACWSD).

**Objective 2:** The ACs and IACs were characterized in order to investigate the chemical structure and physical properties using different analytical approach and identify the best adsorbent in terms of removal efficiency of  $\text{H}_2\text{S}$  (aq) from the simulated

waste water. The three ACs namely (ACCNS, ACPKS, and ACWSD) and the three impregnated activated carbon (IACs) prepared (i.e. Ca-ACCNS, Ca-ACPKS and Ca-ACWSD) were all characterized using the SEM/EDX, FTIR, BET, XRD and XPS analyses. The results obtained concluded that there were no toxic elements from all prepared adsorbents and this showed a good characteristics in terms of high porosity and surface area. The adsorbents are investigated in term of removal efficiency. The results showed that the Ca-ACPKS has the higher RE %.

**Objective3.** The optimization study for Ca-ACPKS are implemented using DoE to investigate the preparation conditions of removal of H<sub>2</sub>S (aq) from simulated petroleum waste water. The preparation conditions of Ca-ACPKS are optimized. The result found that the optimum conditions of prepared Ca-ACPKS are calcination temperature of 880 °C, calcium solution concentration of 49.31 V%, and calcination contact time of 57.5 min with RE of 99.2 % and yield of 33.8 %. The result is also found that calcination temperature has more contribution on the responses of RE and yield of Ca-ACPKS.

The removal operation conditions of H<sub>2</sub>S (aq) from real waste water like initial H<sub>2</sub>S concentration, adsorption contact time, dosage, pH, agitation speed are screened. The result found that the initial H<sub>2</sub>S (aq) concentration, adsorption contact time and dosage are significant. Therefore, the significant factors are optimized. The results present the optimum conditions for removal of H<sub>2</sub>S (aq) from waste water are initial concentration of H<sub>2</sub>S of 440 mg/L, adsorption contact time of 585 min, and amount of Ca-ACPKS of 1.05 g with RE of 99.5 %. However, according to the |DOE standard, the H<sub>2</sub>S removal at an initial concentration of 300 mg/L is acceptable. Hence, an initial concentration below 300 mg/L is within the range of 0.5 mg/L which correspond to the DOE Malaysian standard.

**Objective 4:** The adsorption isotherm and kinetic models studies are conducted using Ca-ACPKS as an adsorbent to investigate the behavior of adsorption process. The results found that the Freundlich isotherm model is more fit to the study and the adsorption kinetic study is followed by pseudo –second order kinetic model. The maximum adsorption capacity of Ca-ACPKS was 543.4 mg/g. The negative value of  $\Delta H^\circ$  indicates the exothermic nature of the current adsorption interaction. However, the positive value of  $\Delta S^\circ$  reflects the affinity of Ca-ACPKS for H<sub>2</sub>S (aq) and increasing randomness at the solid–solution interface during the adsorption process. The negative

value of  $\Delta G^\circ$  indicates the feasibility and the spontaneous nature of the current adsorption process.

The use of optimization tools for the removal of  $H_2S$  (aq) from waste water was not really reported by many researchers. This study made use of optimization tools (RSM) to optimize the removal of  $H_2S$  (aq) at higher concentration by means of ACs and IACs. Also, a detail study on the modification of surface properties of adsorbents using calcium carbonates extracted from egg shells has not been reported. Therefore, this research bridged these knowledge gap by investigating the absorption capacities and removal efficiencies of locally sourced adsorbents obtained from coconut shell, palm kernel shell and wood saw dust for the removal of  $H_2S$  (aq) from simulated waste water. Thus, it is concluded that the activated carbon derived from palm kernel shell and impregnated with calcium extracted from egg shells are very useful green and economical adsorbent due to their easy availability and absence of any toxic. Therefore, it is very suitable for the removal of  $H_2S$  (aq) from petroleum waste wasters.

## 5.2 Future Recommendations

Based on the results from this study the following recommendations be carried out for any future work as continuation:

- i. Looking for greener methods to deal with toxic chemical instead of using dangerous solvents. This study was conducted to determine the feasibility and effectiveness of locally sourced waste materials in the removal of  $H_2S$  (aq) from petroleum waste water.
- ii. Based on the theoretical framework, investigation into different greener adsorption method is of necessity.
- iii. A cheaper yet more efficient method to regenerate spent IACs should be investigated and analysed. The potential of used same adsorbent for removing of  $H_2S$  (g) from stream using continues adsorption process.
- iv. Further investigation is needed to be conducted on used this composite of activated carbon with calcium extracted from egg shells to remove other toxic pollutant such as heavy metals from petroleum industrial waste water. For

instance, further explored should be made based on the results obtained in this study for the treatment of complex mixtures.

- v. A continuous evaluation of use new agricultural wastes as an adsorbent to treatment  $\text{H}_2\text{S}$  (aq) technologies. A collaboration should be made with petroleum refinery waste water companies in order to collect up-to-date data from full scale facilities to identify the real technology needs in the field. This study in  $\text{H}_2\text{S}$  (aq) treatment from solution opens new field that will need strong research to its application in actual field.
- vi. The actual petroleum refinery waste water streams also contain a huge amount of other materials, such as  $\text{NH}_3$ , heavy oil, phenol, hydrocarbons, particulates or grease. Therefore, the effect of these pollutants on adsorption/oxidation process of  $\text{H}_2\text{S}$  (aq) over IACs surface are worth studying when considering industrial application of this process.



UMP

## REFERENCES

- Abdel Ghafar, H. H., Ali, G. A., Fouad, O. A., & Makhlof, S. A. (2015). Enhancement of adsorption efficiency of methylene blue on  $\text{Co}_3\text{O}_4/\text{SiO}_2$  nanocomposite. *Desalination and Water Treatment*, 53(11), 2980-2989.
- Abechi, S. E., Gimba, C. E., Uzairu, A., & Dallatu, Y. A. (2013). Preparation and characterization of activated carbon from palm kernel shell by chemical activation. *Res. J. Chem. Sci.* 3(7), 54-61.
- Agarwal, S., Sadegh, H., Monajjemi, M., Hamdy, A. S., Ali, G. A., Memar, A. O., & Gupta, V. K. (2016). Efficient removal of toxic bromothymol blue and methylene blue from wastewater by polyvinyl alcohol. *Journal of Molecular Liquids*, 218, 191-197.
- Angin, D. (2014). Utilization of activated carbon produced from fruit juice industry solid waste for the adsorption of Yellow 18 from aqueous solutions. *Bioresource technology*, 168, 259-266.
- Amir, R. M., Anjum, F. M., Khan, M. I., Khan, M. R., Pasha, I., & Nadeem, M. (2013). Application of Fourier transform infrared (FTIR) spectroscopy for the identification of wheat varieties. *Journal of food science and technology*, 50(5), 1018-1023.
- Ahmed, S., Rasul, M. G., Martens, W. N., Brown, R., & Hashib, M. A. (2010). Heterogeneous photocatalytic degradation of phenols in waste water a review on current status and developments. *Desalination*, 261(1), 3-18.
- Ahmad, A. A., Hameed, B. H., & Ahmad, A. L. (2009). Removal of disperse dye from aqueous solution using waste-derived activated carbon: Optimization study. *Journal of Hazardous materials*, 170(2), 612-619.
- Al-Degs, Y. S., El-Barghouthi, M. I., El-Sheikh, A. H., & Walker, G. M. (2008). Effect of solution pH, ionic strength, and temperature on adsorption behavior of reactive dyes on activated carbon. *Dyes and pigments*, 77(1), 16-23.
- Allen, S. J., & Koumanova, B. (2005). Decolourisation of water/waste water using adsorption. *Journal of the University of Chemical Technology and Metallurgy*, 40(3), 175-192.
- Almasvandi, M. H., Rahimi, M., & Tagheie, Y. (2016). Microfluidic cold stripping of  $\text{H}_2\text{S}$  from crude oil in low temperature and natural gas consumption. *Journal of Natural Gas Science and Engineering*, 34, 499-508.

- Alonso-Vicario, A., Ochoa-Gómez, J. R., Gil-Río, S., Gómez-Jiménez-Aberasturi, O., Ramírez-López, C. A., Torrecilla-Soria, J., & Domínguez, A. (2010). Purification and upgrading of biogas by pressure swing adsorption on synthetic and natural zeolites. *Microporous and Mesoporous Materials*, 134(1), 100-107.
- Altaş, L., & Büyükgüngör, H. (2008). Sulfide removal in petroleum refinery waste water by chemical precipitation. *Journal of hazardous materials*, 153(1), 462-469.
- Amosa, M. K., Jami, M. S., & Ma'an, F. R. (2016). Electrostatic biosorption of COD, Mn and H<sub>2</sub>S on EFB-based activated carbon produced through steam pyrolysis: an analysis based on surface chemistry, equilibria and kinetics. *Waste and Biomass Valorization*, 7(1), 109-124.
- Ania, C. O., B. Cabal, J. B. Parra, A. Arenillas, B. Arias, and J. J. Pis. 2008. "Naphthalene Adsorption on Activated Carbons Using Solvents of Different Polarity." *Adsorption* 14 (2-3): 343-55. doi:10.1007/s10450-007-9096-3.
- Amosa, M. K. (2015). Process optimization of Mn and H<sub>2</sub>S removals from POME using an enhanced empty fruit bunch (EFB)-based adsorbent produced by pyrolysis. *Environmental Nanotechnology, Monitoring & Management*, 4, 93-105.
- Asaoka, S., Okamura, H., Morisawa, R., Murakami, H., Fukushi, K., Okajima, T., & Ohta, T. (2013). Removal of hydrogen sulfide using carbonated steel slag. *Chemical engineering journal*, 228, 843-849.
- Asaoka, S., Yamamoto, T., Kondo, S., & Hayakawa, S. (2009). Removal of hydrogen sulfide using crushed oyster shell from pore water to remediate organically enriched coastal marine sediments. *Bioresource technology*, 100(18), 4127-4132.
- Asakura, H. (2015). Sulfate and organic matter concentration in relation to hydrogen sulfide generation at inert solid waste landfill site—Limit value for gypsum. *Waste Management*, 43, 328-334.
- Anbia, M., & Haqshenas, M. (2015). Adsorption studies of Pb (II) and Cu (II) ions on mesoporous carbon nitride functionalized with melamine-based dendrimer amine. *International Journal of Environmental Science and Technology*, 12(8), 2649-2664.
- Addington, L., Fitz, C., Lunsford, K., Lyddon, L., & Siwek, M. (2011). Sour Water: Where it Comes from and How to Handle It. In *Prague GPA Europe Annual Conference* (12013-12010).



- Bae, J. W., Kang, S. H., Dhar, G. M., & Jun, K. W. (2009). Effect of Al<sub>2</sub>O<sub>3</sub> content on the adsorptive properties of Cu/ZnO/Al<sub>2</sub>O<sub>3</sub> for removal of odorant sulfur compounds. *International journal of hydrogen energy*, 34(20), 8733-8740.
- Bagreev, A., & Bandosz, T. J. (2000). Study of hydrogen sulfide adsorption on activated carbons using inverse gas chromatography at infinite dilution. *The Journal of Physical Chemistry B*, 104(37), 8841-8847.
- Bagreev, A., & Bandosz, T. J. (2001). H<sub>2</sub>S adsorption/oxidation on unmodified activated carbons: importance of prehumidification. *Carbon*, 39(15), 2303-2311.
- Bagreev, A., & Bandosz, T. J. (2002). A role of sodium hydroxide in the process of hydrogen sulfide adsorption/oxidation on caustic-impregnated activated carbons. *Industrial & engineering chemistry research*, 41(4), 672-679.
- Bagreev, A., Menendez, J. A., Dukhno, I., Tarasenko, Y., & Bandosz, T. J. (2004). Bituminous coal-based activated carbons modified with nitrogen as adsorbents of hydrogen sulfide. *Carbon*, 42(3), 469-476.
- Bagreev, A., Rahman, H., & Bandosz, T. J. (2001). Thermal regeneration of a spent activated carbon previously used as hydrogen sulfide adsorbent. *Carbon*, 39(9), 1319-1326.
- Bagreev, A., & Bandosz, T. J. (2005). On the mechanism of hydrogen sulfide removal from moist air on catalytic carbonaceous adsorbents. *Industrial & engineering chemistry research*, 44(3), 530-538.
- Bandosz, T. J. (2002). On the adsorption/oxidation of hydrogen sulfide on activated carbons at ambient temperatures. *Journal of colloid and Interface Science*, 246(1), 1-20.
- Bandosz, T. J. (2006). *Activated Carbon Surfaces in Environmental Remediation*. Elsevier, UK, Vol. 7, ISBN 978-0-12-370536-5.
- Bansal, R. C., & Goyal, M. (2005). *Activated carbon adsorption*. CRC press.
- Bashkova, S., Armstrong, T. R., & Schwartz, V. (2009). Selective catalytic oxidation of hydrogen sulfide on activated carbons impregnated with sodium hydroxide. *Energy & Fuels*, 23(3), 1674-1682.



- Bastani, A., Lee, C. S., Haghghat, F., Flaherty, C., & Lakdawala, N. (2010). Assessing the performance of air cleaning devices—A full-scale test method. *Building and Environment*, 45(1), 143-149.
- Basu, J. K., Monal, D., & Pinaki, G. (2012). Statistical optimization for the prediction of ibuprofen adsorption capacity by using microwave assisted activated carbon. *Archives of Applied Science Research*, 4(2), 1053-1060.
- Baykara, S. Z., Figen, E. H., Kale, A., & Veziroglu, T. N. (2007). Hydrogen from hydrogen sulphide in Black Sea. *International journal of hydrogen energy*, 32(9), 1246-1250.
- Belmabkhout, Y., De Weireld, G., & Sayari, A. (2009). Amine-bearing mesoporous silica for CO<sub>2</sub> and H<sub>2</sub>S removal from natural gas and biogas. *Langmuir*, 25(23), 13275-13278.
- Baçaoui, A., Yaacoubi, A., Dahbi, A., Bennouna, C., Luu, R. P. T., Maldonado-Hodar, F. J., & Moreno-Castilla, C. (2001). Optimization of conditions for the preparation of activated carbons from olive-waste cakes. *Carbon*, 39(3), 425-432.
- Bagheri, A. R., Ghaedi, M., Asfaram, A., Hajati, S., Ghaedi, A. M., Bazrafshan, A., & Rahimi, M. R. (2016). Modeling and optimization of simultaneous removal of ternary dyes onto copper sulfide nanoparticles loaded on activated carbon using second-derivative spectrophotometry. *Journal of the Taiwan Institute of Chemical Engineers*, 65, 212-224.
- Bergersen, O., & Haarstad, K. (2014). Treating landfill gas hydrogen sulphide with mineral wool waste (MWW) and rod mill waste (RMW). *Waste management*, 34(1), 141-147.
- Boumnijel, I., Amor, H. B., Chekir, H., & Hajji, N. (2016). Hydrogen sulphide removal from the effluents of a phosphoric acid production unit by absorption into chlorinated seawater under alkaline conditions. *Comptes Rendus Chimie*, 19(4), 517-524.
- Box, G. E., & Wilson, K. B. (1992). On the experimental attainment of optimum conditions. In *Breakthroughs in Statistics* (270-310). Springer New York.
- Banerjee, S., & Chattopadhyaya, M. C. (2017). Adsorption characteristics for the removal of a toxic dye, tartrazine from aqueous solutions by a low cost agricultural by-product. *Arabian Journal of Chemistry*, 10, 1629-1638.

- Carrott, P. J. M., & Carrott, M. R. (2007). Lignin—from natural adsorbent to activated carbon: a review. *Bioresource technology*, 98(12), 2301-2312.
- Chang, Y. J., Chang, Y. T., & Chen, H. J. (2007). A method for controlling hydrogen sulfide in water by adding solid phase oxygen. *Bioresource technology*, 98(2), 478-483.
- Chen, M., Kang, X., Wumaier, T., Dou, J., Gao, B., Han, Y. & Zhang, L. (2013). Preparation of activated carbon from cotton stalk and its application in supercapacitor. *Journal of Solid State Electrochemistry*, 17(4), 1005-1012.
- Chen, Q., Wang, Z., Long, D., Liu, X., Zhan, L., Liang, X., & Ling, L. (2010). Role of pore structure of activated carbon fibers in the catalytic oxidation of H<sub>2</sub>S. *Industrial & Engineering Chemistry Research*, 49(7), 3152-3159.
- Chojnacka, K. (2005). Biosorption of Cr (III) ions by egg shell s. *Journal of Hazardous Materials*, 121(1), 167-173.
- Choo, H. S., Lau, L. C., Mohamed, A. R., & Lee, K. T. (2013). Hydrogen sulfide adsorption by alka-line impregnated coconut shell activated carbon. *J. Eng. Sci. Technol.*, 8, 741-753.
- Čmelík, J., Machát, J., Otruba, V., & Kanický, V. (2010). Contribution to vapor generation-inductively coupled plasma spectrometric techniques for determination of sulfide in water samples. *Talanta*, 80(5), 1777-1781.
- Couvert, A., Sanchez, C., Laplanche, A., & Renner, C. (2008). Scrubbing intensification for sulphur and ammonia compounds removal. *Chemosphere*, 70(8), 1510-1517.
- Coelho, A., Castro, A. V., Dezotti, M., & Sant'Anna, G. L. (2006). Treatment of petroleum refinery sourwater by advanced oxidation processes. *Journal of hazardous materials*, 137(1): 178-184.
- Cui, H., Turn, S. Q., & Reese, M. A. (2009). Removal of sulfur compounds from utility pipelined synthetic natural gas using modified activated carbons. *Catalysis Today*, 139(4), 274-279.
- Chaudhuri, M. (2004). Removal of Hydrogen Sulfide from Groundwater Using Ozone and Iron Oxide-coated Sand. University of Missouri.
- Dąbrowski, A., Podkościelny, P., Hubicki, Z., & Barczak, M. (2005). Adsorption of phenolic compounds by activated carbon—a critical review. *Chemosphere*, 58(8), 1049-1070.

- Deng, H., Li, G., Yang, H., Tang, J., & Tang, J. (2010). Preparation of activated carbons from cotton stalk by microwave assisted KOH and K<sub>2</sub>CO<sub>3</sub> activation. *Chemical Engineering Journal*, 163(3), 373-381.
- Davies, N. H., Dennis, J. S., & Hayhurst, A. N. (2007). Reaction between calcium oxide and hydrogen sulphide and also its modelling for a fluidised bed coal gasifier. *Journal of the Energy Institute*, 80(2), 65-72.
- Demiral, H., & Güngör, C. (2016). Adsorption of copper (II) from aqueous solutions on activated carbon prepared from grape bagasse. *Journal of Cleaner Production*, 124, 103-113.
- Derylo-Marczewska, A., Swiatkowski, A., Biniak, S., & Walczyk, M. (2008). Effect of properties of chemically modified activated carbon and aromatic adsorbate molecule on adsorption from liquid phase. *Colloids and Surfaces A: Physicochemical and Engineering Aspects*, 327(1), 1-8.
- Daneshyar, A., Ghaedi, M., & Sabzehmeidani, M. M. (2017). H<sub>2</sub>S adsorption onto Cu-Zn-Ni nanoparticles loaded activated carbon and Ni-Co nanoparticles loaded  $\gamma$ -Al<sub>2</sub>O<sub>3</sub>: optimization and adsorption isotherms. *Journal of colloid and interface science*, 490, 553-561.
- Dutta, P. K., Rabaey, K., Yuan, Z., Rozendal, R. A., & Keller, J. (2010). Electrochemical sulfide removal and recovery from paper mill anaerobic treatment effluent. *Water research*, 44(8), 2563-2571.
- D'Alessandro, W., Brusca, L., Kyriakopoulos, K., Michas, G., & Papadakis, G. (2009). Hydrogen sulphide as a natural air contaminant in volcanic/geothermal areas: the case of Sousaki, Corinthia (Greece). *Environmental geology*, 57(8), 1723-1728.
- De Lomas, J. G., Corzo, A., Gonzalez, J. M., Andrades, J. A., Iglesias, E., & Montero, M. J. (2006). Nitrate promotes biological oxidation of sulfide in waste water s: experiment at plant-scale. *Biotechnol. Bioeng*, 93(4), 801-811.
- Dutta, P. K., Rabaey, K., Yuan, Z., & Keller, J. (2008). Spontaneous electrochemical removal of aqueous sulfide. *Water research*, 42(20), 4965-4975.
- Demirci, Ş., Erdoğan, B., & Özcimder, R. (1998). Waste water treatment at the petroleum refinery, Kirikkale, Turkey using some coagulants and Turkish clays as coagulant aids. *Water research*, 32(11), 3495-3499.
- Das, D., Samal, D. P., & Meikap, B. C. (2015). Preparation of Activated Carbon from Green Coconut Shell and its Characterization. *Journal of Chemical Engineering & Process Technology*, 6(5), 1-7.

- Dehghani, M. H., Dehghan, A., & Najafpoor, A. (2017). Removing Reactive Red 120 and 196 using chitosan/zeolite composite from aqueous solutions: Kinetics, isotherms, and process optimization. *Journal of Industrial and Engineering Chemistry*, 51, 185-195.
- El-Sayed, Y., & Bandosz, T. J. (2004). Adsorption of valeric acid from aqueous solution onto activated carbons: role of surface basic sites. *Journal of colloid and interface science*, 273(1), 64-72.
- Edwards, S., Alharthi, R., & Ghaly, A. E. (2011). Removal of hydrogen sulphide from water. *American Journal of Environmental Sciences*, 7(4), 295.
- El-Naas, M. H., Al-Zuhair, S., Al-Lobaney, A., & Makhlof, S. (2009). Assessment of electrocoagulation for the treatment of petroleum refinery waste water . *Journal of environmental management*, 91(1), 180-185.
- EPA, 2003. Toxicological review of hydrogen sulphide. CAS No. 7783-06-4. Government printing office. Environmental Protection Agency. Washington, DC, USA.
- Elibol, M. (2002). Response surface methodological approach for inclusion of perfluorocarbon in actinorhodin fermentation medium. *Process Biochemistry*, 38(5), 667-673.
- Elsayed, Y., Seredych, M., Dallas, A., & Bandosz, T. J. (2009). Desulfurization of air at high and low H<sub>2</sub>S concentrations. *Chemical Engineering Journal*, 155(3), 594-602.
- Elwakeel, K. Z., & Yousif, A. M. (2010). Adsorption of malathion on thermally treated egg shell material. *Water Science and Technology*, 61(4), 1035-1041.
- Esmaeili Faraj, S. H., Nasr Esfahany, M., Jafari-Asl, M., & Etesami, N. (2014). Hydrogen sulfide bubble absorption enhancement in water-based nanofluids. *Industrial & Engineering Chemistry Research*, 53(43), 16851-16858.
- Estrada, J. M., Kraakman, N. B., Muñoz, R., & Lebrero, R. (2010). A comparative analysis of odour treatment technologies in waste water treatment plants. *Environmental science & technology*, 45(3), 1100-1106.
- Edathil, A. A., Pal, P., & Banat, F. (2017). Alginate derived porous graphitic carbon for highly efficient remediation of sulfide from waste water . *Journal of Environmental Chemical Engineering*, 5(2), 1998-2009.

- Errais, E., Duplay, J., Darragi, F., M'Rabet, I., Aubert, A., Huber, F., & Morvan, G. (2011). Efficient anionic dye adsorption on natural untreated clay: Kinetic study and thermodynamic parameters. *Desalination*, 275(1), 74-81.
- EcA, I. P. I. (2010). Petroleum refining water/waste water use and management. Operations Best Practice Series, London, UK.
- Fang, H. B., Zhao, J. T., Fang, Y. T., Huang, J. J., & Wang, Y. (2013). Selective oxidation of hydrogen sulfide to sulfur over activated carbon-supported metal oxides. *Fuel*, 108, 143-148.
- Farma, R., Deraman, M., Awitdrus, A., Talib, I. A., Taer, E., Basri, N. H., & Hashmi, S. A. (2013). Preparation of highly porous binderless activated carbon electrodes from fibres of oil palm empty fruit bunches for application in supercapacitors. *Bioresource technology*, 132, 254-261.
- Feng, W., Kwon, S., Borguet, E., & Vidic, R. (2005). Adsorption of hydrogen sulfide onto activated carbon fibers: effect of pore structure and surface chemistry. *Environmental science & technology*, 39(24), 9744-9749.
- Florent, M., Wallace, R., & Bandosz, T. J. (2015). Removal of hydrogen sulfide at ambient conditions on cadmium/GO-based composite adsorbents. *Journal of colloid and interface science*, 448, 573-581.
- Foo, K. Y., & Hameed, B. H. (2010). Insights into the modeling of adsorption isotherm systems. *Chemical Engineering Journal*, 156(1), 2-10.
- Foo, K. Y., & Hameed, B. H. (2011). Preparation and characterization of activated carbon from sunflower seed oil residue via microwave assisted  $K_2CO_3$  activation. *Bioresource technology*, 102(20), 9794-9799.
- Foo, K. Y., & Hameed, B. H. (2012). Mesoporous activated carbon from wood sawdust by  $K_2CO_3$  activation using microwave heating. *Bioresource technology*, 111, 425-432.
- Ferguson, M. W. (1982). The structure and composition of the eggshell and embryonic membranes of Alligator mississippiensis. *Journal of Zoology*, 36(2), 99-152.
- Gadekar, S., Nemati, M., & Hill, G. A. (2006). Batch and continuous biooxidation of sulphide by *Thiomicrospira* sp. CVO: reaction kinetics and stoichiometry. *Water research*, 40(12), 2436-2446.

- Gao, P., Liu, Z. H., Xue, G., Han, B., & Zhou, M. H. (2011). Preparation and characterization of activated carbon produced from rice straw by  $(\text{NH}_4)_2\text{HPO}_4$  activation. *Bioresource technology*, 102(3), 3645-3648.
- Ghosh, A., Remorino, A., Tucker, M. J., & Hochstrasser, R. M. (2009). 2D IR photon echo spectroscopy reveals hydrogen bond dynamics of aromatic nitriles. *Chemical physics letters*, 469(4-6), 325-330.
- Gottipati, R., & Mishra, S. (2010). Process optimization of adsorption of Cr (VI) on activated carbons prepared from plant precursors by a two-level full factorial design. *Chemical Engineering Journal*, 160(1), 99-107.
- Guijarro-Aldaco, A., Hernández-Montoya, V., Bonilla-Petriciolet, A., Montes-Morán, M. A., & Mendoza-Castillo, D. I. (2011). Improving the adsorption of heavy metals from water using commercial carbons modified with egg shell wastes. *Industrial & Engineering Chemistry Research*, 50(15), 9354-9362.
- Günay, A., Arslankaya, E., & Tosun, I. (2007). Lead removal from aqueous solution by natural and pretreated clinoptilolite: adsorption equilibrium and kinetics. *Journal of Hazardous Materials*, 146(1), 362-371.
- Guo, J., Luo, Y., Lua, A. C., Chi, R. A., Chen, Y. L., Bao, X. T., & Xiang, S. X. (2007). Adsorption of hydrogen sulphide ( $\text{H}_2\text{S}$ ) by activated carbons derived from oil-palm shell. *Carbon*, 45(2), 330-336.
- Gupta, A. K., Ibrahim, S., & Al Shoaibi, A. (2016). Advances in sulfur chemistry for treatment of acid gases. *Progress in Energy and Combustion Science*, 54, 65-92.
- Gupta, V. K., Ali, I., & Mohan, D. (2003). Equilibrium uptake and sorption dynamics for the removal of a basic dye (basic red) using low-cost adsorbents. *Journal of Colloid and Interface Science*, 265(2), 257-264.
- Gao, B., Han, X., & Zhang, H. (2012). Study on  $\text{H}_2\text{S}$  monitoring technique for high risk wellsite. *Procedia Engineering*, 45, 898-903.
- Guidotti, T. L. (1994). Occupational exposure to hydrogen sulfide in the sour gas industry: some unresolved issues. *International archives of occupational and environmental health*, 66(3), 153-160.
- Haimour, N. M., El-Bishtawi, R., & Ail-Wahbi, A. (2005). Equilibrium adsorption of hydrogen sulfide onto CuO and ZnO. *Desalination*, 181(1-3), 145-152.



- Hamsaveni, D. R., Prapulla, S. G., & Divakar, S. (2001). Response surface methodological approach for the synthesis of isobutyl isobutyrate. *Process Biochemistry*, 36(11), 1103-1109.
- Hariz, I. B., & Monser, L. (2014). Sulfide removal from petroleum refinery waste water by adsorption on chemically modified activated carbon. *International Water Technology Journal*, 4(4), 264-267.
- Hassani, A., Alidokht, L., Khataee, A. R., & Karaca, S. (2014). Optimization of comparative removal of two structurally different basic dyes using coal as a low-cost and available adsorbent. *Journal of the Taiwan Institute of Chemical Engineers*, 45(4), 1597-1607.
- Heinonen, A. (2012). Adsorption of hydrogen sulfide by modified cellulose nano/microcrystals. Master thesis. Lappeenranta University of Technology.
- Hendrickson, R. G., Chang, A., & Hamilton, R. J. (2004). Co-worker fatalities from hydrogen sulfide. *American journal of industrial medicine*, 45(4), 346-350.
- Henshaw, P. F., & Zhu, W. (2001). Biological conversion of hydrogen sulphide to elemental sulphur in a fixed-film continuous flow photo-reactor. *Water Research*, 35(15), 3605-3610.
- Hosseini, M., Mertens, S. F., Ghorbani, M., & Arshadi, M. R. (2003). Asymmetrical Schiff bases as inhibitors of mild steel corrosion in sulphuric acid media. *Materials Chemistry and Physics*, 78(3), 800-808.
- He, S., Hu, Y., Hu, T., Ma, A., Jia, Q., Su, H., & Shan, S. (2017). Investigation of CaO-based sorbents derived from egg shells and red mud for CO<sub>2</sub> capture. *Journal of Alloys and Compounds*, 701, 828-833.
- Hariz, I. B., Halleb, A., Adhoum, N., & Monser, L. (2013). Treatment of petroleum refinery sulfidic spent caustic wastes by electrocoagulation. *Separation and Purification Technology*, 107, 150-157.
- He, R., Xia, F. F., Wang, J., Pan, C. L., & Fang, C. R. (2011). Characterization of adsorption removal of hydrogen sulfide by waste biocover soil, an alternative landfill cover. *Journal of hazardous materials*, 186(1), 773-778.
- Huang, C. C., Chen, C. H., & Chu, S. M. (2006). Effect of moisture on H<sub>2</sub>S adsorption by copper impregnated activated carbon. *Journal of hazardous materials*, 136(3), 866-873.



- Janoszka, K., Wziatek, A., & Gromiec, J. P. (2013). Ocena metod monitoringu stezen siarkowodoru w powietrzu/evaluation of methods for monitoring air concentrations of hydrogen sulfide. *Medycyna pracy*, 64(3), 449.
- Jiang, M., Zhang, J., Xing, L., Zhou, J., Cui, H., Si, W., & Zhuo, S. (2016). KOH-Activated Porous Carbons Derived from Chestnut Shell with Superior Capacitive Performance. *Chinese Journal of Chemistry*, 34(11), 1093-1102
- Joshi, S., & Pokharel, B. P. (2014). Preparation and Characterization of Activated Carbon from Lapsi (*Choerospondias axillaris*) Seed Stone by Chemical Activation with Potassium Hydroxide. *Journal of the Institute of Engineering*, 9(1), 79-88.
- Junior, O. P., Cazetta, A. L., Gomes, R. C., Barizão, É. O., Souza, I. P., Martins, A. C., & Almeida, V. C. (2014). Synthesis of ZnCl<sub>2</sub>-activated carbon from macadamia nut endocarp (*Macadamia integrifolia*) by microwave-assisted pyrolysis: optimization using RSM and methylene blue adsorption. *Journal of Analytical and Applied Pyrolysis*, 105, 166-176.
- Jacukowicz-Sobala, I., Wilk, Ł. J., Drabent, K., & Kociolek-Balawejder, E. (2015). Synthesis and characterization of hybrid materials containing iron oxide for removal of sulfides from water. *Journal of colloid and interface science*, 460, 154-163.
- Jalani, N. F., Aziz, A. A., Wahab, N. A., Hassan, W. H. W., & Zainal, N. H. (2016). Application of Palm Kernel Shell Activated Carbon for the Removal of Pollutant and Color in Palm Oil Mill Effluent Treatment. *Journal of Earth, Environment and Health Sciences*, 2(1), 15.
- Jeon, H. J., Ko, C. H., Kim, S. H., & Kim, J. N. (2009). Removal of refractory sulfur compounds in diesel using activated carbon with controlled porosity. *Energy & Fuels*, 23(5), 2537-2543.
- Kaempfer, W., & Berndt, M. (1998). Polymer modified mortar with high resistance to acid to corrosion by biogenic sulfuric acid. In *Proceedings of the IXth ICPIC Congress, Bologna, Italy, 14<sup>th</sup>* (pp. 681-687).
- Kage, S., Ikeda, H., Ikeda, N., Tsujita, A., & Kudo, K. (2004). Fatal hydrogen sulfide poisoning at a dye works. *Legal medicine*, 6(3), 182-186.
- Kalapala, S. (2014). *Removal of Hydrogen Sulfide from Landfill Gas Using a Solar Regenerable Adsorbent* (Doctoral dissertation, Youngstown State University).

- Kante, K., Nieto-Delgado, C., Rangel-Mendez, J. R., & Bandosz, T. J. (2012). Spent coffee-based activated carbon: specific surface features and their importance for H<sub>2</sub>S separation process. *Journal of hazardous materials*, 201, 141-147.
- Kar, A., Kundu, S., & Patra, A. (2012). Photocatalytic properties of semiconductor SnO<sub>2</sub>/CdS heterostructure nanocrystals. *RSC Advances*, 2(27), 10222-10230.
- Kazemipour, M., Ansari, M., Tajrobehkar, S., Majdzadeh, M., & Kermani, H. R. (2008). Removal of lead, cadmium, zinc, and copper from industrial waste water by carbon developed from walnut, hazelnut, almond, pistachio shell, and apricot stone. *Journal of Hazardous Materials*, 150(2), 322-327.
- Kumar, B. R., Saravanan, S., Rana, D., & Nagendran, A. (2016). Combined effect of injection timing and exhaust gas recirculation (EGR) on performance and emissions of a DI diesel engine fuelled with next-generation advanced biofuel–diesel blends using response surface methodology. *Energy Conversion and Management*, 123, 470-486.
- Kundu, A., Gupta, B. S., Hashim, M. A., & Redzwan, G. (2015). Taguchi optimization approach for production of activated carbon from phosphoric acid impregnated palm kernel shell by microwave heating. *Journal of Cleaner Production*, 105, 420-427.
- Kazmierczak-Razna, J., Gralak-Podemska, B., Nowicki, P., & Pietrzak, R. (2015). The use of microwave radiation for obtaining activated carbons from sawdust and their potential application in removal of NO<sub>2</sub> and H<sub>2</sub>S. *Chemical Engineering Journal*, 269, 352-358.
- Kazmierczak-Razna, J., Nowicki, P., & Pietrzak, R. (2016). Toxic gases removal onto activated carbons obtained from hay with the use of microwave radiation. *Chemical Engineering Research and Design*, 109, 346-353.
- Kennedy, L. J., & Sekaran, G. (2004). Integrated biological and catalytic oxidation of organics/inorganics in tannery waste water by rice husk based mesoporous activated carbon—*Bacillus* sp. *Carbon*, 42(12), 2399-2407.
- Khalid, B., Meng, Q., Akram, R., & Cao, B. (2016). Effects of KOH activation on surface area, porosity and desalination performance of coconut carbon electrodes. *Desalination and Water Treatment*, 57(5), 2195-2202.
- Kose, H. (2010). The effects of physical factors on the adsorption of synthetic organic compounds by activated carbons and activated carbon fibers. Clemson University.

- Karacan, F., Ozden, U., & Karacan, S. (2007). Optimization of manufacturing conditions for activated carbon from Turkish lignite by chemical activation using response surface methodology. *Applied Thermal Engineering*, 27(7), 1212-1218.
- Koumanova, B., Peeva, P., Allen, S. J., Gallagher, K. A., & Healy, M. G. (2002). Biosorption from aqueous solutions by egg shell membranes and *Rhizopus oryzae*: equilibrium and kinetic studies. *Journal of Chemical Technology and Biotechnology*, 77(5), 539-545.
- Köse, T. E., Demiral, H., & Öztürk, N. (2011). Adsorption of boron from aqueous solutions using activated carbon prepared from olive bagasse. *Desalination and Water Treatment*, 29(1-3), 110-118.
- Kanjanarong, J., Giri, B. S., Jaisi, D. P., Oliveira, F. R., Boonsawang, P., Chaiprapat, S., & Khanal, S. K. (2017). Removal of hydrogen sulfide generated during anaerobic treatment of sulfate-laden waste water using biochar: *Evaluation of efficiency and mechanisms*. *Bioresource Technology*, 234, 115-121.
- Ko, J. H., Xu, Q., & Jang, Y. C. (2015). Emissions and control of hydrogen sulfide at landfills: a review. *Critical Reviews in Environmental Science and Technology*, 45(19), 2043-2083.
- Lambert, T. W., Goodwin, V. M., Stefani, D., & Strosher, L. (2006). Hydrogen sulfide (H<sub>2</sub>S) and sour gas effects on the eye. A historical perspective. *Science of the total environment*, 367(1), 1-22.
- Lee, S., Xu, Q., Booth, M., Townsend, T. G., Chadik, P., & Bitton, G. (2006). Reduced sulfur compounds in gas from construction and demolition debris landfills. *Waste Management*, 26(5), 526-533.
- Lemos, B. R., Teixeira, I. F., De Mesquita, J. P., Ribeiro, R. R., Donnici, C. L., & Lago, R. M. (2012). Use of modified activated carbon for the oxidation of aqueous sulfide. *Carbon*, 50(3), 1386-1393.
- Lestari, R. A., Sediawan, W. B., Syamsiah, S., & Teixeira, J. A. (2016). Hydrogen sulfide removal from biogas using a salak fruit seeds packed bed reactor with sulfur oxidizing bacteria as biofilm. *Journal of Environmental Chemical Engineering*, 4(2), 2370-2377.
- Li, H., Monnell, J. D., Alvin, M., & Vidic, R. D. (2008). Factors affecting activated carbon-based catalysts for selective hydrogen sulfide oxidation. *Main Group Chemistry*, 7(3), 239-250.
- Li, J., Chen, F. P., Jin, G. P., Feng, X. S., & Li, X. X. (2015). Removals of aqueous sulfur dioxide and hydrogen sulfide using CeO<sub>2</sub>-NiAl-LDHs coating activated carbon and

its mix with carbon nano-tubes. *Colloids and Surfaces A: Physicochemical and Engineering Aspects*, 476, 90-97.

- Lien, C. C., Lin, J. L., & Ting, C. H. (2014). Water Scrubbing for Removal of Hydrogen Sulfide (H<sub>2</sub>S) Inbiogas from Hog Farms. *Journal of Agricultural Chemistry and Environment*, 3(02), 1-6.
- Liu, M., Deng, Q., Zhao, F., & Liu, Y. (2012). Origin of hydrogen sulfide in coal seams in China. *Safety science*, 50(4), 668-673.
- Lin, H., Williams, N., King, A., & Hu, B. (2016). Electrochemical sulfide removal by low-cost electrode materials in anaerobic digestion. *Chemical Engineering Journal*, 297, 180-192.
- Li, S., Han, K., Li, J., Li, M., & Lu, C. (2017). Preparation and characterization of super activated carbon produced from gulfweed by KOH activation. *Microporous and Mesoporous Materials*, 243, 291-300.
- Liu, S., Xu, W. H., Liu, Y. G., Tan, X. F., Zeng, G. M., Li, X., & Cai, X. X. (2017). Facile synthesis of Cu (II) impregnated biochar with enhanced adsorption activity for the removal of doxycycline hydrochloride from water. *Science of the Total Environment*, 592, 546-553.
- Laca, A., Laca, A., & Díaz, M. (2017). Egg shell waste as catalyst: A review. *Journal of Environmental Management*, 197, 351-359.
- Lu, C., Xu, S., & Liu, C. (2010). The role of K<sub>2</sub>CO<sub>3</sub> during the chemical activation of petroleum coke with KOH. *Journal of Analytical and Applied Pyrolysis*, 87(2), 282-287.
- Mabayoje, O., Seredych, M., & Bandosz, T. J. (2012). Cobalt (hydr) oxide/graphite oxide composites: Importance of surface chemical heterogeneity for reactive adsorption of hydrogen sulfide. *Journal of colloid and interface science*, 378(1), 1-9.
- Marroccoli, M., Montagnaro, F., Telesca, A., & Valenti, G. L. (2010). Environmental implications of the manufacture of calcium sulfoaluminate-based cements. *In Second International Conference on Sustainable Construction Materials and Technologies, Ancona, Italy, Main Proceedings*, ISBN (978-1).
- Mabayoje, O., Seredych, M., & Bandosz, T. J. (2013). Reactive adsorption of hydrogen sulfide on visible light photoactive zinc (hydr) oxide/graphite oxide and zinc (hydr) oxychloride/graphite oxide composites. *Applied Catalysis B: Environmental*, 132, 321-331.

- Martins, A. C., Pezoti, O., Cazetta, A. L., Bedin, K. C., Yamazaki, D. A., Bandoch, G. F., & Almeida, V. C. (2015). Removal of tetracycline by NaOH-activated carbon produced from macadamia nut shells: kinetic and equilibrium studies. *Chemical Engineering Journal*, 260, 291-299.
- Moreno-Azanza, M., Bauluz, B., Canudo, J. I., Puértolas-Pascual, E., & Sellés, A. G. (2014). A re-evaluation of aff. *Megaloolithidae* eggshell fragments from the uppermost Cretaceous of the Pyrenees and implications for crocodylomorph eggshell structure. *Historical Biology*, 26(2), 195-205.
- Ma, F., Guo, J. B., Zhao, L. J., Chang, C. C., & Cui, D. (2009). Application of bioaugmentation to improve the activated sludge system into the contact oxidation system treating petrochemical waste water. *Bioresource technology*, 100(2), 597-602.
- Melo, D. M. D. A., De Souza, J. R., Melo, M. A. D. F., Martinelli, A. E., Cachima, G. H. B., & Cunha, J. D. D. (2006). Evaluation of the zinox and zeolite materials as adsorbents to remove H<sub>2</sub>S from natural gas. *Colloids and Surfaces A: Physicochemical and Engineering Aspects*, 272(1), 32-36.
- Miyawaki, J., Lee, G. H., Yeh, J., Shiratori, N., Shimohara, T., Mochida, I., & Yoon, S. H. (2012). Development of carbon-supported hybrid catalyst for clean removal of formaldehyde indoors. *Catalysis today*, 185(1), 278-283.
- Mochizuki, T., Kubota, M., Matsuda, H., & Camacho, L. F. E. (2016). Adsorption behaviors of ammonia and hydrogen sulfide on activated carbon prepared from petroleum coke by KOH chemical activation. *Fuel Processing Technology*, 144, 164-169.
- Mohamed, E. F. (2011). Removal of organic compounds from water by adsorption and photocatalytic oxidation. PhD Thesis. University of De toulous, France.
- Moreno-Castilla, C. (2004). Adsorption of organic molecules from aqueous solutions on carbon materials. *Carbon*, 42(1), 83-94.
- Muñoz-Guillena, M. J., Macías-Pérez, M. C., Linares-Solano, A., & de Lecea, C. S. M. (1997). CaO dispersed on carbon as an SO<sub>2</sub> sorbent. *Fuel*, 76(6), 527-532.
- Mopoung, S., Moonsri, P., Palas, W., & Khumpai, S. (2015). Characterization and properties of activated carbon prepared from tamarind seeds by koh activation for fe (III) adsorption from aqueous solution. *The Scientific World Journal*, 2015.



- Nguyen-Thanh, D., & Bandosz, T. J. (2005). Activated carbons with metal containing bentonite binders as adsorbents of hydrogen sulfide. *Carbon*, 43(2), 359-367.
- Nikulshina, V., Gebald, C., & Steinfeld, A. (2009). CO<sub>2</sub> capture from atmospheric air via consecutive CaO-carbonation and CaCO<sub>3</sub>-calcination cycles in a fluidized-bed solar reactor. *Chemical Engineering Journal*, 146(2), 244-248.
- Nowicki, P., Skibiszewska, P., & Pietrzak, R. (2014). Hydrogen sulphide removal on carbonaceous adsorbents prepared from coffee industry waste materials. *Chemical Engineering Journal*, 248, 208-215.
- NSDH, 2009. The drop on water: Hydrogen sulphide. Nova Scotia Department of Health. Halifax, Nova Scotia.
- Nowicki, P., Skibiszewska, P., & Pietrzak, R. (2013). NO<sub>2</sub> removal on adsorbents prepared from coffee industry waste materials. *Adsorption*, 19(2-4), 521-528.
- Nakatani, N., Takamori, H., Takeda, K., & Sakugawa, H. (2009). Transesterification of soybean oil using combusted oyster shell waste as a catalyst. *Bioresource Technology*, 100(3), 1510-1513.
- Ozekmekci, M., Salkic, G., & Fellah, M. F. (2015). Use of zeolites for the removal of H<sub>2</sub>S: a mini-review. *Fuel Processing Technology*, 139, 49-60.
- Ouasif, H., Yousfi, S., Bouamrani, M. L., El Kouali, M., Benmokhtar, S., & Talbi, M. (2013). Removal of a cationic dye from waste water by adsorption onto natural adsorbents. *Journal of Materials and Environmental Science*, 4(1), 1-10.
- Ortiz, F. G., Aguilera, P. G., & Ollero, P. (2014). Modeling and simulation of the adsorption of biogas hydrogen sulfide on treated sewage-sludge. *Chemical Engineering Journal*, 253, 305-315.
- Olgun, O., Yildiz, A. Ö., & Cufadar, Y. (2015). The effects of egg shell and oyster shell supplemental as calcium sources on performance, egg shell quality and mineral excretion in laying hens. *Indian Journal of Animal Research*, 49(2), 205-209.
- Pham Xuan, H., Pham Minh, D., Galera Martínez, M., Nzihou, A., & Sharrock, P. (2015). Valorization of Calcium Carbonate-Based Solid Wastes for the Treatment of Hydrogen Sulfide from the Gas Phase. *Industrial & Engineering Chemistry Research*, 54(18), 4915-4922.

- Phooratsamee, W., Hussaro, K., Teekasap, S., & Hirunlabh, J. (2014). Increasing adsorption of activated carbon from palm oil shell for adsorb H<sub>2</sub>S from biogas production by impregnation. *American Journal of Environmental Sciences*, 10(5), 431.
- Poland, A. L., & Sheldon, B. W. (2001). Altering the thermal resistance of foodborne bacterial pathogens with an egg shell membrane waste by-product. *Journal of food protection*, 64(4), 486-492.
- Poulton, S. W., Krom, M. D., Van Rijn, J., & Raiswell, R. (2002). The use of hydrous iron (III) oxides for the removal of hydrogen sulphide in aqueous systems. *Water research*, 36(4), 825-834.
- Pourzolfaghar, H., & Ismail, M. H. S. (2013). Study of H<sub>2</sub>S Removal Efficiency of Virgin Zeolite in POME Biogas Desulfurization at Ambient Temperature and Pressure. *In Developments in Sustainable Chemical and Bioprocess Technology*, 295-301.
- Pourzolfaghar, H., Mohd Halim, S. I., Izhar, S., & Esfahan, Z. M. (2014). Review of H<sub>2</sub>S sorbents at low-temperature desulfurization of biogas. *International Journal of Chemical and Environmental Engineering*, 5(1), 22-28.
- Pamnani, R., Sharma, G. K., Mahadevan, S., Jayakumar, T., Vasudevan, M., & Rao, B. P. C. (2015). Residual stress studies on arc welding joints of naval steel (DMR-249A). *Journal of Manufacturing Processes*, 20, 104-111.
- Przepiórski, J., Czyżewski, A., Pietrzak, R., Toyoda, M., & Morawski, A. W. (2013). Porous carbon material containing CaO for acidic gas capture: Preparation and properties. *Journal of hazardous materials*, 263, 353-360.
- Pundir, C. S., Bhambi, M., & Chauhan, N. S. (2009). Chemical activation of egg shell membrane for covalent immobilization of enzymes and its evaluation as inert support in urinary oxalate determination. *Talanta*, 77(5), 1688-1693.
- Pikaar, I., Li, E., Rozendal, R. A., Yuan, Z., Keller, J., & Rabaey, K. (2012). Long-term field test of an electrochemical method for sulfide removal from sewage. *Water research*, 46(9), 3085-3093.
- Pongener, C., Kibami, D., Rao, K. S., Goswamee, R. L., & Sinha, D. (2015). Synthesis and Characterization of Activated Carbon from the Biowaste of the Plant Manihot Esculenta. *Chem. Sci. Trans.*, 4(1) 59-68.
- Park, W. H., & Polprasert, C. (2008). Roles of oyster shells in an integrated constructed wetland system designed for P removal. *Ecological Engineering*, 34(1), 50-56.



- Pang, B. W., Jiang, C. H., Yeung, M., Ouyang, Y., & Xi, J. (2017). Removal of dissolved sulfides in aqueous solution by activated sludge: mechanism and characteristics. *Journal of hazardous materials*, 324, 732-738.
- Pizzolante, C. C., Kakimoto, S. K., Saldanha, E. S. P. B., Laganá, C., Souza, H. B. A., & Moraes, J. E. (2011). Limestone and oyster shell for brown layers in their second egg production cycle. *Revista Brasileira de Ciência Avícola*, 13(2), 103-111.
- Roosta, M., Ghaedi, M., Daneshfar, A., Sahraei, R., & Asghari, A. (2015). Optimization of combined ultrasonic assisted/tin sulfide nanoparticle loaded on activated carbon removal of erythrosine by response surface methodology. *Journal of Industrial and Engineering Chemistry*, 21, 459-469.
- Radovic, L. R., Moreno-Castilla, C., & Rivera-Utrilla, J. (2001). Carbon materials as adsorbents in aqueous solutions. *Chemistry and physics of carbon*, 227-406.
- Rattanapan, C., Kantachote, D., Yan, R., & Boonsawang, P. (2010). Hydrogen sulfide removal using granular activated carbon biofiltration inoculated with *Alcaligenes faecalis* T307 isolated from concentrated latex waste water. *International Biodeterioration & Biodegradation*, 64(5), 383-387.
- Réguer, A., Sochard, S., Hort, C., & Platel, V. (2011). Measurement and modelling of adsorption equilibrium, adsorption kinetics and breakthrough curve of toluene at very low concentrations on to activated carbon. *Environmental technology*, 32(7), 757-766.
- Rehman, Z. U., Farooqi, I. H., & Ayub, S. (2010). Performance of biofilter for the removal of hydrogen sulphide odour. *International Journal of Environmental Research*, 3(4), 537-544.
- Rene, E. R., Veiga, M. C., & Kennes, C. (2012). Combined biological and physicochemical waste-gas cleaning techniques. *Journal of Environmental Science and Health, Part A*, 47(7), 920-939.
- Reverberi, A. P., Klemeš, J. J., Varbanov, P. S., & Fabiano, B. (2016). A review on hydrogen production from hydrogen sulphide by chemical and photochemical methods. *Journal of Cleaner Production*, 136, 72-80.
- Roy, P., Mondal, N. K., & Das, K. (2014). Modeling of the adsorptive removal of arsenic: a statistical approach. *Journal of Environmental Chemical Engineering*, 2(1), 585-597.

- Rufford, T. E., Hulicova-Jurcakova, D., Khosla, K., Zhu, Z., & Lu, G. Q. (2010). Microstructure and electrochemical double-layer capacitance of carbon electrodes prepared by zinc chloride activation of sugar cane bagasse. *Journal of Power Sources*, 195(3), 912-918.
- Ramasamy, S., Singh, S., Taniere, P., Langman, M. J. S., & Eggo, M. C. (2006). Sulfide-detoxifying enzymes in the human colon are decreased in cancer and upregulated in differentiation. *American Journal of Physiology-Gastrointestinal and Liver Physiology*, 291(2), 288-296.
- Rio, S., Faur-Brasquet, C., Le Coq, L., Courcoux, P., & Le Cloirec, P. (2005). Experimental design methodology for the preparation of carbonaceous sorbents from sewage sludge by chemical activation—application to air and water treatments. *Chemosphere*, 58(4), 423-437.
- Ramesh, A., Lee, D. J., & Wong, J. W. C. (2005). Thermodynamic parameters for adsorption equilibrium of heavy metals and dyes from waste water with low-cost adsorbents. *Journal of Colloid and Interface Science*, 291(2), 588-592.
- Sahu, R. C., Patel, R., & Ray, B. C. (2011). Removal of hydrogen sulfide using red mud at ambient conditions. *Fuel processing technology*, 92(8), 1587-1592.
- Santos, J. M., Lopes, E. S., Junior, N. C. R., de Sá, L. M., & Horan, N. J. (2009). Mathematical modelling of hydrogen sulphide emission and removal in aerobic biofilters comprising chemical oxidation. *Water research*, 43(14), 3355-3364.
- Saien, J., & Nejati, H. (2007). Enhanced photocatalytic degradation of pollutants in petroleum refinery waste water under mild conditions. *Journal of hazardous materials*, 148(1), 491-495.
- Sohrabi, M. R., Moghri, M., Masoumi, H. R. F., Amiri, S., & Moosavi, N. (2016). Optimization of Reactive Blue 21 removal by Nanoscale Zero-Valent Iron using response surface methodology. *Arabian Journal of Chemistry*, 9(4), 518-525.
- Sekirifa, M. L., Hadj-Mahammed, M., Pallier, S., Baameur, L., Richard, D., & Al-Dujaili, A. H. (2013). Preparation and characterization of an activated carbon from a date stones variety by physical activation with carbon dioxide. *Journal of Analytical and Applied Pyrolysis*, 99, 155-160.
- Sen, A., Albarella, J. D., Carey, J. R., Kim, P., & McNamara, W. B. (2008). Low-cost colorimetric sensor for the quantitative detection of gaseous hydrogen sulfide. *Sensors and Actuators B: Chemical*, 134(1), 234-237.

- Seredych, M., & Bandosz, T. J. (2009). Adsorption of hydrogen sulfide on graphite derived materials modified by incorporation of nitrogen. *Materials Chemistry and Physics*, 113(2), 946-952.
- Seredych, M., & Bandosz, T. J. (2008). Role of microporosity and nitrogen functionality on the surface of activated carbon in the process of desulfurization of digester gas. *The Journal of Physical Chemistry C*, 112(12), 4704-4711.
- Seredych, M., Mabayoje, O., & Bandosz, T. J. (2011). Visible-light-enhanced interactions of hydrogen sulfide with composites of zinc (oxy) hydroxide with graphite oxide and graphene. *Langmuir*, 28(2), 1337-1346.
- Seredych, M., Portet, C., Gogotsi, Y., & Bandosz, T. J. (2009). Nitrogen modified carbide-derived carbons as adsorbents of hydrogen sulfide. *Journal of colloid and interface science*, 330(1), 60-66.
- Seredych, M., Strydom, C., & Bandosz, T. J. (2008). Effect of fly ash addition on the removal of hydrogen sulfide from biogas and air on sewage sludge-based composite adsorbents. *Waste management*, 28(10), 1983-1992.
- Shang, G., Li, Q., Liu, L., Chen, P., & Huang, X. (2016). Adsorption of hydrogen sulfide by biochars derived from pyrolysis of different agricultural/forestry wastes. *Journal of the Air & Waste Management Association*, 66(1), 8-16.
- Sahira, J., Mandira, A., Prasad, P. B., & Ram, P. R. (2013). Effects of activating agents on the activated carbons prepared from Lapsi seed stone. *Res. J. Chem. Sci.*, 3, 19-24.
- Siefers, A., Wang, N., Sindt, A., Dunn, J., McElvogue, J., Evans, E., & Ellis, T. (2010). A novel and cost-effective hydrogen sulfide removal technology using tire derived rubber particles. *Proceedings of the Water Environment Federation*, 2010(12), 4597-4622.
- Sitthikhankaew, R., Chadwick, D., Assabumrungrat, S., & Laosiripojana, N. (2014). Effects of humidity, O<sub>2</sub>, and CO<sub>2</sub> on H<sub>2</sub>S adsorption onto upgraded and KOH impregnated activated carbons. *Fuel Processing Technology*, 124, 249-257.
- Skrtic, L. (2006). Hydrogen sulfide, oil and gas, and people's health. University of California Energy and resource group berkeley, USA.
- Song, H. S., Park, M. G., Kwon, S. J., Yi, K. B., Croiset, E., Chen, Z., & Nam, S. C. (2013). Hydrogen sulfide adsorption on nano-sized zinc oxide/reduced graphite oxide composite at ambient condition. *Applied Surface Science*, 276, 646-652.

- Stadelman, W. J. (2000). Encyclopedia of food science and technology. *John Wiley and Sons, New York*, 593-599.
- Startsev, A. N., Kruglyakova, O. V., Chesalov, Y. A., Ruzankin, S. P., Kravtsov, E. A., Larina, T. V., & Paukshtis, E. A. (2013). Low temperature catalytic decomposition of hydrogen sulfide into hydrogen and diatomic gaseous sulfur. *Topics in Catalysis*, 56(11), 969-980.
- Stavropoulos, G. G., & Zabaniotou, A. A. (2005). Production and characterization of activated carbons from olive-seed waste residue. *Microporous and Mesoporous Materials*, 82(1), 79-85.
- Sydney, R., Esfandi, E., & Surapaneni, S. (1996). Control concrete sewer corrosion via the crown spray process. *Water environment research*, 68(3), 338-347.
- Sahu, J. N., Acharya, J., & Meikap, B. C. (2009). Response surface modeling and optimization of chromium (VI) removal from aqueous solution using Tamarind wood activated carbon in batch process. *Journal of hazardous materials*, 172(2), 818-825.
- Sevilla, M., & Fuertes, A. B. (2013). A general and facile synthesis strategy towards highly porous carbons: carbonization of organic salts. *Journal of Materials Chemistry A*, 1(44), 13738-13741.
- Selene, C. H., & Chou, J. (2003). Hydrogen sulfide: human health aspects. *Concise International Chemical Assessment Document*, 53, 7-14.
- Shokrollahzadeh, S., Azizmohseni, F., Golmohammad, F., Shokouhi, H., & Khademhaghighat, F. (2008). Biodegradation potential and bacterial diversity of a petrochemical waste water treatment plant in Iran. *Bioresource technology*, 99(14), 6127-6133.
- Taheri, M., Mohebbi, A., Hashemipour, H., & Rashidi, A. M. (2016). Simultaneous absorption of carbon dioxide (CO<sub>2</sub>) and hydrogen sulfide (H<sub>2</sub>S) from CO<sub>2</sub>-H<sub>2</sub>S-CH<sub>4</sub> gas mixture using amine-based nanofluids in a wetted wall column. *Journal of Natural Gas Science and Engineering*, 28, 410-417.
- Tao, Y., Li, P., & Shi, S. Q. (2016). Effects of Carbonization Temperature and Component Ratio on Electromagnetic Interference Shielding Effectiveness of Woodceramics. *Materials*, 9(7), 540.

- Terzyk, A. P. (2004). Molecular properties and intermolecular forces—factors balancing the effect of carbon surface chemistry in adsorption of organics from dilute aqueous solutions. *Journal of colloid and interface science*, 275(1), 9-29
- Thompson, M. A., Kelkar, U. G., & Vickers, J. C. (1995). The treatment of groundwater containing hydrogen sulfide using microfiltration. *Desalination*, 102(1), 287-291.
- Tomar, M., & Abdullah, T. H. (1994). Evaluation of chemicals to control the generation of malodorous hydrogen sulfide in waste water . *Water Research*, 28(12), 2545-2552.
- Treviño-Cordero, H., Juárez-Aguilar, L. G., Mendoza-Castillo, D. I., Hernández-Montoya, V., Bonilla-Petriciolet, A., & Montes-Morán, M. A. (2013). Synthesis and adsorption properties of activated carbons from biomass of *Prunus domestica* and *Jacaranda mimosifolia* for the removal of heavy metals and dyes from water. *Industrial Crops and Products*, 42, 315-323.
- Thommes, M., Kaneko, K., Neimark, A. V., Olivier, J. P., Rodriguez-Reinoso, F., Rouquerol, J., & Sing, K. S. (2015). Physisorption of gases, with special reference to the evaluation of surface area and pore size distribution (IUPAC Technical Report). *Pure and Applied Chemistry*, 87, 1051-1069.
- Tsai, W. T., Yang, J. M., Lai, C. W., Cheng, Y. H., Lin, C. C., & Yeh, C. W. (2006). Characterization and adsorption properties of egg shells and egg shell membrane. *Bioresource technology*, 97(3), 488-493
- Tsai, W. T., Hsien, K. J., Hsu, H. C., Lin, C. M., Lin, K. Y., & Chiu, C. H. (2008). Utilization of ground egg shell waste as an adsorbent for the removal of dyes from aqueous solution. *Bioresource technology*, 99(6), 1623-1629.
- Tsang, Y. F., Wang, L., & Chua, H. (2015). Simultaneous hydrogen sulphide and ammonia removal in a biotrickling filter: crossed inhibitory effects among selected pollutants and microbial community change. *Chemical Engineering Journal*, 281, 389-396.
- Tseng, R. L., Tseng, S. K., Wu, F. C., Hu, C. C., & Wang, C. C. (2008). Effects of micropore development on the physicochemical properties of KOH-activated carbons. *Journal of the Chinese Institute of Chemical Engineers*, 39(1), 37-47.
- Tran, H. N., You, S. J., & Chao, H. P. (2016). Thermodynamic parameters of cadmium adsorption onto orange peel calculated from various methods: a comparison study. *Journal of Environmental Chemical Engineering*, 4(3), 2671-2682.



- Tumin, N. D., Chuah, A. L., Zawani, Z., & Rashid, S. A. (2008). Adsorption of copper from aqueous solution by Elais Guineensis kernel activated carbon. *Journal of Engineering Science and Technology*, 3(2), 180-189.
- Tong, K., Zhang, Y., Liu, G., Ye, Z., & Chu, P. K. (2013). Treatment of heavy oil waste water by a conventional activated sludge process coupled with an immobilized biological filter. *International Biodeterioration & Biodegradation*, 84, 65-71.
- Theivandran, G., Ibrahim, M., & Murugan, M. (2015). Fourier Transform Infrared (Ft-Ir) Spectroscopic Analysis of Spirulina fusiformis. *Journal of Medicinal Plants Studies*, 3(4), 30-32.
- US Environmental Protection Agency. (1991). Hydrogen Sulphide Corrosion in Waste water Collection and Treatment System. *US Environmental Protection Agency*.
- Vincke, E., Van Wanseele, E., Monteny, J., Beeldens, A., De Belie, N., Taerwe, L., & Verstraete, W. (2002). Influence of polymer addition on biogenic sulfuric acid attack of concrete. *International biodeterioration & biodegradation*, 49(4), 283-292.
- Vaiopoulou, E., Melidis, P., & Aivasidis, A. (2005). Sulfide removal in waste water from petrochemical industries by autotrophic denitrification. *Water Research*, 39(17), 4101-4109.
- Vollertsen, J., Nielsen, A. H., Jensen, H. S., Wium-Andersen, T., & Hvitved-Jacobsen, T. (2008). Corrosion of concrete sewers—the kinetics of hydrogen sulfide oxidation. *Science of the total Environment*, 394(1), 162-170.
- Van Hamme, J. D., Singh, A., & Ward, O. P. (2003). Recent advances in petroleum microbiology. *Microbiology and molecular biology reviews*, 67(4), 503-549.
- Wang, C., & Pei, Y. (2012). The removal of hydrogen sulfide in solution by ferric and alum water treatment residuals. *Chemosphere*, 88(10), 1178-1183.
- Wang, N., Park, J., & Ellis, T. G. (2013). The mechanism of hydrogen sulfide adsorption on fine rubber particle media (FRPM). *Journal of hazardous materials*, 260, 921-928.
- Ward, A. J., Hobbs, P. J., Holliman, P. J., & Jones, D. L. (2008). Optimisation of the anaerobic digestion of agricultural resources. *Bioresource technology*, 99(17), 7928-7940.

- Wallace, R., Seredych, M., Zhang, P., & Bandosz, T. J. (2014). Municipal waste conversion to hydrogen sulfide adsorbents: Investigation of the synergistic effects of sewage sludge/fish waste mixture. *Chemical Engineering Journal*, 237, 88-94.
- White, A. J. (2010). Development of an activated carbon from anaerobic digestion by-product to remove hydrogen sulfide from biogas (Doctoral dissertation, University of Toronto (Canada)).
- Wiemann, M., Schenk, H., & Hegemann, W. (1998). Anaerobic treatment of tannery waste water with simultaneous sulphide elimination. *Water research*, 32(3), 774-780.
- Wiheeb, A. D., Shamsudin, I. K., Ahmad, M. A., Murat, M. N., Kim, J., & Othman, M. R. (2013). Present technologies for hydrogen sulfide removal from gaseous mixtures. *Reviews in Chemical Engineering*, 29(6), 449-470.
- Xiao, Y., Wang, S., Wu, D., & Yuan, Q. (2008). Experimental and simulation study of hydrogen sulfide adsorption on impregnated activated carbon under anaerobic conditions. *Journal of hazardous materials*, 153(3), 1193-1200.
- Xu, S., Huang, S., Guo, D., Zhao, Y., & Song, M. (2017). Failure analysis of a carbon steel pipeline exposed to wet hydrogen sulfide environment. *Engineering Failure Analysis*, 71, 1-10.
- Xu, X., Cao, X., Zhao, L., & Sun, T. (2014). Comparison of sewage sludge-and pig manure-derived biochars for hydrogen sulfide removal. *Chemosphere*, 111, 296-303.
- Yang, J., & Qiu, K. (2010). Preparation of activated carbons from walnut shells via vacuum chemical activation and their application for methylene blue removal. *Chemical Engineering Journal*, 165(1), 209-217.
- Yang, K., Peng, J., Srinivasakannan, C., Zhang, L., Xia, H., & Duan, X. (2010). Preparation of high surface area activated carbon from coconut shells using microwave heating. *Bioresource technology*, 101(15), 6163-6169.
- Yaşyerli, S., Ar, I., Doğu, G., & Doğu, T. (2002). Removal of hydrogen sulfide by clinoptilolite in a fixed bed adsorber. *Chemical Engineering and Processing: Process Intensification*, 41(9), 785-792.
- Yuan, W., & Bandosz, T. J. (2007). Removal of hydrogen sulfide from biogas on sludge-derived adsorbents. *Fuel*, 86(17), 2736-2746.



- Zaman, J., & Chakma, A. (1995). Production of hydrogen and sulfur from hydrogen sulfide. *Fuel processing technology*, 41(2), 159-198.
- Zhang, J., Sun, Y., Woo, M. W., Zhang, L., & Xu, K. Z. (2016). Preparation of steam activated carbon from black liquor by flue gas precipitation and its performance in hydrogen sulfide removal: experimental and simulation works. *Journal of the Taiwan Institute of Chemical Engineers*, 59, 395-404
- Zhang, L., De Schryver, P., De Gusseme, B., De Muynck, W., Boon, N., & Verstraete, W. (2008). Chemical and biological technologies for hydrogen sulfide emission control in sewer systems: a review. *Water research*, 42(1), 1-12.
- Zhang, S., Shao, T., & Karanfil, T. (2011). The effects of dissolved natural organic matter on the adsorption of synthetic organic chemicals by activated carbons and carbon nanotubes. *Water Research*, 45(3), 1378-1386.
- Zhang, X., Li, A., Jiang, Z., & Zhang, Q. (2006). Adsorption of dyes and phenol from water on resin adsorbents: effect of adsorbate size and pore size distribution. *Journal of hazardous materials*, 137(2), 1115-1122.
- Zhen-shan, L., Ning-sheng, C., & Croiset, E. (2008). Process analysis of CO<sub>2</sub> capture from flue gas using carbonation/calcination cycles. *AIChE journal*, 54(7), 1912-1925.
- Zhou, L. (2005). Progress in fundamental research into supercritical adsorption and its impact on clean energy technology. *Adsorption Science & Technology*, 23(7), 509-518.
- Zhi, L. L., & Zaini, M. A. A. (2017). Adsorption properties of cationic rhodamine B dye onto metals chloride-activated castor bean residue carbons. *Water Science and Technology*, 75(4), 864-880.

**APPENDIX A**  
**THE IMAGES OF MATERIALS, SIMULATED, AND REAL WASTE WATER**  
**BEFORE AND AFTER ADSORPTION PROCESS**

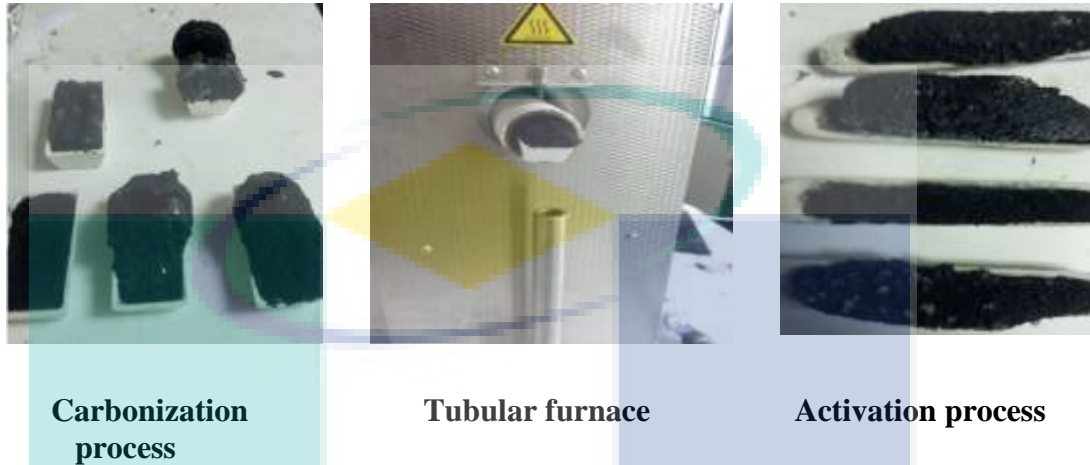
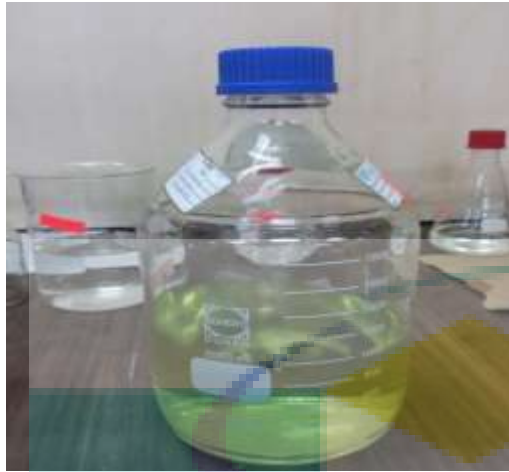


**Figure A.1:** Carbonization and activation process of ACs using tubular furnace



**Figure A.2:** Sample of prepared ACs and IACs



**Simulated waste water**

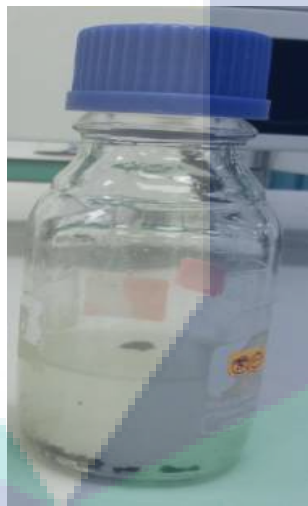


**Real waste water**

**Figure A.3:** Stock solution of simulated and real waste water



Before treatment with  
adsorbent



During the adsorption  
process



After adsorption  
process

**Figure A.4:** real waste water before, during the adsorption process and after treatment

## APPENDIX B CALCULATIONS AND RESULTS

### CALCULATIONS B. 1: Determination of the initial concentration of dissolved H<sub>2</sub>S (aq)

$$\text{Number of moles of atoms} = \frac{\text{mass in gram}}{\text{molar mass of atoms}}$$

For concentration of 100 mg/L

$$\text{Number of moles of sulfur} = \frac{0.1\text{g}}{32\text{ g/mol}} = 0.003125\text{ mol}$$

$$W = M \times V \times MW$$

$$W = 0.003125\text{ mol} \times 1\text{L} \times 240.04\text{ g/mol} = 0.750\text{ g/L}$$

Where *W* is weight of Na<sub>2</sub>S.9H<sub>2</sub>O g/L, *MW* is molecular weight of Na<sub>2</sub>S.9H<sub>2</sub>O, *M* is the number of moles of sulfide, *V* is the volume of solution.

Determination of Removal efficiency (RE)

$$RE = \frac{C_o - C}{C_o} \times 100$$

For 500 mg/L of dissolved H<sub>2</sub>S<sub>(aq)</sub>

$$RE = \frac{500 - 30}{500} \times 100 = 94$$

Where, *C<sub>o</sub>* is the initial concentration of dissolved H<sub>2</sub>S<sub>(aq)</sub> (mg/L), *C* is the concentration of dissolved H<sub>2</sub>S<sub>(aq)</sub> at equilibrium (mg/L)

$$\text{Yield (\%)} = \frac{W_c}{W_o} \times 100$$

Where, *W<sub>c</sub>* and *W<sub>o</sub>* are the dry weight of the final sample and the dry weight of precursor, respectively.

$$\text{Yield (\%)} = \frac{1.205}{3.566} \times 100 = 33.8$$

$$R_L = \frac{1}{1 + bC_0}$$

Where  $C_0$  is the initial concentration of  $H_2S$  ( $mg L^{-1}$ ) and  $b$  is the Langmuir constant, the value of  $R_L$  indicates the shape of the isotherm.

$$R_L = \frac{1}{1 + (0.0495 \times 500)} = 0.0388$$



UMP

**APPENDIX C**  
**OPTIMIZATION OF THE PREPARATION AND OPERATION CONDITIONS**  
**OF CA-ACPKS**

**Table C.1:** The design matrix and the response of preparations factors of Ca-ACPKS

Runs	Ca-ACPKS preparation conditions variables			RE (%)	Yield (%)
	A: calcination temperature (°C)	B: calcination contact time	C: concentration of calcium V%		
1	900	60	50	98	35.2
2	800	30	75	89.5	35
3	900	60	92	92	33.4
4	1068	60	50	91	25
5	800	30	25	89.3	35.6
6	900	110	50	91	33
7	1000	30	75	92	29.3
8	900	10	50	91	36.3
9	800	30	75	89.8	35.2
10	800	30	25	89	35.5
11	1000	30	25	90.2	31
12	1000	90	75	91	28.4
13	1000	90	25	90.5	28.5
14	900	60	50	98.2	35
15	1000	90	25	91	28.6
16	1068	60	50	91	25.1
17	900	60	50	99	35.1
18	900	60	50	98.4	35
19	800	90	25	91.3	34.6
20	731	60	50	89	35
21	1000	90	75	90.3	28.2
22	1000	30	75	92.4	29.5
23	1000	30	25	90.5	31.2
24	900	60	92	92	33
25	731	60	50	88.7	35
26	900	60	8	91.1	35
27	900	60	50	99	36
28	900	60	8	91	35.1
29	800	90	75	90.2	34
30	800	90	25	91	34
31	900	10	50	91	36
32	900	60	50	98	35
33	900	110	50	91.3	33
34	800	90	75	90.5	34

**Table C.2:** Analysis of variance (ANOVA) for the screening of operation condition of removal of H<sub>2</sub>S using Ca-ACPKS (2 level factorial)

Sources	Sum of squares	Contribution (%)	F-value	P-value
Model	131.31		94.98	< 0.0001
A-Initial H <sub>2</sub> S concentration	31.36	23.6	158.78	< 0.0001
B-adsorption contact time	70.56	53.10	357.27	< 0.0001
C-adsorbent dosage	5.29	3.98	26.78	0.0008
D-pH	0.36	0.27	1.82	0.2139
E-agitation speed	0.81	0.61	4.10	0.0774
AB	17.64	13.27	89.32	< 0.0001
BC	5.29	3.98	26.78	0.0008
Residual	1.58			
Cor Total	132.89			

**Table C.3:** Validation of optimization of operating conditions using Ca-ACPKS

Runs	Factors			Response	
	A: Initial conc.	B: Time	C: Dosage	RE (Actual)	RE predicted
1	700	660	1.25	94	94.11
2	300	660	1.25	95.4	95.86
3	500	540	1.4	95.6	95.8
4	500	540	1	98.7	98.08
5	163	540	1	95.8	95.67
6	500	741	1	96	95.21
7	500	540	1	97.8	98.08
8	700	420	1.25	90.2	90.1
9	500	338	1	88	88.4
10	500	540	1	98	98.017
11	500	540	1	98	98.081
12	500	540	0.58	94.7	94.34
13	700	420	0.75	88.9	88.63
14	836	540	1	91.7	91.49
15	500	540	1	98.3	98.08
16	300	660	0.75	95.6	95.84
17	300	420	0.75	91.8	91.87
18	500	540	1	97.7	98.08
19	300	420	1.25	94.63	94.15
20	700	660	0.75	94.2	94.86



**APPENDIX D  
THE RESULT OF MEASURING CALCIUM CONCENTRATION**

Method: Untitled Page 1 Date: 11/24/2011 10:28:21 PM

**Analysis Begun**

Logged In Analyst: Administrator Technique: AA Flame  
Spectrometer: AAnalyst 400, S/N 201812010501 Autosampler:

Sample Information File: C:\Documents and Settings\All Users\PerkinElmer\AA\Data\Sample Information\  
Ca230916Omar.sif

Batch ID:  
Results Data Set: Ca230916Omar  
Results Library: C:\Documents and Settings\All Users\PerkinElmer\AA\Data\Results\Results.mdb

**Method Loaded**

Method Name: Ca230916Omar Method Last Saved: 11/24/2011 9:26:13 PM  
Method Description: Ca230916Omar

Sequence No.: 1  
Sample ID: Blank  
Analyst:

Autosampler Location:  
Date Collected: 11/24/2011 9:31:54 PM  
Data Type: Original

**Replicate Data: Blank**

Repl #	Sample Conc mg/L	Std Conc mg/L	Blk Corr Signal	Time	Analyte: Ca 422.67 Signal Stored
1	[0.00]	[0.00]	0.371	9:31:56 PM	No
2	[0.00]	[0.00]	0.379	9:32:00 PM	No
3	[0.00]	[0.00]	0.388	9:32:04 PM	No
Mean:	[0.00]	[0.00]	0.379		
SD:	0.0000	0.0000	0.0084		
%RSD:	0.00%	0.00%	2.23		

Auto-zero performed.

Sequence No.: 2  
Sample ID: Calib Std 1  
Analyst:

Autosampler Location:  
Date Collected: 11/24/2011 10:07:22 PM  
Data Type: Original

**Replicate Data: Calib Std 1**

Repl #	Sample Conc mg/L	Std Conc mg/L	Blk Corr Signal	Time	Analyte: Ca 422.67 Signal Stored
1	[1]	[1]	0.045	10:07:24 PM	No
2	[1]	[1]	0.026	10:07:28 PM	No
3	[1]	[1]	0.024	10:07:32 PM	No
Mean:	[1]	[1]	0.032		
SD:	0.00	0.00	0.0114		
%RSD:	0.00%	0.00%	36.30		

Standard number 1 applied. [1]  
Correlation Coef.: 1.000000 Slope: 0.03152 Intercept: 0.00000

Sequence No.: 3  
Sample ID: Calib Std 2  
Analyst:

Autosampler Location:  
Date Collected: 11/24/2011 10:08:01 PM  
Data Type: Original

**Replicate Data: Calib Std 2**

Repl #	Sample Conc mg/L	Std Conc mg/L	Blk Corr Signal	Time	Analyte: Ca 422.67 Signal Stored
1	[2]	[2]	0.077	10:08:02 PM	No
2	[2]	[2]	0.072	10:08:07 PM	No
3	[2]	[2]	0.071	10:08:11 PM	No
Mean:	[2]	[2]	0.073		
SD:	0.00	0.00	0.0031		
%RSD:	0.00%	0.00%	4.20		

Standard number 2 applied. [2]  
Correlation Coef.: 0.983970 Slope: 0.03565 Intercept: 0.00000



-----  
Replicate Data: Ca-Eggshell

Analyte: Ca 422.67

Repl #	SampleConc mg/L	StndConc mg/L	BlnkCorr Signal	Time	Signal Stored
1	72.52	72.52	2.350	10:11:06 PM	No
Sample concentration is greater than that of the highest standard.					
2	69.85	69.85	2.264	10:11:10 PM	No
Sample concentration is greater than that of the highest standard.					
3	72.55	72.55	2.351	10:11:15 PM	No
Sample concentration is greater than that of the highest standard.					
Mean:	71.64	71.64	2.321		
SD:	1.546	1.546	0.0501		
%RSD:	2.16%	2.16%	2.16		
Sample concentration is greater than that of the highest standard.					

Sequence No.: 8

Autosampler Location:

Sample ID: Ca-Oyester shell

Date Collected: 11/24/2011 10:12:09 PM

Analyst:

Data Type: Original

-----  
Replicate Data: Ca-Oyester shell

Analyte: Ca 422.67

Repl #	SampleConc mg/L	StndConc mg/L	BlnkCorr Signal	Time	Signal Stored
1	64.61	64.61	2.094	10:12:10 PM	No
Sample concentration is greater than that of the highest standard.					
2	69.97	69.97	2.267	10:12:14 PM	No
Sample concentration is greater than that of the highest standard.					
3	67.58	67.58	2.190	10:12:19 PM	No
Sample concentration is greater than that of the highest standard.					
Mean:	67.39	67.39	2.184		
SD:	2.685	2.685	0.0870		
%RSD:	3.99%	3.99%	3.99		
Sample concentration is greater than that of the highest standard.					

Sequence No.: 9

Autosampler Location:

Sample ID: Ca-After treatment

Date Collected: 11/24/2011 10:13:01 PM

Analyst:

Data Type: Original

-----  
Replicate Data: Ca-After treatment

Analyte: Ca 422.67

Repl #	SampleConc mg/L	StndConc mg/L	BlnkCorr Signal	Time	Signal Stored
1	9.046	9.046	0.293	10:13:02 PM	No
Sample concentration is greater than that of the highest standard.					
2	4.945	4.945	0.160	10:13:06 PM	No
3	1.732	1.732	0.056	10:13:11 PM	No
Mean:	5.241	5.241	0.170		
SD:	3.6661	3.6661	0.1188		
%RSD:	69.95%	69.95%	69.95		

Sequence No.: 10

Autosampler Location:

Sample ID: Ca-After treatment

Date Collected: 11/24/2011 10:13:46 PM

Analyst:

Data Type: Original

-----  
Replicate Data: Ca-After treatment

Analyte: Ca 422.67

Repl #	SampleConc mg/L	StndConc mg/L	BlnkCorr Signal	Time	Signal Stored
1	-3.208	-3.208	-0.104	10:13:48 PM	No
2	-3.705	-3.705	-0.120	10:13:52 PM	No
3	-3.683	-3.683	-0.119	10:13:56 PM	No
Mean:	-3.532	-3.532	-0.114		
SD:	0.2810	0.2810	0.0091		
%RSD:	7.96%	7.96%	7.96		



## APPENDIX E LIST OF PUBLICATIONS

### Published papers

#### Book chapter

1. Omar Abed Habeeb, Ramesh Kanthasamy, Sumathi Sethupathib, Rosli Mohd. Yunus. Optimization and Characterization Study of Preparation Factors of Activated Carbon Derived from Coconut shell to Remove of H<sub>2</sub>S from Waste water . *Activated carbon: prepared from various precursors. Ideal International E – Publication Pvt. Ltd. ISBN: 978-93-86675-07-1. P-(44-61).*

#### Journal Articles

2. Omar Abed Habeeb, K. Ramesh, Gomaa A.M. Ali, S. Sumathi, Rosli bin Mohd. (2017). Hydrogen Sulfide Emission Sources, Regulations and Cleaning Techniques Using Physiochemical, Chemical and Biological Approaches: A Review. *Reviews in Chemical Engineering journal*. DOI: 10.1515/revce-2017-0004.(Q1 - IF:3.19).

3. Omar Abed Habeeb, K. Ramesh, Gomaa A.M. Ali, Rosli bin Mohd. Yunus. (2017). Low Cost and Eco–friendly Activated Carbon from Modified Palm Kernel Shell for Hydrogen Sulfide Removal from Waste water : Adsorption and Kinetic Studies. *Desalination and Water Treatment*, 84: 205-214.(Q2 - IF:1.6).

4. Omar Abed. Habeeb, K. Ramesh, & Gomaa, A. A., Rosli bin Mohd. Yunus. (2017). Experimental design technique on removal of hydrogen sulfide using CaO-egg shell s dispersed onto palm kernel shell activated carbon: Experiment, optimization, equilibrium and kinetic studies. *Journal of Wuhan University of Technology-Mater. Sci. Ed.*, 32(2): 305-320. (Q3 - IF:0.44).

5. Omar Abed Habeeb, K. Ramesh, Gomaa A. M. Ali, Rosli bin Mohd. Yunus. (2017). Application of Response Surface Methodology for Optimization of Palm Kernel Shell Activated Carbon Preparation Factors for Removal of H<sub>2</sub>S from Industrial Waste water . *Jornal Teknologi*. 79: 1–10. (SCOPUS Index).

6. Omar Abed Habeeb, K. Ramesh, Ali, G. A. M., & Yunus, R. M. (2017). Isothermal modelling based experimental study of dissolved hydrogen sulfide adsorption from waste water using egg shell based activated carbon. *Malaysian Journal of Analytical Sciences*, 21(2): 334-345. (SCOPUS Index).

7. Omar Abed Habeeb, K. Ramesh, Ali, G. A., & bin Mohd, R. (2017). Optimization of activated carbon synthesis using response surface methodology to enhance H<sub>2</sub>S removal from refinery waste water . *Journal of Chemical Engineering and Industrial Biotechnology*, 1: 1-17.
8. Omar Abed Habeeb, K. Ramesh, Ali, G. A., Yunus, R. M., & Olalere, O. A. (2017). Kinetic, isotherm and equilibrium study of adsorption capacity of hydrogen sulfide-waste water system using modified egg shell s. *IIUM Engineering Journal*, 18(1): 13-25.
9. Omar Abed Habeeb, K. Ramesh, Ali, G. A., Yunus, R. M., Thanusha, T. K., & Olalere, O. A. (2016). Modelling and Optimization for H<sub>2</sub>S Adsorption from Waste water Using Coconut Shell Based Activated Carbon. *Australian Journal of Basic and Applied Sciences*, 10(17): 136-147.
10. Omar Abed Habeeb, Ramesh Kanthasamy, Ayodele Bamidele Victor, Rosli bin Mohd. Yunus. Predictive modelling for the removal of hydrogen sulfide from waste water by calcium-modified coconut shell based activated carbon using Artificial Neural Network. *Journal of King Saud University - Science*(Submitted).
11. Omar Abed Habeeb, K. Ramesh, Ali, G. A. High surface area mesoporous silica (MCM-41) for hydrogen sulfide effective removal. *Turkish Journal of Chemistry*. (under review).
12. Omar Abed Habeeb, Ramesh Kanthasamy, Ayodele Bamidele Victor, Rosli bin Mohd. Yunus. Optimization and modeling of H<sub>2</sub>S removal from downstream waste water using calcium-coated wood sawdust-based activated carbon. (under preparation).

#### Conference Proceeding

1. Omar Abed Habeeb, Ramesh Kanthasamy, Rosli Mohd Yunus, Mani Malam Ahmad, Olalere Olusegun Abayomi. (2016). Experimental Study of the Effect of PH on the Adsorption Capacity of H<sub>2</sub>S from Waste water by Using Calcination of Egg shell as an Adsorbent. Paper presented in The National Conference for Postgraduate Research (NCON-PGR) (2016).
2. Omar Abed. Habeeb, K. Ramesh, Gomaa A. M. Ali, R. M. Yunus, T. K. Thanusha, O.A. Olalere. (2016). Modeling and Optimization for H<sub>2</sub>S Adsorption from Waste water Using Coconut Shell Based Activated Carbon. Paper presented in 4<sup>th</sup> International Conference of Chemical Engineering & Industrial Biotechnology (ICCEIB) (2016).